Geochemistry and mineralization of the Archean Titan (Roaring River) intrusion, Thunder Bay, Ontario

Tianna Groeneveld

A thesis submitted in partial fulfillment of the requirements

of the degree of Master of Science

Department of Geology

Lakehead University

February 2023

Abstract

The 2690 ± 3.2 Ma Titan intrusion is an approximately 7 by 3 km, roughly ovoid, mafic-ultramafic intrusion, located just north of the inferred boundary between the Winnipeg River and Marmion terranes. Outcrop in the area is relatively sparse, largely due to cover from pervasive glacial till and Proterozoic diabase sills associated with the Midcontinent Rift. Titan consists of a variety of lithologies, including leucogabbros, melagabbros, gabbros, and pyroxenites, which are distributed throughout the intrusion. Both mafic and felsic dikes are observed in outcrop, as are felsic breccias. Titan consists of a single magma body, with one pulse of magma which has subsequently undergone fractional crystallization within a closed system. This is supported by smooth linear trends in the major element bivariate plots, with moderate amounts of scatter, and consistent, tight primitive mantle normalized REE trends. Titan samples have a range of $(La/Sm)_N$ from 0.7 to 3.8, a range of $(Gd/Yb)_N$ from 2.3 to 7.4, and a range of Nb/Nb* values from 0.02 to 0.47.

Titan likely formed in a supra subduction zone setting, as evidenced by the negative HFSE anomalies. This is consistent with the regional context of the Winnipeg River and Marmion terranes during this time period (~2.74-2.69 Ga). Small amounts of crustal material appear to have been incorporated into Titan, as evidenced by ε_{Nd} values of 0.70 to 1.82, compared to an estimated depleted mantle at 2.7 Ga which would have a ε_{Nd} value of +3. The exact source of the contamination can only be speculated due to the similarity in geochemical and ε_{Nd} values for the surrounding Roaring River complex, and lack of data from the basement rocks in that area.

Sulphides are found ubiquitously throughout the intrusion, though generally at low abundances (~3%). The most common sulphide is pyrite, often found as very fine-grained blebs with a rim of magnetite, whereas larger aggregates of pyrrhotite, chalcopyrite, and pentlandite are much rarer. Pyrite is considered to be a hydrothermal phase, likely as secondary precipitation. Sulphide isotopes were gathered from pyrite and a smaller amount of chalcopyrite grains, providing $\delta^{34}S$ values with a range of -10.02 to +5.41‰ and $\Delta^{33}S$ values with a range of -0.26 to +0.1‰. The sulphur isotope values are consistent with an initial magmatic sulphur phase, responsible for the large aggregates of pyrrhotite, pentlandite, and chalcopyrite, and a later low temperature (< 400 °C) hydrothermal system. The hydrothermal system is also likely to have oxidizing conditions, causing the preferential mobility of Se over S.

Titan is compared to the nearby Lac des Iles suite, a collection of mafic to ultramafic intrusions within the Marmion terrane, which includes the Lac des Iles Complex and Tib Lake intrusion. There are broad similarities between Titan and the Lac des Iles suite, particularly in the regional context of the intrusions, general lithology, age, and in tectonic setting. However, there are key differences. Titan consists of one magmatic body, while the Lac des Iles complex consists of several intrusions and Tib Lake has multiple magmatic pulses. The environment around the Lac des Iles suite is also more dynamic, with roughly coeval felsic and mafic magmatism. The Lac des Iles complex and Tib Lake are interpreted to have assimilated country rock and felsic magmas associated with surrounding tonalite. In contrast, Titan is intruded into the middle of a felsic complex, but the magmatism is not coeval. In general, Titan appears to be a much simpler intrusion, when compared to intrusions of similar size in the Lac des Iles suite.

Acknowledgements

First and foremost, thank you to my supervisor, Pete Hollings, for this opportunity and for the guidance thereafter. I know I had a stranger path than many to this degree and project, and I appreciate you taking a chance on that.

Thank you to David Good for your time and attention to this thesis. Your comments have made it a better body of work.

Within Lakehead University, I would like to thank Matt Brzozowski, who has always been a generous source of information and a huge help. I would also like to thank Justin Jonsson and Vicky Currie. The advice has sometimes been questionable, but the support has always been there.

A huge thank you to Impala Canada. This project would not exist without their support, and I have been hugely thankful to have worked on a Lac des Iles project. There are also many individuals within Impala Canada who have helped this project come to life. A huge thank you to Lionnel Djon and Jami Brown, for their help in facilitating this project and sampling. An even larger thank you to Liam Fay, Jeff Pinksen, Doug Nikkila, and Mike Garrett. They had the dubious honour of hiking around the woods with me while sampling, and then answering all my questions after. Without them, I am sure that I would be still be lost in the wilds of northern Ontario.

Lastly, I would like to thank my family. They've been with me throughout all of this, if not physically then emotionally. I would not have been able to start this project, let alone finish it, without their support.

Table of Contents

List of Figures

List of Tables

1. Introduction

Ontario, Quebec, parts of Manitoba, and the northern United States are all partially underlain by the Superior Province, which consists of roughly linear belts of Archean rock (Card and Ciesielski, 1986; Stott, 1997). The Superior Province is host to a variety of different lithologies, ranging from volcanic to sedimentary to mafic and felsic intrusions (Stott, 1997). Many of these intrusions are host to economic mineralization and many more are active areas of exploration, both to determine other intrusions and areas of economic interest and to understand the geologic history of the Superior Province.

Titan is one of many mafic-ultramafic intrusions within the Superior Province and is situated within more than 300 contiguous claim cells all owned by Impala Canada. It was flagged for anomalous Pd and Pt concentrations in a lake sediment survey completed by the Ontario Geological Survey (OGS) and more recently as an area of interest in their Recommendations for Exploration (2000, 2018). In the 23 years since the lake sediment survey, small amounts of work have been done on the property, including geophysics, multiple rounds of prospecting and soil sampling, and an aborted drilling program (Fingler and McCrindle, 2001; McCrindle, 2001; Staargaard, 2002; Barr, 2003; Heerema, 2004; Tshimbalanga, 2004). Together this body of work is not cohesive, with poor reproducibility and a patchwork of exploration. The body of work that does exist has flagged Titan as possibly comparable to the Lac des Iles suite, which lies ~50 km south in the Marmion terrane. The regional context of Titan is similar to that of the Lac des Iles suite, as are the general lithologies and ages. The Lac des Iles suite is also host to a palladium mine, hosted in a Ni-Cu-PGE deposit. The similarities between Titan and Lac

des Iles, along with the more recent Recommendation of Exploration from the Ontario Geological Survey have Titan being reconsidered as a possible source of economic Ni-Cu-PGE mineralization.

The main objective of this study was to produce a cohesive body of work based on available outcrops at Titan. The goal was to characterize the intrusion using petrography, geochemistry, and sulphide and radiogenic isotope analysis to better understand the lithology, formation conditions, tectonic setting, the source of sulphur, and any evidence for crustal contamination. The research focused mainly on what could be observed in outcrop, though the limited drill core is discussed when applicable.

2. Regional Geology

2.1 The Superior Province

The Superior Province is the world's largest relatively undisturbed Archean craton, covering an area of ~1,572,000 km^2, largely over Ontario, Quebec, Manitoba, and parts of the Northern USA (Stott, 1997). The craton is surrounded on all sides by Proterozoic orogenic belts, with the Grenville Province lying to the south-east, the Churchill Province to the east, north, and west, and the Southern Province to the south (Card and Ciesielski, 1986). The Superior Province largely consists of roughly linear belts, each consisting of either volcanic, sedimentary, or granitoid lithologies (Stott, 1997). In the western Superior Province, where this study is focused, the belts are largely east-west trending. The belts, termed subprovinces or terranes, are commonly bounded by strike-slip faults which are traditionally interpreted to have formed during the terminal stages of Archean collisional orogeny (Bethune et al., 2006). A range of metamorphic grades are observed across the Province and include both regional and intrusion specific metamorphic effects (Card and Ciesielski, 1986; Stott, 1997).

There have been multiple attempts to subdivide the Superior Province based on shifting criteria as geologic knowledge and techniques have improved. The criteria used as the basis for the subdivision include all, or some combination of, structural trends and styles, lithology, absolute and relative ages of rock units and events, metamorphic grade, metallogenesis, and geophysical characteristics (Card and Ciesielski, 1986; Tomlinson et al., 2004; Stott et al., 2010). The subprovinces of the Superior Province are based on empirical contrasts in lithology, structure, metamorphism, and geophysics, and these

criteria are still used today as a method of dividing the western Superior Province (Card and Ciesielski, 1986; Stott, 1997). Later refinement in age dating and isotopic analysis created the terrane and domain subdivisions of the Superior Province, with this classification having its basis in the discrete tectonic history of each craton (Stott, 1997; Stott et al., 2010).

Although the terrane system is the newer classification method, the older subprovince system is still widely used and its descriptive, lithology-based categorization can be helpful when discussing broad differences across the western Superior Province. Additionally, the study area lies within an ambiguous area between the subprovince and terrane classification systems, so familiarity with both is often helpful (Fig. 2.1). Within the western Superior Province there are three broad lithologic categories of subprovinces: volcano-plutonic, metasedimentary, and plutonic. The volcano-plutonic subprovinces, including the Wabigoon, Uchi, Sachigo, and Wawa-Abitibi, are characterized by dominantly metavolcanic supracrustal sequences, greenstone belts, regional sub-to-greenschist facies metamorphism, and tend to make up many of the most economically important parts of the Superior Province (Card and Ciesielski, 1986). Metasedimentary subprovinces, such as the English River and Quetico, consist of dominantly sedimentary supracrustal rocks, linear structural characteristics, and metamorphism that tends to increase inward from greenschist to low-pressure amphibolite facies (Card and Ciesielski, 1986). The plutonic subprovinces, Winnipeg River and Berens, are characterized by a near absence of supracrustal rocks and granitoid batholiths derived by partial melting of the mantle (Card and Ciesielski, 1986). Each subprovince has its own unique characteristics, however these basic subdivisions are still widely used.

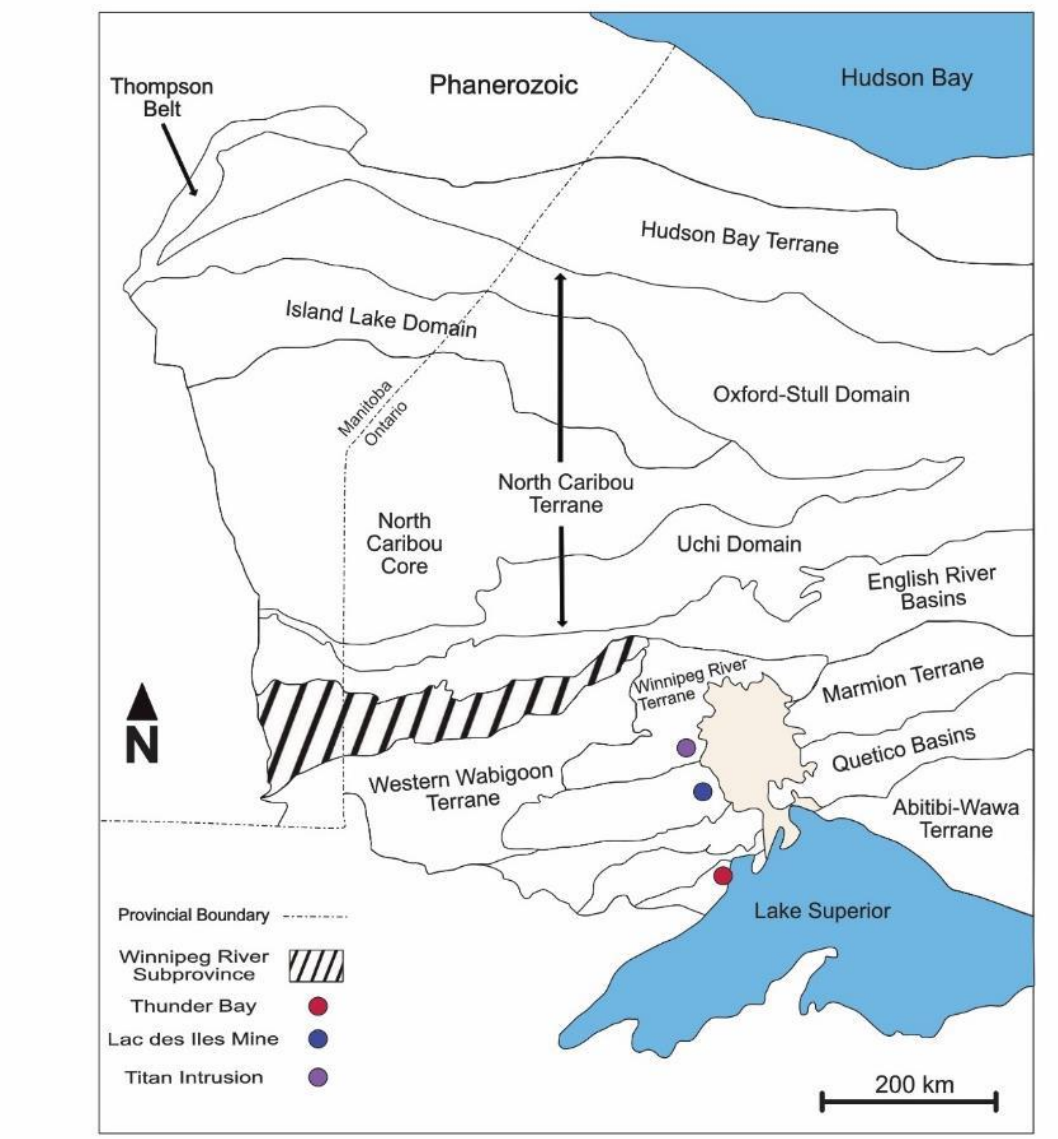

Figure 2.1. Terrane map of the western Superior Province, additionally highlighting the split between the Winnipeg River subprovince and the Winnipeg River terrane. The locations of the Titan intrusion, Lac des Iles mine, and Thunder Bay have been highlighted. Modified from Stott et al. (2010).

With improvements to age dating and geophysics, the limitations of the primarily descriptive subprovince system began to be apparent when attempting to understand the formation of the Superior Province and lead to the development of the terrane classification (Fig. 2.1; Percival et al., 2006). The terrane system is primarily used to determine tectonic divisions within the western Superior Province, with each terrane

being a tectonically bounded region with internal characteristics unique to those terranes adjacent to it (Percival et al., 2006). The recognition of tectonic boundaries suggests that the Superior Province grew through accretion, with the different terranes being stitched together during the Northern Superior (~2.72-2.71 Ga), Uchian (~2.72-2.70 Ga), Central Superior (~2.71-2.70 Ga), Shebandowanian (~2.69 Ga) and Minnesotan (~2.68 Ga) orogenies (Percival et al., 2006). The North Caribou terrane is interpreted to be the continental nucleus upon which all other terranes were accreted, with the Superior Province in general becoming younger to the south (Sanborn-Barrie and Skulski, 2006; Stott et al., 2010). The accretion and orogenic stitching of individual cratons can account for the discrete lithological domains, >1000 km long orogenic belts, and the aforementioned systematic age variation of the western Superior Province (Percival et al., 2006).

The majority of the names used in the terrane system are the same as those used in the subprovince one, though the boundaries vary between the two (Card and Ciesielski, 1986; Tomlinson et al., 2004; Stott et al., 2010). However, in certain areas the boundaries are remarkably similar, and as such the subprovince system often persists in literature. As the study area lies in an area where the subprovince and terrane systems diverge, this study will mainly be using the terrane classification system but will also be referring to the subprovince one as necessary.

2.2 Winnipeg River Terrane

The Winnipeg River terrane comprises the east-west trending Winnipeg River subprovince as well as the north-central and north-eastern parts of the Wabigoon subprovince (Fig. 2.1; Tomlinson et al., 2004). The Winnipeg River terrane is bounded

by the Marmion to the south, the Western Wabigoon to the northwest, and the English River terrane to the north. The main boundary between the western Wabigoon and the Winnipeg River terrane has been interpreted to be due to a collision at ~2.71 Ga, though this boundary has been obscured with younger intrusions (Tomlinson et al., 2004). Similar obfuscation by younger intrusions occurs at the boundary between the Marmion and Winnipeg River terranes (Tomlinson et al., 2004). Together the Winnipeg River, western Wabigoon, and Marmion terranes make up the central Superior superterrane, with the central Superior orogeny accreting them together into one superterrane shortly before they were accreted to the North Caribou superterrane (Percival et al., 2006).

Overall, the Winnipeg River terrane contains roots as old as 3.4 Ga with an overall range of 3.4-2.8 Ga, and as such it hosts some of the oldest crust within the western Superior Province (Tomlinson et al., 2004; Percival et al., 2006). The linear east-west portion of the terrane is composed mainly of Neoarchean plutonic rocks with some areas dating back to the Mesoarchean and Paleoarchean, whereas the western Wabigoon subprovince portion of the terrane consists solely of Neoarchean plutonic rocks (Percival et al., 2006). Similar to the rest of the western Superior Province, the metamorphic grade in the Winnipeg River terrane is largely limited to regional greenschist-facies (Sanborn-Barrie and Skulski, 2006).

2.3 Roaring River Complex

The Roaring River complex lies within the Winnipeg River terrane, in the Western Wabigoon subprovince portion, just west of the Nipigon Embayment. The Roaring River complex is bounded by the Garden Lake granite-greenstone belt to the south, and to the north by the Obonga Lake granite-greenstone belt (Fig. 2.2). These two greenstone belts

are both Neoarchean in age (Tomlinson et al., 2004). Proterozoic diabase sills related to the 1.1 Ga Midcontinent Rift are intruded into basement rocks for a considerable distance away from the current limits of the Nipigon Embayment, including into the Roaring River complex.

The Roaring River intrusive complex is ~70 by 1-15 km, forming a roughly crescent shape, and is comprised of diorite, monzodiorite, quartz monzodiorite, and granodiorite, which together constitute the Archean sanukitoid suite (Fig. 2.2; Stern and Hanson, 1991; Smyk and Franklin, 2007). Mesocratic to melanocratic dykes crosscut all other phases and are interpreted to be lamprophyre dykes (Stern and Hanson, 1991). The complex is emplaced into foliated to gneissic biotite-hornblende tonalite, granodiorite, and quartz diorite country rock (Stern and Hanson, 1991). The Roaring River complex is interpreted to have been emplaced late in the evolution of the Winnipeg River terrane, with a date of 2697 Ma obtained for the complex through U-Pb geochronology (Stone et al., 2003; Hart and MacDonald, 2007).

Prior to 2020 the Titan intrusion was either referred to as the Roaring River mafic intrusion or the Highway 811 gabbro (Stern and Hanson, 1991). The Titan intrusion is located within the larger Roaring River complex and is comprised of gabbro and pyroxenite (Stern and Hanson, 1991; Bowdidge, 2010). The Titan intrusion is ~ 7 km long and ~3 km wide, with a roughly ovoid shape (Fig. 2.2; Bowdidge, 2010). The shape and size are largely inferred from geophysics, as outcrop is sparse in the area due to pervasive glacial till and the aforementioned diabase sills (Bowdidge, 2010). A date of 2690 ± 3.2 Ma has been obtained for the Titan intrusion through zircon geochronology (Djon, 2018).

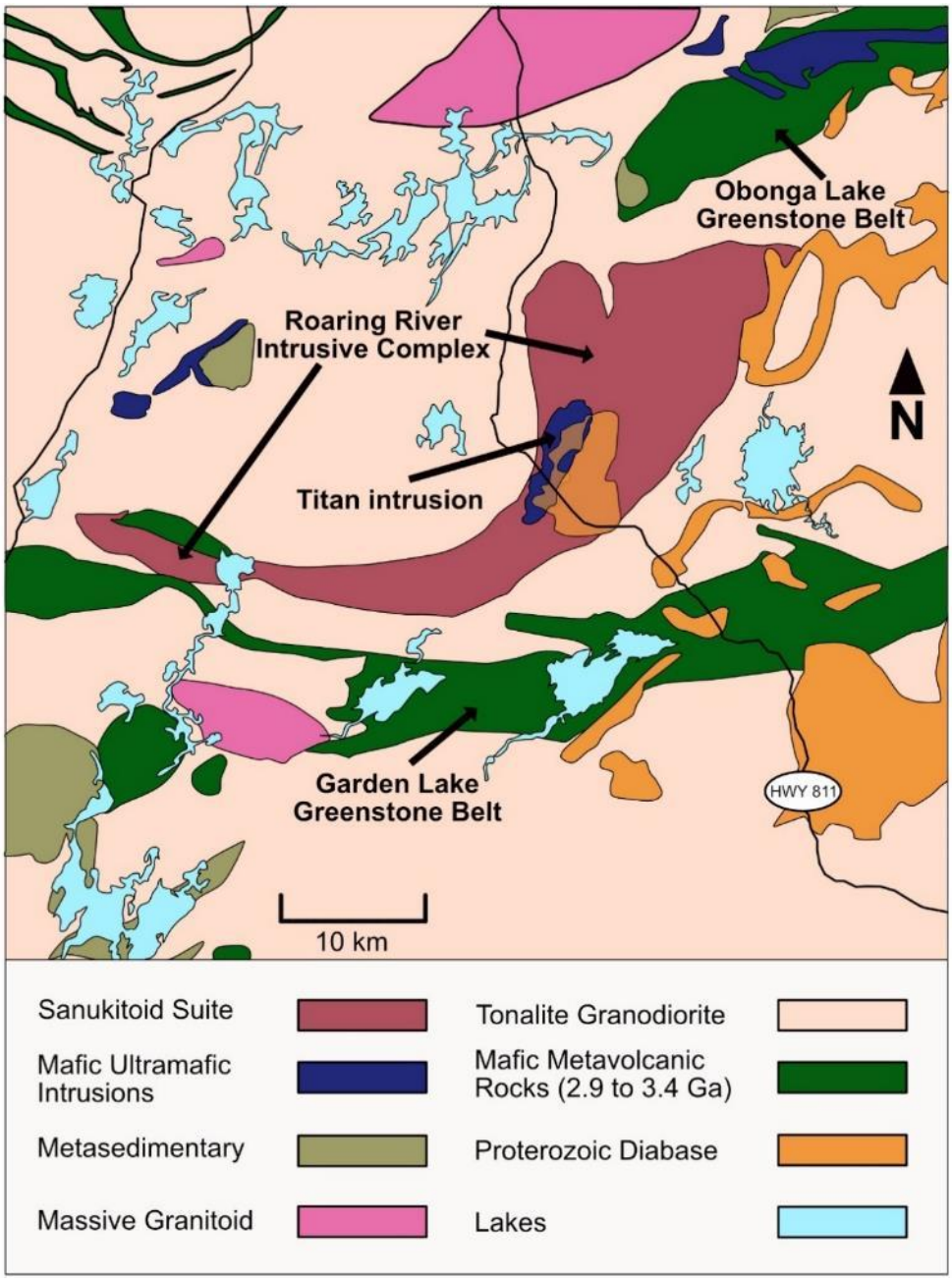

Figure 2.2. Geological map of the Roaring River Intrusive Complex area, highlighting the Titan intrusion and two nearby greenstone belts. Modified from Ontario Geological Survey (2000, 2018), and Bowdidge (2010).

The Titan intrusion was first noted as an area of interest due to anomalous Pd and Pt values from a lake sediment survey (OGS, 2000). In the following years, two separate prospecting programs were completed across the Titan intrusion, as well as three soil

surveys, trenching of primary outcrops discovered through prospecting, two induced polarization (IP) surveys, and finally a diamond drilling program (Fingler and McCrindle, 2001; McCrindle, 2001; Staargaard, 2002; Barr, 2003; Heerema, 2004; Tshimbalanga, 2004). The prospecting and trenching reports make note of primarily gabbro lithology, with fine-grained pyrite and pyrrhotite (Fingler, and McCrindle, 2001; McCrindle, 2001; Barr, 2003). The reports also noted two intrusive trends with the primary difference between the two being the amount of magnetite present and otherwise noting that they are mineralogically and texturally similar (McCrindle, 2001). However, since only fire assay analysis was performed for all rocks prospected and trenched the data from these reports is of variable help to this study. The soil survey results returned values below detection limits and showed poor reproducibility over field duplicates, and as such provide limited information (Staargaard, 2002; Barr, 2003).

Diamond drilling was generally more helpful, though the actual success of the program was limited. A total of five holes were drilled, with the locations picked from the interpretation of IP survey and magnetic anomalies (Heerema, 2004). Of these five drill holes, three intersected only diabase though their depths were variable and two intersected some portion of the mafic Titan intrusion. The holes that encountered only diabase are RR04-001, going to a depth of 141 m, RR04-002, going to a depth of 102 m, and RR04-004, going to a depth of 9 m (Heerema, 2004). The third drill hole, RR04-003, was drilled for 126 m and consisted of diabase until ~53 m at which point melanogabbro was observed (Heerema, 2004). The final drill hole, RR04-005, was drilled for 150 m and reached melanogabbro at a depth of ~120.5 m, with the overlying lithology being diabase (Heerema, 2004). Note that the drill holes which encountered mafic lithologies stopped

within the mafic material, though there was no indication that the lithology would change.

Once diamond drilling on the Titan intrusion was completed work on the property stopped until 2010, when a versatile time domain electromagnetic (VTEM) survey was completed. The VTEM survey notes some interesting geophysical anomalies, particularly in the northern section of the intrusion and provides the main interpretation for the shape of the Titan intrusion, particularly where outcrop is limited (Bowdidge, 2010). Once the VTEM survey was completed work on the Titan intrusion stopped, until work related to this project began in 2020.

2.4 Lac des Iles Suite

The Lac des Iles (LDI) suite is a series of mafic and ultramafic intrusions, occurring within the Marmion Terrane. The ultramafic and mafic intrusions are subcircular to ovoid in shape, and lie around the perimeter of a rough circle, with a diameter of ~30 km (Fig. 2.3; Brugmann et al., 1997). The suite is potentially part of a longer, linear belt of mafic intrusions that extend into the western Wabigoon terrane, and possibly all the way to the Quetico (Brugmann et al., 1997). The suite includes the LDI complex, as well as the Tib Lake, Dog River, Buck Lake, and Taman Lake intrusions (Fig. 2.3). The intrusions range in size from ~1-10 km and vary compositionally from leucogabbro and gabbronorite to peridotite and pyroxenite (Stone et al., 2003).

The LDI suite crosscuts three east-trending Archean greenstone belts, which north to south are the Garden Lake, Heaven Lake, and Lac des Iles belts (Stone et al., 2003). These greenstone belts are separated by felsic plutonic domains, including gneissic, biotite tonalite, hornblende tonalite, biotite granite, and sanukitoid lithologies, with each

lithology having varying degrees of prevalence in the area (Stone et al., 2003). The Archean rocks of the LDI suite and surrounding area are cut by Proterozoic diabase dikes and sills of the 1.1 Ga Midcontinent Rift (Stone et al., 2003).

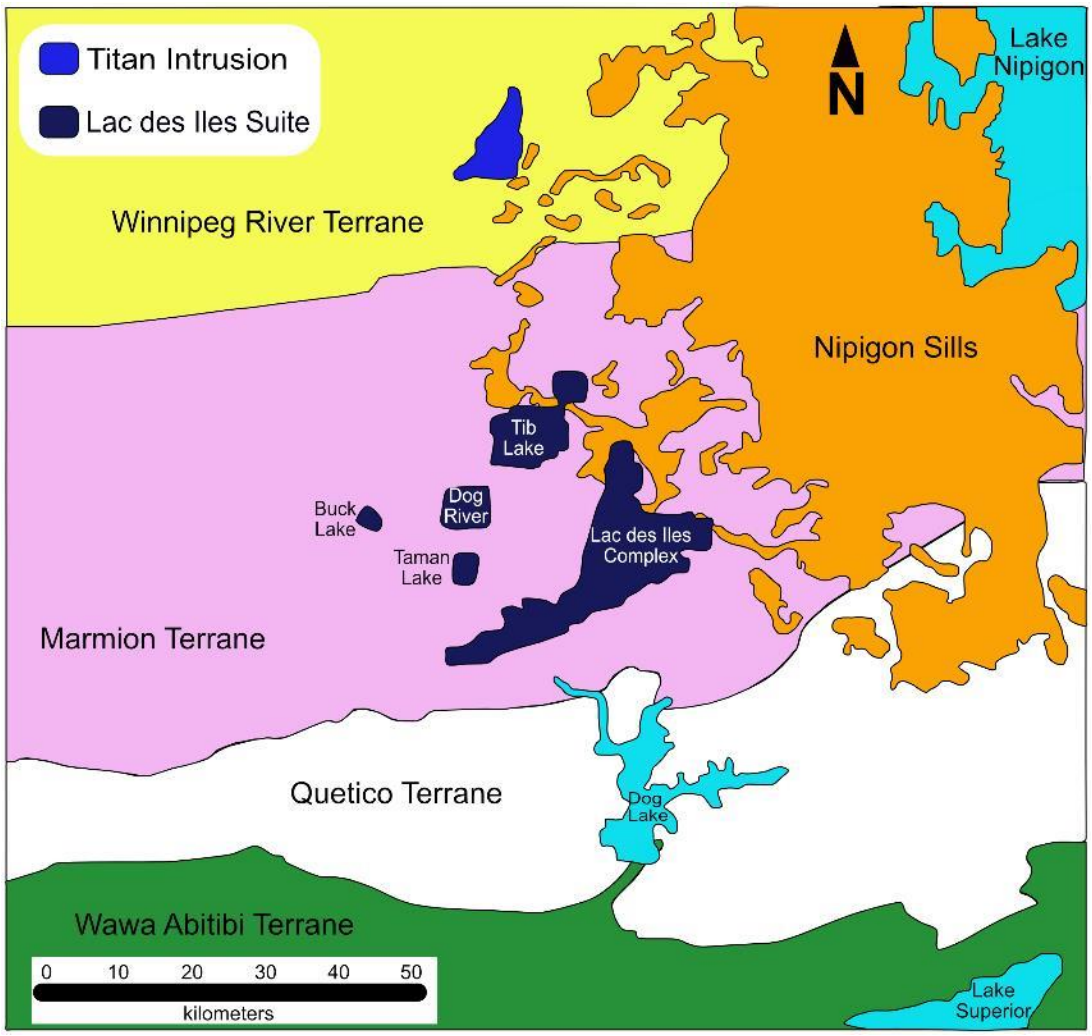

Figure 2.3. Map of the Lac des Iles suite and Titan intrusion, underlain by the terrane the intrusions lie within. Modified from Peck and Djon, (2020).

Two regional faults are mapped in the LDI area: the Gull Lake and the Shelby Lake faults (Stone et al., 2003). These variably affect the individual intrusions within the LDI suite. A splay of the Gull Lake fault offsets the Tib Lake intrusion, cuts through the very northern part of the Dog River intrusion, and extends into the Buck Lake intrusion,

whereas the Shelby Lake fault is present just to the south of the Mine Block intrusion, within the main LDI complex (Stone et al., 2003). There is a strong association between the mafic and ultramafic intrusions of the LDI suite and faults, and it has been interpreted that the faults may have acted as conduits for magma emplacement (Stone et al., 2003).

Within the LDI suite, the LDI complex is the largest of the plutons and has intruded into foliated tonalitic gneisses (Sutcliffe, 1989). The LDI complex consists of three main chambers: an ultramafic intrusion known as North LDI, a gabbroic intrusion known as the Mine Block intrusion, and a homogenous hornblende gabbro known as the Camp Lake intrusion (Brugmann et al., 1989; Lavigne and Michaud, 2001). The Camp Lake and Mine Block intrusions are sometimes referred to as South LDI (Brugmann et al., 1989). The three intrusions of the LDI complex are partially separated by tonalites, however, each intrusion is lithologically distinct (Lavigne and Michaud, 2001). The distribution of lithologies within each intrusion is generally quite chaotic suggesting that there were multiple magma pulses occurring within a dynamic environment (Lavigne and Michaud, 2001).

Many of the smaller intrusions within the LDI suite have similar lithologies, though the overall complexity of each intrusion varies considerably. Tib Lake, the second largest of the intrusions, is similar to the LDI complex, with peridotite, pyroxenite, gabbro, and gabbronorite cumulates being present in four main zones within the intrusion (Brugmann et al., 1997; Stone et al., 2003). The three smaller intrusions, Dog River, Buck Lake, and Taman Lake, mainly consist of hornblende-rich gabbro and hornblendite (Brugmann et al., 1997; Stone et al., 2003). Outcrop exposure is variable amongst these smaller intrusions, and it is possible that some lithologies are not present at surface. Overall, the

LDI suite intrusions tend to have a well-preserved igneous mineralogy that has not been significantly deformed, though greenschist facies metamorphism is prevalent (Sutcliffe, 1989). Mineralization within the suite varies, both in grade and occurrence. LDI and Tib Lake have strong to variable mineralization, whereas Buck Lake, Taman Lake, and Dog River are only very weakly mineralized (Stone et al., 2003). The LDI Complex is currently the only economic resource, and as of 2021 the LDI mine property was estimated to host 6.34 million ounces of palladium hosted within 92.9 million tonnes of measured, indicated, and inferred resources (Implats, 2021).

The LDI suite seem to be roughly coeval, as well as contemporaneous with hornblende-rich tonalite in the region (Sutcliffe, 1989). North LDI has been dated to 2687 ± 1.6 Ma, while the Mine Block intrusion has been dated to 2693.3 ± 1.3 Ma in the Eastern portion, and 2689.0 ± 1.0 Ma in the western portion, with all ages being U-Pb zircon ages (Heaman and Easton, 2006; Hart and Macdonald, 2007). The ages of the smaller intrusions are similar, with Tib Lake being dated to 2685.9 ± 1.6 Ma, whereas Taman Lake, Dog River, and Buck Lake have been dated to 2691.0 ± 1.0 Ma (Stone et al., 2003; Hart and Macdonald, 2007). It has been suggested based on the ages and lithologies of the LDI suite that the intrusions formed from the same widespread magmatic event, which may also include other mafic and ultramafic intrusions in the area such as the Shelby Lake, Wakinoo Lake, Camp Lake, and Legris Lake intrusions (Stone et al., 2003; Hart and Macdonald, 2007). Further identification of smaller mafic intrusions, typically weakly deformed, altered, and with similar ages to the LDI suite, would suggest a widespread magmatic event stretching north of the LDI area to the

Obonga Lake Greenstone Belt, which would potentially include the mafic portion of the Roaring River complex (Hart and Macdonald, 2007).

3. Methods

3.1 Sampling

Sampling of the Titan intrusion was carried out in the summer of 2021. The entire extent of the intrusion was traversed, with the goal of following up on previously sampled outcrops and discovering new ones. In total, ~120 kms were traversed, with the very furthest northern reaches of the intrusion being accessed by helicopter. A total of 144 samples were taken, with field notes made for each sample and outcrop. Field notes included a general description of the area and sample, field lithology, structure, and magnetic susceptibility measurements. Of the 144 samples, 108 were taken from the Titan intrusion, with the remaining 36 being a mix of diabase dikes and sills, and felsic country rock.

3.2 Petrography

Samples were submitted to Lakehead University's lapidary facility for preparation of polished thin sections. Fifty-one samples were submitted to provide representative coverage of the intrusion and all lithologies observed in the field. Five additional thin sections were prepared from historical drill core from the Titan intrusion, with contact areas between different mafic lithologies or between the mafic intrusion and felsic dikes being selected for additional assessment. Petrographic analysis was completed using an Olympus BX 51 microscope, with all photomicrographs taken using an Olympus SC180 camera at Lakehead University. Full petrographic descriptions of each thin section can be found in Appendix I.

3.3 Whole Rock Geochemistry

Samples were submitted to ALS Geochemistry in Thunder Bay, using their complete characterization package (CCP-PKG01), with a platinum group mineral (PGM-ICP23) fire assay add on. All 144 samples were analyzed, as was one additional sample obtained from historical drill core. Samples were prepared for analysis by crushing at least 70% of the sample to <2mm, with a representative 250g subdivision being further pulverized until 85% could pass through 75 μm. The complete characterization package combines whole rock analysis, trace elements by fusion, aqua regia digestion for volatile trace elements, and carbon and sulphur by combustion analysis in order to analyze a complete suite of elements, including rare earth elements. The platinum group minerals fire assay was done by standard lead oxide collection fire assay with inductively coupled plasma-atomic emission spectroscopy (ICP-AES) finish. The full data set can be found in Appendix II, along with detection limits.

3.4 Scanning Ion Mass Spectroscopy (SIMS)

Ten polished thin sections were submitted to the Canadian Centre for Isotopic Microanalysis (CCIM) facility at the University of Alberta for sulphur isotope analysis using scanning ion mass spectroscopy (SIMS). Areas of interest were selected during petrographic analysis, to encompass a representative sampling of sulphide minerals and their habits and occurrences (Fig. 3.1). The selected areas of interest were ~2 mm in diameter and were cored from the polished thin sections and arranged along with CCIM reference materials into a 25 mm diameter epoxy mount (Fig. 3.1). Reflected light microscopy was completed to characterize the sulphide minerals and allow precise spot selection before microprobe analysis was started. Scanning electron microscopy (SEM)

was completed on the regions of interest to ensure that any zoning within the sulphides was considered for analysis.

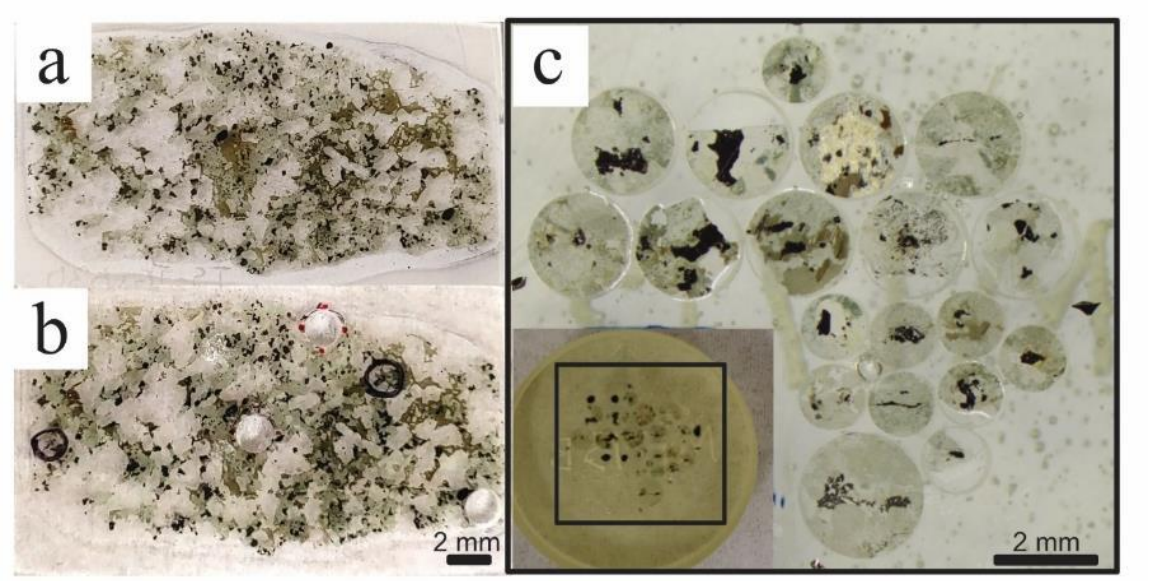

Figure 3.1. Images illustrating the preparation process for SIMS analysis. a) the clean, thin section, where sulphides are chosen and imaged to make a guide for drilling. b) the thin section with both guide marks and drill holes visible. The holes are drilled very carefully, so that any damage to the thin section is minimal and it can still be used after SIMS analysis. c) the epoxy mount, with a zoomed in image so the removed rounds with sulphide grains in them can clearly seen within the mount.

Sulphur isotope ratios ($^{34}S/^{33}S/^{32}S$) were determined using an IMS-1280 multi-collector microprobe at the CCIM. The primary beam conditions included the use of 20 keV $^{133}Cs^{+}$ ions focused to form a probe with diameter ~15 µm and beam current ~1.5 nA. All minerals of interest were assumed to have no significant mass independent isotopic anomalies for the purpose of this study, i. e., $\Delta^{33}S = 0$, where

$$\Delta^{33}\mathrm{S} = \left[\left(\frac{\delta^{33}S}{1000} + 1\right) - \left(\frac{\delta^{34}S}{1000} + 1\right)\right] \times 1000‰,$$

with δ values expressed in ‰, the exponential mass fractionation constant from Farquhar et al. (2010), and the VCDT values for $^{33}S/^{32}S = 0.00787725$ and $^{34}S/^{32}S = 0.0441626$ (Ding et al., 2001). Final uncertainties in $\delta^{33}S_{VCDT}$, $\delta^{34}S_{VCDT}$, and $\Delta^{33}S$ are reported at

95% confidence level and have typical values at ± 0.15‰. In house reference materials were used, with analyses of these reference materials measured as a baseline and intermittently throughout data collection. The full data set can be found in Appendix III.

3.5 Sm-Nd isotopes

Fourteen samples were sent for Sm-Nd isotope analysis at the Isotope Geochronology and Geochemistry Research Centre (IGGRC) at Carleton University. Samples were selected to address the spread of LREE trends observed from whole rock geochemistry, as well as a few outlier samples that did not exhibit the main REE anomalies.

Rock powders were spiked with ^{148}Nd-^{149}Sm and then dissolved in a series of acids before being dried down. Neodymium isotope ratios were measured using IGGRC's Thermo-Finnigan Neptune MC-ICP-MS. Neodymium isotopic ratios were normalized against $^{146}Nd/^{144}Nd=0.7219$. $^{143}Nd/^{144}Nd$ ratios were corrected for the offsets using bracketing JNdi-1 average values against an average JNdi-1 value of 0.512100 of IGGRC's Thermo-Finnigan Triton TIMS (Tanaka et al., 2000). Isotope results were then re-calculated using the previously determined age date of 2690 Ma for the Titan intrusion. The full data set can be found in Appendix IV.

3.6 Laser Ablation Inductively Coupled Plasma Mass Spectrometry (LA-ICP-MS)

The twelve thin sections and mounts used for SIMS were submitted to the University of Windsor for laser ablation-inductively coupled plasma-mass spectrometry (LA-ICP-MS) analysis on sulphide grains. These samples yielded 45 separate analyses, primarily on pyrite grains with a smaller amount of chalcopyrite grains. Samples were chosen from the thin sections sent for SIMS analysis, with three additional thin sections

added to make the dataset more robust. The samples were checked to ensure there was a representative spatial spread across the intrusion, that a spread of sulphur isotope results obtained from SIMS were included, as well as a range of Pt and Pd values from geochemical analysis.

A G8403A mass spectrometer was used, with a spot size of 20 μm, traverse speed of 5 μm/s, fluence of 2.2 J/cm^2, laser energy set at 3 mJ, a repetition rate of 20 Hz, gas background collection time of 30 seconds, and an integration time of 0.01 seconds. The following analytes were used as standards, calibration references, and to correct for PGE's: ^{29}Si, ^{33}S, ^{34}S, ^{51}V, ^{57}Fe, ^{59}Co, ^{61}Ni, ^{63}Cu, ^{65}Cu, ^{66}Zn, ^{68}Zn, ^{75}As, ^{77}Se, ^{78}Se, ^{101}Ru, ^{103}Rh, ^{105}Pd, ^{106}Pd, ^{108}Pd, ^{109}Ag, ^{111}Cd, ^{118}Sn, ^{120}Sn, ^{121}Sb, ^{123}Sb, ^{125}Te, ^{101}Ru, ^{103}Rh, ^{105}Pd, ^{106}Pd, ^{108}Pd, ^{197}Au, ^{208}Pb, and ^{209}Bi. Calibration and standard checks were done before beginning each laser ablation session as well as periodically throughout to ensure accuracy. Data was collected along a traverse across the sulphide grain, rather than drilling vertically into it.

Once data was collected, it was processed using the Iolite4 program to select areas of interest for each analysis (Paton et al., 2011). These areas were selected as consistently as possible, with the following criteria in place to make this process easier: large spikes in PGEs were avoided, as that might indicate a PGM inclusion within the sulphide; if there was low and high Co-Ni regions in pyrite they were integrated separately, so to avoid zonation; spikes of Zn were avoided in chalcopyrite grains, as this would indicate sphalerite inclusions; and Cu spikes within pyrite grains were also avoided, as this would indicate a chalcopyrite inclusion. These criteria allowed for 'clean' integration, ensuring that the area selected represented the sulphide grain originally selected and not an

inclusion within the grain. Additionally, the SEM was used to do energy dispersive X-ray (EDX) analysis to collect qualitative elemental composition for each sulphide grain. This compositional data was used in the processing of the laser ablation data as an internal standard. The full data set, including processing criteria, can be found in Appendix V.

4. Results

4.1 Petrography

Four main petrographic subtypes were observed: gabbros, leucogabbros, melagabbros, and ultramafic lithologies (Fig. 4.1). Gabbros make up the majority of the samples with 22 samples, leucogabbros account for seven samples, melagabbros have nine, ultramafic lithologies have 15 samples, and the remaining three samples were from dikes. The leucogabbros and ultramafic lithologies tend to occur together, whereas the gabbros and melagabbros are spread out across the entire Titan intrusion (Fig. 4.1). Minerals such as hornblende, orthopyroxene, and quartz vary within each of the petrographic groups, so that each group is not completely homogenous. The degree of alteration varies amongst the petrographic groups, though it shows no particular pattern across Titan. Many, though not all, of the alteration minerals are inferred to be related to the metamorphic grade of the intrusion, which goes up to greenschist-facies. This includes minerals such as actinolite, chlorite, and epidote, all in varying levels of abundance.

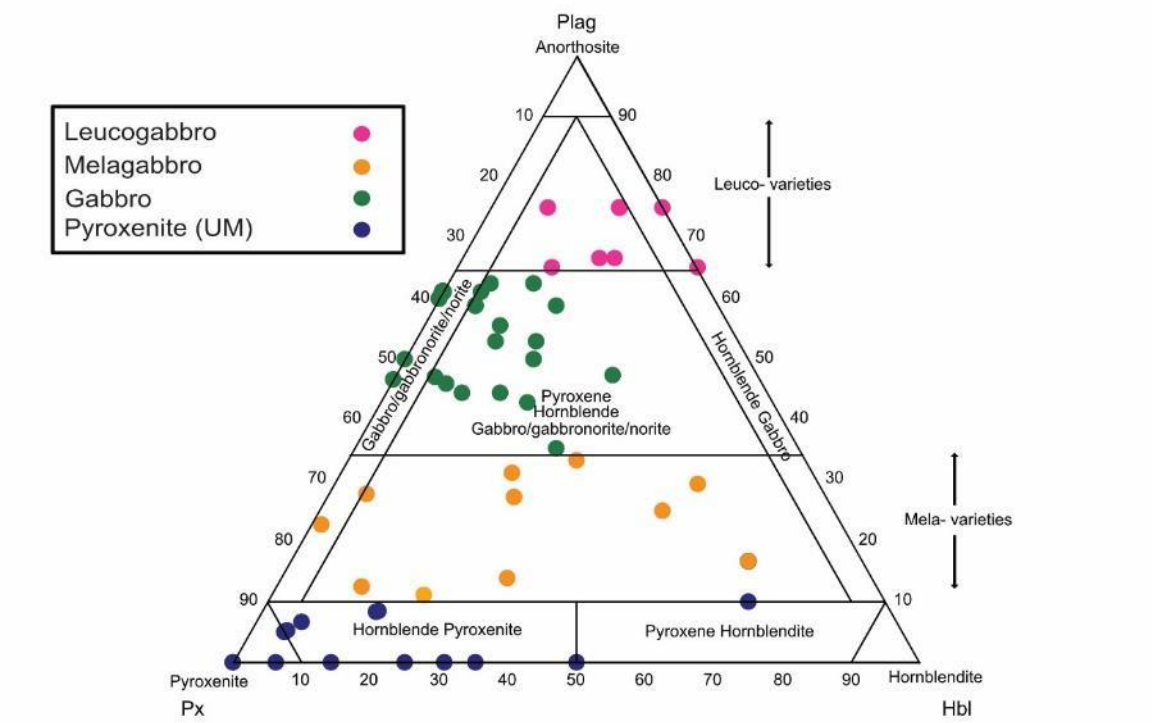

Figure 4.1. Ternary diagram of pyroxene, hornblende, and plagioclase normalized modal abundances for Titan rocks from surface samples.

A total of 51 thin sections were made from surface samples, across the entirety of the Titan intrusion. The distribution of the samples reflects the amount of Titan outcrop that was exposed at surface (Fig. 4.2). An additional five sections were selected from historical drill core. Drilling at Titan is limited, with five holes yielding a total of 528 m of core. However, only two of the five holes (RR04-003 and -005) intersected Titan, yielding ~103 m of core from the intrusion, with the rest being magnetite-rich diabase (Fig. 4.2). Select areas of core were chosen for thin sections which represented morphologies absent in outcrop. Three of the thin sections represent contact areas, either with mafic dikes or two varieties of felsic veinlets. The other two thin sections represent less and more altered versions of the melagabbro unit, which are a more mafic rock type than was typically observed in outcrop.

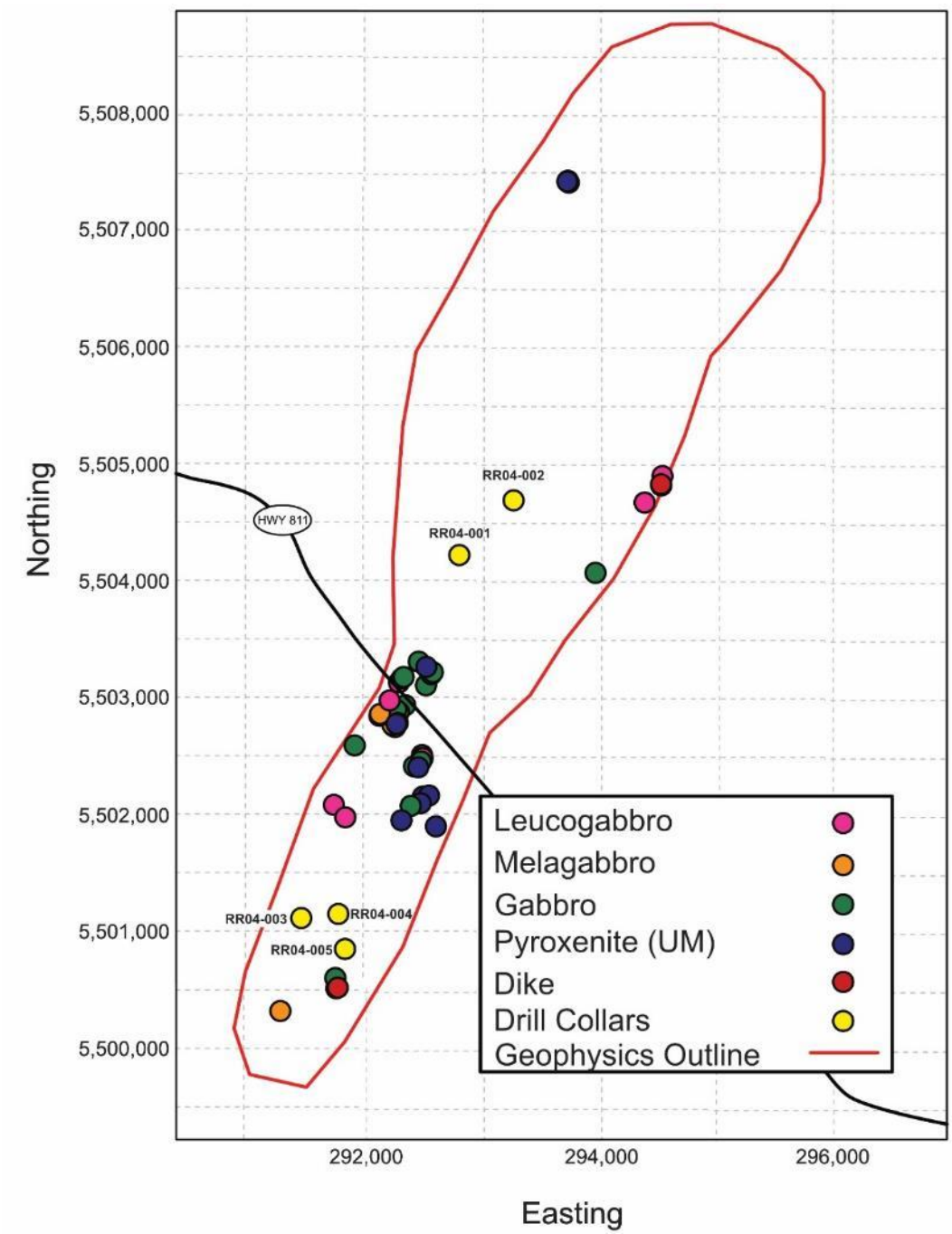

Figure 4.2. Extent and sampling of the Titan intrusion, showing the key lithological divisions observed in outcrop samples and the locations of the drill hole collars. The red outline denotes the inferred extent and boundary of the Titan intrusion, as interpreted by geophysics.

Gabbros

Gabbros occur throughout the intrusion, ranging from the very furthest south outcrops to the very furthest north (Fig. 4.2). There is some variation amongst the gabbros, including orthopyroxene gabbros, hornblende gabbros, quartz gabbros, pyroxene amphibole gabbros, and gabbronorites. The gabbros are composed of 15-45% clinopyroxene and 15-45% plagioclase, with varying amounts of other minerals, which include amphibole, orthopyroxene, biotite, quartz, and olivine. The majority of the gabbros have ≤ 10% amphibole, though a couple of samples have up to 45%. The amphibole is considered to be a primary mineral and is not included in the alteration assemblage as a metamorphic mineral. This decision was based on the overall texture and relationship between the amphibole and the other silicate minerals, as well as the texture and habits of the alteration assemblages (Fig. 4.3). Orthopyroxene ranges from 5-35% in the nine samples that host it, though all but one are <15%. Biotite occurs in six samples and is generally < 5% of the total, with one sample having 10%. Quartz is present in two samples and ranges from 5-10%. Olivine occurs in a single sample, at ~5%. The gabbros are variably altered, ranging from 5-65% alteration assemblages, though the majority of the rocks comprise ≤ 30%.

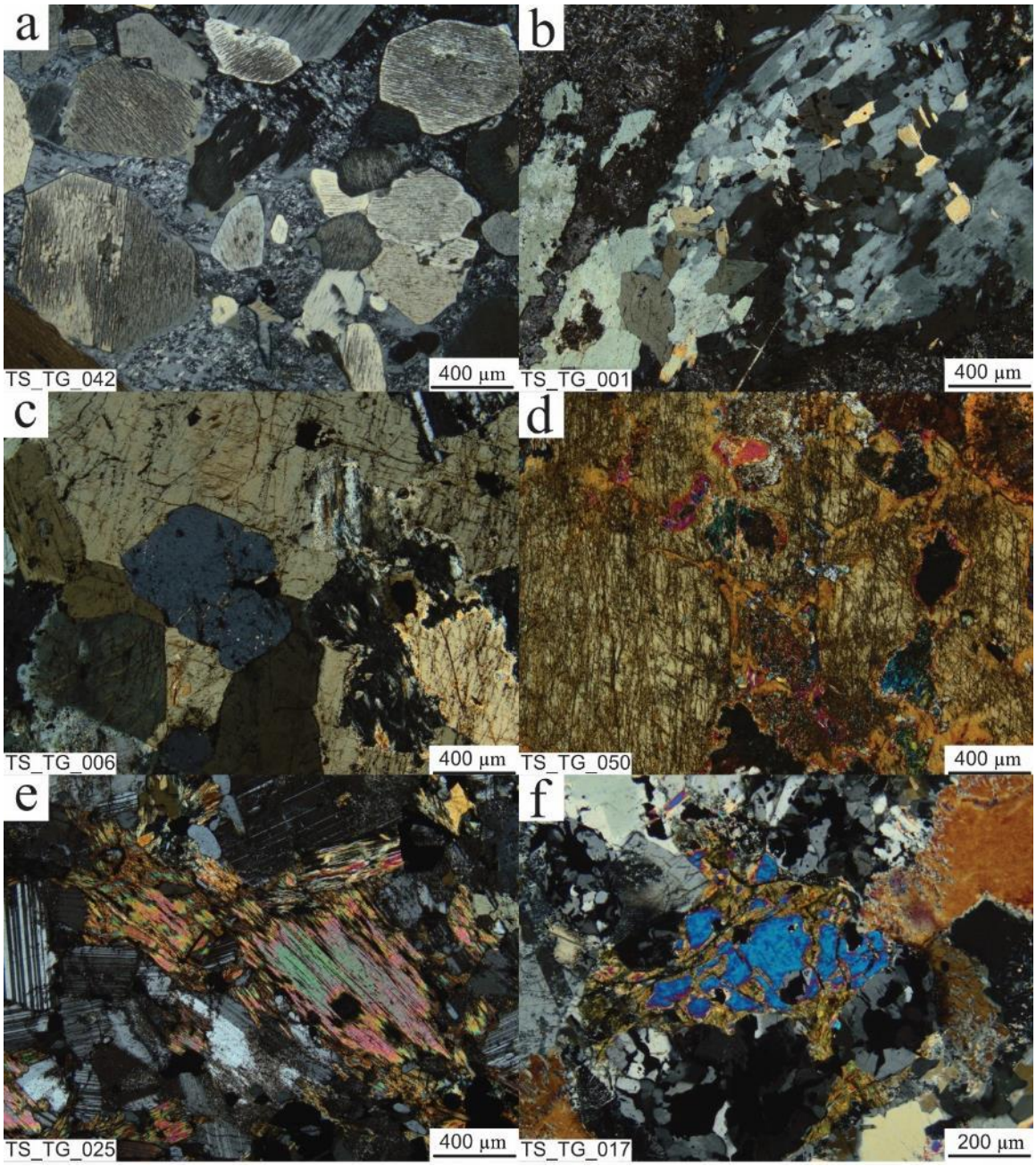

Figure 4.3. Minerals observed in Titan samples. a) euhedral to subhedral orthopyroxene crystals occurring with sericite altered plagioclase. b) fine-grained quartz, occurring with plagioclase and amphibole. c) fresh amphibole, surrounding pyroxene crystals. d) altered amphibole, which has replacement by alteration minerals at grain boundaries. e) tabular biotite occurring interstitial to plagioclase crystals. f) an anhedral olivine crystal, with iddingsite propagating along the edges and cracks in the crystal, occurring with plagioclase and clinopyroxene.

Clinopyroxene in the gabbros tends to be fine- to medium-grained, ranging from euhedral to anhedral (Fig. 4.4b). Clinopyroxene can also be found enclosed by medium-grained amphibole masses (Fig. 4.4c). Clinopyroxene crystals often have indistinct grain boundaries, as replacement by alteration minerals often occurs at the edge (Fig. 4.4d). If the clinopyroxene grain boundary is distinct, then they are either fresh and intact or have alteration that is central to the crystal, often occurring along cleavage planes (Fig. 4.4a, b, d, e). Indistinct grain boundaries, along with overprinting by alteration both within and around the clinopyroxene grains, creates a variety of different appearances and textures within clinopyroxene. The effect can give clinopyroxene a more granular appearance, but also sometimes gives it a mottled appearance depending on the smoothness of the alteration minerals and crystal grain boundaries (Fig. 4.4e, f). Within a single thin section, both highly altered and completely intact clinopyroxene have been observed, with no observed pattern or preference for when each occurs.

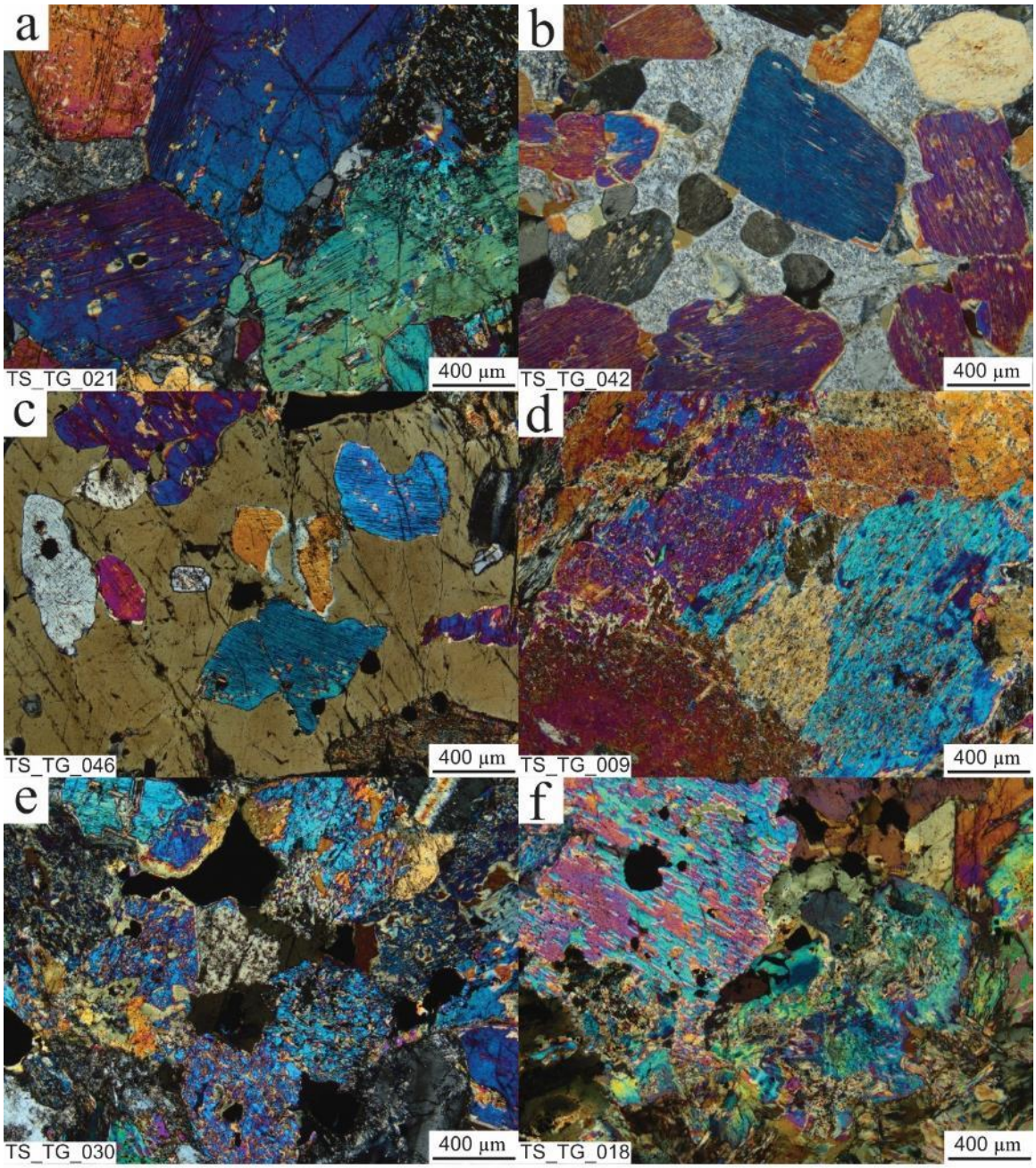

Figure 4.4. Typical clinopyroxene (CPX) textures observed in Titan samples. a) intergrown CPX crystals with minor amounts of alteration minerals occurring along grain boundaries. b) subhedral CPX crystals within a matrix of plagioclase with moderate sericite alteration. c) subhedral to anhedral CPX crystals within a massive amphibole crystal. d) intergrown CPX crystals which display internal granularity. e) CPX crystals with a high degree of internal granularity, which also display replacement rims. f) mottled recrystallized CPX next to an alteration assemblage of epidote and clay group minerals.

Plagioclase crystals range from fine- to medium-grained and are often subhedral to euhedral (Fig. 4.5a). Sericite alteration of the plagioclase grains is common, and ranges from weak to intense (Fig. 4.5b). In most cases the original plagioclase grain boundary can still be observed, though in the more pervasive cases only small parts of the original grain are preserved. Sericite alteration is typically concentrated towards the center of the plagioclase crystal.

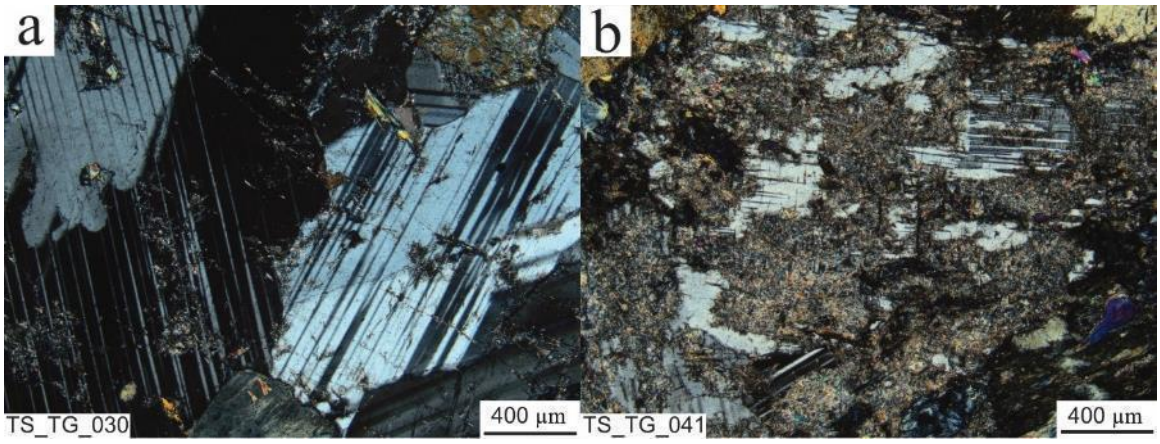

Figure 4.5. Typical plagioclase occurrences observed in Titan samples. a) intergrown euhedral plagioclase crystals, with minor amounts of sericite alteration. b) plagioclase grains with moderate to intense levels of sericite alteration. Plagioclase can still be recognized, but sericite obscures many of the features.

Amphibole is the next most common mineral, aside from plagioclase and clinopyroxene, in the gabbro samples, occurring in 24 of 29 samples. Amphibole ranges from fine- to medium-grained, and can occur as massive, medium-grained crystals enclosing plagioclase and clinopyroxene or as anhedral, fine-grained crystals occurring interstitial to these phases (Figs. 4.3c, 4.5c). Alteration minerals often occur as replacement at amphibole grain edges and along cleavage planes (Fig. 4.3d). Accessory biotite occurs in twelve of the gabbro samples and tends to be very fine- to medium-grained and tabular, occurring interstitial to clinopyroxene and plagioclase (Fig. 4.3e). Orthopyroxene occurs in nine gabbro samples. Orthopyroxene is typically fine- to

medium-grained and subhedral (Fig. 4.3a). In general, orthopyroxene lacks the internal granularity observed in clinopyroxene crystals. Quartz occurs in only two gabbro samples and is very fine-grained and interstitial to plagioclase and amphibole (Fig. 4.5b). Olivine occurs in a single gabbro sample, is fine-grained and rounded, and has been mostly replaced by iddingsite (Fig. 4.3f).

Leucogabbros

The leucogabbros are the least common rock sampled, other than dikes, with only seven samples (Figs. 4.1 and 4.2). Similar to the gabbros, there are a number of subtypes in this category including hornblende leucogabbros, leuco-orthopyroxene gabbros, and leuconorites but since each of these lithologies consist of only one or two samples the leucogabbros will be discussed as a group. The leucogabbros mostly occur in the northeast of the intrusion and sparsely throughout the centre (Fig. 4.2).

The leucogabbros are composed primarily of plagioclase and clinopyroxene cumulates. There are no systematic differences in the appearance of the minerals that compose the leucogabbros, and the largest difference is the modal percentage of plagioclase and clinopyroxene. Plagioclase content ranges from 45-60%, and typically occurs as medium-grained tabular to equant crystals (Fig. 4.5a). In contrast, the mafic mineral content is never greater than 30%, with ≤ 25% clinopyroxene and ≤15% orthopyroxene. Clinopyroxene displays the same granular textures observed in the gabbros (Fig. 4.4). Other minerals include amphibole in all samples, with contents ≤20%. Amphibole is generally subhedral to anhedral and medium-grained, and generally occurs interstitial to plagioclase. Biotite occurs in five of the leucogabbros, ranging from 5-10%. Biotite typically occurs interstitial to other mineral phases, as very fine- to fine-grained

tabular crystals. Quartz occurs in a single sample, at 5%, as a fine-grained, granular phase, which occurs interstitial to plagioclase and clinopyroxene. Alteration assemblages range from 5-25%, and are typically very fine- to fine-grained and anhedral.

Melagabbros

Nine melagabbros were sampled in the Titan intrusion. The melagabbro samples are most common through the very centre of the Titan intrusion, with rare examples in the south and north extremes (Fig. 4.2). They are typically composed of clinopyroxene and amphibole, with two samples also containing orthopyroxene. Clinopyroxene varies between 25-35%, whereas amphibole ranges from 10-45%. In the samples that contain orthopyroxene, it can represent as much as 30% of the sample. The pyroxenes have the same general textures as observed in the gabbros and leucogabbros, with alteration minerals being present in the centre of the majority of clinopyroxene grains (Fig. 4.4). Amphibole is similar to those observed in gabbro and leucogabbro samples, typically occurring interstitial to pyroxene crystals and the limited amount of plagioclase present (Fig. 4.3c, d). Olivine is present in two samples, as subhedral crystals and is almost completely replaced by iddingsite.

Although the melagabbro is relatively rare in outcrop, the historical drill core is almost entirely logged as melagabbro, which implies that the lithology may be more widespread than surface samples suggest. Two of the thin sections taken from the Titan drill core represent an area where both samples were logged as melagabbro, but an increase in alteration with depth was noted. The upper sample occurs near a contact with overlying diabase and the second was taken twenty metres lower (Fig. 4.6). The thin section closest to the diabase contact has a small amount of recognizable plagioclase,

with clinopyroxene, olivine, and amphibole making up ~50% of the thin section and alteration assemblages making up ~40%. Sericite makes up a large proportion of the alteration assemblage, suggesting that plagioclase was once a larger proportion of the sample. The lower thin section lacks any recognizable plagioclase, has a larger percentage of olivine, increasing from 20-30%, and similar amounts of amphibole and clinopyroxene, both around 10-15%. The upper thin section is classed as an olivine melagabbro, but the lower sample is classed as an olivine clinopyroxenite, despite being logged as a melagabbro. The two samples are roughly equivalent in terms of the level of alteration and amount of alteration minerals, contrary to what was noted during logging.

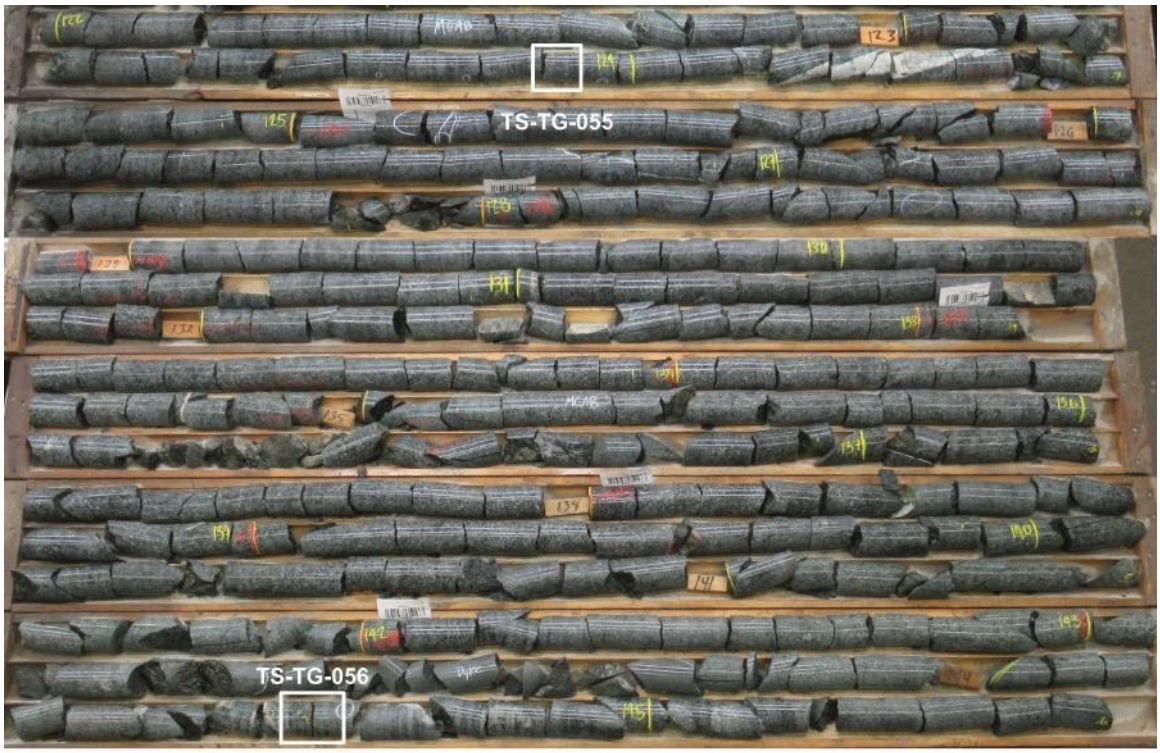

Figure 4.6. Picture of wet drill core from hole RR004-005, showing the interval 122.00-145.60 m, from which thin sections TG-055 and TG-056 were taken.

Pyroxenites and Peridotites

The ultramafic rocks are concentrated in the middle of the intrusion, forming a cluster at the very centre and expanding towards the south, with one sample occurring at the very furthest north outcrops (Fig. 4.2). There are thirteen ultramafic samples, consisting of pyroxenites and two peridotites. Overall, the ultramafic rocks are composed of predominantly clinopyroxene and olivine. Clinopyroxene ranges from 0-80%, though the majority of the pyroxenites have modal percentages closer to 80%. In rocks with less clinopyroxene, olivine forms the rest of the main mineralogy, up to 50%, with amphibole and alteration assemblages forming the rest of the sample. Plagioclase occurs in some samples, but is ≤5%. Other minerals include orthopyroxene, <30%, amphibole, <10%, biotite, <5%, and alteration assemblages, ranging from 5-65%.

The clinopyroxene and olivine ranges from very fine- to medium-grained, with varying degrees of alteration. There are small patches of fresh, euhedral pyroxene and olivine crystals. However, the majority of each thin section is composed of more anhedral grains, which have often been replaced around the rim or along cracks in the crystal structure. Orthopyroxene forms subhedral crystals, generally fine- to medium-grained, which occur as cumulates with clinopyroxene (Fig. 4.3a). Other minerals include biotite, which occurs as very fine- to fine-grained tabular crystals, and amphibole, which generally occurs as fine- to medium-grained crystals that are interstitial to clinopyroxene and olivine (Fig. 4.3e).

Dikes and Contacts

Dikes are not uncommon across the Titan intrusion and were observed at surface and in drill core. The dikes observed across Titan are mafic in composition and crosscut

the intrusion. Dikes were difficult to sample in outcrop, with only two taken, although other dikes were observed during sampling. Three other samples were taken from drill core to represent the contacts between the dikes and the surrounding mafic lithology. These contacts included a mafic dike, felsic veinlets, and a pegmatitic felsic dike.

The two dike samples taken from surface are similar in composition, with one being an amphibole gabbro and the other a gabbronorite. In general, both are very fine- to fine-grained, with a homogenous mixture of the main silicate minerals (Fig. 4.7). Plagioclase, clinopyroxene, and amphibole are common, with the gabbronorite having orthopyroxene as an additional phase (Fig. 4.7). The gabbronorite dike has two small veins of sericite-altered plagioclase, but otherwise alteration minerals are a very minor phase.

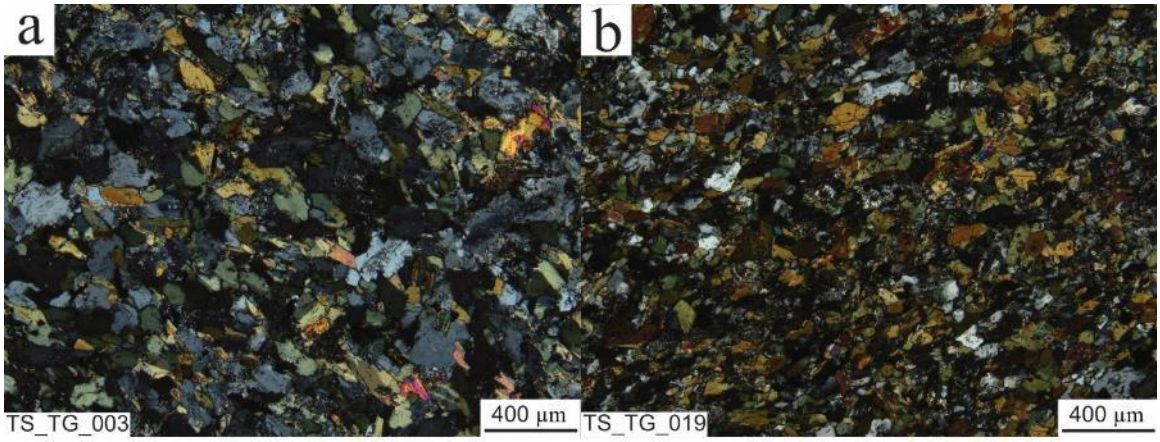

Figure 4.7. Photomicrographs from two different dike samples. a) a gabbronorite dike b) a pyroxene amphibole gabbro dike.

One thin section represents a contact between three different lithologies: a pyroxenite, gabbro, and then a gabbro dike (Fig. 4.8). Gradation between the gabbro and pyroxenite lithologies was noted from drill logs, but the contact was observed to be more abrupt in thin section (Fig. 4.8c). Texture and grain size are the main difference between

the mafic dike and gabbro, while the plagioclase content is the main difference between the pyroxenite and gabbro. No zonation of the constituent minerals was observed within each subsection.

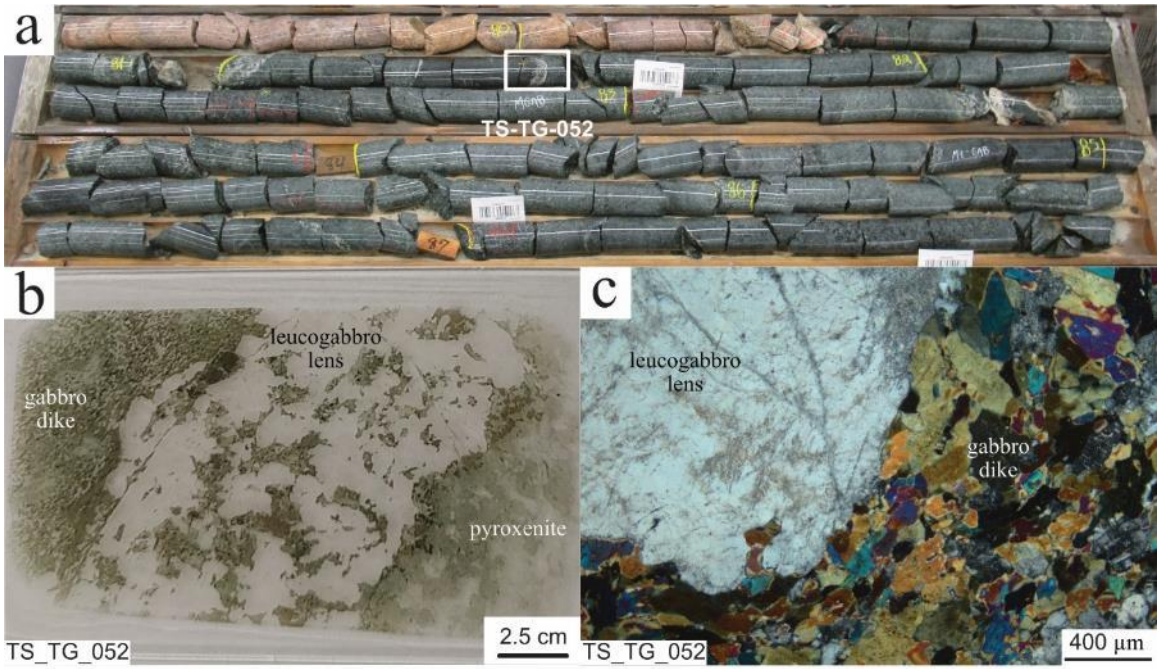

Figure 4.8. Three different views of the contact between the mafic dike and melagabbro. a) Picture of wet drill core from RR004-003, 79.43-73.76 m. The contact point between the mafic dike and pyroxenite is highlighted, with a cap of plagioclase rich material on the dike. b) thin section TS-TG-052, which highlights the dike to the far left, the inner vein of leucogabbro material, and the pyroxenite on the far right. c) a photomicrograph showing the contact between the mafic dike and leucogabbro.

The two thin sections of contacts with felsic material are quite different. In one the contact between a pegmatitic felsic dike is completely obscured by the alteration assemblage. The hand sample appears to be quite felsic, with lots of coarse-grained plagioclase crystals, but under the microscope the crystals are mostly talc, chlorite, epidote, and clay group minerals which obscure the original grain boundaries (Fig. 4.9a). In the second thin section there is a clear divide between the mafic and felsic units, with a gradational area between the two which is filled with fine-grained quartz, plagioclase, and various clay group minerals. The felsic side is a granodiorite and mostly consists of

fine- to medium-grained potassium feldspar and minor amounts of quartz, whereas the mafic side is an orthopyroxene gabbro (Fig. 4.9b). Alteration assemblages make up the majority of the mafic material in the sample, replacing the pyroxene and plagioclase. In contrast the felsic material is quite fresh, with a cumulate occurrence.

Figure 4.9. Pictures of wet drill core from hole RR004-003. a) 92.06-99.61 m, showing the contact sampled for TS-TG-053 of melagabbro and a pegmatitic felsic veinlet. b) 107.85-116.04 m, showing the contact sampled for TS-TG-054 of melagabbro and felsic dike.

Sulphides and Fe-Oxides

Sulphides and Fe-oxides are ubiquitous throughout the samples from the Titan intrusion. Every sample has at least a small amount of either sulphides or Fe-oxides, and usually both. Together they make up a small percentage of any given thin section, generally in the 1-3% range. The sulphides and Fe-oxides are generally very fine-grained, with the very occasional assemblages being fine-grained.

Sulphides appear in all but one thin section, with pyrite being the most common sulphide. Euhedral pyrite is extremely rare. Most of the pyrite occurs as blebs, with rounded grain boundaries (Fig. 4.10b). These blebs can aggregate together into more lobate structures (Fig. 4.10a). Occasionally, pyrite occurs as veins, though this is confined

to only a few thin sections. Magnetite rims are quite common in pyrite grains (Fig. 4.10c). The magnetite rims can range from a very thin outer rim to almost completely enveloping the pyrite grain. In the case of the completely replaced pyrite grains, the habit and slightly banded appearance of the magnetite means the grain can still be identified as originally being pyrite.

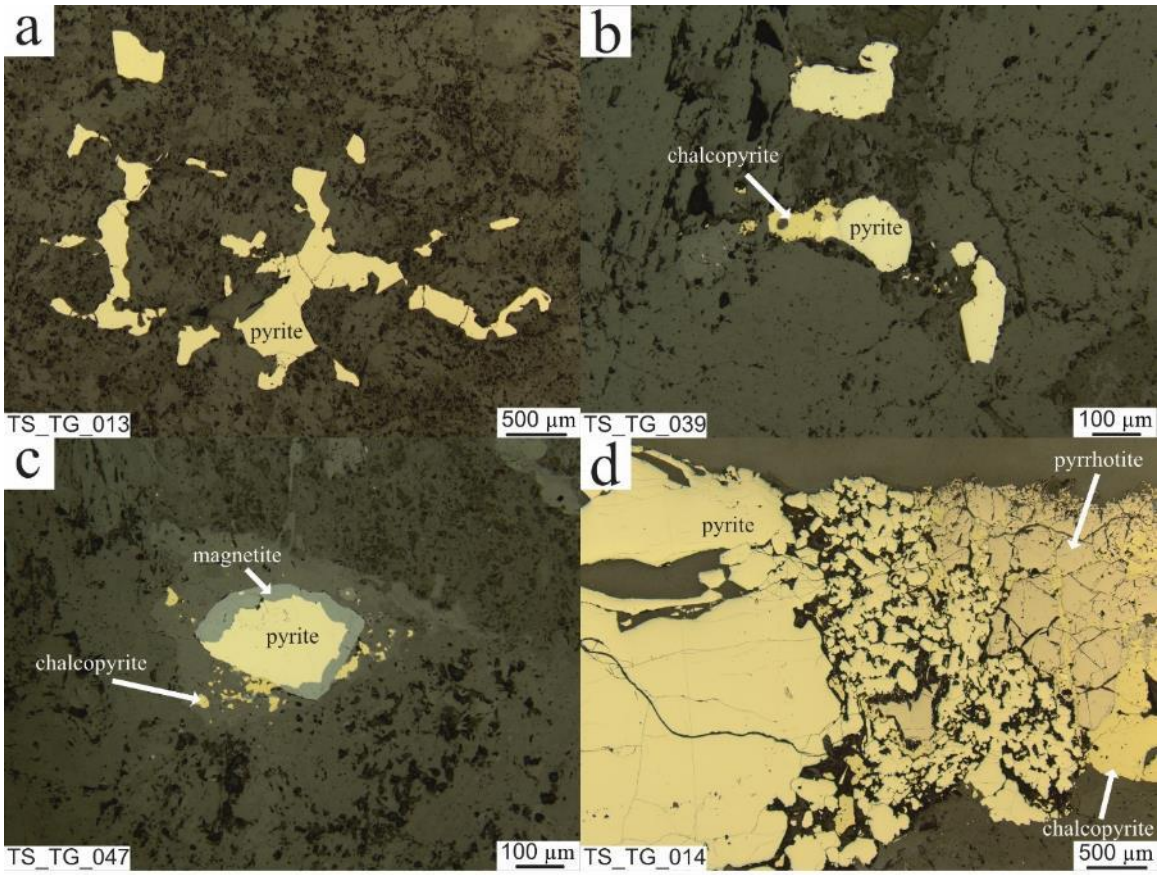

Figure 4.10. Common sulphide occurrences. a) blebby pyrite, occurring nearly as stringers. b) blebby pyrite and chalcopyrite, forming a small cluster. Similar clusters are generally distributed throughout the whole sample. c) pyrite bleb with a rim of magnetite and a cluster of anhedral chalcopyrite. d) a larger magmatic sulphide assemblage, which shows pyrite, pyrrhotite, and chalcopyrite.

Chalcopyrite is the next most common sulphide, and typically occurs as either small inclusions within pyrite crystals or as discrete grains in close association with pyrite. Similar to the pyrite crystals, chalcopyrite generally has a subhedral to anhedral

form, appearing as blebs (Fig. 4.10b). Rims were not observed in chalcopyrite, though chalcopyrite inclusions do occur in larger pyrite grains that have magnetite rims. Pyrrhotite is the next most common sulphide, occurring with pentlandite in the occasional larger sulphide assemblage that exist in the samples (Fig. 4.10d). When these sulphide assemblages are present, they tend to be fine-grained and comprise a larger proportion of the sample, with the majority of these samples occurring in the centre of the intrusion where the largest outcrops are located. However, pyrrhotite and pentlandite are quite rare, with only eight thin sections having pyrrhotite and three having pentlandite.

Magnetite is the most common Fe-oxide, occurring in varying degrees in all but ten of the thin sections. Magnetite is typically subhedral to anhedral, and forms either disseminated blebs or blockier aggregates (Fig. 4.11a, b). Occasionally, hematite exsolution was observed in the larger aggregates, typically forming at 30° angles to one another. Magnetite has one other, less common habit, occurring as swirled, elongate droplets, typically in association with other magnetite habits (Fig. 4.11c). This swirled occurrence gives the magnetite a myrmekitic texture or the appearance of a fingerprint and can appear either as a small offshoot of larger aggregates of blocky magnetite or on its own (Fig. 4.11c). Ilmenite occurs in the majority of the samples, but as a minor phase compared to magnetite. Ilmenite typically occurs in association with aggregates of magnetite and tends to have a more lath shaped habit. Magnetite exsolution within ilmenite grains was observed in the majority of ilmenite crystals (Fig. 4.11a).

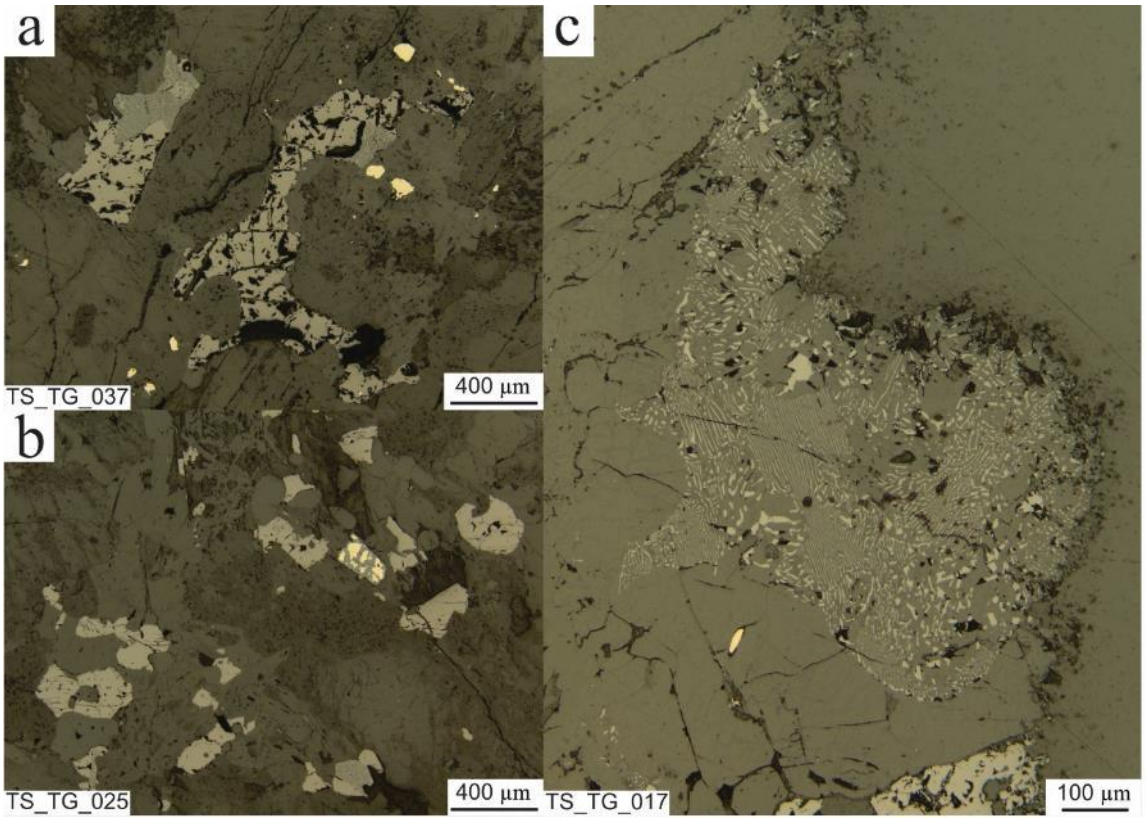

Figure 4.11. Typical Fe-oxide occurrences. a) an aggregate of magnetite, with blebs of pyrite occurring nearby. Ilmenite occurs within each aggregate and has magnetite exsolution within each grain. b) blebby magnetite with pyrite. Often magnetite is more disseminated throughout the samples. c) myrmekitic magnetite with occasional larger blebs. Each individual droplet is very fine-grained, but the entire structure is much larger than any individual droplet.

Alteration

Alteration assemblages are fairly ubiquitous throughout the Titan intrusion, ranging from 3-65% of the thin sections. The alteration assemblages are consistent across lithologies. The main alteration assemblages include tremolite, actinolite, epidote, sericite, talc, and chlorite. Calcite and clay group minerals occur occasionally, and typically only as a small proportion (<5%) of the overall alteration assemblage. The alteration assemblages can occur as replacement rims around the main silicate crystals, as discrete crystals, or as granular groundmasses occurring interstitial to the main silicate crystals (Fig. 4.3d, f, 4.4e, 4.5bd, 4.12). There is little in the way of systematic zoning in

the alteration assemblages across the intrusion, although there may be clusters of specific minerals they do not vary systematically across individual thin sections or lithologies.

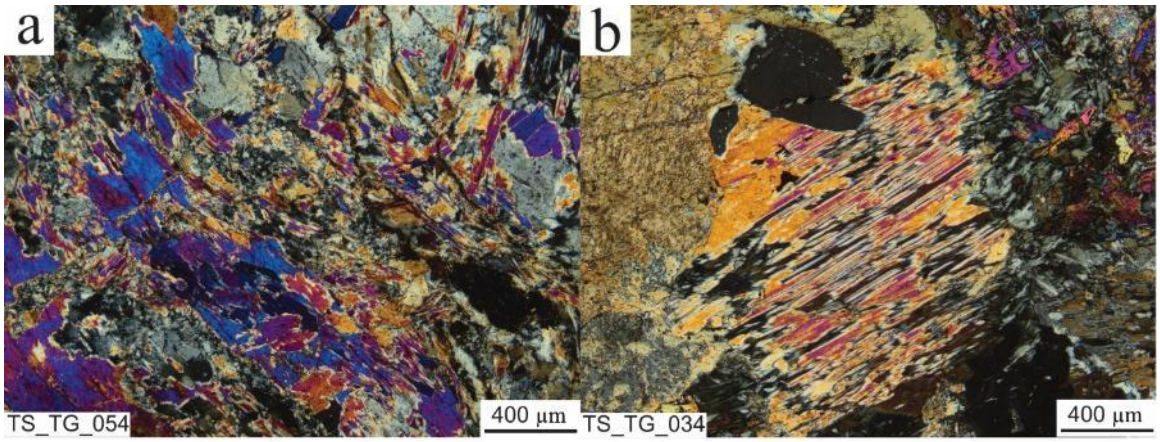

Figure 4.12. Typical tremolite occurrences in Titan samples. a) anhedral tremolite crystals, occurring as a groundmass infringing on other phases in the sample. b) a pyroxene that has been replaced by bladed tremolite crystals. Tremolite crystals occur in close association to a groundmass of very fine-grained alteration minerals.

Tremolite, actinolite, and epidote are the phases most likely to form discrete crystals, they are typically very fine- to medium-grained, usually bladed or equant in habit (Fig. 4.12b). Tremolite and actinolite additionally form chaotic masses of tabular to acicular crystals (Fig. 4.12a). Epidote occurs as smaller, granular crystals, along with talc and chlorite (Fig. 4.13). Talc and chlorite also form very fine-grained fibrous crystals (Fig. 4.13d). These granular and fibrous crystals tend to form large masses that occur interstitial to the main silicate phases, and often replace the silicate minerals.

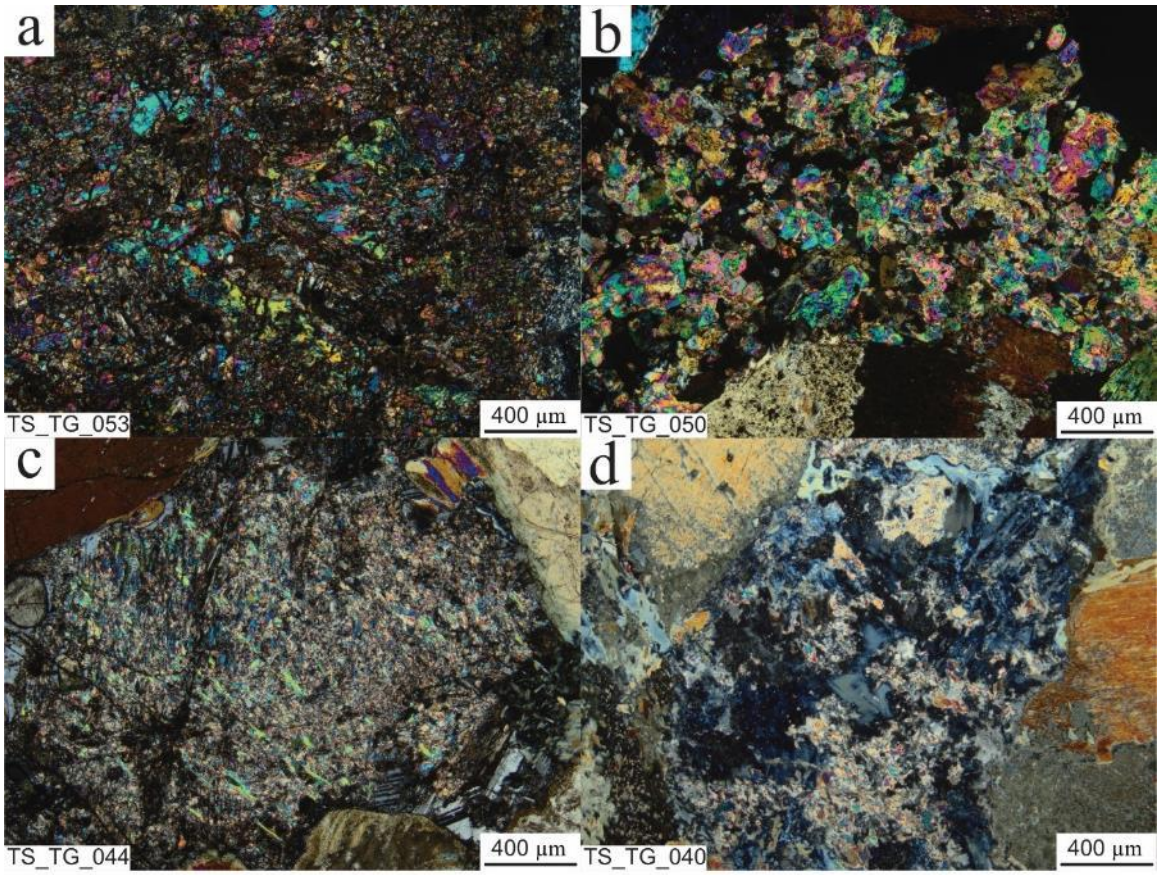

Figure 4.13. Common occurrences of alteration mineral assemblages. a) very fine-grained, granular epidote occurring in the groundmass. b) slightly larger, anhedral epidote crystals, occurring interstitial to the main mineral phases. c) very fine-grained groundmass of talc, which is replacing plagioclase. d) very fine-grained chlorite and talc occurring interstitial to pyroxene phases.

Sericite replaces plagioclase, ranging from weak to intense. Weak sericite alteration tends to be confined to the centre of the grain, but is a dispersed phase. As the degree of sericite alteration increases, the middle of the grain becomes almost entirely obscured and the sericite spreads towards the edges. Moderate sericite alteration begins to obscure the diagnostic plagioclase twinning, although it is usually still possible to recognize the primary phase and grain boundaries are still intact. Intense sericite alteration almost completely replaces the plagioclase grain, with only small patches of plagioclase available to determine the primary mineralogy. The plagioclase grain

boundary can usually still be recognized, but it becomes much more difficult to determine the edges. At the most intense level, sericite is still recognizable but primary plagioclase can no longer be recognized.

4.2 Geochemistry

The detailed petrographic work showed that the distinct lithologies are heterogeneously distributed across the intrusion and do not always align perfectly with field observations. As such the geochemical results of the Titan intrusion are discussed for the entire intrusion, without inference from field or petrographic analysis.

Major Elements

Samples from the Titan intrusion contain between 40 to 60 wt% SiO_2, 0.1 to 1.5 wt% TiO_2, 4 to 20 wt% Al_2O_3, 5 to 18 wt% Fe_2O_3, 4 to 21 wt% MgO, 5 to 19 wt% CaO, 0.4 to 4 wt% Na_2O, 0.1 to 2.8 wt% K_2O, and 0.02 to 1.4 wt% P_2O_5 (Appendix II). Loss on ignition (LOI) values range from 0.47 to 5.59, however ~90% of the samples have values below 3.00 wt% (Appendix II).

The major elements show a continuous trend across the samples, with the exception of MgO which shows bimodal distribution with 51 samples above 11.0 wt% and 57 samples below 10.3%. There is a slight spatial relationship to this bimodal MgO distribution, with the farthest north and south extremes as well as one cluster of rocks just south of the centre of the intrusion having higher MgO values (Fig. 4.14). However, this is not a strict relationship. The continuous trend observed in the major element concentrations does not have a strong spatial aspect, with each element displaying a chaotic distribution.

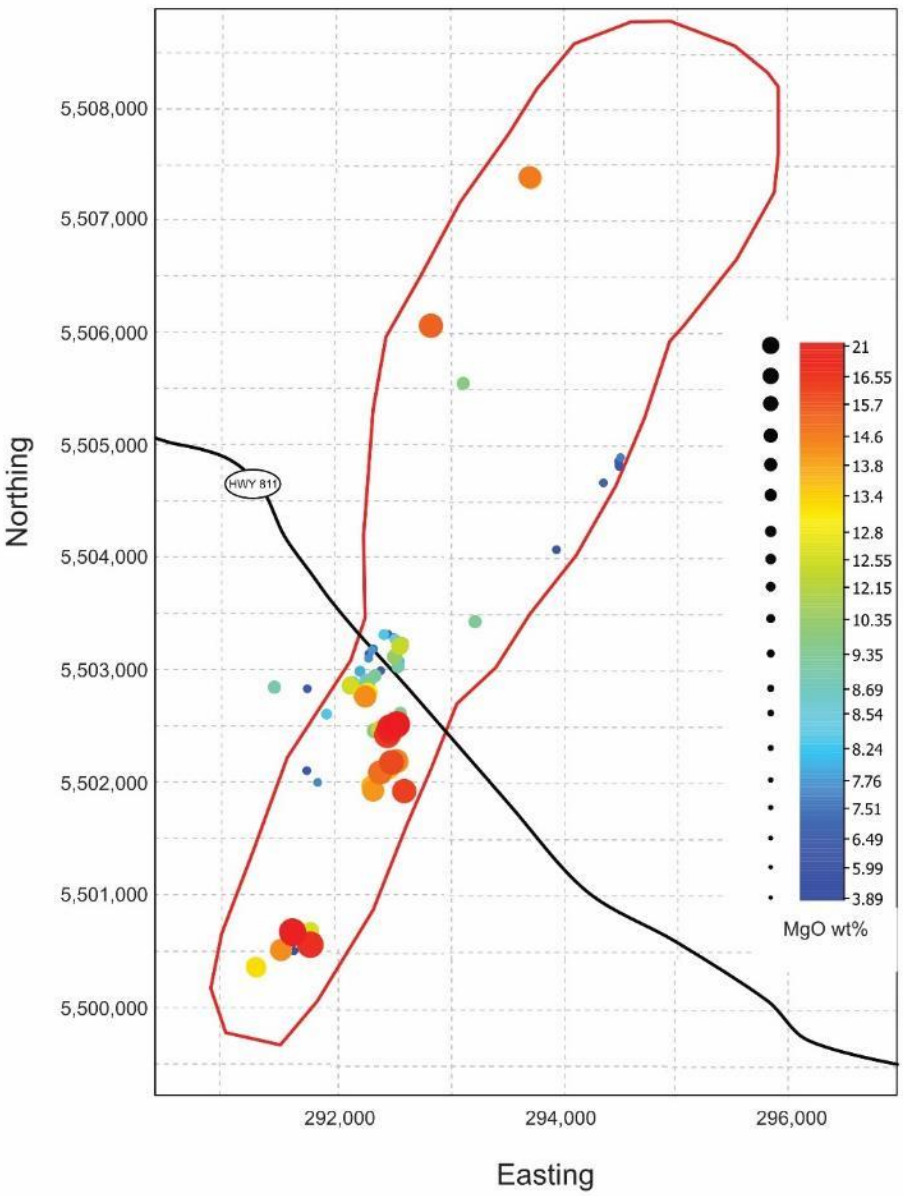

Figure 4.14. Map of the Titan intrusion denoting the MgO wt% for each sample.

The SiO_2 concentration has a slight positive correlation with CaO and shows a slight negative correlation with Fe_2O_3 and Al_2O_3 (Fig. 4.15). No correlation appears between SiO_2 and P_2O_5, TiO_2, K_2O and Na_2O. In general, there is a negative correlation between MgO and Al_2O_3, Na_2O, and K_2O (Fig. 4.15). There is a roughly positive correlation between MgO and CaO, but no correlation between MgO and SiO_2, Fe_2O_3,

P_2O_5, and TiO_2, with Fe_2O_3, P_2O_5, TiO_2, and K_2O showing slightly more variation in the low MgO samples (Fig. 4.15). Al_2O_3 is negatively correlated with CaO and positively correlated with Na_2O, whereas CaO has a negative correlation with Na_2O and K_2O. Overall, there is a medium to large degree of scatter in all the elements (Fig. 4.15). The spread of major elements was compared to representative mineral compositions to determine if a relationship between geochemical data and petrography exists (Fig. 4.16).

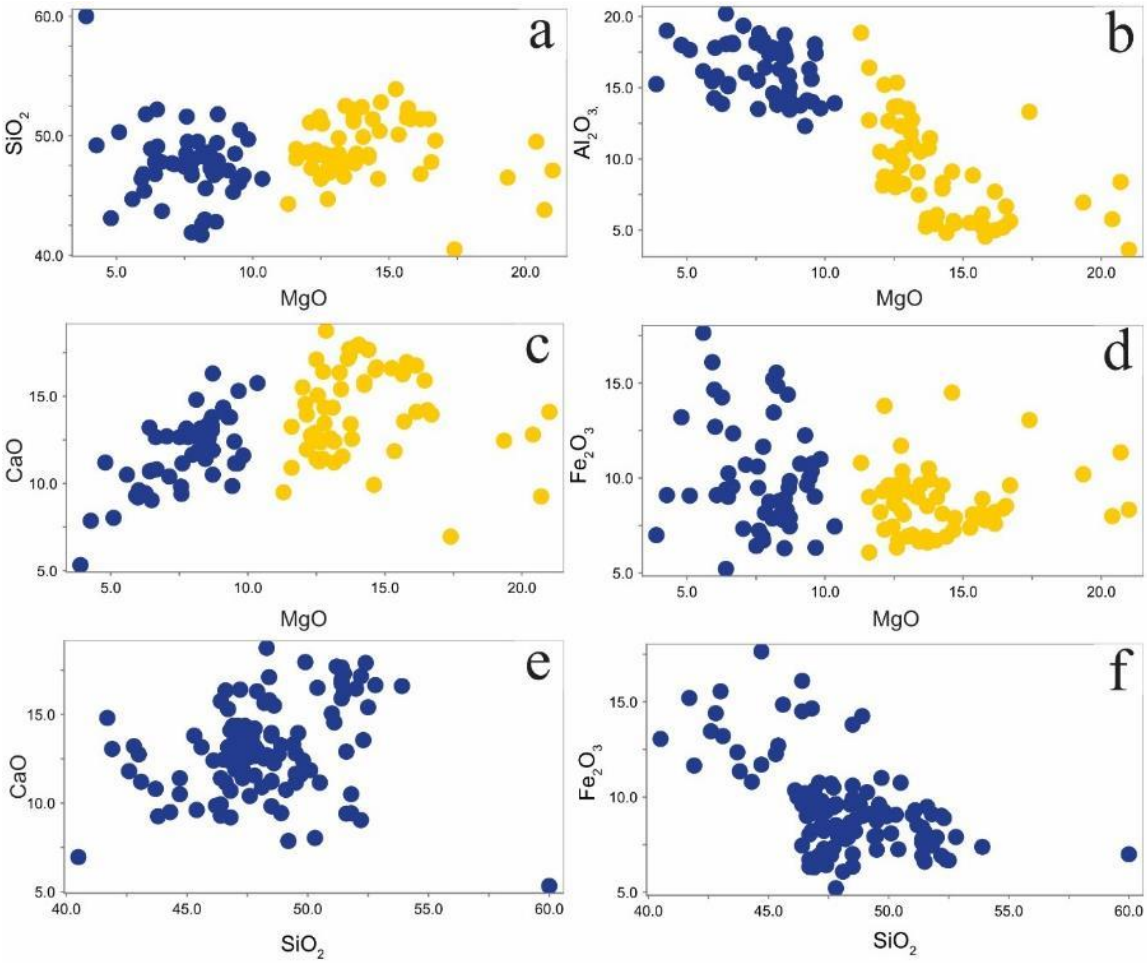

Figure 4.15. Geochemical plots of Titan rocks. Blue denotes the low MgO group, while yellow dots are the high MgO samples for figures a), b), c), and d). a) SiO_2 vs MgO, b) Al_2O_3, vs MgO, c) CaO vs MgO, d) Fe_2O_3 vs MgO, e) CaO vs SiO_2, and f) Fe_2O_3 vs SiO_2

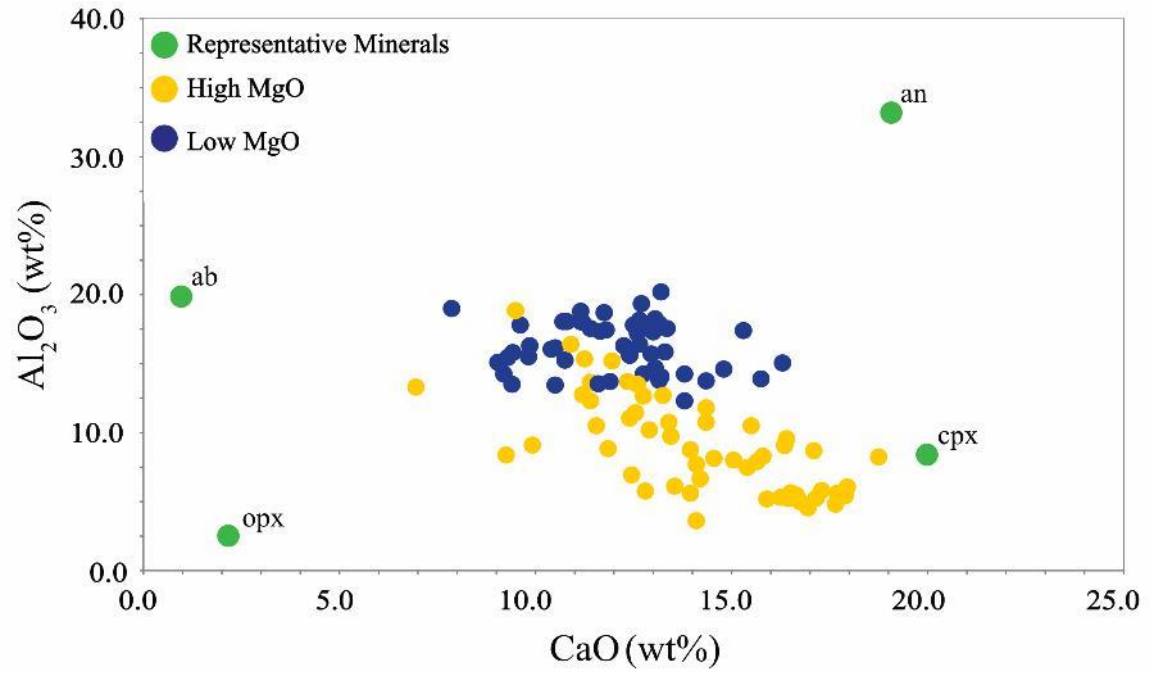

Figure 4.16. Geochemical plot of Titan rocks showing Al_2O_3 vs CaO (wt%), as well as representative mineral compositions of orthopyroxene (opx), clinopyroxene (cpx), albite (ab), and anorthite (an). Mineral compositions from IMDEX ioGAS-64, ver 7.4.2.

Trace Elements

Samples from the Titan intrusion contain between 4.2-86.5 ppm La, 5.7-82.4 ppm Nd, 1.6-12.65 ppm Sm, 1.01-9.45 ppm Gd, 0.22-2.65 ppm Yb, 16-1850 ppm Ni, 4-3560 ppm Cu, 0.56-18.8 ppm Nb, 10-3080 ppm Cr, 40-603 ppm V, 2.5-219 ppb Pt, and 0.5-717 ppb Pd (Appendix II). Sulphur ranges from 0.01 to 1.53 wt% (Appendix II).

There is a weak positive correlation between Ni and MgO concentrations (Fig. 4.18b). A positive correlation exists between Sc and SiO_2 and MgO, however, there is a large amount of scatter in the relationship between Sc and SiO_2 and only slightly less between Sc and MgO (Fig. 4.17c, d). Neither Ni or Cu are correlated with SiO_2 concentration, while V is not correlated with either MgO or SiO_2. A positive correlation was observed between Cr and MgO, while Cr and SiO_2 display a more erratic spread with

no correlation (Fig. 4.17a). With all of the trace elements there does not appear to be a strong spatial distribution.

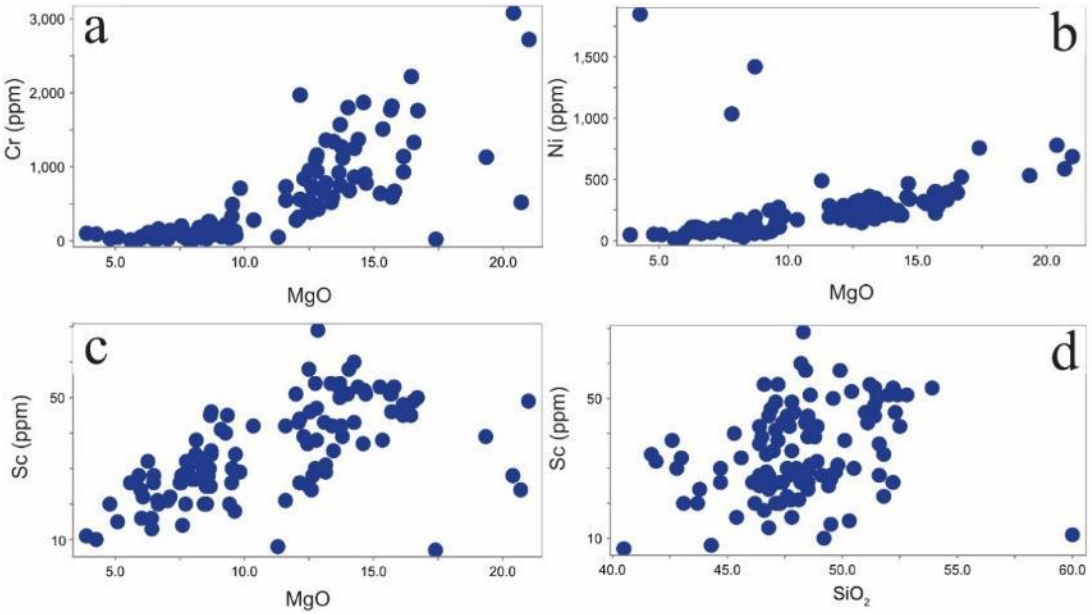

Figure. 4.17. Trace elements plotted against major elements. a) Cr vs MgO, b) Ni vs MgO, c) Sc vs MgO, and d) Sc vs SiO_2

Primitive mantle normalized multi-element diagrams were plotted for the Titan intrusion (Fig. 4.18). In general, the REEs have similar trends across the intrusion, with LREE elements being enriched, HREEs being fractionated, and consistent negative Nb, Zr, Hf, and Ti anomalies. Primitive mantle normalized ratios of La/Sm_N, Gd/Yb_N, Nb/Nb*, Hr/Hf*, Zr/Zr*, and Ti/Ti* were calculated to better understand REE behaviour in the intrusion. La/Sm_N ranges from 0.69 to 4.88, with a mean of 1.91. The values of Gd/Yb_N range from 1.24 to 7.44, with a mean of 4.38. The Nb/Nb* values range from 0.02 to 0.66 and is the most consistently negative of all the observed negative anomalies with a mean of 0.15. Hf/Hf* ranges from 0.05 to 1.08 and has a mean of 0.28, while Zr/Zr* ranges from 0.05 to 0.96 and has a mean 0.27. Ti/Ti* has the smallest range, from

0.13 to 0.73, with a mean of 0.26. The negative Hf and Zr anomalies are consistent, with 95% of the Hf/Hf* values being <0.52 and 95% of the Zr/Zr* values being <0.59.

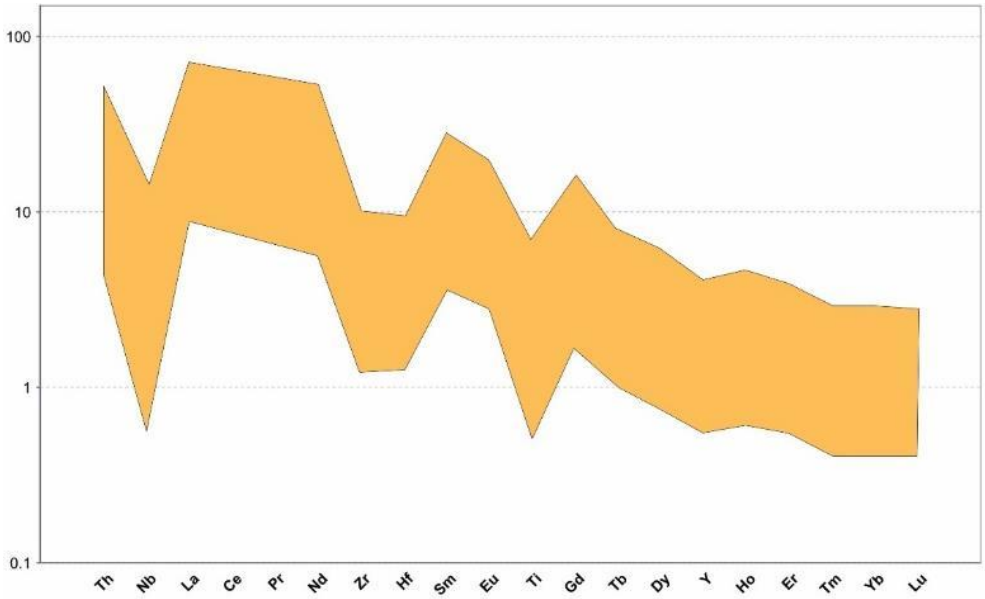

Figure 4.18. Primitive mantle normalized diagrams of the range of values for Titan samples. Normalizing values from Sun and McDonough (1989).

4.3 Isotopes

Sulphur Isotopes

Samples chosen for sulphur isotope analysis were chosen to cover the entire spatial range of the intrusion, and were also chosen to represent the most common sulphide habits and mineral associations (Fig. 4.19). Note that because of the overall sampling distribution and the criteria for data collection there is a bias towards the middle of the intrusion (Fig. 4.19).

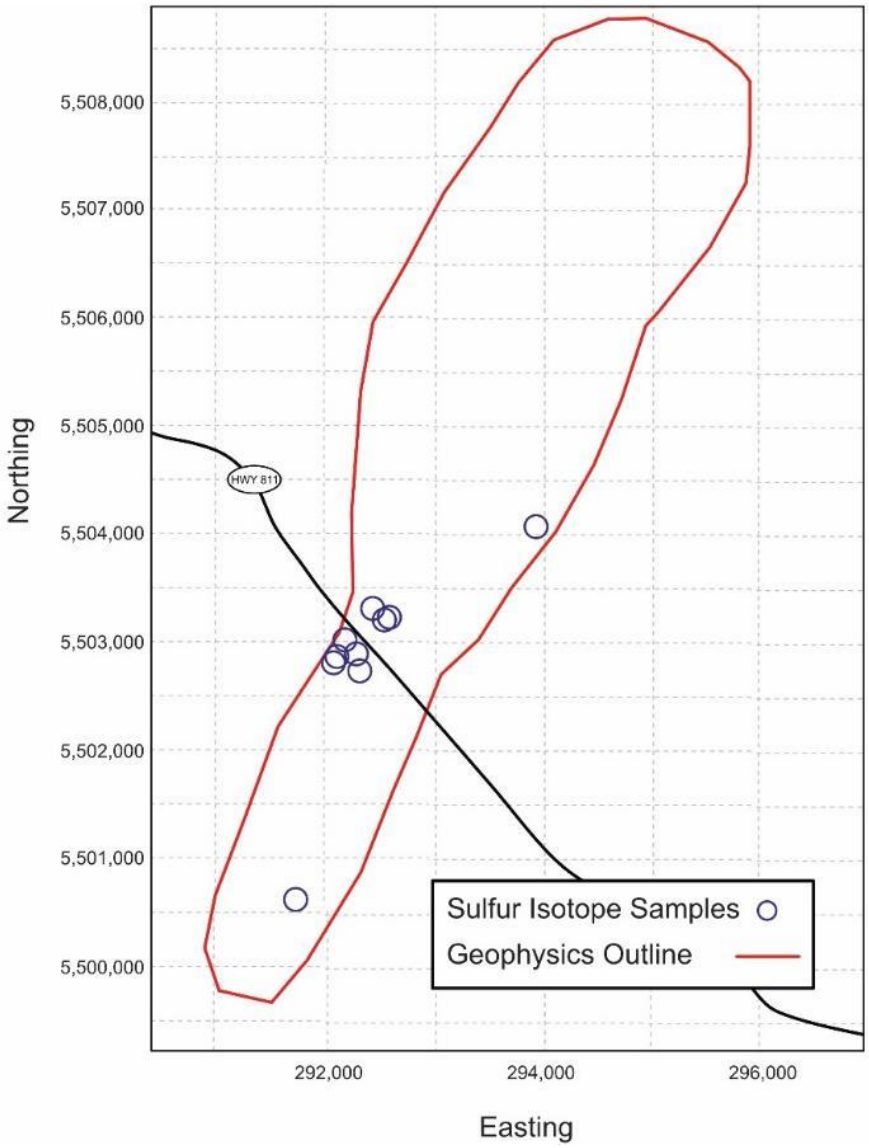

Figure. 4.19. Representation of the Titan intrusion showing the ten samples selected for sulphur isotope work.

Regions of interest ranged in size from 550-2300 µm, with the actual sulphides analyzed being <100-1000 µm in size. Seven to ten spots were analyzed from each region of interest, distributed across all the sulphides within the area. In the case of smaller crystals, sulphide clusters and aggregates were chosen in order to generate enough spots for analysis (Fig. 4.20a, c, d). For pyrite, a range of euhedral to anhedral habits were chosen. Pyrite grains in close association with chalcopyrite were prioritized where

possible, though due to availability and size of chalcopyrite throughout the intrusion, most samples had either no chalcopyrite or the grains were too small to be analyzed (Fig. 4.20b). Two regions of interest had inclusions of either pyrrhotite or pentlandite (Fig. 4.20b). As magnetite rims and magnetite are common in the Titan samples, regions of interest were chosen that included these associations (Fig. 4.20c, d).

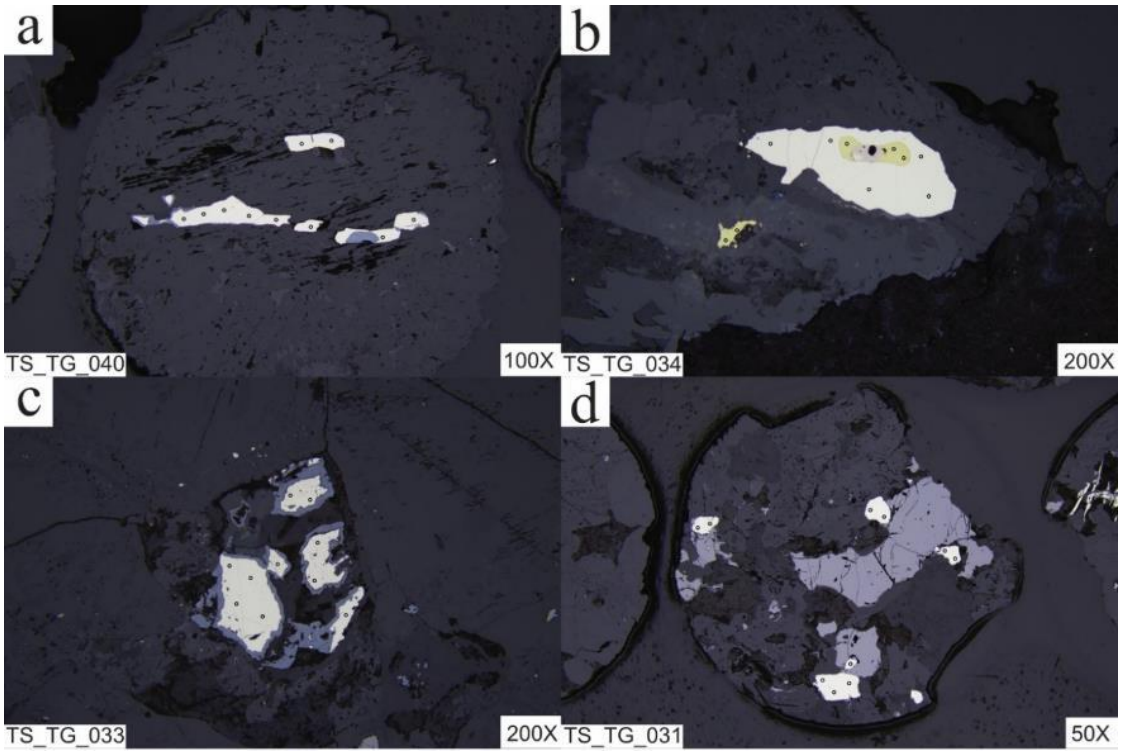

Figure. 4.20. SEM images of four different regions of interest drilled from Titan thin sections. Small black circles represent spot analyses points. Multiple regions of interest may come from the same thin section.

Pyrite and chalcopyrite were the only sulphides large and plentiful enough to be analyzed, with 146 pyrite spots analyzed and 46 chalcopyrite spots analyzed. Pyrrhotite and pentlandite had less then five individual mineral grains throughout the intrusion, and thus were not chosen for analysis. All 19 of the regions of interest included pyrite, while 13 of the 19 regions of interest included chalcopyrite (Table 4.1). For all regions of

interest, ^{32}S, ^{33}S, and ^{34}S were measured. Full results for pyrite and chalcopyrite can be found in Appendix III.

Table 4.1. Denotes the original thin section, the region of interest (ROI), what sulphide was analyzed for each ROI, and the number of individual spots were analyzed per type of sulphide

Thin Section ID	ROI #	# of spots for pyrite analysis	# of spots for chalcopyrite analysis
TS_TG_049	1	8	3
TS_TG_047	2	5	5
TS_TG_047	3	8	2
TS_TG_047	4	5	6
TS_TG_043	5	5	6
TS_TG_043	6	10	1
TS_TG_043	7	8	2
TS_TG_042	8	3	8
TS_TG_042	9	10	
TS_TG_042	10	6	2
TS_TG_040	11	10	
TS_TG_040	12	9	
TS_TG_037	13	11	1
TS_TG_034	14	5	5
TS_TG_033	15	10	
TS_TG_031	16	10	
TS_TG_030	17	8	
TS_TG_030	18	8	1
TS_TG_030	19	7	4

For $\delta^{34}S$, the values range from -11.62 to +6.22‰ with the majority of the values for both pyrite and chalcopyrite falling within 0.0 ± 2.0‰ (Fig. 4.21). For pyrite, 13 of the 19 regions of interests yielded $\delta^{34}S$ within 0.0 ± 2.0‰ (Fig. 4.21). These results are also shown for the chalcopyrite, where chalcopyrite from regions of interest with pyrite $\delta^{34}S$ within 0.0 ± 2.0‰ also have $\delta^{34}S$ within 0.0 ± 2.0‰.

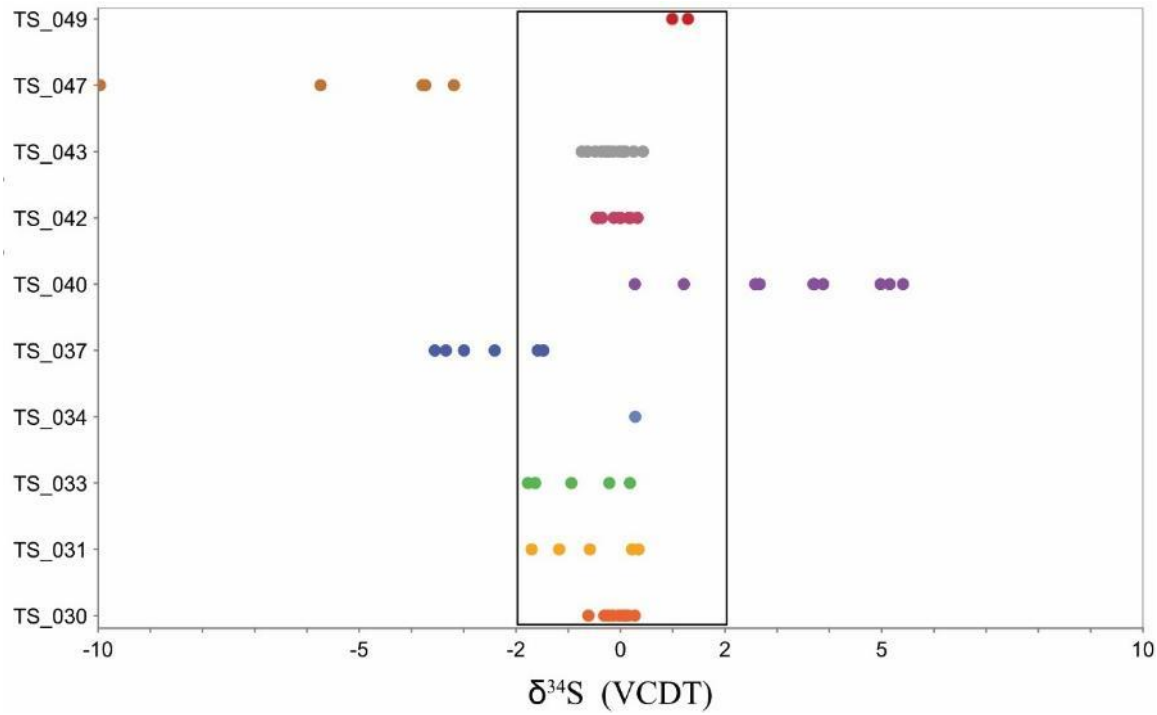

Figure 4.21. $\delta^{34}S$ values for pyrite per sample. Each thin section may contain multiple regions of interest. Red box denotes the region between -2.00 and 2.00, often denoted as the mantle range (Ripley and Li, 2003).

The remaining six regions of interest, from three thin sections, have $\delta^{34}S$ values outside of 0.0 ± 2.0‰. Two thin sections, comprising four regions of interest, have pyrite with negative $\delta^{34}S$ values, ranging from -10.02 to -1.47‰ (Fig. 4.21). One thin section, which hosts the remaining two regions of interest, has positive $\delta^{34}S$ values, ranging from +0.28 to +5.41‰ (Fig. 4.21). These three thin sections are all near the very centre of the intrusion, just south of Highway 811 (Fig. 4.22). The $\delta^{34}S$ values observed in chalcopyrite, ranging from -10.06 to +1.34‰, follow the same general trend observed in pyrite (Appendix III).

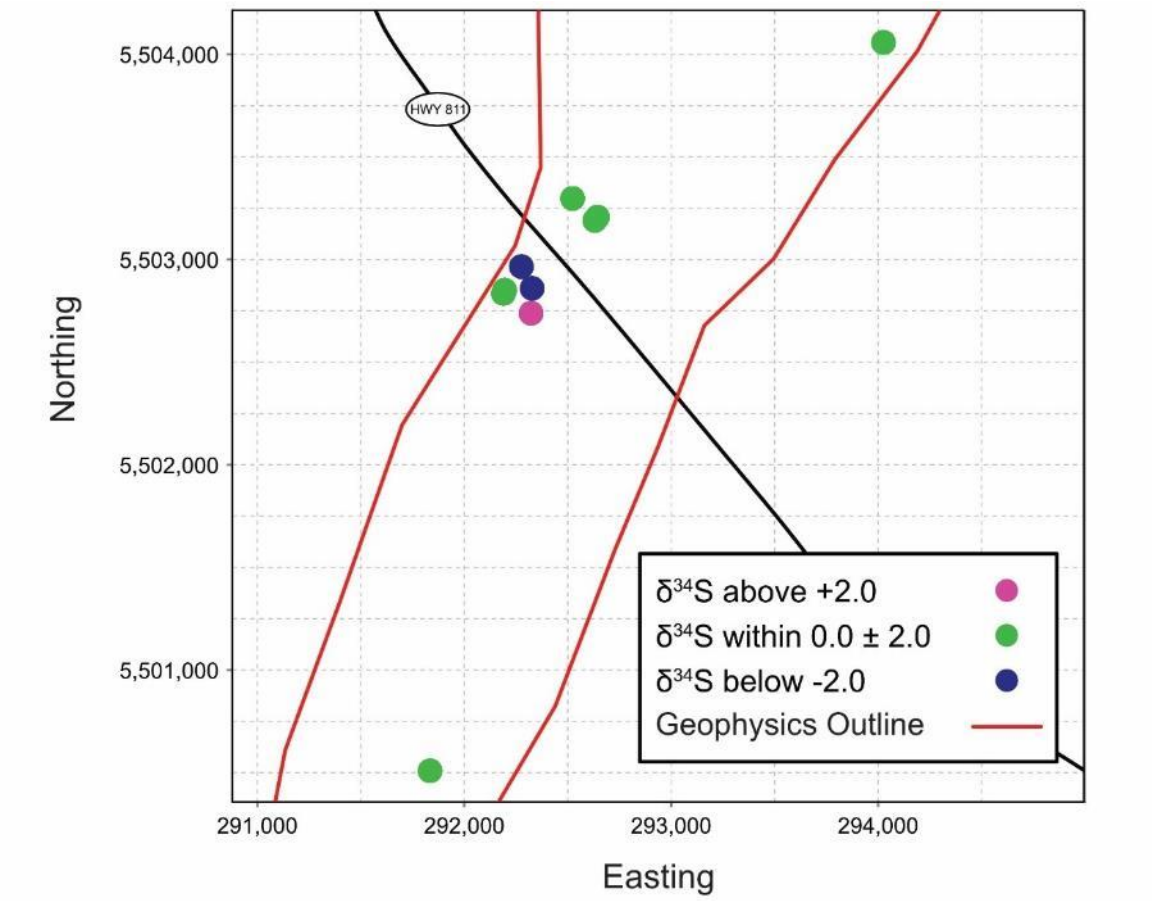

Figure 4.22. Representation of the Titan intrusion, showing the sulphur isotope samples. Anomalous $\delta^{34}S$ samples are highlighted.

Using the $\delta^{33}S$ and $\delta^{34}S$ values, $\Delta^{33}S$ could be calculated for each spot analyses generated for pyrite and chalcopyrite. Pyrite and chalcopyrite show the same trends, with all values falling in between -0.3 to 0.1‰.

Sm-Nd Isotopes

. The samples chosen for Sm-Nd analysis were picked based on whole rock geochemistry, to encompass the different trends in the LREEs of the Titan intrusion (Fig. 4. 23). Three samples were chosen which had a LREE pattern dipping to the left (group A), three with a LREE pattern dipping to the right (group B), and three with a flat LREE trend (Group C; Fig. 4.24a, b, c). For each of these groups a high, middle, and low LREE

trend was chosen (Fig. 4.24a, b, c). Two additional samples were selected, one of which lacked the negative Nb anomaly and the other lacking the negative Ti anomaly (Fig. 4.24d). A further three samples were chosen to capture variation in Zr and Hf trends (Group E), once again selecting a high, middle, and low sample (Fig. 4.24e).

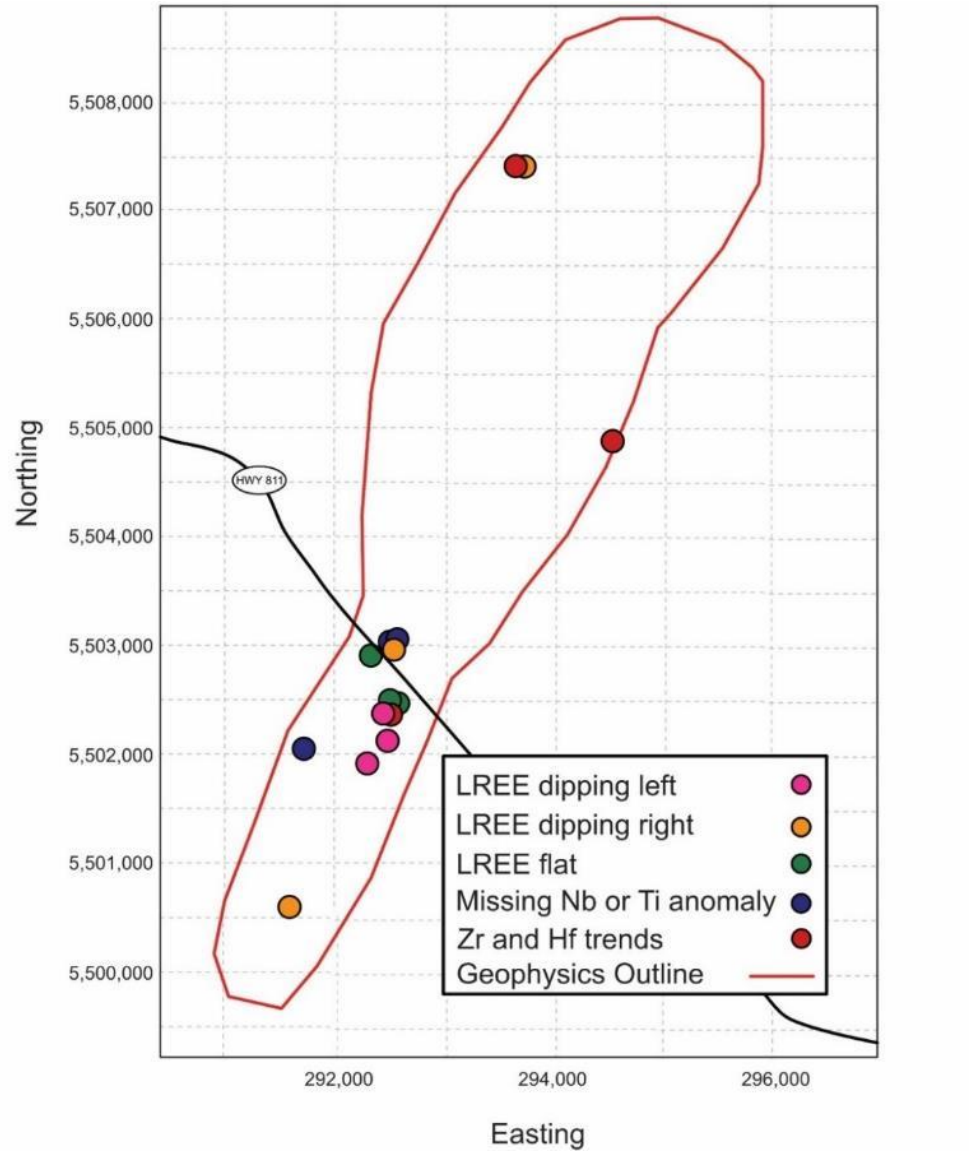

Figure 4.23. Representation of the Titan intrusion denoting where the Sm-Nd samples were taken. The map also highlights the location of the different LREE trends that were being investigated.

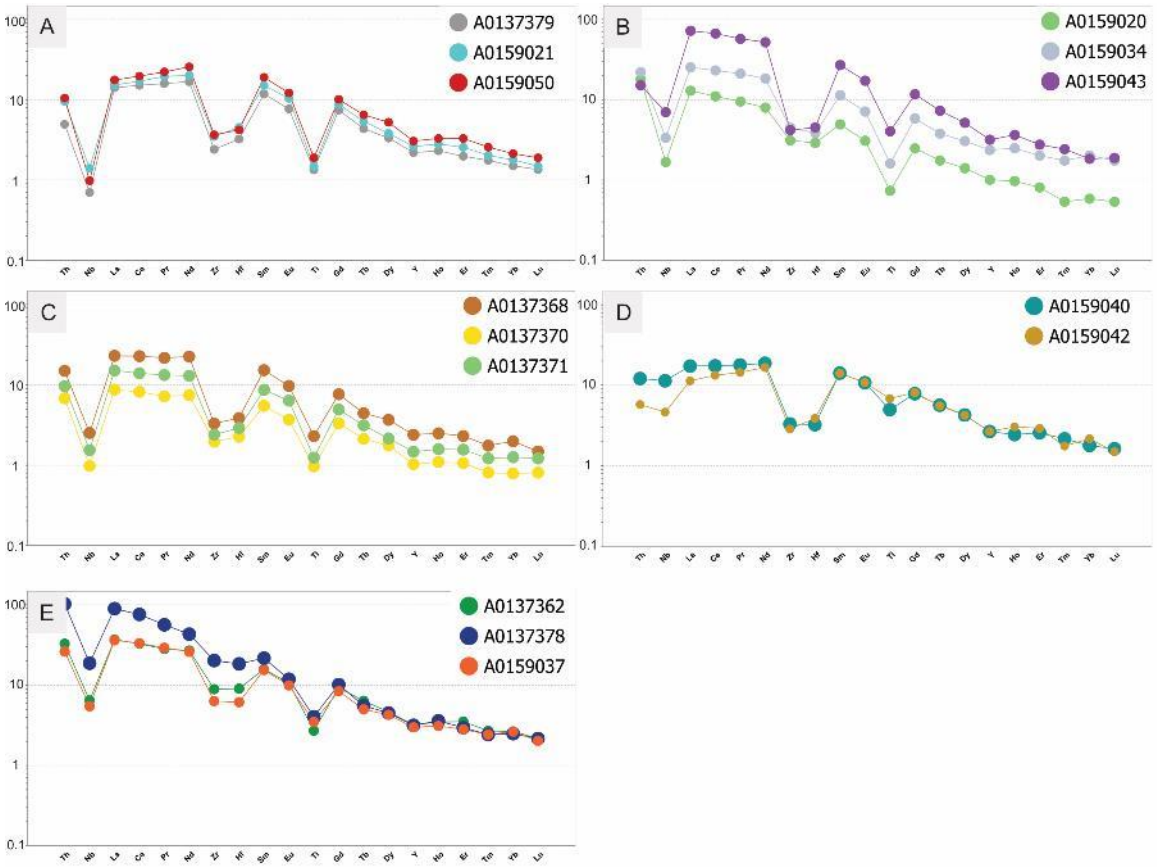

Figure 4.24. Extended trace element plots showing the variation in LREE and HFSE used for picking Sm-Nd samples. A) LREE dipping to left trend, B) LREE dipping to right trend, C) LREE flat trend, D) Nb or Ti anomalies missing from REE trend, E) HFSE variation

The Sm-Nd isotope data was recalculated using a U-Pb zircon age of 2690 Ma for the Titan intrusion (Appendix IV). Overall, the recalculation of the Sm-Nd isotope values yielded positive ε_{Nd} values ranging from 0.70-1.82, with $^{143}Nd/^{144}Nd$ values ranging from 0.510812-0.511998 (Table 4.2). Group A samples have a $^{143}Nd/^{144}Nd$ range of 0.511819-0.511892 and a ε_{Nd} range of 1.14-1.82. Group B samples have a $^{143}Nd/^{144}Nd$ range of 0.511067-0.511349 and the tightest ε_{Nd} range, from 1.29-1.38. Group C samples have $^{143}Nd/^{144}Nd$ values ranging from 0.511528-0.511691 and a ε_{Nd} range of 1.19-1.63. The sample lacking the negative Ti anomaly has a $^{143}Nd/^{144}Nd$ value of 0.511998 and a ε_{Nd} value of 1.35 while the sample missing the negative Nb anomaly has a $^{143}Nd/^{144}Nd$ value

of 0.511816 and a ε_{Nd} value of 1.55. Group E samples have a $^{143}Nd/^{144}Nd$ range of 0.510812-0.51139 and an ε_{Nd} range of 0.70-1.18. Given the range, it is deemed that the different LREE trends have no effect on ε_{Nd} values.

Table 4.2. The groups selected for Sm-Nd sampling, as previously referenced on Figure 4.22, demonstrating the $^{143/144}Nd$ and ε_{Nd} spread appearing in each group

Sample Group	Sample Name	Nd (ppm)	Sm (ppm)	$^{143}Nd/^{144}Nd$	εNd
Group A	A0159050	32.21	8.065	0.511892	1.14
Group A	A0159021	26.2	6.457	0.511861	1.36
Group A	A0137379	22.63	5.44	0.511819	1.82
Group B	A0159043	68.46	11.77	0.511067	1.48
Group B	A0159034	23.66	4.643	0.511323	1.39
Group B	A0159020	9.898	1.971	0.511349	1.29
Group C	A0137371	18.81	4.068	0.511528	1.19
Group C	A0137370	9.911	2.273	0.511691	1.63
Group C	A0137368	31.69	6.938	0.511566	1.37
Missing Nb	A0159040	24.7	5.962	0.511816	1.55
Missing Ti	A0159042	23.66	6.135	0.511998	1.35
Group E	A0159037	34.81	6.658	0.511259	1.18
Group E	A0137378	60.72	9.218	0.510812	0.72
Group E	A0137362	35.39	7.245	0.511379	0.70

4.4 Mineral Chemistry (LA-ICP-MS)

Out of all the samples, five analyses were done on sulphides that were also used for SIMS analyses, 21 analyses were done on sulphides from thin sections that had sulphides drilled out for SIMS analysis, and 17 were taken from sulphides that had not had any other analysis done on them. Forty-one of these analyses were completed on pyrite, with the remaining four on chalcopyrite. The difficultly in finding chalcopyrite grains of suitable size for the laser ablation traverses prevented more analyses from being done at this time. Note that of the five analyses done on sulphides which have undergone

SIMS analysis that two of them have negative $\delta^{34}S$ values outside of the range of 0.0 ± 2.0‰. The other three samples have $\delta^{34}S$ values which are within the mantle range of 0.0 ± 2.0‰.

The sulphides picked for laser ablation were representative of those observed throughout the intrusion. Pyrite is typically subhedral, with the majority occurring as disseminated grains (Fig. 4.25a, b). Some, but not all, of the pyrite grains have magnetite rims, or were associated with larger magnetite aggregates (Fig. 4.25a, b). A couple of larger aggregates of pyrite were also chosen (Fig. 4.25c, d). The few chalcopyrite grains analyzed tend to be anhedral and occurring in close association to very fine-grained pyrite blebs.

Trace elements concentrations were gathered during each analysis and for some of these elements different isotopes were gathered. Sulphur content was gathered from SEM and ranged from 514,500 to 528,000 ppm. ^{59}Co and ^{61}Ni, the only isotopes measured for these elements, had somewhat similar magnitudes of values where ^{59}Co ranged from 3-43,000 ppm and ^{61}Ni ranged from 24-7,000 ppm. These two are much more similar to each other than ^{63}Cu, ^{65}Cu, ^{66}Zn, and ^{68}Zn. All of these elements ranged between 0.20-20.00 ppm. The PGEs had similar values when they were above the limit of detection, with ^{101}Ru, ^{103}Rh, ^{105}Pd, ^{106}Pd, ^{108}Pd, ^{101}Ru, ^{103}Rh, ^{105}Pd, ^{106}Pd, ^{108}Pd all having values between 0.0002-0.005 ppm.

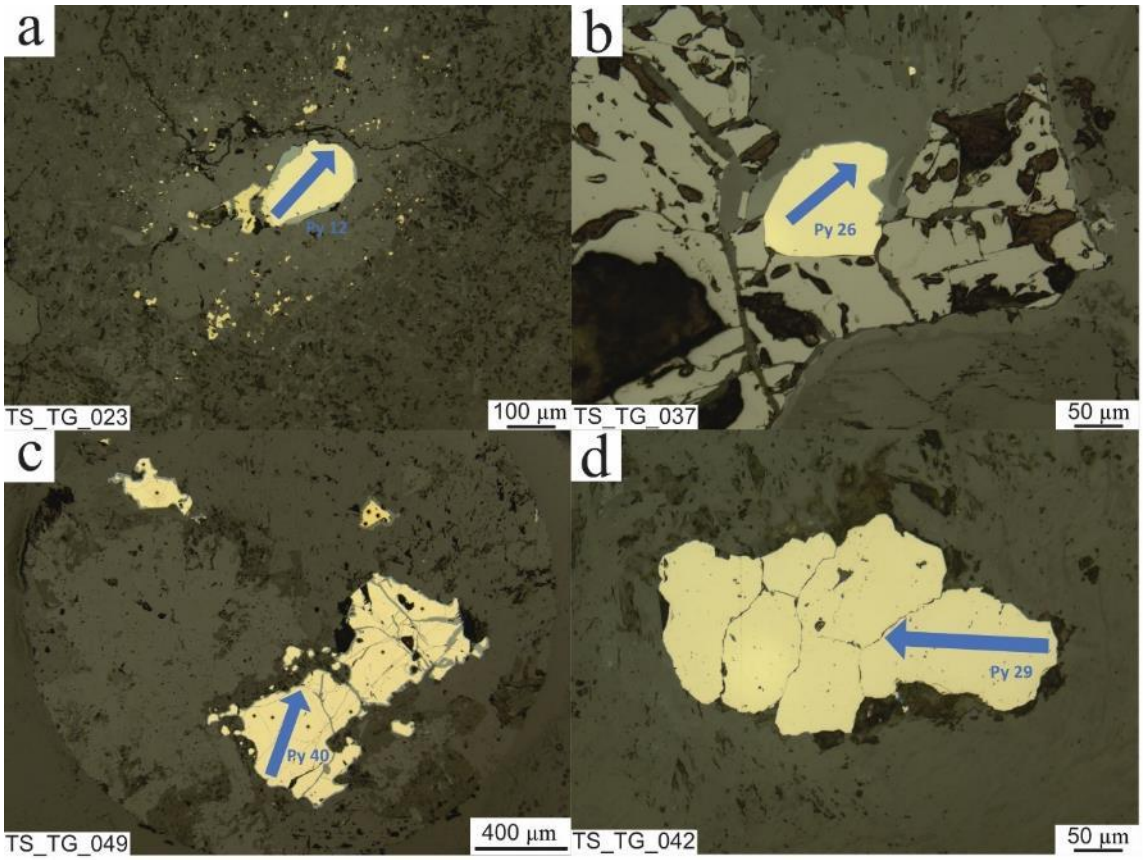

Figure 4.25. Examples of pyrite grains picked for laser ablation analysis. Blue lines show the path of ablation across the pyrite grain. a) pyrite analysis 12, from TS_TG_023, which is unassociated with SIMS analysis. b) pyrite analysis 26, from TS_TG_037. Other pyrite grains from this thin section were used for SIMS analysis. c) pyrite analysis 40, from a region of interest used for SIMS analysis. d) pyrite analysis 29, from TS_TG_042. Other pyrite grains from this thin section have been used for SIMS analysis.

5. Discussion

The Titan intrusion was emplaced within the larger Roaring River complex, a 2697 Ma sanukitoid suite comprised of diorites, monzodiorites, granodiorites, and granites all characterized by high Mg contents and LREE enrichment (Stern and Hanson, 1991; Halla, 2005). The Titan intrusion has been dated at 2690 ± 3.2 Ma, and is thus very close in age, but slightly younger than the Roaring River complex (Djon, 2018). They all lie near the boundary between the Winnipeg River, Marmion, and Western Wabigoon terranes (Fig. 2.1). The basement rocks for both the Roaring River complex and Titan are foliated to gneissic biotite-hornblende tonalite, granodiorite, and quartz diorite country rock, ranging in age from 2930-2723 Ma (Tomlinson et al., 2004).

The data gathered in this study, as well as all available historical data, has been used to characterize the Titan intrusion and relate it to the larger Roaring River complex and the regional LDI suite. This chapter will discuss the petrology of Titan, possible tectonic settings, the role of crustal contaminants, sulphur history, and how metamorphism and alteration have modified all the above.

5.1 Petrology of Titan

Previously, the Titan intrusion has been described as either a melagabbro-pyroxenite intrusion or as a gabbro-melagabbro-pyroxenite intrusion (Fig. 5.1; Fingler and McCrindle, 2001; McCrindle, 2001; Barr, 2003; Heerema, 2004; Bowdidge, 2010). This was based upon previous field sampling and a limited drilling program, neither of which were very extensive nor included detailed petrographic studies. The aim of this research was to provide a more in-depth analysis of the petrography, as well as a more thorough investigation of the intrusion as a whole.

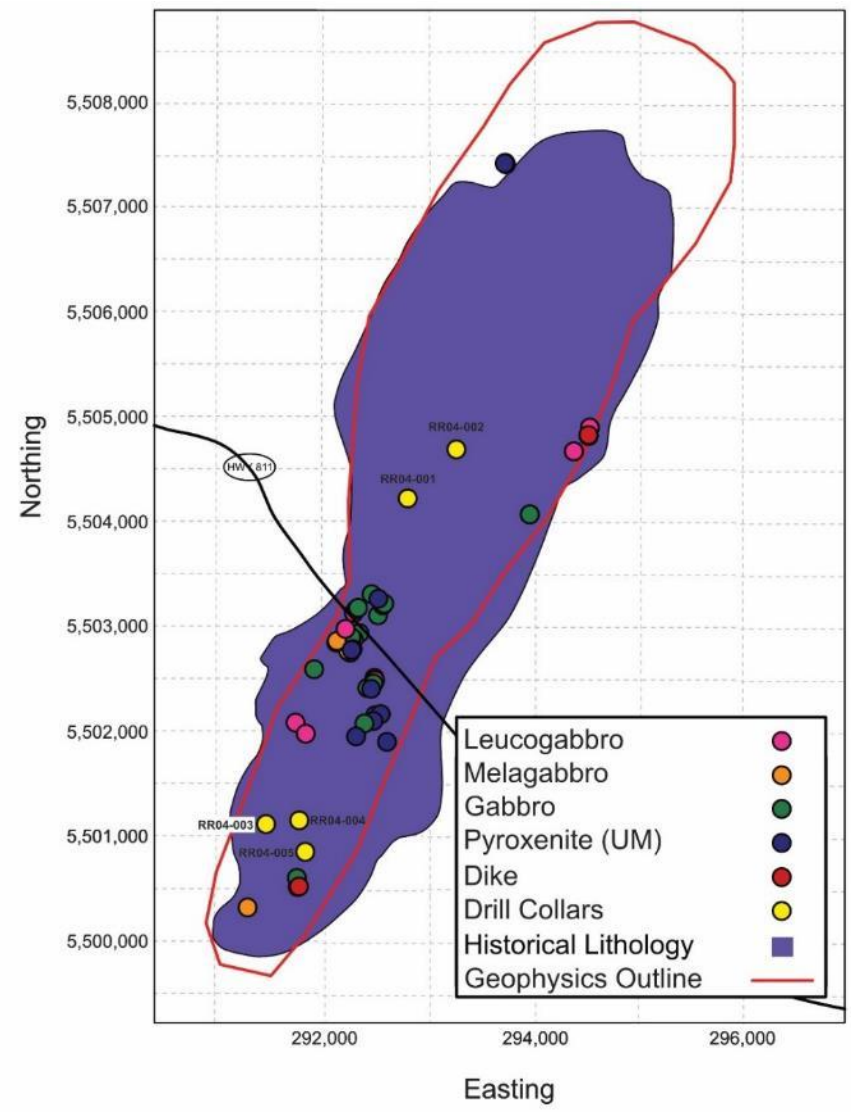

Figure 5.1 Inferred extent and sampling of Titan, with the previously described lithologies shown in purple. Earlier work describes Titan as either a melagabbro-pyroxenite or a gabbro-melagabbro-pyroxenite (Bowdidge, 2010). Sampling shows the lithologies defined in this study.

Petrographic analysis has identified a variety of rock types, indicating a less homogenous intrusion then previously described. It should be noted that while sampling was more comprehensive than previous work, there is a pronounced sampling bias towards the centre of the intrusion (Fig. 5.1). This is due to the availability of outcrops in the area. Pervasive glacial till and Proterozoic diabase sills related to the ~1.1 Ga Midcontinent Rift obscure large swaths of Titan, particularly in the northern and southern

extremes. These factors also obscure contacts within the intrusion, particularly those between the Roaring River complex and Titan.

Petrographic analysis revealed the majority of the Titan rocks are composed of plagioclase and clinopyroxene, with lesser amounts of orthopyroxene, hornblende, olivine, quartz, biotite, Fe-oxides, sulphides, and alteration assemblages. Plagioclase and clinopyroxene generally alternate as the most abundant mineral present, and occur as cumulates, with each mineral tending to be equigranular and intergrown with little in the way of groundmass (Fig. 5.2). The plagioclase and clinopyroxene are generally similar in size, ranging from fine- to medium-grained, while the less abundant minerals tend to be smaller. There is no consistent trend in terms of the orientation of grains, nor was any sort of layering observed in thin section. One small section of mild to moderate layering was observed in outcrop but could not be sampled due to outcrop orientation. Alteration has destroyed some of the primary textures observed in thin section, particularly where grain boundaries, portions of crystals, or whole crystals have been replaced.

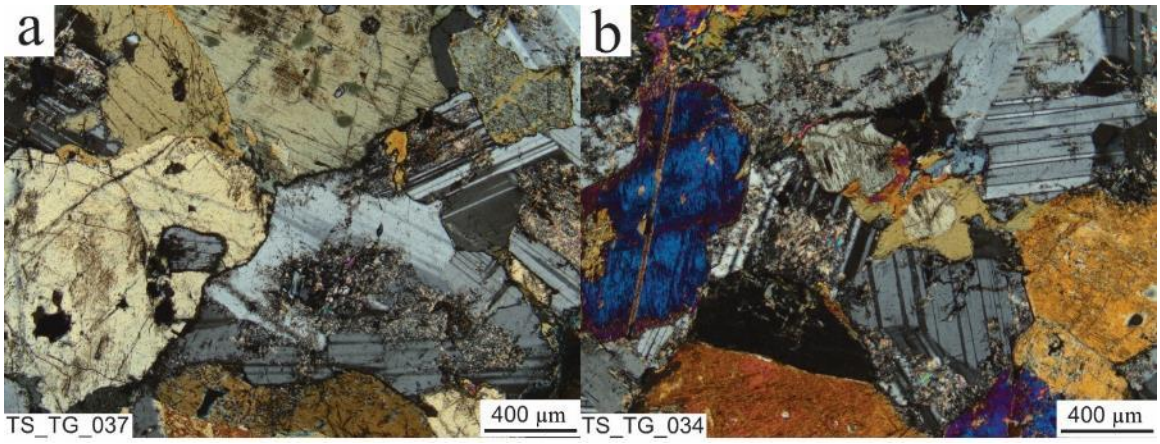

Figure 5.2. Two occurrences of intergrown plagioclase, clinopyroxene, and hornblende. Both exhibit little alteration; therefore grain boundaries are relatively sharp.

Poikilitic textures were observed, however, they are found in only a couple of samples, representing minor proportions (Fig. 5.3). The poikilitic texture generally has amphibole occurring as the enclosing mineral and either clinopyroxene or plagioclase occurring as enclosed anhedral phases (Fig. 5.3). The other occurrence of the poikilitic texture has plagioclase with intense sericite alteration as the enclosing phase, and pyroxene crystals, with minor amounts of alteration at the rim, as the phase enclosed (Fig. 5.3).

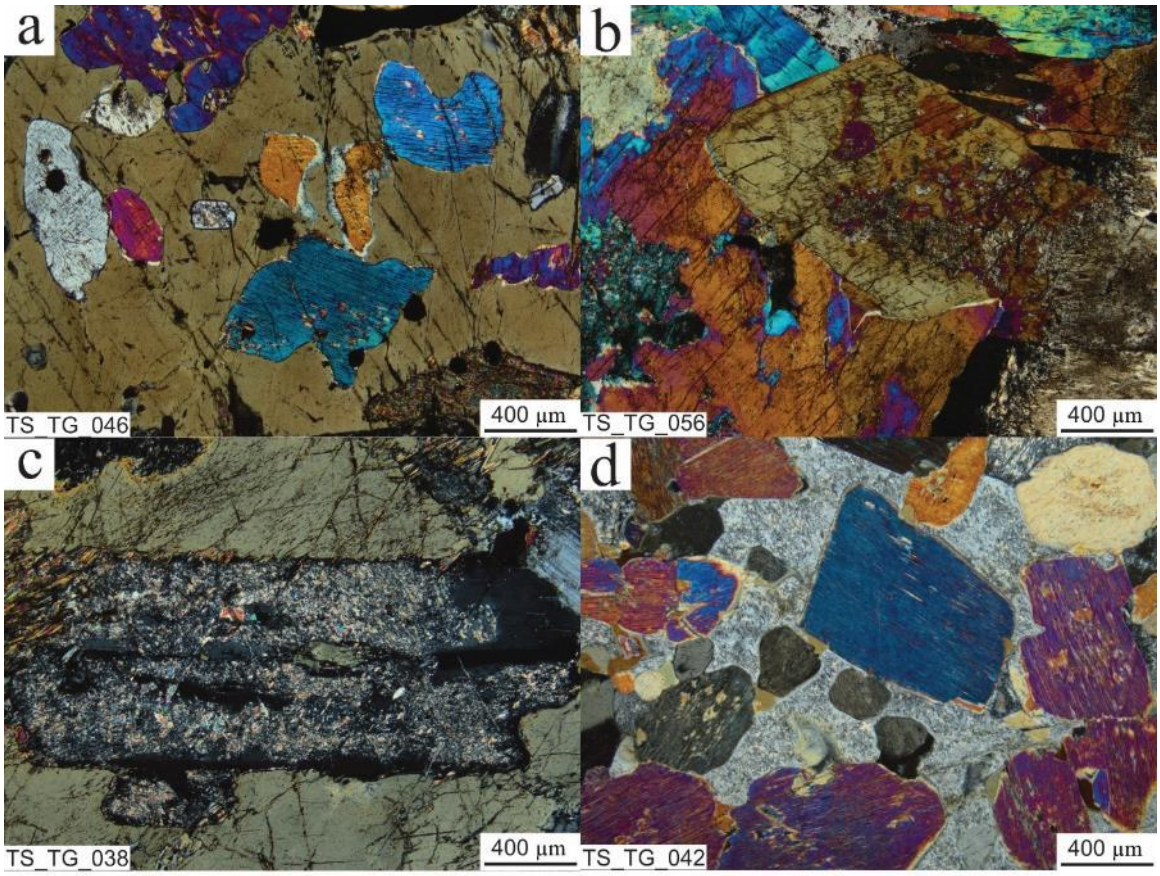

Figure 5.3. Various occurrences of poikilitic textures as well as a more common amphibole occurrence. a) poikilitic hornblende enclosing clinopyroxene grains. b) hornblende intergrown with clinopyroxene grains. The centre of the hornblende grain is altered, which is also observed in clinopyroxene grains. c) a crystal of plagioclase that has been almost completely replaced by sericite, enclosed by amphibole. The amphibole has been replaced by alteration assemblages at the edges and along the boundary between the plagioclase and amphibole. d) plagioclase that has almost completely been replaced by sericite alteration surrounding subhedral clinopyroxene grains, with alteration along the grain boundaries.

Hornblende is interpreted to be a primary mineral based on its occurrence and habit, as it is generally very fine- to medium-grained, intergrown with the other silicates, and has similar amounts and styles of alteration as observed in the plagioclase and clinopyroxene. In the poikilitic patches, amphibole is interpreted to have formed later as it encloses clinopyroxene and plagioclase crystals (Fig. 5.3). It is unlikely to be the product of metamorphism, as the enclosed minerals are generally euhedral to subhedral with similar amounts of alteration to the amphibole (Fig. 5.3). There is no indication of foliation in the hornblende, nor are they particularly associated with other alteration assemblages. This is consistent with a primary magmatic origin.

The proportion of the minerals observed in Titan samples varies throughout the intrusion giving rise to the variety of rock types, which include leucogabbros, gabbros, melagabbros, and pyroxenites. There is a rather chaotic distribution of lithologies, with gabbro outcrops found metres away from ultramafic ones. This lack of systematic variation is consistent with Titan being composed of one large mafic body, rather than multiple separate ones. In general, regular variation in mineral abundances, without significant textural variations indicates a closed magmatic system where fractional crystallization is the primary mechanism of crystal formation (Shahabi Far et al., 2019). As the variation that occurs throughout Titan is generally a matter of modal abundance rather than completely different minerals, with similar textures observed across the intrusion, the processes of formation seem to favour fractional crystallization within a closed system. The presence of primary hornblende indicates that the magma was hydrous, but knowledge of how lithology changes at depth within the intrusion would provide more context about the magma system (Murphy, 2007). There are no observed

mafic breccias observed at surface, which could serve as additional evidence of a volatile-rich magma, though minor amounts of felsic breccias have been observed in outcrop (Lavigne and Michaud, 2001; Barnes and Gomwe, 2010). Currently, there is no observed large-scale layering within the intrusion, again consistent with a single magma body with little recharge or subsequent magma pulses, but it is possible that any layering is only present at depth (Lavigne and Michaud, 2001; Djon et al., 2017). Without knowledge of the shape and lithology of Titan at depth, combined with the poor exposure in the far north and south of the intrusion, and the general lack of contacts, there are limits to what surface lithology can indicate about the parent magma.

Sulphides and Fe-oxides are ubiquitous throughout the intrusion, though are generally very low abundance in each sample. They occur as very fine- to fine-grained, blebby crystals that are disseminated throughout the samples. The sulphides consist primarily of pyrite, with chalcopyrite, pyrrhotite, and pentlandite occurring less often. Pyrite occurs as disseminated, rounded blebs, often with chalcopyrite inclusions and a magnetite rim. Chalcopyrite, pyrrhotite, and pentlandite occur as fine-grained, anhedral aggregates, but are rare. Their importance will be discussed later when the sulphur history of Titan is explored. The Fe-oxides within the intrusion are almost entirely magnetite, with only a small number of grains showing any exsolution lamellae with hematite (Fig. 5.4). There are also separate, discrete grains of ilmenite, which sometimes have exsolution lamellae of magnetite, but overall, they comprise a very minor proportion of the total of Fe-oxides (Fig. 5.4). While small aggregates of magnetite occur, there is no suggestion of any widespread accumulation or layering. This, along with the overall lack of layering in the intrusion, suggests that density separation or settling did not have a

large effect on Titan, and is consistent with a single large magma chamber (Wiebe and Snyder, 1993; Nebel et al., 2013). The general ubiquity of magnetite throughout the samples is consistent with a hydrous magma as suggested by primary amphibole, as H_2O-rich melts can lead to oxidation and thus the early precipitation of oxide minerals (Murphy, 2007; Polivchuk, 2017). However, the magnetite is not confirmed to be primarily magmatic and it is possible that the magnetite present at Titan could be partially or completely related to secondary processes, such as alteration, and is an area of potential follow up for future studies (Nebel et al., 2013; Boutroy et al., 2014; Polivchuk, 2017).

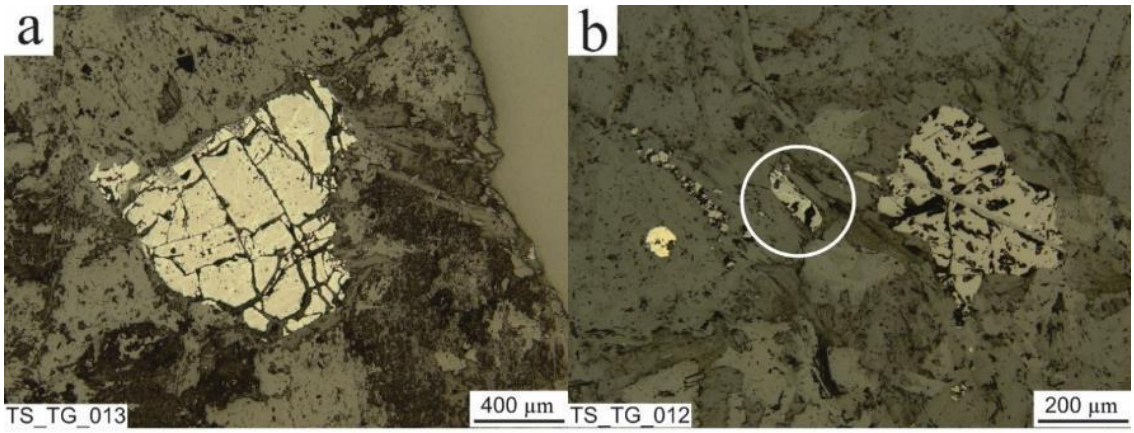

Figure 5.4. Photomicrographs of exsolution within Fe and Fe-Ti oxides in Titan. a) magnetite exsolution lamellae within an ilmenite grain. b) a small grain of magnetite (circled) with ilmenite exsolution.

The occurrence of a swirled droplet habit observed in magnetite is reminiscent of myrmekite (Fig. 4.11). This texture occurs in five samples, with varying amounts in each. This habit is not observed in any other mineral, and there is no specific mineral association or other textural association for samples that have this texture. A similar myrmekite texture in Fe-Ti oxides has been observed in the Marathon deposit as well as in deposits in Norway, though both occurrences are specifically intergrown with

orthopyroxene crystals, which is not observed in Titan (Barton and Van Gaans, 1988; Shahabi Far et al., 2019). Nevertheless, it is possible that the conditions of formation between these two types of myrmekite are similar. In the Marathon occurrence the texture was interpreted to be a late-stage mineral, though there is uncertainty in regard to the onset or mechanism of formation (Shahabi Far et al., 2019). The Norway occurrences were interpreted to have occurred through re-equilibration occurring during retrograde metamorphism and likely through subsolidus cooling (Barton and Van Gaans, 1988). Barton and Van Gaans (1988) noted that the formation conditions are complex, which likely contributes to their rarity. Given the differing mineralogical associations it is possible that Titan's magnetite textures were produced through different processes than these other occurrences. However, the formation conditions are likely to be similarly complex, and possibly suggests that there is an element of re-equilibration and alteration involved in the formation of some of the magnetite grains.

In addition to the main lithology observed in outcrop, mafic dikes are present throughout the intrusion and in drill core, as are felsic veins, veinlets, and breccias (Fig. 5.5). The mafic dikes are very fine- to fine-grained, gabbro to gabbronorite in composition, with minor amounts of alteration assemblages. They are observed in drill core and at surface, with no consistent orientation observed. The composition of the mafic dikes is similar to the gabbros observed throughout the entirety of the intrusion, with sharp contacts between the dike and host rock (Fig. 5.5c). The sharp contacts and absence of any comingling between the host rock and the dike, indicates that the host was solidified before dike emplacement (Wiebe and Snyder, 1993). The mafic dikes are quite thin (10-20 cm) in outcrop but can range in size in drill core (up to a metre; Figs. 4.8;

5.5). In drill core it is not uncommon to find a comingling of felsic veinlets (<5 cm) with the mafic dikes, possibly indicating that the mafic dikes incorporated some amount of felsic material (Fig. 4.8). Felsic veins (>5 cm) were not observed at surface; however, they do occur in drill core (Fig. 5.5d). Because of the nature of the drill core, it was not possible to determine if the felsic veins represent dikes, large clasts, or xenoliths of unincorporated country rock. Felsic veinlets and breccias were found at surface, though they only formed a minor feature in outcrops (Fig. 5.5a, b). The occurrence of the felsic material varies, with one felsic dike having euhedral and well-defined silicate grain boundaries and little to no alteration assemblages while another shows almost complete replacement by alteration assemblages. Overall, most felsic dikes tend to have quite sharp contacts with mafic host rock, while the felsic breccias have more diffuse contacts. The difference between the two types of felsic contacts implies multiple phases of felsic intrusions, with the breccias and felsic veinlets occurring early in Titan's emplacement, and thus being more incorporated into the magma. In contrast, the felsic dikes appear to be a later stage, as evidenced by the sharp contacts and lesser amounts of alteration.

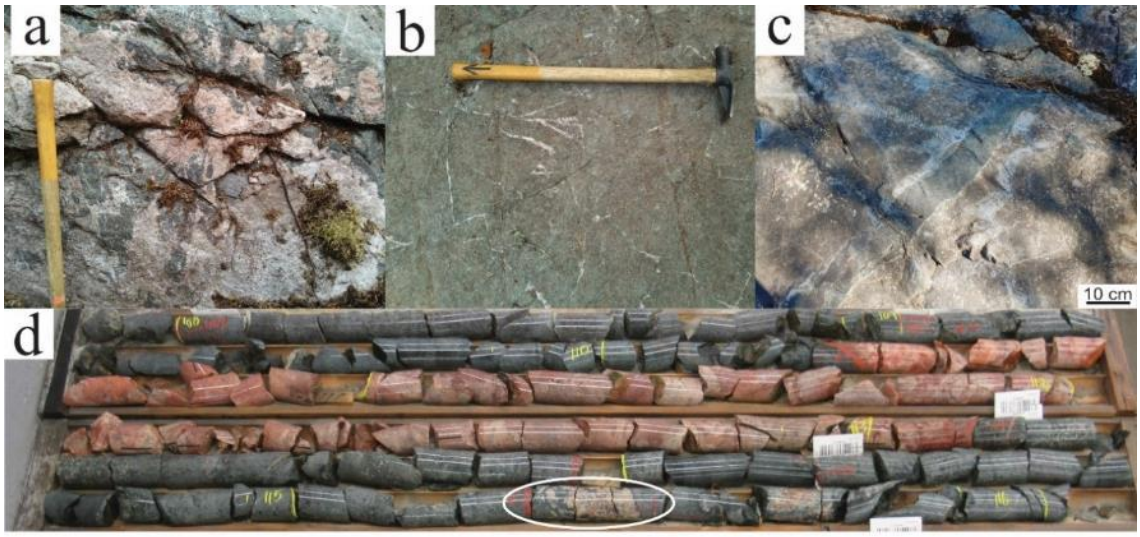

Figure 5.5. Outcrop pictures from Titan. a) felsic breccia observed in pyroxenite outcrop. b) small cross-cutting felsic veinlets observed in pyroxenite outcrop. c) mafic dike cross-cutting gabbro outcrop. d) drill core from RR04-003 (107.85-116.00 m), showing a felsic dike and felsic breccia, highlighted with the white circle.

Alteration

Across Titan, there are a variety of alteration minerals, ranging in abundance from 5-65%. The alteration minerals tend to have two main occurrences, one where they have replaced pyroxene and plagioclase along grain boundaries and cleavage planes and another as discrete minerals. The assemblages of discrete alteration minerals range in habit from granular to bladed, depending on the minerals in the assemblage. The most common alteration minerals are chlorite, actinolite, tremolite, talc, epidote, and sericite (Figs. 4.12; 4.13). Minor amounts of calcite, iddingsite, and unidentified clay group minerals were also observed. All samples are altered to some extent, though samples from the very farthest southern extents seem to have a consistently higher degree of alteration minerals, from 45-65%. Samples with this much alteration have both high amounts of discrete alteration minerals and replacement of silicate minerals, making it difficult to determine original grain boundaries or even identify the primary silicates in

some cases. Regional greenschist facies metamorphism can account for much of the alteration observed. Given that the original mineralogy of Titan consists primarily of pyroxenes and plagioclase, minerals such as chlorite, actinolite, tremolite, talc, and epidote are consistent with greenschist facies metamorphism (Fletcher et al., 1997; Essaifi et al., 2004). These minerals make up the majority of the alteration observed, both as replacement minerals and as large masses (Figs. 4.12; 4.13). There does not appear to be any consistent orientation or foliation to the alteration minerals, suggesting that shearing or compaction had a minimal effect on the samples taken (Essaifi et al., 2004).

The cumulate lithology of Titan makes it difficult to interpret the parental magma, and doubly so when the amount and type of alteration makes it generally impractical to undertake quantitative mineral analysis. Even the most common and abundant silicate minerals have consistent levels of alteration that render mineral analysis challenging. Given those limitations, the next best tool is whole-rock geochemistry. However, in addition to the effects of cumulate lithology, the amount and nature of alteration needs to be considered when interpreting whole-rock geochemistry. As minerals are altered by metamorphism and hydrothermal alteration, the interaction with fluids can cause chemical changes within the rocks (Pearce, 1976; Gélinas et al., 1982). In terms of the major elements, Na_2O, and K_2O are generally quite mobile under both hydrothermal conditions and greenschist facies metamorphism, whereas CaO, FeO, and MgO are variably mobile under greenschist facies metamorphism (Fig. 5.6; Pearce, 1976; Gélinas et al., 1982). Trace elements generally fare better, and HFSE are generally used in geochemical diagrams because they are resistant to water-rich solutions and low grades of metamorphism, as they are concentrated in phases such as zircon, ilmenite, and titanite

(Fig. 5.6; Murphy, 2007). Loss on ignition (LOI) values for Titan range from 0.78 to 5.59, without any spatial trend to the values. The majority of samples have relatively low LOI wt% values (<3.1), indicating that despite the amount of alteration minerals observed in thin section, large amounts of volatiles are not present in Titan's samples. However, the mobility of elements will be assessed when considering trends in geochemical data moving forward.

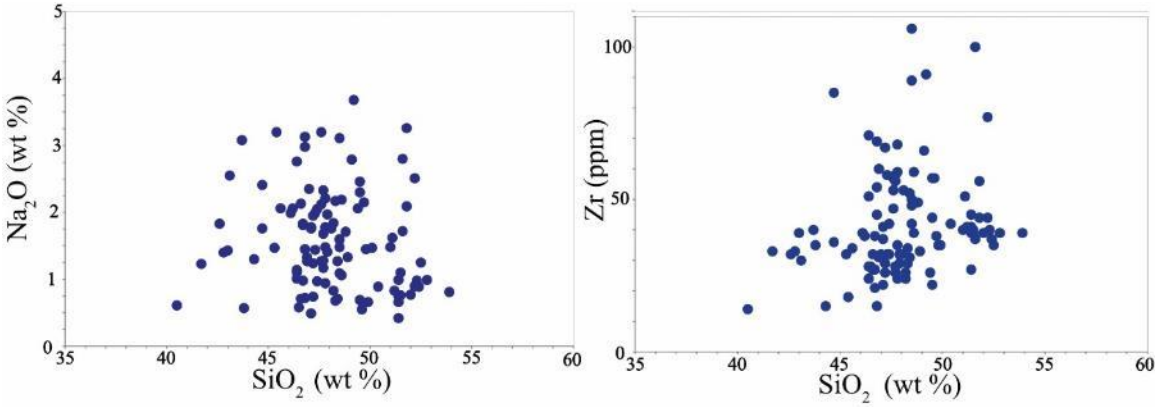

Figure 5.6. Bivariate diagrams of Na_2O (wt%) and Zr (ppm) vs SiO_2 (wt%). Na_2O has a much greater degree of scatter then Zr, showing the relative mobility of Na_2O vs an immobile trace element.

5.2 Geochemistry

Just as the petrology of Titan varies throughout the intrusion, so does the geochemistry. On bivariate diagrams, the majority of elements have a continuous span of data, with no gaps but moderate to large degrees of scatter (Fig. 4.16). Generally, there is no systematic distribution of the major elements across the intrusion. The only exception to this is MgO, which has a roughly bimodal distribution with a 'low' population ranging from 4.3-10.3 wt% and a 'high' population ranging from 11.3-21.0 wt% (Fig. 4.15). High MgO samples tend to be more concentrated around the inferred margins of Titan, while low MgO samples are generally confined to the centre (Fig. 4.15). However, this is not a clear-cut division and it is difficult to determine how much of this trend is affected by

sample distribution from outcrop availability (Fig. 4.15). There is some correlation between geochemistry and petrographic data, at least as far as is able to be determined by samples that have both. Some of the other major elements show correlation to individual mineral abundances. A positive correlation between plagioclase abundance and Al_2O_3 and Na_2O is observed as are negative correlations between plagioclase abundance and CaO and MgO. There is a positive correlation between clinopyroxene abundance and CaO and negative correlations between clinopyroxene abundance and Al_2O_3 and Na_2O. Plotting the lithology data against the representative composistions of various minerals reveals that these correlations are useful only for broad scale comparisons (Fig. 5.7). Within the petrographic data it isn't possible to correlate lithology with geochemistry in very fine detail, and as such it is not possible to use geochemical data alone to determine lithology (Fig. 5.7). Broad distinctions can be made, with high Al2O3 content correlating to leucogabbros and gabbros, for example (Fig. 5.7). However any further refinement is impossible at this time and as these are broad distinctions, with plenty of outliers, major element behaviour will generally be discussed on its own merit, with only very broad petrographic inferences.

The major elements can be used to investigate broad fractionation behaviour in the intrusion. Broadly Fe_2O_3 content decreases as SiO_2 increases (Fig. 5.8). Both CaO and Al_2O_3 correlate to MgO content (Fig. 5.8). There is a straightforward negative correlation between Al_2O_3 and MgO, and generally for CaO and MgO as well (Fig. 5.8). In the some of the highest MgO samples there begins to be a reversal in the correlation to CaO, possibly indicating the crystallization of Ca-rich pyroxenes (Fig. 5.8). This possibility would need to be confirmed by mineral chemistry on relatively fresh grains. In general,

the smooth major element trends suggest fractional crystallization of a single magma, without disruption from subsequent magma pulses.

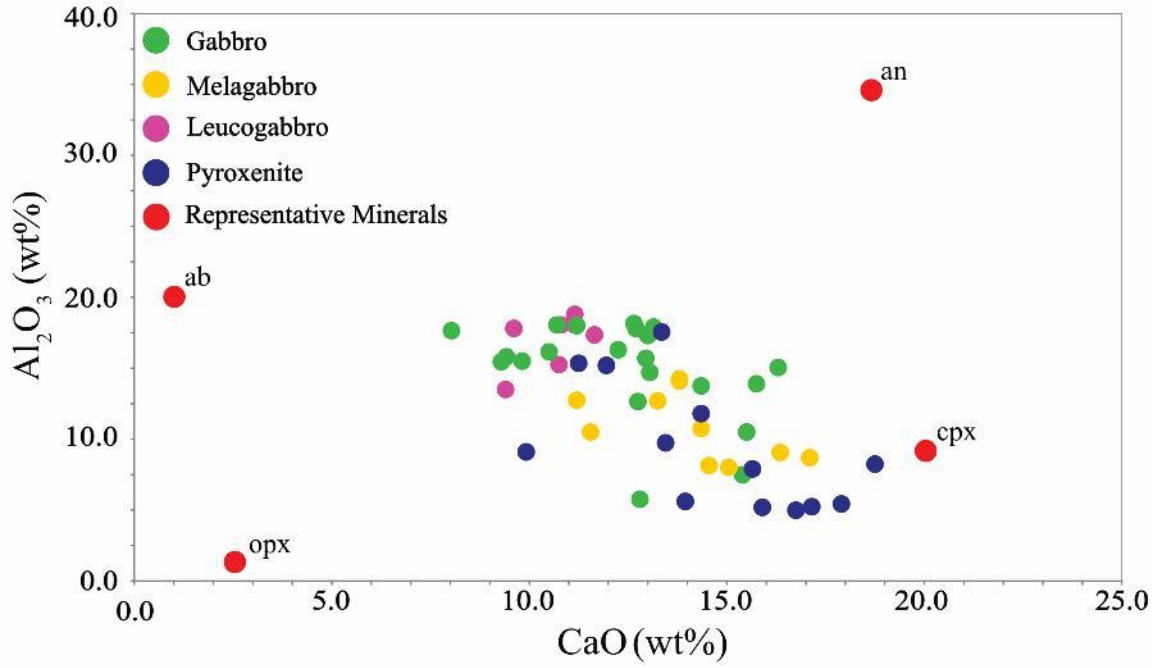

Figure 5.7. Bivariate plot of Al_2O_3 and CaO (wt%) for thin section samples, which also denotes the main divisions in rock type. The red dots are representative compositions for select minerals, including orthopyroxene (opx), clinopyroxene (cpx), albite (ab), and anorthite (an). Mineral compositions from IMDEX ioGAS-64, ver 7.4.2.

In general, there are only weak levels of correlation between trace and major element behaviour, and often relatively large amounts of scatter for Titan rocks. As incompatible trace elements stay in the melt, this appears to reflect the cumulate nature of Titan. Both Ni and Cr have positive correlations with MgO, and thus a slight positive correlation to rock type (Fig. 4.16). Nickel is correlated with Cu and is likely associated with the sulphides present in Titan. Also associated with the sulphides are Pt and Pd, which range from below detection limits to 0.219 and 0.717 ppm respectively. The Pd/Pt ratios therefore range from 0.2 to 5.6, which is within and above the range for most PGE-dominated deposits (0.5 to 2; Barnes and Gomwe, 2011). The range of Pt and Pd values

indicate that there is possibly some enrichment of Pd over Pt in the sulphides in Titan. Additionally, vanadium is positively correlated with Fe_2O_3, which is consistent with the presence of magnetite (Fig. 5.8).

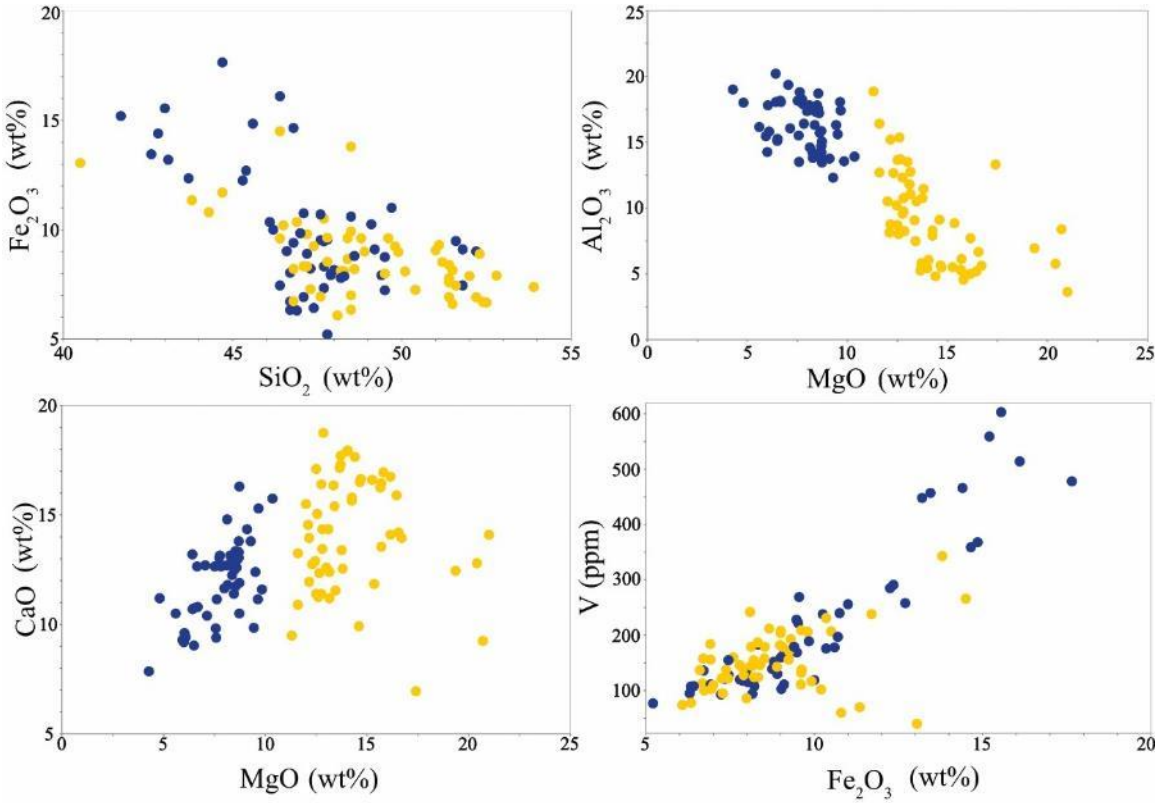

Figure 5.8. Bivariate diagrams for major elements. Yellow dots indicate high MgO group and blue dots indicate low MgO group. Diagrams show Fe_2O_3 vs SiO_2, Al_2O_3 vs MgO, CaO vs MgO, and V (ppm) vs Fe_2O_3. All major elements are in wt% oxide.

Narrowing down from trace elements to REEs, the primitive mantle normalized profiles of Titan are all similar, with consistent LREE enrichment, HREE fractionation, and negative Nb and Ti anomalies (Fig. 4.17). The spread of values does not systematically change with lithology, major element, or spatial variation. The tight spread of REEs and consistency in anomalies is consistent with a single magma source. The variations noted over the process of picking samples for Sm-Nd isotope analysis exist in a continuous fashion, and could be produced through crustal contamination or fractional

crystallization (Fig. 4.24). Furthermore, the trends selected cannot be observed in the spread of REE data, which shows a continuous, roughly linear trend (Fig. 5.9). The smooth linear behaviour observed in the major element data and REE data, as well as the variation in minerals and lithology are all consistent with a single magma body, in a closed system that has fractionated over time (Fig. 5.9).

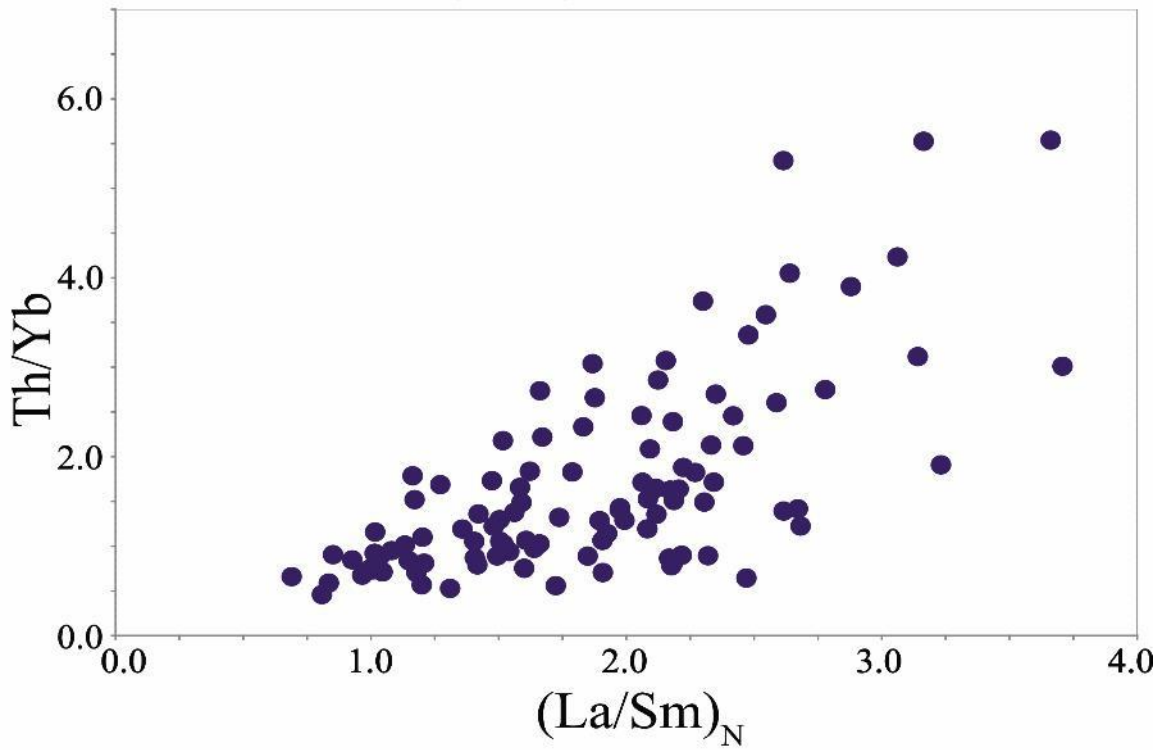

Figure 5.9. Bivariate plot of Th/Yb vs $(La/Sm)_N$. Note the continuous spread of data present in the REEs.

Crustal Contamination

Primitive mantle normalized plots and REE data can also be used to investigate if crustal contamination occurred in Titan, as well as being useful for determining tectonic setting. In particular, the negative Nb, Zr, Hf, and Ti anomalies and general systematic changes to the HFSE are indicative of either crustal contamination or a subduction zone setting (Sun and McDonough, 1989; Lightfoot et al., 1991). Considering where Titan is

located, there is the possibility of contamination from the surrounding Roaring River complex and Archean tonalite basement rocks. In general, continental crust is enriched in incompatible trace elements such as Th and the LREEs, relative to moderately incompatible trace elements, such as Zr, Hf, the middle REEs, and negative Nb and Ti anomalies (Sun and McDonough, 1989; Lightfoot et al., 1991). The range of $(La/Sm)_N$ and Th/Yb values for the Titan samples cannot conclusively indicative whether crustal contamination has occurred or is from a subduction source (Fig. 5.10). The range of Nb/Nb* values indicate the size of the negative Nb anomaly, and is also not conclusive of either process (Fig. 5.10). However, specific geochemical and radiogenic isotope data from the potential contaminants can better constrain if any contamination has occurred and the potential source.

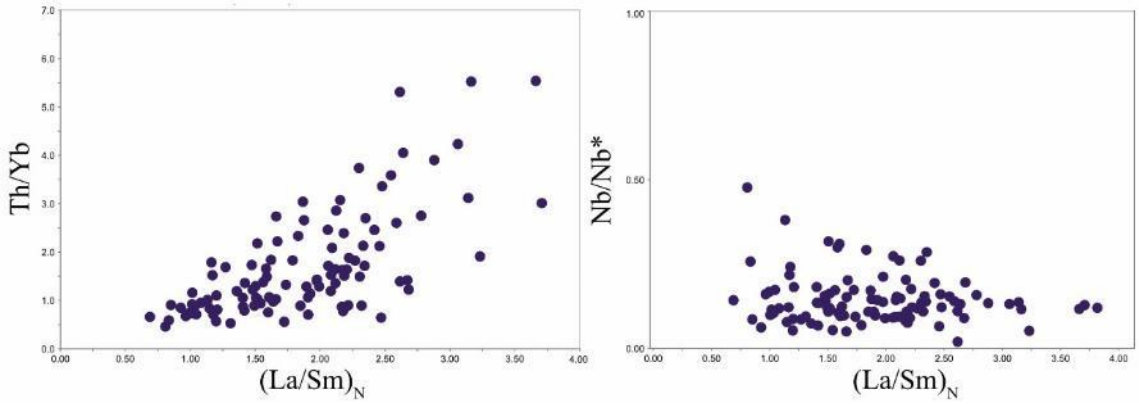

Figure 5.10. Bivariate plots of $(La/Sm)_N$ vs Th/Yb and Nb/Nb for Titan samples.*

The first possible contaminant to consider is the Roaring River complex, into which Titan was intruded. The Roaring River complex is characterized by steeply fractionated, subparallel REE patterns with no Eu anomalies (Fig. 5.11; Stern and Hanson, 1991). This LREE enrichment, along with other distinct geochemical features, has been attributed to the addition of a LREE enriched melt or hydrous fluids, which are

sourced either from the mantle or from a subduction source during emplacement (Stern et al., 1989; Stern and Hanson, 1991; Halla, 2005). When the data from Roaring River is plotted on a primitive mantle normalized diagram, the general trend is in line with the highest range of data from Titan (Fig. 5.11). Note that the data used for Roaring River's primitive mantle normalized diagram is historical, and as such only a small proportion of REE data was reported, meaning that certain similarities cannot be evaluated (Fig. 5.11; Stern and Hanson, 1991). Overall, the primitive mantle normalized trends for Roaring River and Titan are similar, and if Titan assimilated any of Roaring River it would be difficult to tell from trace elements alone. Given the presence of minor amounts of felsic breccias at surface it appears likely that at the very least small amounts of Roaring River were incorporated into Titan, but the geochemical data cannot further distinguish any role for a Roaring River contaminant.

Figure 5.11. Primitive mantle normalized spider plot, showing the span of values for historical Roaring River data, and Titan. Concentrations normalized to primitive mantle (Sun and McDonough, 1989). Historical Roaring River data from Stern and Hanson (1991).

The next possibility for crustal contamination is the underlying Archean basement rocks, which consist of foliated to gneissic biotite-hornblende tonalite, granodiorite, and quartz diorite (Tomlinson et al., 2004). There is little in the way of detailed geochemical data from the basement rock in this particular area, but as Archean tonalite and granodiorite rocks it is likely they are high in SiO_2 and Na_2O, with enrichment in LREE and strong to moderate fractionation of REEs, and thus are a general possibility as a contaminant (Martin, 1986).

As the geochemical data for the possible contaminants are not conclusive, the possibility of crustal contamination was also investigated using Sm-Nd isotopes. Radiogenic isotopes are generally better able to constrain the source and magnitude of crustal contamination, with the half-lives of the isotopes involved able to produce measurable differences over several million years (Dickin, 2005). The usefulness of Sm-Nd isotopes occurs because Nd is typically more concentrated in magmas than Sm due its larger ionic size, meaning that the average Sm/Nd ratios is lower in the crust than it is in the depleted mantle (DePaolo, 1981; Murphy, 2007). Therefore, over time the crust typically evolves to a negative ε_{Nd} signature, whereas the depleted mantle evolves to positive ε_{Nd} values (DePaolo, 1981; Murphy, 2007).

For Titan the overall range of ε_{Nd} values is 0.70-1.82, with all but two samples yielding values within a range of 1.18-1.82, a fairly tight spread. The two outlying values range from 0.70-0.72, but are within error of the other samples. These ε_{Nd} values are

consistent with a magma that has assimilated small amounts of continental crust, as the estimated depleted mantle at 2.7 Ga has an ε_{Nd} of +3 (Tomlinson et al., 2004; Dickin, 2005; Sanborn-Barrie and Skulski, 2006). The Titan ε_{Nd} values are similar to the single ε_{Nd} value published for the Roaring River complex of 1.17 (Tomlinson et al., 2004). Since Titan and Roaring River are similar in age (2690 ± 3.2 and 2697 Ma respectively), it is likely that both have assimilated small amounts of continental crust (Tomlinson et al., 2004; Dickin, 2005). It is also not possible to say if Titan assimilated Roaring River, as the ε_{Nd} values are too similar to indicate if contamination has occurred. The tonalite and tonalite gneisses to the west of the Roaring River complex have ε_{Nd} values ranging from 0.97-1.43, with an age range of 2713-2746 Ma, and are the closest values available to represent the Archean basement rocks underlying Titan (Tomlinson et al., 2004). Taken together with the geochemical data, this suggests that small amounts of older Archean tonalite basement rocks were likely incorporated into both the Roaring River complex and Titan. It is still possible for Roaring River to have been incorporated into Titan, perhaps in the form of the multiple generations of felsic dikes and breccias observed at surface and in drill core, but overall, the isotopes are not conclusive. The amount of contamination in Titan seems to be relatively small, and is likely not the main source of the HFSE anomalies observed in Titan's primitive mantle normalized diagrams (Fig. 5.11).

Tectonic Setting

As crustal contamination does not fully explain the trends observed in Titan's trace element data, tectonic setting will be considered as a possible explanation. Large ultramafic and mafic intrusions are generally associated with the development of large

igneous provinces (LIPs) and mantle plumes, often exploiting faults or other large-scale structures to ascend to the surface (Murphy, 2006; Lightfoot and Evans-Lamswood, 2014). There is a strong association between large igneous provinces, mantle plumes, and rifted environments where voluminous amounts of ultramafic and mafic magmas would be emplaced, however, extensional and compressional environments are also possible settings for emplacement of such intrusions (Barnes et al., 2016). As such, there are a number of tectonic settings in which Titan could have formed, and the geochemistry of the rocks can be used to constrain that environment. Starting with major elements, the total alkali and silica (TAS) diagram is one option for understanding the broad alkalinity of the rocks. Note that K_2O and Na_2O can be mobile under greenschist metamorphism, so there is some degree of ambiguity to the y-axis (Fig. 5.12). The samples from Titan generally fall within the gabbro field, though some of the samples do not plot into any field (Fig. 5.12). If the bimodal MgO is considered, then it becomes clear that high MgO samples are more likely not to plot within the fields of the TAS diagram (Fig. 5.12). Some of this effect in likely due to the mobility of Na_2O and K_2O, as well as the presence of ultramafic rocks being plotted on the TAS diagram (Fig. 5.12). As geochemistry alone cannot accurately discern between melagabbros and other ultramafic rocks observed at Titan, the group is left as is. Overall, the Titan rocks show a broadly gabbroic composition.

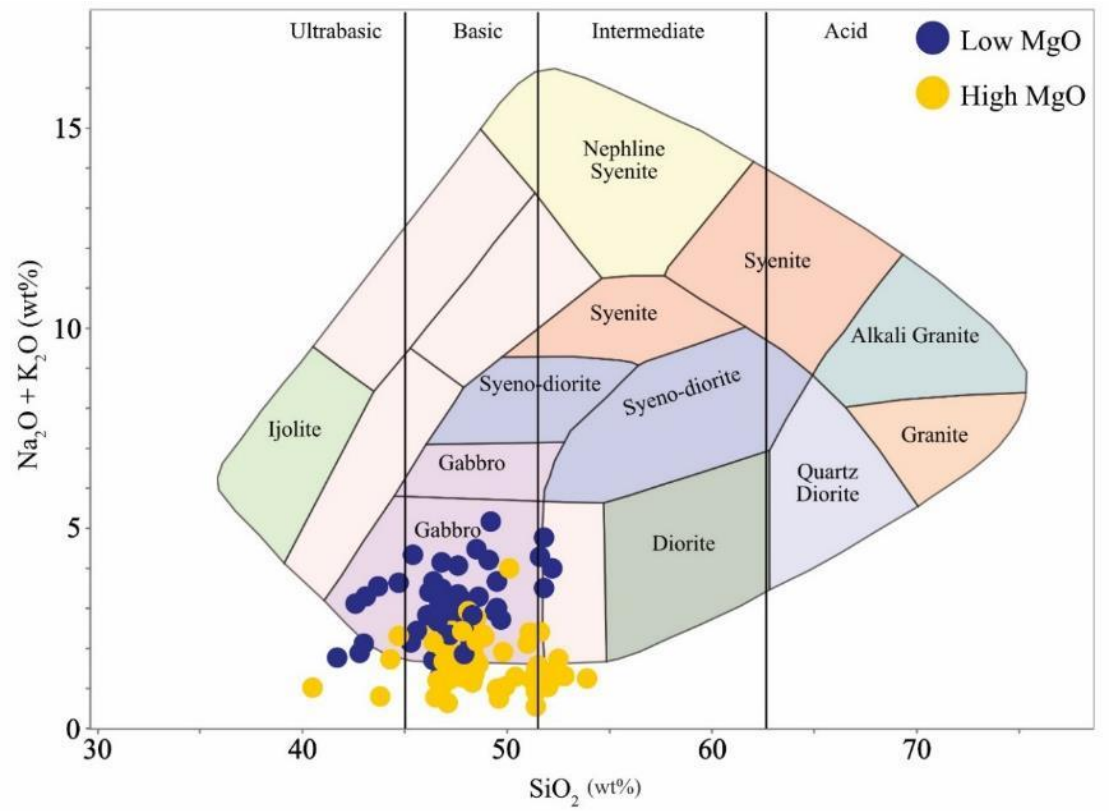

Figure 5.12. Total alkali vs silica (TAS) diagram for Titan samples. Adapted from Cox et al. (1979) and Wilson (1989).

Given the mobility of the major elements, trace elements are considered to better define possible tectonic settings. Primitive mantle normalized plots can be used to make comparisons between the patterns observed in Titan and those of 'typical' rocks from different magma sources, and the processes that cause these patterns. Mafic and ultramafic intrusions associated with sulphides, including many large deposits, are often associated with the most primitive magmas available, generally occurring along the margins of LIPs (Kerrich et al., 2005; Barnes et al., 2016). In turn, LIPs are often associated with plumes, where the long-lived and voluminous amounts of magmatism create favourable environments for ore deposition (Kerrich et al., 2005; Barnes et al., 2016). Mantle plumes often consist of ocean island basalt (OIB) magma and are a good

starting point for comparison. There are some similarities between the Titan samples and the OIB signature, particularly in the overall LREE enrichment (Fig. 5.13; Sun and McDonough, 1989). However, Titan's typical signature is more depleted and has strong persistent negative Nb, Zr, Hf, and Ti anomalies that differ from the idealized OIB signature (Fig. 5.13; Sun and McDonough, 1989). Negative Nb and Ti anomalies are a signature of supra subduction zone magmatism or of contamination by continental crust derived from supra subduction, as is the enrichment of LREEs (Sun and McDonough, 1989; Kerrich et al., 2005; Tatsumi, 2005; Mansur et al., 2021). As Titan has likely seen only small amounts of crustal assimilation, the negative Nb and Ti anomalies are more likely indicative of supra subduction source (Sun and McDonough, 1989; Kerrich et al., 2005). Comparing Titan's REE signature to two subduction zone settings; oceanic and continental arc rocks, a similar Nb anomaly can be observed (Fig. 5.13; Kerrich et al., 2005; Murphy, 2007; Keleman et al., 2014). On average Titan is more LREE enriched and HREE depleted, with a more negative Ti anomaly than either arc signature (Fig. 5.13). In either case, Titan appears more similar to arc rocks then to OIBs, with a hydrous magma associated with subduction zone also consistent with the amount of primary hornblende observed in thin section (Murphy, 2007). In the absence of evidence for extensive contamination, the HFSE anomalies are likely the result of supra-subduction zone processes.

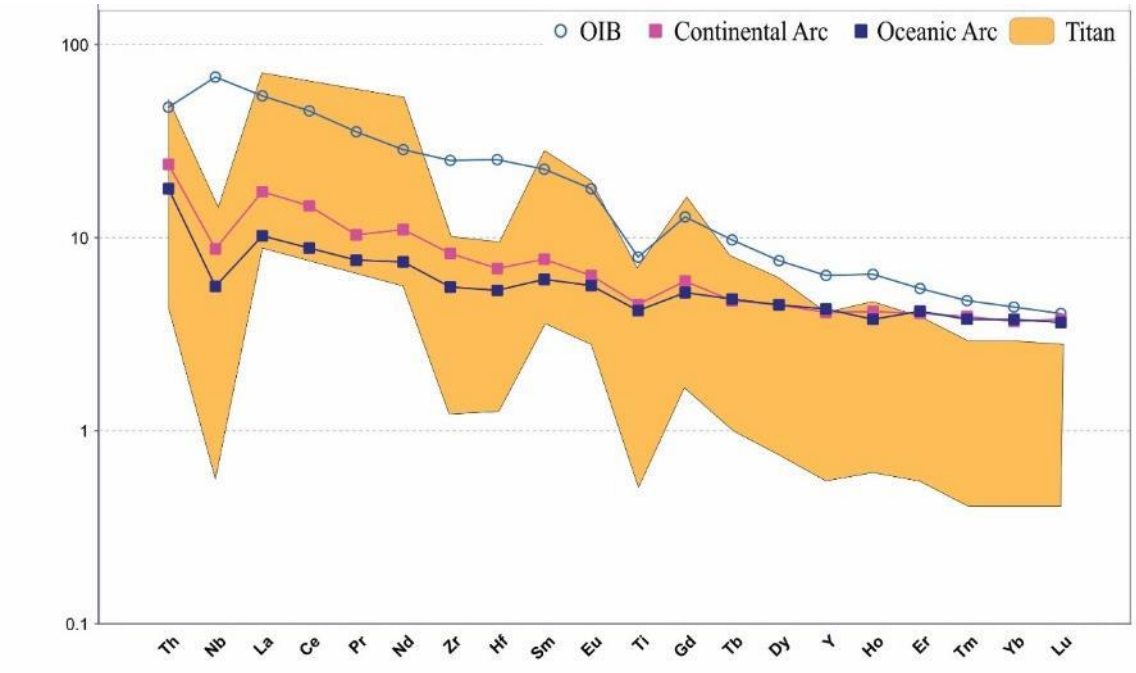

Figure 5.13. Primitive mantle normalized spider plot, showing representative values for oceanic island basalts (OIB), continental arc, oceanic arc, and the span of values for Titan. Concentrations normalized to primitive mantle (Sun and McDonough, 1989). OIB from Sun and McDonough (1989), continental and oceanic arcs from Kelemen et al. (2014).

The possibility of an arc setting can be evaluated in the context of the larger Winnipeg River terrane to help discern if this idea holds in the larger, regional context. The Titan intrusion lies within the Winnipeg River terrane, which is comprised primarily of Neoarchean plutonic rocks (Percival et al., 2006). Specifically, Titan lies near the boundary between the Winnipeg River and Marmion terranes, a boundary which is not well-defined (Tomlinson et al., 2004). The collision between the Marmion and Winnipeg River terranes is interpreted to have occurred between 2.93-2.92 Ga, and likely brought about a period of magmatism at 2.90 Ga due to crustal thickening (Tomlinson et al., 2004). Continental arc magmatism resurges in the Winnipeg River, Marmion, and western Wabigoon terranes from ~2.74-2.69 Ga, as a result of subduction along its margins (Tomlinson et al., 2004). Titan's age is consistent with the end of this period of

magmatism, and its position near the boundary between the Marmion and Winnipeg River terranes indicates that a subduction zone tectonic setting is consistent with the regional setting.

5.3 Sulphide saturation history

Sulphides are ubiquitous throughout Titan, though at generally small percentages (≤ 3%). The majority of this is pyrite, while pyrrhotite, pentlandite, and chalcopyrite are generally rare within the intrusion (Fig. 5.14). Pyrite is the most common sulphide present in Titan, occurring as very fine-grained, blebby, and commonly with a rim of magnetite (Fig. 4.11). Where pyrrhotite, pentlandite, and chalcopyrite are observed, they form relatively large aggregates, while still being very fine-grained, and are euhedral to subhedral (Fig. 4.11). Pyrrhotite, pentlandite, and chalcopyrite are base metal sulphides and crystallize directly from either one or a combination of monosulphide and intermediate solid solutions (MSS and ISS respectively; Barnes and Lightfoot, 2005; Duran et al., 2016; Mansur et al., 2021). The presence of base metal sulphides indicates that Titan's magma became saturated in sulphide during its emplacement, though the mechanism for reaching saturation is unclear based on petrographic evidence alone (Barnes et al., 2016; Mansur et al., 2021). Early sulphide saturation does not explain the abundance of pyrite observed in Titan. Pyrite is a common sulphide in a variety of ore deposits, but is much less common in magmatic Ni-Cu-PGE deposits (Duran et al., 2015). In magmatic Ni-Cu-PGE deposits, pyrite can exsolve from S-rich MSS, usually as euhedral grains, though this process is not common due to the amount of sulphur required (Duran et al., 2015; Mansur et al., 2021). The other processes of pyrite formation occur during post-cumulus re-equilibration or precipitation from hydrothermal or metamorphic

fluids, where it is likely to replace pre-existing pyrrhotite (Duran et al., 2015; Holwell et al., 2017; Mansur et al., 2021). In deposits that have undergone hydrothermal alteration, magnetite and hydrous silicate minerals such as chlorite, talc, and actinolite are often found in association with the pyrite (Holwell, et al., 2017; Mansur et al., 2021). Magnetite can also replace pyrrhotite during oxidation, indicating that in the right hydrothermal environment it could be forming from the replacement of pyrrhotite and precipitation from fluids (Barnes and Lightfoot, 2005; Holwell et al., 2017; Mansur et al., 2021). In hydrothermal deposits, these altered pyrite grains often occur with millerite and chalcopyrite (Holwell et al., 2017). In Titan's case, no millerite was observed, though chalcopyrite often occurs as an inclusion within pyrite grains or in very close proximity (Figs. 4.11; 4.22). Additionally, no direct association is observed between the pyrite grains in Titan and chlorite or actinolite, though alteration minerals are abundant throughout the thin sections. Magnetite is observed as rims or in close proximity to many of Titan's pyrite grains (Figs. 4.11; 4.22). As such, the pyrite at Titan is unlikely to be magmatic in origin and appears to have occurred through hydrothermal processes.

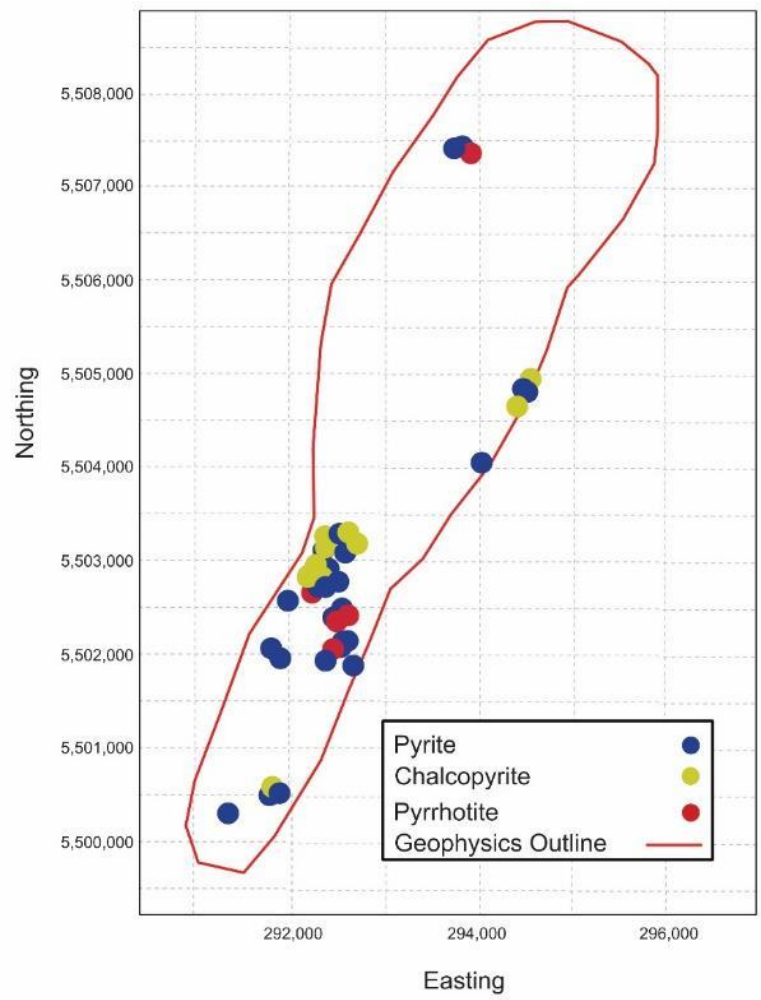

Figure 5.14. Map of the Titan intrusion showing the sulphides found in thin sections. Note that samples with pyrrhotite also have chalcopyrite and pyrite present, and samples with chalcopyrite also have pyrite present.

Given the presence of sulphides in the Titan intrusion, there is likely to be a source of sulphur within the intrusive plumbing system. In situ sulphur isotopes were gathered from pyrite and chalcopyrite to better constrain the origin and history of sulphur in Titan's history. Samples with pyrrhotite and pentlandite were not analyzed due to the limited number of grains available for analysis, though future work in this area would be beneficial. Sulphur isotope values obtained from in situ analyses ($\Delta^{33}S$ and $\delta^{34}S$) can be used to try to constrain the source of sulphur (Farquhar et al., 2010). The range of both S

isotopes has varied with time, due to a change from mass-independent atmospheric processes to mass-dependent processes (Farquhar and Wing, 2003; Farquhar and Wing, 2005; Seal, 2006). This transition is due to differences in the terrestrial sulphur cycle, atmospheric chemistry, and atmospheric content, and consists of a rather abrupt change at 2.45 Ga, likely due to the development of an oxygenated atmosphere (Farquar and Wing, 2005; Seal, 2006; Farquar et al., 2010) Pre-2.45 Ga, mass-independent atmospheric sulphur processes occurred, so that crustal $\Delta^{33}S$ values had a range greater than ± 0.5‰ (from -4 to +12‰), in contrast to crustal $\Delta^{33}S$ values after 2.45 Ga, which are consistently between -0.5 to +0.5‰ (Farquhar and Wing, 2003; 2005). In contrast, pre-2.45 Ga crustal $\delta^{34}S$ values had a smaller range, similar to that of mantle sulphur (0.0 ± 2.0‰VCDT), whereas after 2.45 Ga the range extends widely to anywhere between -60 to +80‰, but on average between -16 to +4‰ (Farquhar and Wing, 2003; 2005; Farquhar et al., 2010; Ripley and Li, 2003; Ripley et al., 2017). Additionally, variations in $\Delta^{33}S$ cannot be modified by equilibrium and kinetic fractionation reactions generated by metamorphic processes, whereas $\delta^{34}S$ can be more easily modified by these reactions, sulphur devolatilization, and hydrothermal alteration so that an originally magmatic $\delta^{34}S$ signature is modified (Baillie et al., 2010; Caruso et al., 2020).

Given what is known about the range of sulphur isotopes with time, Titan's small range of $\Delta^{33}S$ values (-0.26 to 0.1‰) is not consistent with the large range expected for Archean derived crustal sulphur (Appendix III; Farquhar and Wing, 2005; Farquhar et al., 2010; Djon, 2018). Titan's range of $\Delta^{33}S$ values indicates that the sulphur source was likely mantle derived, and therefore that mass-independent processes are not responsible

for the isotope composition (Fig. 5.15; Farquhar and Wing, 2003; 2005; Farquhar et al., 2010; Bekker et al., 2016). The range of mantle derived $\Delta^{33}S$ values is not as well constrained as it is for $\delta^{34}S$ values, with the most commonly used range being 0.00 ± 0.1‰ (Bekker et al., 2009; Benson et al., 2020). The majority of Titan's $\Delta^{33}S$ values fall within the mantle range and none are in the range of Archean crustal $\Delta^{33}S$ values (± 0.5‰) (Fig 5.15). This conclusion is somewhat supported by the $\delta^{34}S$ values, which together with the $\delta^{33}S$ values fall quite closely along the mass-fractionation line, indicating that mass-dependent processes are responsible for these values (Fig. 5.16).

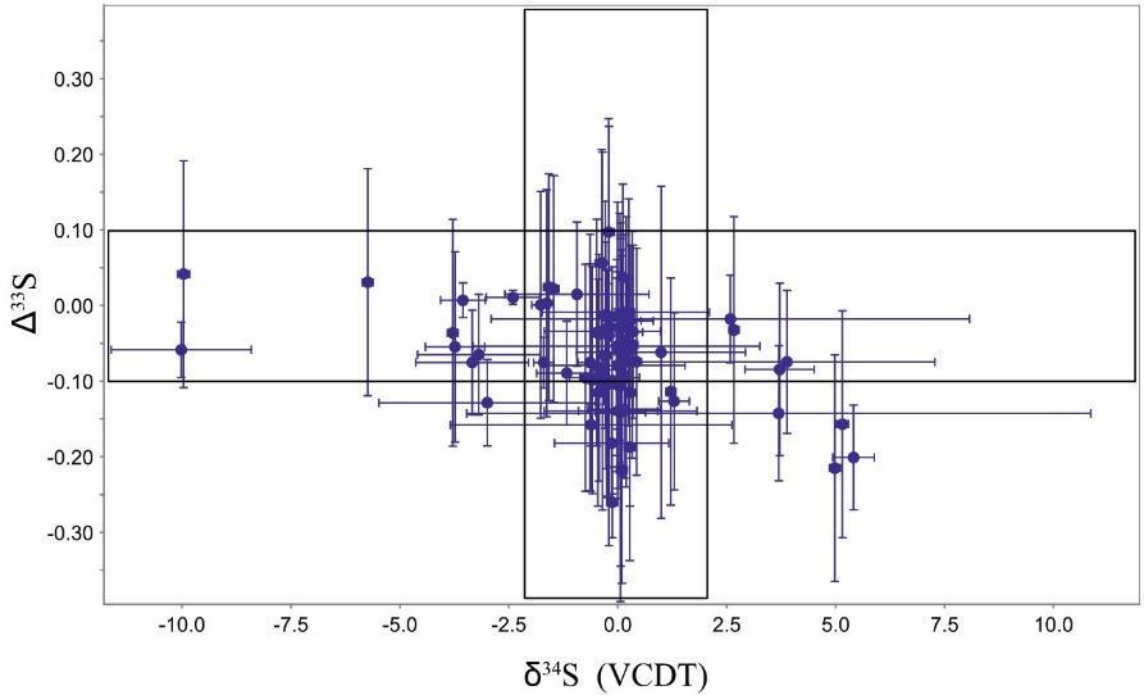

Figure 5.15. A bivariate diagram displaying $\Delta^{33}S$ vs $\delta^{34}S$ values, with sulphur values coming from in situ isotope work. Each point represents the average of all analysis points taken within a single sulphide grain. Error bars are 2σ. Mantle values for $\Delta^{33}S$ vs $\delta^{34}S$ are shown as boxes (Ripley and Li, 2003; Bekker et al., 2016).

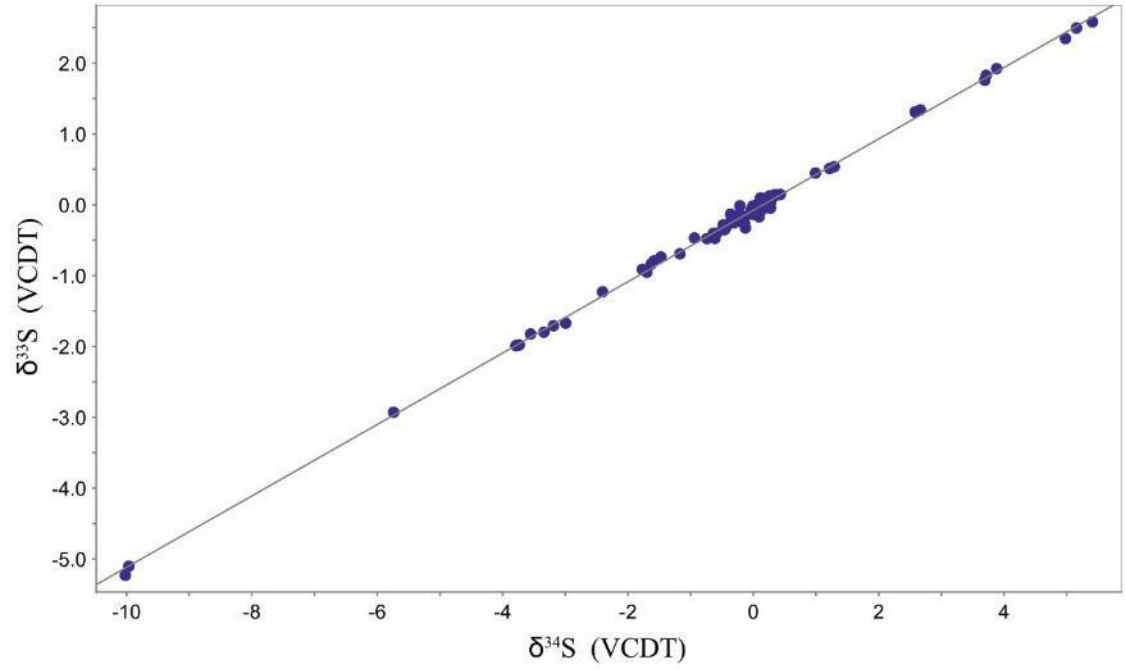

Figure 5.16. A bivariate diagram displaying $\delta^{33}S$ vs $\delta^{34}S$ for the Titan intrusion. The slope of the line is 0.5048, very close to the slope of the mass-fractionation line (0.515) (Seal, 2006).

There is a relatively large spread of $\delta^{34}S$ values (-10.02 to +5.41‰), which is not consistent with a mantle source, but is more consistent with post-2.45 Ga crustal sulphur values, which would record mass-dependent values (Appendix III; Fig. 4.23; Farquhar and Wing, 2003; 2005; Farquhar et al., 2010). The spread of Titan's $\delta^{34}S$ values divide into three populations, one within the mantle range, one below, and one above (Fig. 5.15). There is a slight preference for the centre of the intrusion for the samples with non-mantle values, however samples with mantle $\delta^{34}S$ values also occur in close proximity to these outlying samples so this trend seems more coincidental than systematic. Just as there is no strong spatial trend to the $\delta^{34}S$ values, there is also no difference in silicate association or sulphide habit between the outlying and mantle range samples. Altogether there is no way to predict which samples would give non-mantle $\delta^{34}S$ values based on spatial, lithological, or geochemical data. It is possible that the three $\delta^{34}S$ populations

observed represent different processes occurring in the intrusion, all preserved in samples occurring in close proximity to each other that have no distinguishing habit or occurrence to differentiate them, however this seems unlikely given the other geochemical data (Fig. 5.15).

Generally, $\delta^{34}S$ values outside of the mantle range are considered to be indicative of externally derived (crustal) sulphur (Li et al., 2002; Ding et al., 2012; Ripley and Li, 2013; Ripley et al., 2017). In Titan's case the source of any externally derived sulphur is ambiguous, given the limited amount of crustal contamination that appears to have occurred. Additionally, Archean-age, felsic basement rocks are unlikely to be responsible for the $\delta^{34}S$ values outside of the mantle range, though sulphur isotope data from the Roaring River complex and the surrounding basement rocks would be needed to assess this. Combined with the $\Delta^{33}S$ values, the $\delta^{34}S$ values for Titan do not seem to indicate externally derived sulphur, and are more consistent with a fluid source (Smith et al., 2016; Wernette et al., 2018; Caruso et al., 2019).

The pyrite observed at Titan seems to be the result of precipitation from a fluid rather then from the re-equilibration of base metal sulphides, given the lack of other common re-equilibration sulphides such as millerite and cubanite (Holwell et al., 2017; Mansur et al., 2021). The effect of hydrothermal fluids can be highly variable, depending on the composition, pH, oxygen fugacity, and temperature of the fluids, all of which can be affected by the source of the fluids and any interactions between the fluid and wall rock (Ohmoto, 1972; Ripley and Li, 2007; Wernette et al., 2018; Caruso et al., 2019). The crystallization of pyrite at low temperatures (<400 °C) can cause large fractionation between oxidized and reduced S species and fractionate $\delta^{34}S$ in a positive or negative

direction out of mantle range without any addition of S (Smith et al., 2016; Wernette et al., 2018; Caruso et al., 2019). Additionally, the oxygen fugacity and pH of the fluids could cause relatively large variations in $\delta^{34}S$ within a heterogenous fluid system (Ohmoto, 1972; Smith et al., 2016; Caruso et al., 2019). It is therefore possible that a fluid system could have produced the variety of $\delta^{34}S$ values while keeping a fairly strong mantle $\Delta^{33}S$ signature, within fluid derived pyrite grains (Ohmoto, 1972; Smith et al., 2016; Wernette et al., 2018; Caruso et al., 2019).

In addition to in situ sulphur isotopes, laser ablation data was collected from pyrite, and a select few chalcopyrite grains (Appendix IV). The amount of chalcopyrite analyses was limited by their small grain size, and therefore is generally insufficient to draw meaningful conclusions from. In six of the 44 pyrite grains, there was some zonation observed in Ni and Co concentrations, which was not observed petrographically. This zonation only occurred in Ni and Co content, and did not appear to have any strong effect on other elements analyzed. This indicates a possible change in source for a minority of the grains observed, possibly as a result from a changing fluid system (Li et al., 2018). Similar zoning has been found in pyrite from other deposits, though it often includes zonation of platinum group elements which was not observed in the sulphides analyzed (Duran et al., 2015).

The laser ablation results can be used in conjunction with whole rock geochemistry in order to constrain magmatic and post-magmatic processes, using S/Se ratios from mineral analyses and Cu/Pd ratios from whole rock data. Sulphur/Se ratios have a constrained mantle range (2,632-4350) and both S and Se behave differently in the mantle and during hydrothermal alteration (Eckstrand and Hulbert, 1987; Queffurus and

Barnes, 2015; Smith et al., 2016; Brzozowski et al., 2020). Sulphur-undersaturated primary magmas typically have Cu/Pd ratios similar to that of the mantle, which is 1,000 to 10,000 (Barnes et al., 1993; Barnes et al., 2015). Titan's S/Se ratio ranges from 4,080 to 215,624, with an average of 46,122, and is therefore generally much higher than the mantle range. Titan's Cu/Pd ratios range from 50-350,000, with an average of 61,000, indicating that the primary magma was sulphur-saturated and that some of the sulphide liquid was lost at depth (Fig. 5.17; Zhang et al., 2021). The moderate to high Cu/Pd and S/Se ratios, along with the exponential decrease in Se as S/Se increases suggests that Se loss is responsible for the high S/Se ratios (Fig. 5.17). Sulphur/Se ratios can be modified by low temperature hydrothermal alteration, metamorphism, and supergene weathering (Queffurus and Barnes, 2015; Smith et al., 2016). In hydrothermal systems, S is generally more mobile than Se, unless the fluid is saline, acidic, and highly oxidizing (Prichard et al., 2013; Smith et al., 2016).

All together, it appears that some amount of magmatic sulphides formed, but the majority of sulphides were precipitated from low temperature hydrothermal fluids, likely under oxidizing conditions. The hydrothermal system affected $\delta^{34}S$ isotopes and mobilized Se but did not affect $\Delta^{33}S$. Further work on base metal sulphides (pyrrhotite, pentlandite, and chalcopyrite unassociated with pyrite) would be beneficial for understanding the initial magmatic stage of sulphides at Titan. Additionally, laser ablation work on magnetite may be able to correlate to the laser ablation work on pyrite to better constrain the hydrothermal system.

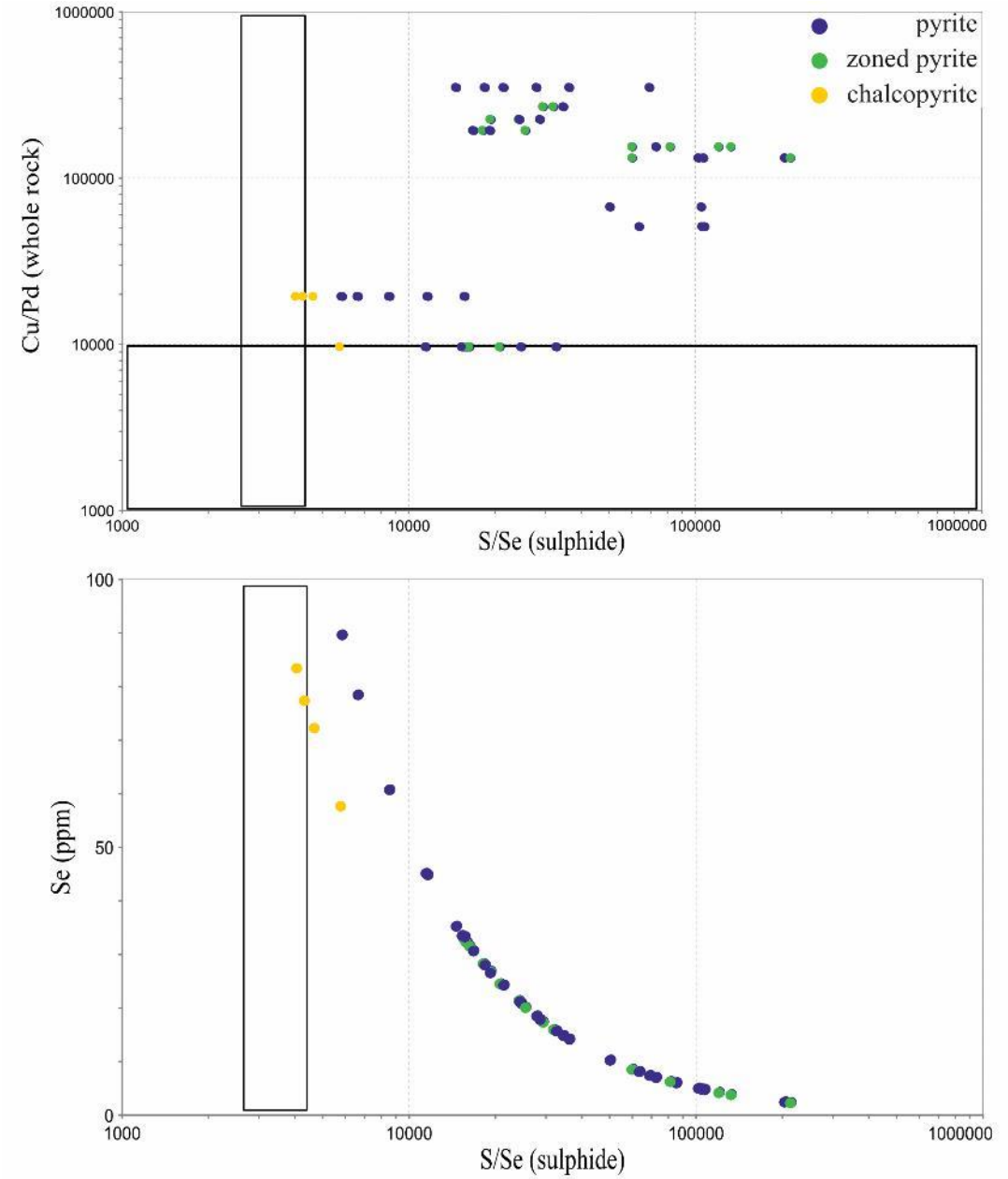

Figure 5.17. Bivariate plot of whole rock Cu/Pd (whole rock) vs laser ablation S/Se (sulphide) and Se (ppm) vs S/Se (sulphide), where the boxes represent the mantle range for both values (Brzozowski et al., 2020; Zhang et al., 2021).

5.4. Comparisons with the Lac des Iles Complex

The Titan intrusion lies within the Roaring River complex, in between the Garden Lake and Obonga Lake greenstone belts, north of the inferred boundary between the Winnipeg River and Marmion terranes (Figs. 2.2; 2.3; Stern and Hanson, 1991). The age

of Titan (2690 ± 3.2 Ma), its association with the sanukitoid Roaring River complex, the presence of sulphide mineralization, and its proximity to the border between terranes has broad similarities to the nearby Lac des Iles suite (Djon, 2018). The Lac des Iles suite is a series of mafic and ultramafic intrusions, occurring in a rough circle near the border between the Quetico and Marmion terranes, and is thought to be a continuation of a series of intrusions that stretch 200 km south-southwest into the southern Wabigoon and northern Quetico terranes (Fig. 2.3; Brugmann et al., 1997; Stone et al., 2003). The LDI suite is underlain by three Archean greenstone belts, is associated with sanukitoid lithologies, has variable levels of sulphide mineralization, and ranges in age from 2685.9 ± 1.6 to 2693.3 ± 1.3 Ma, a range that is roughly contemporaneous to Titan (Stone et al., 2003; Heaman and Easton, 2006; Hart and Macdonald, 2007; Djon, 2018). One of the greenstone belts, Garden Lake, lies just south of the Roaring River intrusion (Fig. 2.2; Ontario Geological Survey, 2000; 2018; Stone et al., 2003; Bowdidge, 2010). The broad regional similarities between Titan and the LDI suite, as well as the similarities in general lithologies make it a good point of comparison within the Superior Province.

Overall, the LDI suite is composed of both ultramafic and mafic lithologies, with the intrusions ranging in size from ~1 to 10 km (Stone et al., 2003). Titan is ~7 by 3 km in size, in the same range as the intrusions of the LDI suite (Stone et al., 2003; Bowdidge, 2010). Starting with the largest and most studied of the LDI suite, the LDI complex is commonly described as being composed of two different centers, an ultramafic body known as North LDI, and a mafic body, South LDI (Fig. 5.18; Brugmann et al., 1989; Lavigne and Michaud, 2001). South LDI has been divided into two intrusions, the Mine Block and Camp Lake intrusions (Fig. 5.18; Brugmann et al., 1989; Lavigne and

Michaud, 2001). The Mine Block intrusion is a texturally and lithologically complex gabbroic complex, with compositions ranging from mela- to leuco-gabbronorite, whereas the Camp Lake intrusion is a more homogenous hornblende gabbro (Lavigne and Michaud, 2001; Hinchey et al., 2003; Barnes and Gomwe, 2011). In both intrusions, altered chlorite-actinolite schist is also a major component, and is found throughout the intrusion (Brugmann et al., 1989; Hinchey et al., 2005; Barnes and Gomwe; 2011; Djon and Barnes, 2012). North LDI is composed of a cyclical layering of pyroxenites, wehrlite, websterite, and gabbronorite (Sutcliffe et al., 1988; Djon et al., 2017). Both the mafic and ultramafic bodies show a chaotic distribution of lithologies in outcrop (Lavigne and Michaud, 2001; Hinchey et al., 2003). In the gabbroic intrusions, outcrop relationships can range from well-defined intrusive contacts to diffuse, magma mingling textures, and wide-scale brecciation and pegmatitic pods have been observed (Lavigne and Michaud, 2001; Hinchey et al., 2003). In the ultramafic North LDI intrusion the presence of layering in outcrop is uncommon, despite the presence of cyclical layering throughout the entirety of North LDI (Lavigne and Michaud, 2001; Barnes and Gomwe; 2011).

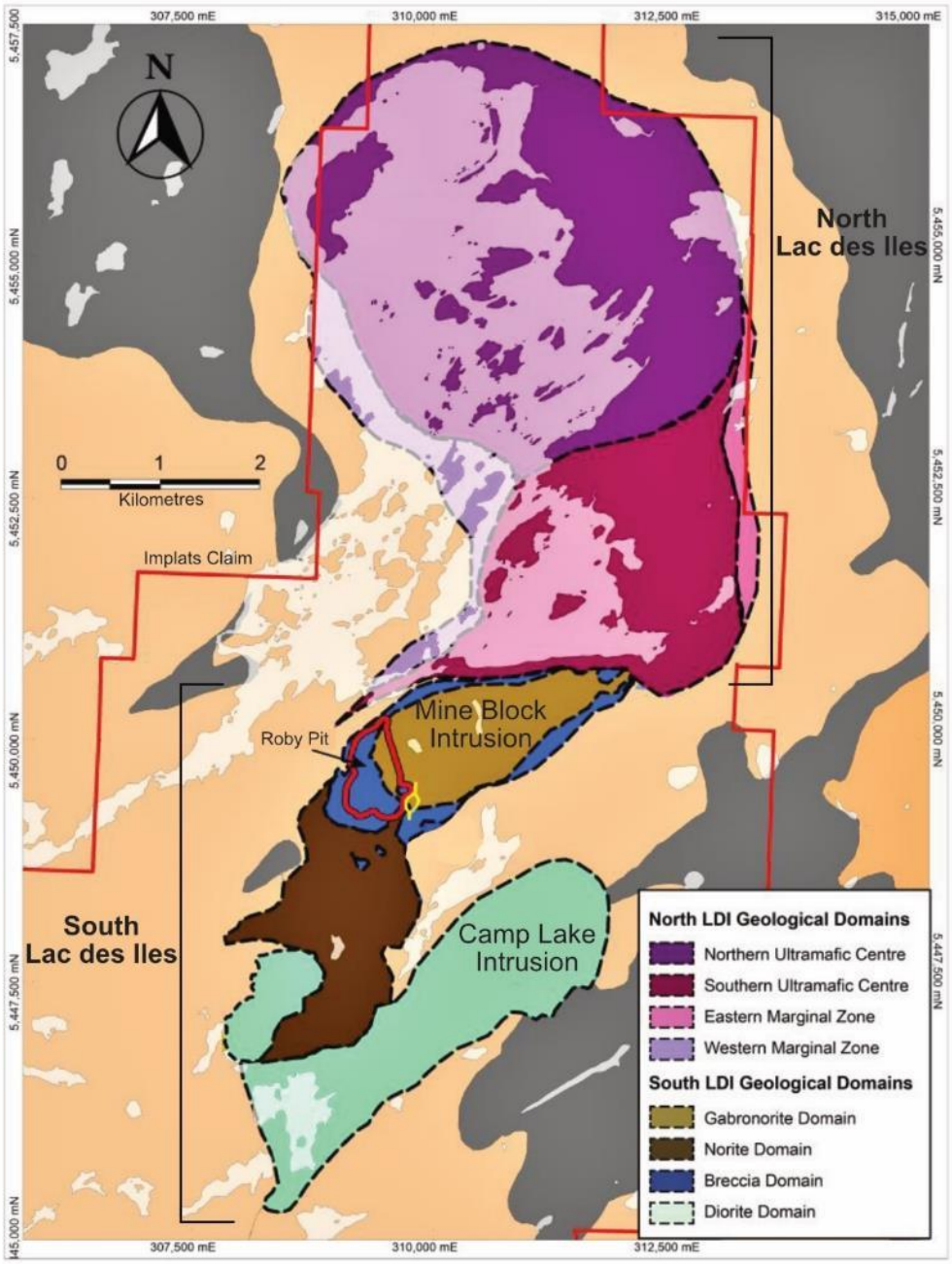

Figure 5.18. Geological map of the main Lac des Iles complex, highlighting the North LDI intrusion, and two South LDI intrusions—the Mine Block and Camp Lake intrusions. Modified from Peck and Djon (2020).

The other intrusions of the LDI suite; Buck Lake, Taman Lake, Dog River, and Tib Lake, are all smaller then the LDI complex, and each has its own unique lithology

and characteristics (Fig. 2.3). In similar fashion to Titan, outcrop exposure for each is highly variable and generally poor. Buck Lake is elongate and appears to be a single body composed of a majority of hornblende gabbro with lesser amounts of hornblendite, pyroxenite, and gabbro breccia, whereas intrusions like Dog River and Taman Lake are comprised of two to six smaller bodies, with a range of lithologies represented amongst them (Brickner, 2002; Stone et al., 2003). Tib Lake is the second largest of the LDI suite intrusions, and has been divided into four different zones, with each comprised of coarse-grained to pegmatitic gabbro, gabbronorite, hornblende gabbronorite, and hornblende gabbronorite with layers of magnetite-bearing gabbronorite respectively (Smith and Sutcliffe, 1986; Brickner, 2002; Stone et al., 2003). It is interpreted to have formed from two distinct magma pulses, with a gradation upwards from ultramafic cumulates near the base to magnetite-rich gabbro at the top (Smith and Sutcliffe, 1986; Brickner, 2002). All of the intrusions contain sulphides, though only the mafic centre of the LDI complex hosts economic concentrations (Brickner, 2002; 2002; Stone et al., 2003; Implats, 2021).

In general, the LDI suite intrusions have broad lithologic and metallogenic similarities, as well as similar age dates (2685.9 ± 1.6 to 2693.3 ± 1.3 Ma) which has led to their grouping together as a suite (Lavigne and Michaud, 2001; Heaman and Easton, 2006; Hart and Macdonald, 2007; Djon, 2018). Many of these broad similarities are also observed in Titan, particularly in terms of lithology, though there are differences. Titan is made up of both ultramafic and mafic lithologies, however, they do not appear to comprise separate mafic bodies, unlike the LDI complex, Dog River, and Taman Lake intrusions (Brugmann, 1997; Lavigne and Michaud, 2001; Brickner, 2002; Stone et al., 2003). The concentric zoning observed at Tib Lake or the cyclical layering at North LDI

is also not present at Titan (Brugmann, 1997; Lavigne and Michaud, 2001; Stone et al., 2003; Djon et al., 2017). However, the chaotic mix of lithologies seen at surface for the mafic LDI intrusions is somewhat reminiscent of what is observed at Titan, where the distribution of lithologies can range considerably over small (metre scale) distances. Other key components observed in the LDI outcrops, namely wide scale brecciation and pegmatites, have not been observed at Titan, though it is possible that these textures exist in unexposed areas (Lavigne and Michaud, 2001; Hinchey et al., 2005). Despite similarities in lithology, there are stark differences in geochemistry between Titan and the LDI complex, both in major and trace element behaviour (Figs. 5.19; 5.20). Figure 5.19 highlights how consistent the REE patterns of Titan are, as well as how much more enriched the LREEs are as well as the steeper slope for the HREEs, compared to LDI (Fig. 5.19). The negative Nb, Zr, and Hf anomalies are another large difference between the two intrusions (Fig. 5.20). Note that many of the LDI samples have a negative Nb anomaly, but it is obscured by the behaviour of the LREEs (Fig. 5.20). The range of REE behaviours occurring in LDI reflects the influence of multiple magma sources affecting each other, in contrast to Titan's single source. There are also differences in major element behaviour (Fig. 5.20). Titan has a larger spread of SiO_2 and TiO_2 values, excluding a small number of outliers in the LDI data (Fig. 5.20). Titan also has smaller $(La/Sm)_N$ and larger $(Gd/Yb)_N$ values then LDI, which goes along with the REE behaviour observed in the primitive normalized diagrams (Figs. 5.19; 20). The range of SiO_2 observed in Titan is likely indicative of the wide variety of lithologies and the large amount of each, while LDI has a variety of lithologies, but amounts vary due to brecciation (Fig. 5.20).

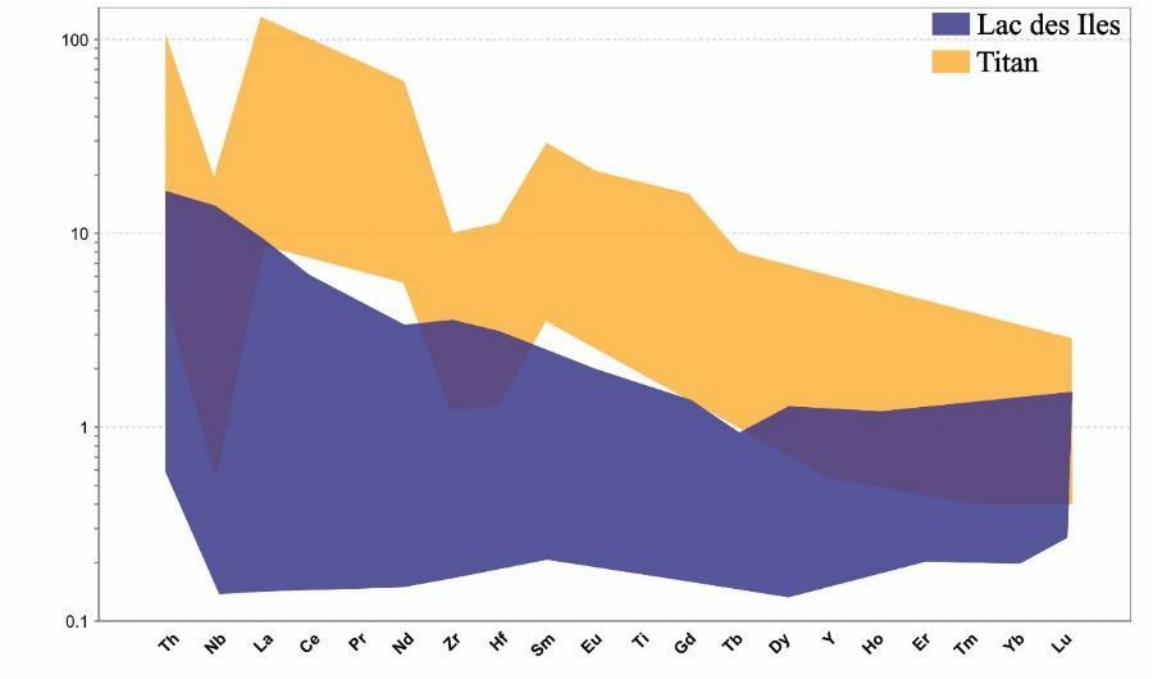

Figure 5.19. Primitive mantle normalized diagram of the full spread of values for Titan and the LDI complex. Titan values are from surface rocks, while the LDI values come from the Twilight, Roby, and Offset zones at depth (Peck, 2016). Normalizing values from Sun and McDonough (1989).

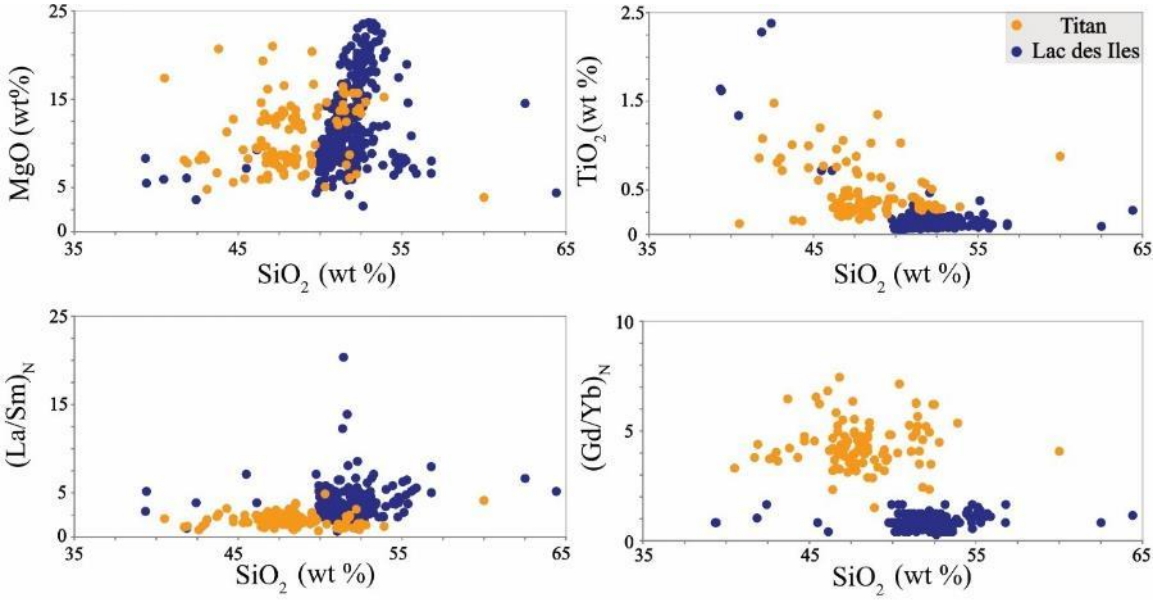

Figure 5.20. Bivariate plots of MgO, TiO_2, $(La/Sm)_N$ and $(Gd/Yb)_N$ vs SiO_2 for Titan (orange dots) and the LDI complex (blue dots). LDI data from Peck (2016).

The three intrusions that make up the LDI complex are separated by tonalitic country rock, which combined with the differing lithologies and presence of widespread breccias indicate a dynamic environment with multiple magmatic pulses (Lavigne and Michaud, 2001; Hinchey et al., 2005). The granitoid plutons surrounding or intruded by the LDI complex are roughly coeval to the complex, indicating that this dynamic environment included both felsic and mafic magmatism (Sutcliffe et al., 1989; Brugmann et al., 1997; Stone et al., 2003; Barnes and Gomwe, 2011). This contemporaneous mafic and felsic magmatism, and the potential mixing between the two has been argued to be the cause for many of the complicated textures observed in the complex (Sutcliffe, 1989; Djon et al., 2017). The widescale brecciation combined with the proximity to varitextured units and silicate alteration suggests a magma with dissolved fluids, at least within the two intrusions that make up the mafic south area of the LDI complex (Lavigne and Michaud, 2001; Hinchey et al., 2003).

The LDI complex, as well as the other intrusions of the suite, form funnel- and basin-shaped bodies, which differ from most PGE deposits which are more laterally extensive stratiform complexes, such as the Stillwater Complex or the Bushveld Complex (Gupta and Sutcliffe, 1990; Barnes and Gomwe, 2010.) The shape of the intrusions is consistent with multiple pulses of mantle-derived magma, where the surrounding granitoid plutons and magmatism prevented lateral spread in the mafic intrusion (Gupta and Sutcliffe, 1990). Various magma compositions have been suggested for the LDI complex, with differing tectonic settings. This has included both an E-MORB magma, and thus an oceanic setting, as well as a continental arc setting (Brugmann et al., 1997; Hinchey et al., 2005; Barnes and Gomwe, 2010). Currently, the continental arc setting is

favoured based on geochemical characteristics and regional context (Brugmann et al., 1997; Barnes and Gomwe, 2010; Djon et al., 2017). This is a similar interpretation to Titan, where a supra subduction zone setting is favoured for similar reasons.

In addition to geochemistry, Sm-Nd isotope analysis has been completed for both Titan and the LDI complex. In the LDI suite, Sm-Nd isotope work was done on rocks within the Mine Block intrusion, the ultramafic North LDI, gabbro, the Tib Lake intrusion, and tonalite surrounding the LDI complex (Brugmann et al., 1997). Overall, the complete range of ε_{Nd} across the entire suite is 0 to 2, though Tib Lake is consistently closer to 0 while North LDI is consistently around 1.5 (Brugmann et al., 1997). The tonalite surrounding the LDI complex has ε_{Nd} ranging from 0.3 to 2.0, while the country rock sample taken has a ε_{Nd} of -1.1 (Brugmann et al., 1997). In contrast, Titan and the Roaring complex have ε_{Nd} values ranging from 0.70 to 1.82, with the majority of the samples clustered from 1.14 to 1.82 (Appendix IV). The LDI complex and Tib Lake are interpreted to have assimilated country rock, but also possibly magmas associated with the surrounding tonalite (Brugmann et al., 1997). Titan appears to have assimilated less crustal material and lacks the range of possible sources proposed for LDI complex (Brugmann et al., 1997). Overall, Titan appears to have formed in a less dynamic environment than the LDI complex and assimilated less felsic material as a possible consequence.

Overall, there are similarities between Titan and the LDI suite. Many of these similarities are broad, considering regional characteristics which may indicate shared factors leading to the emplacement of these intrusions. There are also some similarities in lithology, with the LDI complex representing an even more complex and chaotic mix of

lithologies. However, there are also differences between the two, which geochemistry makes quite plain. Titan has a larger spread in SiO_2 and TiO_2 and differing $(La/Sm)_N$ and $(Gd/Yb)_N$ values, with a much tighter spread of REEs then the LDI complex (Figs. 5.20; 21). Both the LDI complex and Titan represent rocks formed in a supra subduction setting, however Titan appears to represent a single pulse of magma with a less complicated history than the LDI complex. As such while there are similarities between Titan and the LDI complex, these similarities do not necessarily indicate any deeper connection. The regional similarities likely indicate more about the processes occurring in this time period in the Superior Province, rather than indicating anything about the individual intrusions.

Table 5.1. Comparison Summary between Titan and the South LDI Complex

Intrusion	**Titan**	**South LDI Complex**
Age	2690 +/- 3.2	2689.0 +/- 1.0
Inferred tectonic setting	Supra-subduction	Supra-subduction
Terrane	Winnipeg River	Marmion
Intrusive breccias present	No	Yes
Number of dominant intrusive units	1	3 discrete mafic intrusions
Dominant primary silicate minerals	clinopyroxene, plagioclase, amphibole	plagioclase, orthopyroxene, clinopyroxene
Igneous layering present	No	No
Presence of primary clinopyroxene	Yes	yes, but much less than Titan
Presence of primary hornblende	Yes	No

Range of ε_{Nd}	0.70-1.82	0.0-1.9
Crustal contamination	minimal	moderate
Steepness of trace element pattern	La/Yb: 7.28-57	La/Yb: 1-21
Negative Zr anomaly	Yes, present	Variable
Range of Zr/Sm values	Zr/Sm: 1.53-23.35	Zr/Sm: 10-100
Negative Nb anomaly	Yes	Yes
Range of La/Nb values	La/Nb: 2.36-41.57	La/Nb: 0.3-19
Primary sulfide minerals present	chalcopyrite, pyrrhotite	pyrrhotite, pentlandite, chalcopyrite
Presence of secondary pyrite	Yes	Yes
Sulphur isotope conclusion	Small amount primary S, currently majority low temperature hydrothermal	magmatic, primary S. Possibly some redistribution by fluids
Range of δ34 S values	-10.02-5.41	-0.5-1.5
Ni/Cu ratio for those samples with greater than 100 ppm Cu	Ni/Cu: 0.28-4.8	Ni/Cu: 0.42-27.3
Pd/Pt ratio for those samples with greater than 50 ppb Pd	Pd/Pt: 0.99-4.1	Pd/Pt: 2-29.33

(Brugmann et al., 1997; Stone et al., 2003; Heaman and Easton, 2006; Hart and Macdonald, 2007; Duran et al., 2015; Peck, 2016; Djon, 2018)

6. Conclusions

The objective of this study was to characterize the Titan intrusion and compare it to the nearby LDI suite. The work to characterize the intrusion consisted of petrographic analyses, whole rock geochemistry analyses, Sm-Nd radiogenic isotopes, sulphur isotopes, and laser ablation analyses of sulphides.

Overall, Titan consists of cumulate leucogabbro, melagabbro, gabbro, and pyroxenite lithologies, which are distributed across the intrusion. The intrusion includes both mafic and felsic dikes, as well as felsic breccias. Hornblende is common and is interpreted to be a primary mineral based on occurrence and habit. The cumulate habit and chaotic distribution of the lithologies within Titan is consistent with one large mafic body, with a closed magmatic system where fractional crystallization is the main mechanism of formation (Shahabi Far et al., 2019). The presence of hornblende indicates that the primary magma was hydrous (Murphy, 2007). The samples are consistently altered, with the main alteration minerals consisting of actinolite, tremolite, sericite, chlorite, and epidote. Sulphides and Fe-oxides are ubiquitous across the intrusion, though at generally low abundances (~3%). The sulphides consist mainly of pyrite, with lesser amounts of pyrrhotite, chalcopyrite, and pentlandite, while the Fe-oxides mainly consist of magnetite, with lesser amounts of ilmenite. Overall, there is no suggestion of widespread layering of the magnetite, nor was any layering observed in any of the outcrops, which is again consistent with a single large magma chamber (Wiebe and Snyder, 1993; Nebel et al. 2013).

In terms of geochemistry, the major element data forms a continuous span with large degrees of scatter. There is some correlation between geochemistry and petrography, but not enough to use geochemistry as the sole proxy for lithology. In terms of REEs, the primitive mantle normalized diagrams for Titan are extremely similar, with consistent LREE enrichment, HREE fractionation, and strongly negative Nb and Ti anomalies. The smooth trend of the major element data and the consistent spread of REE data is consistent with fractional crystallization of a single magma chamber, with no disruption from subsequent magma pulses.

Together, the geochemical and radiogenic isotope data indicate that small amounts of crustal material was assimilated into Titan. The two most likely sources of contamination are the surrounding Roaring River complex or the tonalite and granodiorite basement rocks in the area. Neither the geochemical and radiogenic isotope data were able to determine if Roaring River is a contaminant due to similarities in REE values and ε_{Nd} values. It is more likely that small amounts of the Archean tonalite basement rocks were incorporated into both the Roaring River complex and Titan, though the possibility of Titan assimilating some material from Roaring River still exists. The geochemical data supports Titan having formed in a supra subduction zone setting, which is consistent with the REE data, particularly the enrichment of the LREEs and strongly negative Nb and Ti anomalies. This setting is also consistent with the regional context of the Winnipeg River and Marmion terranes, with Titan near the boundary between these two terranes (Tomlinson et al., 2004; Percival et al., 2006).

In terms of sulphides, there appear to be at least two generations within Titan. The first is magmatic base metal sulphides, which are generally rare across the samples. The

second is fluid derived, and mostly consists of the pyrite found in samples. The pyrite, and often accompanying magnetite, appears to have formed through precipitation in a hydrothermal environment (Duran et al., 2015; Holwell et al., 2017; Mansur et al., 2021). The hydrothermal system was likely a low temperature (<400 °C) system, which would cause fractionation within $\delta^{34}S$ values and cause a wide variety of $\delta^{34}S$ values (Smith et al., 2016; Wernette et al., 2018; Caruso et al., 2019). This low temperature hydrothermal system could have also caused the increased mobility of Se, provided that the fluid had suitable oxidizing conditions (Prichard et al., 2013; Smith et al., 2016).

In general, there are some broad similarities between Titan and the LDI suite, which include regional context, general lithology, and their respective ages. However, overall Titan appears to be less complicated than the intrusions of similar size in the LDI suite. Titan consists of a single magma body, without any systematic zoning or layering as observed in Tib Lake or North LDI (Brugmann, 1997; Lavigne and Michaud, 2001; Stone et al., 2003; Djon et al., 2017). In terms of geochemistry, Titan has a much more homogenous geochemical signature consistent with a single magma body compared to the more complicated bodies and magma history seen in the LDI suite. In summary while there are definitely similarities between Titan and the LDI suite, overall Titan appears to have a less complicated formation history.

References

Bailie, R., Gutzmer, J., Strauss, H., Stüeken, E., McClung, C., 2010. Sulfur isotope characteristics of metamorphosed Zn-Cu volcanogenic massive sulfides in the Areachap Group, Northern Cape Province, South Africa. Miner Deposita, vol. 45, p. 481-496.

Barnes, S.-J., Couture, J.-F., Sawyer, E.W., Bouchaib, C., 1993. Nickel-Copper Occurrences in the Belleterre-Angliers Belt of the Pontiac Subprovince and the Use of Cu-Pd Ratios in Interpreting Platinum-Group Element Distributions. Economic Geology, vol. 88, p. 1402-1418.

Barnes, S.J., Cruden, A.R., Arndt, N., Saumur, B.M., 2016. The mineral system approach applied to magmatic Ni-Cu-PGE sulphide deposits. Ore Geology Reviews, vol. 76, p. 296-316.

Barnes, S.-J., Gomwe, T.S., 2010. Composition of the Lac des Iles Magma and Implications for the Origin of the Ore. Ontario Geological Survey, Miscellaneous Release-Data 269, 11th International Platinum Symposium.

Barnes, S.-J., Gomwe, T.S., 2011. The Pd Deposits of the Lac des Iles Complex, Northwestern Ontario. Reviews in Economic Geology, vol. 17, p. 351-370.

Barnes, S.-J., Lightfoot, P.C., 2005. Formation of magmatic nickel-sulfide ore deposits and processes affecting their copper and platinum-group element contents. *In* Hedenquist, J.W., Thompson, J.F.H., Goldfarb, R.J. and Richards, J.P. (eds.) Economic Geology 100th Anniversary Volume, p. 179-213.

Barnes, S.J., Mungall, J.E., Maier, W.D., 2015. Platinum group elements in mantle melts and mantle samples. Lithos, vol. 232, p. 395-417.

Barr, C., 2003. Report on Soil Geochemical Survey, Roaring River Property, NTS 52H/12, Northwestern Ontario for North American Palladium Ltd., Lac des Iles Mine Ltd., assessment report 2.25956.

Barr, C., 2003. Summary of 2003 Work, Roaring River Property, NTS 52H/12, Northwestern Ontario for North American Palladium Ltd., Lac des Iles Mine Ltd., assessment report 2.26728.

Barton, M., Van Gaans, C., 1988. Formation of orthopyroxene-Fe-Ti-oxide symplectites in Precambrian intrusives, Rogaland, southwestern Norway. American Mineralogist, vol. 73, p. 1046-1059.

Bekker, A., Barley, M.E., Fiorentini, M.L., Rouxel, O.J., Rumble, D., Beresford, S.W., 2009. Atmospheric Sulfur in Archean Komatiite-Hosted Nickel Deposits. Science, vol. 326, p. 1086-1088.

Bekker, A., Grokhovskaya, T.L., Hiebert, R., Sharkov, E.V., Bui, T.H., Stadnek, K.R., Chashchin, V. V., Wing, B.A., 2016. Multiple sulfur isotope and mineralogical constrains on the genesis of Ni-Cu-PGE magmatic sulfide mineralization of the Monchegorsk Igneous Complex, Kola Peninsula, Russia. Miner Deposita, vol. 51, p. 1035-1053.

Benson, E.K., Ripley, E.M., Li, C., Underwood, B.W., Mahin, R., 2020. Multiple S Isotopes and S Isotope Heterogeneity at the East Eagle Ni-Cu-Platinum Group Element Deposit, Northern Michigan. Economic Geology, vol. 47 (7), p. 1-16.

Bethune, K.M., Helmstaedt, H.H., McNicoll, V.J., 2006. Structural analysis of the Miniss River and related faults, western Superior Province: post-collisional displacement initiated at terrane boundaries. Canadian Journal of Earth Sciences, vol. 43, p. 1031-1054.

Boutroy, E., Dare, S.A.S., Beaudoin, G., Barnes, S-J., Lightfoot, P., 2014. Magnetite composition in Ni-Cu-PGE deposits worldwide: application to mineral exploration. Journal of Geochemical Exploration, vol. 145, p. 64-81.

Bowdidge, C., 2010. Report on an airborne magnetic and VTEM electromagnetic survey for Ringbolt Ventures Ltd. Ontario Geological Survey, Open File Report 10039, p. 1-19.

Brickner, R., 2002. Report of Exploration on Buck Lake Property, Lac des Iles Area, Northwestern Ontario, Buck Lake Ventures, Ltd.. Assessment Report, Reference No. 2.25151.

Brickner, R., 2002. Report of Exploration on Tib Lake Property, Lac des Iles Area, Northwestern Ontario, Buck Lake Ventures Ltd.. Assessment Report, Reference No. 2.23721.

Brugmann, G.E., Naldrett, A.J., Macdonald, A.J., 1989. Magma Mixing and Constitutional Zone Refining in the Lac des Iles Complex, Ontario: Genesis of Platinum-Group Element Mineralization. Economic Geology, vol. 84, p. 1557-1573.

Brugmann, G.E., Reischmann, T., Naldrett, A.J., Sutcliffe, R.H., 1997. Roots of an Archean volcanic arc complex: the Lac des Iles area in Ontario, Canada. Precambrian Research, vol. 81, p. 223-239.

Brzozowski, M. J., Samson, I. M., Gagnon, J. E., Good, D. J., Linnen, R. L., 2020. On the Mechanisms for Low-Sulfide, High-Platinum Group Element and High-Sulfide, Low-Platinum Group Element Mineralization in the Eastern Gabbro, Coldwell Complex, Canada: Evidence from Textural Associations, S/Se Values, and Platinum Group Element Concentrations of Base Metal Sulfides. Economic Geology, vol. 115 (no. 2), p. 355-384.

Card., K.D., Ciesielski, A., 1986. Subdivisions of the Superior Province of the Canadian Shield. Geoscience Canada, vol. 13, p. 5-13.

Caruso, S., Fiorentini, M.L., Barnes, S.J., LaFlamme, C.K., Martin, L.A.J., 2020. Microchemical and sulfur isotope constraints on the magmatic and hydrothermal evolution of the Black Swan Succession, Western Australia. Mineralium Deposita, vol. 55, p. 535-553.

Cox, K., Bell, J., Pankhurst, R., 1979. The interpretation of igneous rocks. Allen and Unwin, London, p. 528.

DePaolo, D.J., 1981. Neodymium isotopes in the Colorado Front Range and crust-mantle evolution in the Proterozoic. Nature, vol. 291, p. 193-196.

Dickin, A.P., 2005. Radiogenic Isotope Geology. Cambridge University Press, p. 70-101.

Ding, T., Valkiers, S., Kipphardt, H., De Bièvre, P., Taylor, P. D. P., Gonfiantini, R., &Krouse, R., 2001. Calibrated sulfur isotope abundance ratios of three IAEA sulfur isotope reference materials and V-CDT with a reassessment of the atomic weight of sulfur. Geochimica et Cosmochimica Acta, vol. 65 (15), p. 2433–2437.

Ding, X., Ripley, E.M., Shirey, S.B., Li, C., 2012. Os, Nd, O, and S isotope constraints on country rock contamination in the conduit-related Eagle Cu-Ni-(PGE) deposit, Midcontinent Rift System, Upper Michigan. Geochimica et Cosmochimica Acta, vol. 89, p. 10-30.

Djon, L., 2018. Lac des Iles geochronology data. Unpublished data, Impala Canada.

Djon, M.L., Barnes, S-J., 2012. Changes in sulfides and platinum-group minerals with the degree of alteration in the Roby, Twilight, and High Grade Zones of the Lac des Iles Complex, Ontario, Canada. Miner Deposita, vol. 48, p. 875-896.

Djon, M.L., Olivo, G.R., Miller, J.D., Peck, D.C., Joy, B., 2017. Stratiform platinum-group element mineralization in the layered Northern Ultramafic Center of the Lac des Iles Intrusive Complex, Ontario, Canada. Ore Geology Reviews, vol. 90, p. 697-722.

Duran, C.J., Barnes, S-J., Corkery, J.T., 2015. Chalcophile and platinum-group element distribution in pyrite from the sulfide-rich pods of the Lac des Iles Pd deposits, Western Ontario, Canada: Implications for post-cumulus re-equilibration of the ore and the use of pyrite compositions in exploration. Journal of Geochemical Exploration, vol. 158, p. 223-242.

Duran, C.J., Barnes, S-J., Corkery, J.T., 2016.Geology, petrography, geochemistry, and genesis of sulfide-rich pods in the Lac des Iles palladium deposits, western Ontario, Canada. Miner Deposita, vol. 51, p. 509-532.

Duran, C.J., Barnes, S-J., Corkery, J.T., 2016. Trace element distribution in primary sulfides and Fe-Ti oxides from the sulfide-rich pods of the Lac des Iles Pd deposits, Western Ontario, Canada: Constraints on processes controlling the composition of the ore and the use of pentlandite compositions in exploration. Journal of Geochemical Exploration, vol. 166, p. 45-63.

Eckstrand, O.R., Hulbert, L.J., 1987. Selenium and the source of sulfur in magmatic nickel and platinum deposits. Geological Associations of Canada-Mineralogical Association of Canada (GAC-MAC) Saskatoon, Canada, May 25-27, 1987, Abstracts.

Essaifi, A., Capdevila, R., Fourcade, S., Lagarde, J.L., Ballèvre, M., Marignac, CH., 2004. Hydrothermal alteration, fluid flow, and volume change in shear zones: the layered mafic-ultramafic Kettara intrusion (Jebilet Massif, Variscan belt, Morocco). Journal of Metamorphic Geology, vol. 22, p. 25-43.

Farquhar, J., Wing, B.A., 2003. Multiple sulfur isotopes and the evolution of the atmosphere. Earth and Planetary Science Letters, vol. 213, p. 1-13.

Farquhar, J., Wing, B.A., 2005. The terrestrial record of stable sulphur isotopes: a review of the implications for evolution of Earth's sulphur cycle. Mineral Deposits and Earth Evolution, vol. 248, p. 167-177.

Farquhar, J., Wu, N., Canfield, D., &Oduro, H., 2010. Connections between sulfur cycle evolution, sulfur isotopes, sediments, and base metal sulfide deposits. Economic Geology, vol. 105, p. 509–533.

Fingler, J. and McCrindle, W., 2001. Exploration Report, Berland Resources Ltd., Roaring River Property, Ontario, NTS 52H, Assessment report, Reference No. 2.22861.

Fletcher, J.M., Stephens, C.J., Petersen, E.U., Skerl, L., 1997. Greenschist Facies Hydrothermal Alteration of Oceanic Gabbros: A Case Study of Element Mobility

and Reaction Paths. In Proceedings of the Ocean Drilling Program: Scientific Results, vol. 153, p. 389-398.

Gélinas, L., Mellinger, M., Trudel, P., 1982. Archean mafic metavolcanics from the Rouyn-Noranda district, Abitibi greenstone belt, Quebec. 1. Mobility of the major elements. Canadian Journal of Earth Sciences, vol. 19, p. 2258-2275.

Gupta, V.K., Sutcliffe, R.H., 1990. Mafic-ultramafic intrusives and their gravity field: Lac des Iles area, northern Ontario. Geological Society of America Bulletin, vol. 102, p. 1471-1483.

Halla, J., 2005. Late Archean high-Mg granitoids (sanukitoids) in the southern Karelian domain, eastern Finland: Pb and Nd isotopic constraints on crust-mantle interactions. Lithos, vol. 79, p. 161-178.

Hart, T.R., MacDonald, C.A., 2007. Proterozoic and Archean geology of the Nipigon Embayment: implications for emplacement of the Mesoproterozoic Nipigon diabase sills and mafic to ultramafic intrusions. Canadian Journal of Earth Sciences, vol. 44, p. 1021-1040.

Heaman, L.M. and Easton, R.M., 2006. Preliminary U/Pb geochronology results: Lake Nipigon Geoscience Initiative. Ontario Geological Survey, Miscellaneous Release – Data 191.

Heerema, D., 2004. Report on Surface Diamon Drilling, Roaring River Property, NTS 52H/12, Northwestern Ontario for North American Palladium Ltd., Lac des Iles Mine Ltd., assessment report 2.28328.

Hinchey, J., Hattori, K.H., Lavigne, M.J., 2003. Preliminary Report of Field Descriptions and Contact Relationships of Lithological Units in the South Roby and Twilight Zones, Lac des Iles Deposit, Northwestern Ontario. Ontario Geological Survey, Open File Report 6107, p. 1-16.

Hinchey, J.G., Hattori, K.H., 2005. Magmatic mineralization and hydrothermal enrichment of the High Grade Zone at the Lac des Iles palladium mine, northern Ontario, Canada. Mineralium Deposita, vol. 40, p. 13-23.

Hinchey, J.G., Hattori, K.H., Lavigne, MJ., 2005. Geology, Petrology, and Controls on PGE mineralization of the Southern Roby and Twilight Zones, Lac des Iles Mine, Canada. Economic Geology, vol. 100, p. 43-61.

Holwell, D.A., Adeyemi, Z., Ward, L.A., Smith, D.J., Graham, S.D., McDonald, I., Smith, J.W., 2017. Low temperature alteration of magmatic Ni-Cu-PGE sulfides as a source for hydrothermal Ni and PGE ores: A quantitative approach using automated mineralogy. Ore Geology Reviews, vol. 91, p. 718-740.

Implats, 2021. Mineral Resource and Mineral Reserve Statement. https://www.implats.co.za/mineral-resources-and-reserves.php

Kelemen, P.B., Hanghøj, K., Greene, A.R., 2014. One View of the Geochemistry of Subduction-Related Magmatic Arc, with an Emphasis on Primitive Andesite and Lower Crust. Treatise on Geochemistry, vol. 4, p. 749-806.

Kerrich, R., Goldfarb, R.J., Richards, JP., 2005. Metallogenic Provinces in an Evolving Geodynamic Framework. Economic Geology 100th Anniversary Volume, p. 1097-1136.

Lavigne, M.J., Michaud, M.J., 2001. Geology of North American Palladium Ltd.'s Roby Zone Deposit, Lac des Iles. Exploration Mining Geology, vol. 10, p. 1-17.

Li, C., Ripley, E.M., Maier, W.D., Gomwe, T.E.S., 2002. Olivine and sulfur isotopic compositions of the Uitkomst Ni-Cu sulfide ore-bearing complex, South Africa: evidence for sulfur contamination and multiple magma emplacements. Chemical Geology, vol. 188, p. 149-159.

Li, X-H., Fan, H-R., Yang, K-F., Hollings, P., Liu, X., Hu, F-F., Cai, Y-C., 2018. Pyrite textures and compositions from the Zhuangzi Au deposit, southeastern North China Craton: implications for ore-forming processes. Contributions to Mineralogy and Petrology, vol. 173 (73), p. 1-20.

Lightfoot, P.C., Evans-Lamswood, D., 2014. Structural controls on the primary distribution of mafic-ultramafic intrusions containing Ni-Cu-Co-(PGE) sulfide

mineralization in the roots of large igneous provinces. Ore Geology Reviews, vol. 64, p. 354-386.

Lightfoot, P.C., Sutcliffe, R.H., Doherty, W., 1991. Crustal Contamination Identified in Keweenawan Osler Group Tholeiites, Ontario: A Trace Element Perspective. The Journal of Geology, vol. 99, p. 739-760.

Mansur, E.T., Barnes, S-J., Duran, C.J., 2021. An overview of chalcophile element contents of pyrrhotite, pentlandite, chalcopyrite, and pyrite from magmatic Ni-Cu-PGE sulfide deposits. Mineralium Deposita, vol. 56, p. 179-204.

Martin, H., 1986. Effect of steeper Archean geothermal gradient on geochemistry of subduction-zone magmas. Geology, vol. 14, p. 753-756.

McCrindle, W., 2001. Geophysical Report, Berland Resources Ltd., Roaring River Property, Ontario, NTS 52H, Assessment report, Reference No. 2.22983.

McCrindle, W., 2001. Prospecting Report, Berland Resources Ltd., Roaring River Property, Ontario, NTS 52H, Assessment report, Reference No. 2.20983.

Murphy, J.B., 2006. Arc Magmatism I: Relationship Between Subduction and Magma Genesis. Geoscience Canada, vol. 33, p. 145-167.

Murphy, J.B., 2007. Arc Magmatism II: Geochemical and Isotopic Characteristics. Geoscience Canada, vol. 34, p. 7-36.

Nebel, O., Arculus, R.J., Ivanic, T.J., Rapp, R., Wills, K.J.A., 2013. Upper Zone of the Archean Windimurra layered mafic intrusion, Western Australia: insights into fractional crystallization in a large magma chamber. Journal of Mineralogy and Geochemistry, vol. 191 (1), p. 83-107.

Ohmoto, H., 1972. Systematics of Sulfur and Carbon Isotopes in Hydrothermal Ore Deposits. Economic Geology, vol. 67, p. 551-578.

Ontario Geological Survey, 2000. Garden-Obonga Lake area lake sediment survey: gold and PGE data. Open File Report 6028, p. 1-76.

Ontario Geological Survey, 2018. Fe-Ti-V and PGE-Cu-Ni Potential in the Roaring River Complex. Recommendations for Exploration 2018-2019, p. 27-31.

Paton, C., Hellstrom, J., Paul, B.,Woodhead, J. and Hergt, J. (2011) Iolite: Freeware for the visualisation and processing of mass spectrometric data. Journal of Analytical Atomic Spectrometry.

Pearce, J.A., 1976. Statistical analysis of major element patterns in basalts. Journal of Petrology, vol. 17, p. 15-43.

Peck, D., 2016. Roaring River Geochem Comparison. Unpublished internal report, Implats.

Peck, D., and Djon, L., 2020. The Lac des Iles Palladium Deposits. North American Palladium Report, p. 1-193.

Percival, J.A., Sanborn-Barrie, M., Skulski, T., Stott, G.M., Helmstaedt, H., White, D.J., 2006. Tectonic evolution of the western Superior Province from NATMAP and Lithoprobe studies. Canadian Journal of Earth Sciences, vol. 43, p. 1085-1117.

Polivchuk, M., 2017. The formation of vanadium deposits in the Archean Rivière Bell Complex, Quebec: Insights from Fe-Tx oxide chemistry. M.Sc thesis. University of Ottawa, p. 119-121.

Prichard, H.M., Knight, R.D., Fisher, P.C., McDonald, I., Zhou, M.-F., Wang, C.Y., 2013. Distribution of platinum-group elements in magmatic and altered ores in the Jinchuan intrusion, China: An example of selenium remobilization by postmagmatic fluids. Mineralium Deposita, vol. 48, p. 767-786.

Queffurus, M., Barnes, S.-J., 2015. A review of sulfur to selenium ratios in magmatic nickel-copper and platinum-group element deposits. Ore Geology Reviews, vol. 109, p. 785-794.

Ripley, E.M., Li, C., 2003. Sulfur isotope exchange and metal enrichment in the formation of magmatic Cu-Ni-(PGE) deposits. Economic Geology, vol. 98, p. 635-641.

Ripley, E.M., Li, C., 2007. Applications of Stable and Radiogenic Isotopes to Magmatic Cu-Ni-PGE Deposits: Examples and Cautions. Earth Science Frontiers, vol. 14 (5), p. 124-132.

Ripley, E.M., Li, C., 2013. Sulfide Saturation in Mafic Magmas: Is External Sulfur Required for Magmatic Ni-Cu-(PGE) Ore Genesis? Economic Geology, vol. 108, p. 45-58.

Ripley, E.M., Wernette, B.W., Ayre, A., Li, C., Smith, J.M., Underwood, B.S., Keays, R.R., 2017. Multiple S isotope studies of the Sillwater Complex and country rocks: An assessment of the role of crustal S in the origin of PGE enrichment found in the J-M Reef and related rocks. Geochimica et Cosmochimica Acta, vol. 214, p. 226-245.

Sanborn-Barrie, M., Skulski, T., 2006. Sedimentary and structural evidence for 2.7 Ga continental arc-oceanic-arc collision in the Savant-Sturgeon greenstone belt, western Superior Province, Canada. Canadian Journal of Earth Sciences, vol. 43, p. 995-1030.

Seal, R.R. II., 2006. Sulfur Isotope Geochemistry of Sulfide Minerals. Review in Mineralogy and Geochemistry, vol. 61, p. 633-677.

Shahabi Far, M., Samson, I.M., Gagnon, J.E., Good, D.J., Linnen, R.L., Ames, D., 2019. Evolution of a Conduit System at the Marathon PGE-Cu Deposit: Insights from Silicate Mineral Textures and Chemistry. Journal of Petrology, vol. 0, p. 1-33.

Smith, A.R., Sutcliffe, R.H., 1986. Geology of the Tib Gabbro, Lac des Iles area, District of Thunder Bay. Summary of Field Work and Other Activities 1986, Ontario Geological Survey, Miscellaneous Paper, vol. 132, p. 76-79.

Smith, J.W., Holwell, D.A., McDonald, I., Boyce, A.J., 2016. The applications of S isotopes and S/Se ratios in determining ore-forming processes of magmatic Ni-Cu-PGE sulfide deposits: A cautionary case study from the northern Bushveld Complex. Ore Geology Reviews, vol. 73, p. 148-174.

Smyk, M.C., Franklin, J.M., 2007. A synopsis of mineral deposits in the Archean and Proterozoic rocks of the Lake Nipigon Region, Thunder Bay District, Ontario. Canadian Journal of Earth Sciences, vol. 44, p. 1041-1053.

Staargaard, C.F., 2002. Geochemical Soil Survey on the Roaring River Property, Thunder Bay District, Ontario, assessment report 2.25849.

Stern, R.A., Hanson, G.N., 1991. Archean High-Mg Granodiorite: A derivative of Light Rare Earth Element-enriched Monzodiorite of Mantle Origin. Journal of Petrology, vol. 32, p. 201-238.

Stern, R.A., Hanson, G.N., Shirey, S.B., 1989. Petrogenesis of mantle-derived, LILE-enriched Archean monzodiorites and trachyandesites (sanukitoids) in southwestern Superior Province. Canadian Journal of Earth Sciences, vol. 26, p. 1688-1712.

Stone, D., Lavigne, M.J., Schnieders, B., Scott, J., Wagner, D., 2003. Regional Geology of the Lac des Iles Area, in Summary of Field Work and Other Activities, 2003. Ontario Geological Survey, Open File Report 6120, p. 15-1 to 15-25.

Stott, G. M., 1997. The Superior Province, Canada, *in* de Wit, M.J. and Ashwal, L.D., ed., Greenstone Belts. Oxford Monograph on Geology and Geophysics, vol. 35, p. 480-507.

Stott, G.M., Corkery, M.T., Percival, J.A., Simard, M., Goutier, J., 2010. A Revised Terrane Subdivision of the Superior Province, in Summary of Field Work and Other Activities, 2010. Ontario Geological Survey, Open File Report 6260, p. 20-1 to 20-10.

Sun, S.S., McDonough, W.F., 1989. Chemical and isotopic systematics of oceanic basalts: implications for mantle composition and processes. Geological Society, London, Special Publications, vol. 42, p. 313-345.

Sutcliffe, R.H., 1989. Magma Mixing in Late Archean Tonalitic and Mafic Rocks of the Lac des Iles Area, Western Superior Province. Precambrian Research, vol. 44, p. 81-101.

Sutcliffe, R.H., Sweeny, J.M., Edgar, A.D., 1988. The Lac des Iles Complex, Ontario: petrology and platinum-group-elements mineralization in an Archean mafic intrusion. Canadian Journal of Earth Sciences, vol. 26, p. 1408-1427.

Tanaka, T., Togashi, S., Kamioka, H., Amakawa, H., Kagami H., Hamamoto, T., Yuhara, M., Orihashi, Y., Yoneda, S., Shimizu, H., Kunimaru, T., Takahashi, K., Yanagi, T., Nakano, T., Fujimaki, H., Shinjo, R., Asahara, Y., Tanimizu, M., Dragusanu, C., 2000. JNdi-1: a neodymium isotopic reference in consistency with LaJolla neodymium. Chemical Geology, vol. 168, p. 279-281.

Tatsumi, Y., 2005. The subduction factory: How it operates in the evolving Earth. Geological Society of America Today, vol. 15, no. 7, p. 4-10.

Tomlinson, K. Y., Stott, G.M., Percival, J.A., Stone, D., 2004. Basement terrane correlations and crustal recycling in the wester Superior Province: Nd isotopic character of granitoid and felsic volcanic rocks in the Wabigoon subprovince, N. Ontario, Canada. Precambrian Research, vol. 132, p. 245-274.

Tshimbalanga, S., 2004. Induced Polarization Survey, Roaring River Property, Gillard Lake Area, 52H/12 for North American Palladium Ltd., Lac des Iles Mine Ltd., assessment report 2.28329.

Wernette, B.W., Ripley, E.M., Li, C., Wintsch, R.P., 2018. Strongly negative $\delta^{34}S$ values associated with secondary pyrite above and below the J-M Reef, Sillwater Complex, Montana. Chemical Geology, vol. 493, p. 58-66.

Wiebe, R.A., Snyder, D. 1993. Slow, dense replenishments of a basic magma chamber: the layered series of the Newark Island layered intrusion, Nain, Labrador. Contributions to Mineralogy and Petrology, vol. 113, p. 59-72.

Wilson, M., 1989. Igneous Petrogenesis. A Global Tectonic Approach. Harper Collins Academic. London, p. 466.

Zhang, A.-P., Sun, T., Zhao, Z.-F., Zhou, J.-X, Li, W.-T., Qi, Q.-J., Wei, X.-Z., 2021. Genesis of the Neoarchean subduction-related Taoke Ni-Cu-(PGE) sulphide

deposit in the North China Craton: Constraints from Os-S isotopes and PGE geochemistry. Geological Journal, vol. 1, p. 1-16.

Appendix I

Thin section descriptions

Key	
PPL	Plane polarized light
XPL	Crossed polarized Light
Coarse-grained	>5 mm
Medium-grained	1-5 mm
Fine-grained	0.5-1 mm
Very fine-grained	<0.5 mm
OPX	Orthopyroxene
CPX	Clinopyroxene
GAB	Gabbro
GABVT	Varitextured gabbro
GAB-Mt	Magnetite Gabbro
MGAB	Melanogabbro
LGAB	Leucogabbro
PYXT	Pyroxenite

Thin Section ID: TS-TG-001	**Sample ID:** A0137362	**Latitude:** 49.66149717	**Longitude:** -89.84634151	**Rock Name:** Hornblende leucogabbro
Field Description: small outcrop, granular texture with subhedral plagioclase-pyroxene-hornblende laths, abundant dilatant felsic veins with quartz in center, cross-cutting mafic dikes observed, no observed texture or lithology changes.				
Mineralogy	**Abundance (%)**	**Habit**	**Grain size**	**Notes**
Plagioclase	60	Tabular to equant, when intact	Medium-grained	~40% of the plagioclase is heavily altered to sericite to the point that grain boundaries are ambiguous.
Quartz	~5	Granular	Fine-grained	Interstitial to plagioclase and amphibole.
Amphibole	20	Massive, subhedral	Medium-grained	Interstitial to plagioclase grains. Portions of the amphibole have alteration in the centre of the grain.
Fe-Ti oxides	~2	Subhedral to anhedral, disseminated throughout sample	Fine-grained	Majority magnetite. Ilmenite occurs as discrete crystals with internal magnetite exsolution.
Sulphides	~2	Subhedral to anhedral blebs, disseminated throughout sample	Majority very fine-grained, up to fine-grained	Majority pyrite. Minor amounts of chalcopyrite occurs in close proximity to pyrite crystals.

Alteration assemblage	~10	Anhedral, granular to tabular	Very fine- to fine-grained	Chlorite + epidote, both common around heavily altered plagioclase and amphibole. Chlorite has the tabular habit, while epidote has a granular habit.
Comments: Varying levels of alteration are observed in the sample, ranging from weak to moderate. There is one vein cross-cutting the thin section, which is filled with very fine-grained epidote, plagioclase, and chlorite.				
Thin Section ID: TS-TG-002	**Sample ID:** A0137363	**Latitude:** 49.66077303	**Longitude:** -89.84644317	**Rock Name:** Leucogabbro
Field Description: on southeast edge of main LGAB outcrop, at least 100x30m, late-stage felsic veins and mafic dikes brecciated LGAB, some pegmatitic minor pods observed, granular plagioclase-pyroxene-hornblende composition anhedral-subhedral, chaotic outcrop with no Fe-oxides observed.				
Mineralogy	**Abundance (%)**	**Habit**	**Grain size**	**Notes**
Plagioclase	50	Anhedral	Medium-grained, when grain boundaries intact	Majority of plagioclase has been almost completely altered by sericite, which obscures grain boundaries.
Clinopyroxene	20	Anhedral	Medium-grained	Internal alteration is present, which gives CPX a patchy and pockmarked appearance.
Biotite	5	Tabular	Fine-grained	Primarily occurs around edges of clinopyroxene crystals.
Amphibole	15	Subhedral to anhedral	Medium-grained	Interstitial to plagioclase and pyroxene. Chlorite replacement occurs at edges.

Fe-Ti oxides	~2	Subhedral to anhedral, forming aggregates	Very fine- to fine-grained	Majority magnetite, lathes of ilmenite occur in the clusters. Magnetite has exsolution flames of hematite, ilmenite has magnetite and hematite exsolution.
Sulphides	<1	Anhedral, disseminated throughout	Very fine-grained	Rimmed with magnetite.
Alteration assemblage	5	Anhedral,	Very fine-grained	Chlorite + epidote, preferentially occurs with amphibole and magnetite grains.
Comments: Alteration seems to be mostly confined to plagioclase grains, with pyroxene having more weak alteration. One of the rare samples with hematite exsolution in magnetite.				
Thin Section ID: TS-TG-003	**Sample ID:** A0137364	**Latitude:** 49.66086386	**Longitude:** -89.8464745	**Rock Name:** Pyroxene hornblende gabbronorite dike
Field Description: 75cm wide mafic dike cross-cutting LGAB, sharp contacts, minor shearing, no sulphides.				
Mineralogy	**Abundance (%)**	**Habit**	**Grain size**	**Notes**
Plagioclase	50	Subhedral	Very fine-grained	Two veins of heavily sericitized plagioclase run across the sample, otherwise plagioclase is fresh.
Clinopyroxene	10	Subhedral	Very fine-grained	
Orthopyroxene	20	Subhedral, rounded	Very fine-grained	No particular zoning or distribution between CPX and OPX.

Amphibole	10	Subhedral, rounded	Very fine-grained	Slight preference around sericite veins, but also distributed throughout the rest of the sample.
Biotite	5	Tabular	Very fine-grained	Slight preference away from sericite veins.
Opaques	2	Subhedral, blebby	Very fine-grained	Pyrite and ilmenite, disseminated throughout sample. Larger ilmenite grains have magnetite exsolution within them.
Alteration assemblage	3	Equant	Very fine-grained	Occurs within the sericite veins.

Comments:
Very fine-grained dike. The main alteration occurs within two veins that cross cut the thin section

Thin Section ID:	**Sample ID:**	**Latitude:**	**Longitude:**	**Rock Name:**
TS-TG-004	A0137366	49.65940533	-89.84832107	Leuco-pyroxene hornblende gabbro

Field Description:
Isolated outcrops within areas of lowland, this section of outcrop has coarse-grained to pegmatitic material with felsic pods and near pyroxenite composition, similar to varitextured gabbro at LDI with exception of sulfides and increase in cross-cutting felsic veinlets, pyrite associated with mafic components of cumulus pyroxenite, felsic blebs dominantly plagioclase with potassium alteration.

Mineralogy	**Abundance (%)**	**Habit**	**Grain size**	**Notes**
Plagioclase	60	Anhedral	Very fine-grained	Vast majority of plagioclase has been altered to sericite to the point where it obscures grain boundaries.

Clinopyroxene	5	Anhedral	Fine-grained	Alteration internal to crystal is pervasive. Chlorite replacement around rims is common.
Amphibole	15	Anhedral, massive	Very fine- to fine-grained	Interstitial to plagioclase, chlorite and epidote occurs near edges. Less altered than pyroxene or plagioclase crystals.
Fe-Ti oxides	1	Subhedral, blebby	Very fine-grained	Disseminated throughout the sample, magnetite is the main phase with smaller crystals of ilmenite also present. Ilmenite has magnetite exsolution present.
Sulphides	2	Subhedral, blebby	Very fine- to medium-grained	Most very fine-grained. Pyrite main phase, minor amounts of chalcopyrite occurs in close association to pyrite or as inclusions.
Alteration assemblage	20	Subhedral to anhedral, granular.	Very fine-grained	Chlorite + epidote + muscovite, occurs as portions of discrete alteration assemblages or interstitial to plagioclase. Epidote preferentially occurs with magnetite.
Comments: High levels of alteration overall, particularly within plagioclase and sections composed entirely of alteration minerals.				
Thin Section ID: TS-TG-005	**Sample ID:** A0137362	**Latitude:** 49.64313857	**Longitude:** -89.87557145	**Rock Name:** Orthopyroxene gabbro

Field Description: Medium-grained cumulus pyroxenite with interstitial plagioclase-magnetite, disseminated pyrite-magnetite observed within groundmass, homogeneous with little structure on outcrop which continues west and north, overgrown but appears to be contacts with MGAB and other mafic units, including cross-cutting mafic dikes.				
Mineralogy	**Abundance (%)**	**Habit**	**Grain size**	**Notes**
Plagioclase	35	Tabular-equant	Fine- to medium-grained	Variable amounts of sericitization, with alteration typically heavier towards the middle of the grain
Clinopyroxene	30	Subhedral to anhedral	Fine- to medium-grained	Alteration internal to crystal is common. Intergrown with OPX and plagioclase. Replacement around rims by chlorite.
Orthopyroxene	10	Subhedral, rounded	Fine-grained	Replacement around rims by chlorite.
Biotite	<5	Tabular	Very fine-grained	Interstitial to plagioclase and CPX.
Fe-Ti oxides	3	Anhedral, blebby. One area of myrmekitic texture	Very fine-grained	Magnetite and ilmenite; ilmenite has magnetite exsolution, while magnetite has hematite exsolution.
Sulphides	2	Blebby	Very fine-grained	Mainly pyrite, with magnetite rims of varying thickness. Inclusions of chalcopyrite are also common.

Alteration assemblage	~15	Granular	Very fine-grained	Chlorite + talc + epidote; chlorite either occurs around rims of pyroxene crystals, or as a fine-grained granular groundmass with talc. Epidote is a minor phase and occurs interstitial to pyroxene.
Thin Section ID: TS-TG-006	**Sample ID:** A0159011	**Latitude:** 49.63890159	**Longitude:** -89.87344853	**Rock Name:** Hornblende leucogabbro
Field Description: GAB - medium-grained, green-grey-black-white-purple, weak to moderate pervasive chlorite-actinolite-epidote alteration. 1.5% very fine- to medium-grained anhedral to subhedral disseminated to cluster/patchy pyrite. Pyroxene: plagioclase 55:45 to 60:40.				
Mineralogy	**Abundance (%)**	**Habit**	**Grain size**	**Notes**
Plagioclase	45	Tabular	Fine- to medium-grained	Weak to moderate alteration by talc and sericite. Grain boundaries are preserved.
Amphibole	25	Subhedral	Fine- to medium-grained	Encloses opaque phases.
Fe-Ti oxides	2	Anhedral, blebby	Very fine- to fine-grained	Mostly magnetite, with minor amounts of ilmenite. Closely associated with pyrite.
Sulphides	3	Subhedral, blebby	Very fine- to fine-grained	Majority pyrite, with a couple blebs of chalcopyrite. Inclusions of pyrrhotite and chalcopyrite occur in larger pyrite grains.

Alteration assemblage	25	Bladed	Fine- to medium-grained	Tremolite + clay group minerals + chlorite, but majority tremolite and clay group minerals.

Comments:
Thin section is roughly graded. The end with the label consists of mostly plagioclase and grades into a section that mostly consists of alteration assemblages and then on the far side into a section that is mostly amphibole. Opaque minerals are concentrated on side with amphibole.

Thin Section ID:	**Sample ID:**	**Latitude:**	**Longitude:**	**Rock Name:**
TS-TG-007	A0159008	49.6389698	-89.87346428	Pyroxene hornblende orthopyroxene gabbro

Field Description:
Fine-grained, green-grey-black-white. Weak to moderate pervasive chlorite-actinolite-epidote alteration. Millimeter-scale pyrite veins.

Mineralogy	**Abundance (%)**	**Habit**	**Grain size**	**Notes**
Plagioclase	30	Equant to tabular, subangular	Very fine-grained	Varying levels of sericitization from weak to moderate.
Clinopyroxene	25	Anhedral, rounded to elongate	Very fine- to fine-grained	Alteration internal to crystal is common.
Orthopyroxene	5	Anhedral, rounded	Very fine- to fine-grained	Minor replacement by chlorite around grain edges.
Amphibole	30	Massive	Medium-grained	Interstitial and enclosed around plagioclase and pyroxene. Fresh compared to other silicate phases.
Fe-Ti oxides	2	Blebby to cubic	Very fine-grained	Magnetite the only phase, no exsolution.

Sulphides	1	Blebby	Very fine-grained	Some grains have magnetite rims to varying levels of thickness
Alteration assemblage	~5	Bladed, granular	Very fine-grained	Talc + epidote + chlorite + clay group minerals, generally interstitial to plagioclase and pyroxene.
Comments: Alteration in plagioclase and pyroxene is dependent on size. Larger grains have more alteration.				
Thin Section ID: TS-TG-008	**Sample ID:** A0159005	**Latitude:** 49.63910799	**Longitude:** -89.87342547	**Rock Name:** Gabbro
Field Description: GAB - green-grey-black-white-purple-pink. Pyroxene: plagioclase 60:40 to 40:60. Weak pervasive chlorite-actinolite-epidote alteration. Intermittent pervasive potassium alteration. Very fine-grained trace disseminated pyrite.				
Mineralogy	**Abundance (%)**	**Habit**	**Grain size**	**Notes**
Plagioclase	45	Tabular to blocky	Very fine- to medium-grained	Cumulate texture. Alteration by sericite is weak to moderate.
Clinopyroxene	30	Blocky or anhedral depending on side of thin section	Fine- to medium-grained	Chlorite and tremolite replacement around edges is common, as is alteration internal to crystal.
Amphibole	10	Subhedral to anhedral	Very fine-grained	Associated with alteration assemblage.
Fe-Ti oxides	2	Blocky to blebby	Very fine-grained	Magnetite + ilmenite; ilmenite is more abundant. Magnetite exsolution occurs within ilmenite grains. Disseminated throughout sample.

Sulphides	3	Blebby, minor amounts of more skeletal habit	Very fine-grained	Pyrite, with variable amounts of magnetite rims. Disseminated throughout sample.
Alteration assemblage	10	Subhedral, blocky to bladed	Very fine-grained	Chlorite + epidote + calcite + actinolite, overprints other phases or occurs as a replacement rim.

Comments:
Sample is roughly divided in half, with one section less altered and more plagioclase rich and the other hosting more pyroxene and alteration assemblage minerals.

Thin Section ID:	**Sample ID:**	**Latitude:**	**Longitude:**	**Rock Name:**
TS-TG-009	A0159009	49.63899322	-89.87344219	Quartz gabbro

Field Description:
GAB - green-grey-black-white-pink. Weak to moderate pervasive chlorite-actinolite-epidote-potassium alteration. Pyroxene: plagioclase ratio 55:45 to 65:35. No observed sulphide.

Mineralogy	**Abundance (%)**	**Habit**	**Grain size**	**Notes**
Plagioclase	30	Tabular to blocky	Fine- to medium-grained	Variable amounts of sericite alteration and alteration assemblage overprint.
Clinopyroxene	30	Anhedral	Fine- to medium-grained	Grain boundaries are often poorly defined and replaced by alteration assemblages. Pits and alteration minerals towards the centre of the crystal is common.
Quartz	10	Subhedral, rounded	Very fine-grained	Associated with plagioclase, as well as the cataclasis vein.

Sulphides	1	Blebby	Very fine-grained	Pyrite, disseminated, propagates along cracks in silicates. Magnetite rims majority of pyrite grains.
Alteration assemblage	30	Anhedral, bladed to granular	Very fine-grained	Epidote + chlorite + calcite + talc + tremolite, generally, forms a groundmass that has overprinted plagioclase and pyroxene.

Comments:
On the end of the thin section opposite from the label there is a vein of material that has undergone cataclasis.

Thin Section ID:	**Sample ID:**	**Latitude:**	**Longitude:**	**Rock Name:**
TS-TG-010	A0137499	49.63934983	-89.8733662	Leuco-pyroxene hornblende gabbro

Field Description:
GAB-Mt - medium-grained, grey-green-black-white-purple. Weak pervasive chlorite-actinolite alteration. 0.3% disseminated anhedral to subhedral pyrite. 0.3% disseminated magnetite. On one of historical Mere outcrops.

Mineralogy	**Abundance (%)**	**Habit**	**Grain size**	**Notes**
Plagioclase	60	Tabular to equant	Fine- to medium-grained	Well formed cumulate texture. Weak level of sericite alteration.
Clinopyroxene	10	Anhedral	Fine-grained	Tremolite replacement occurs near edges and cleavage planes. Alteration internal to crystal is common. Grains are often enclosed by amphibole.

Amphibole	20	Subhedral	Very fine- to fine-grained	Aggregates interstitial to plagioclase. Quite fresh.
Fe-Ti oxides	3	Blocky to tabular	Very fine-grained	Magnetite + ilmenite, grains are generally disseminated, sometimes forming larger aggregates. Magnetite is pitted.
Sulphides	2	Blebby	Very fine-grained	Pyrite, commonly with rims of magnetite. Larger grains may have inclusions of chalcopyrite within them.
Alteration assemblage	5	Bladed	Very fine-grained	Tremolite + actinolite, generally, occurs in close association with amphibole.
Thin Section ID: TS-TG-011	**Sample ID:** A0137500	**Latitude:** 49.63907512	**Longitude:** -89.87331063	**Rock Name:** Pyroxene hornblende gabbro
Field Description: GAB – fine- to medium-grained, green-grey-black-white-purple. Weak pervasive chlorite-actinolite alteration. Very fine-grained disseminated pyrite. Trace disseminated magnetite. On one of Mere outcrops.				
Mineralogy	**Abundance (%)**	**Habit**	**Grain size**	**Notes**
Plagioclase	40	Equant to tabular	Fine- to medium-grained	Cumulate texture. Little sericite alteration.
Clinopyroxene	35	Anhedral	Fine-grained	Alteration internal to crystal is common. Chlorite and tremolite replacement around rims is common.

Amphibole	15	Subhedral	Fine-grained	Aggregated, usually interstitial to plagioclase. Minor amounts of chlorite replacement around rims.
Fe-Ti oxides	1	Subangular to blebby	Very fine-grained	Magnetite + minor amounts of ilmenite, disseminated. Ilmenite has exsolution blebs of magnetite.
Sulphides	1	Blebby	Very fine-grained	Disseminated throughout.
Alteration assemblage	10	Anhedral	Very fine-grained	Talc + epidote + chlorite + tremolite, occurs as a replacement rim around amphibole and CPX grains, or in close proximity to those phases.
Thin Section ID: TS-TG-012	**Sample ID:** A0159004	**Latitude:** 49.63914193	**Longitude:** -89.87328664	**Rock Name:** Pyroxene hornblende gabbro
Field Description: GAB - medium-grained, green-grey-black-white-purple. Pyroxene: plagioclase ratio 60:40. Weak pervasive chlorite-actinolite alteration. Very fine- to fine-grained disseminated pyrite.				
Mineralogy	**Abundance (%)**	**Habit**	**Grain size**	**Notes**
Plagioclase	40	Tabular to blocky	Fine-grained	Variable levels of sericite alteration from weak to moderate. Grain boundaries preserved.
Clinopyroxene	40	Anhedral	Fine-grained	Alteration internal to crystal is pervasive. Chlorite and tremolite replacement of rims is common.

Amphibole	10	Anhedral	Very fine-grained	Interstitial to plagioclase and CPX.
Fe-Ti oxides	2	Blebby	Very fine-grained	Magnetite + minor amounts of ilmenite. Ilmenite has exsolution of magnetite, and occurs with aggregates of magnetite. In general, all phases are disseminated.
Sulphides	2	Blebby	Very fine-grained	Pyrite, disseminated throughout with some larger aggregates. Larger grains often have inclusions of chalcopyrite. Minority of grains have magnetite rims.
Alteration assemblage	~5	Anhedral, bladed to granular	Very fine-grained	Epidote + chlorite + tremolite + actinolite + talc + calcite. Overprints all other phases to varying degrees.
Thin Section ID: TS-TG-013	**Sample ID:** A0137377	**Latitude:** 49.63846983	**Longitude:** -89.87425637	**Rock Name:** Gabbro
Field Description: Medium-grained cumulus pyroxene in anhedral plagioclase matrix, potassium-epidote alteration within plagioclase matrix, 60-40 ratio plagioclase-pyroxene.				
Mineralogy	**Abundance (%)**	**Habit**	**Grain size**	**Notes**
Pyroxene	~35	Anhedral	Fine-grained	Difficult to tell pyroxene species due to alteration assemblage overprint.

Fe-Ti oxides	~2	Blocky	Very fine-grained	Ilmenite, with exsolution of hematite within the grains. Disseminated or forming small aggregates.
Sulphides	~2	Blebby	Very fine- to fine-grained, with the majority being very fine-grained.	Pyrite, disseminated throughout.
Alteration assemblage	~65	Anhedral	Very fine- to medium-grained	Epidote + talc + chlorite + sericite. Epidote and talc are the primary phase, and form crystals up to 1.5 mm. Alteration phases have almost completely replaced silicate phases.
Thin Section ID: TS-TG-014	**Sample ID:** A0159015	**Latitude:** 49.638871	**Longitude:** -89.873458	**Rock Name:** Pyroxene hornblende gabbro
Field Description: GABVT green-grey-black-white-purple, weak pervasive chlorite-actinolite-epidote alteration. Pyroxene: plagioclase ratio 60:40. 5% blebby chalcopyrite-pyrrhotite-pentlandite-pyrite (2-1-1-1%). Collected in proximity to historic Mere channel sample.				
Mineralogy	**Abundance (%)**	**Habit**	**Grain size**	**Notes**
Plagioclase	40	Tabular to blocky	Very fine- to medium-grained	Cumulate texture. Weak to heavy amounts of sericite alteration.
Clinopyroxene	40	Subhedral to anhedral	Medium-grained	Alteration internal to crystal is common. Cumulate texture along with plagioclase.

Amphibole	<5	Subhedral	Very fine- to fine-grained	Interstitial to plagioclase and CPX.
Biotite	1	Tabular	Fine-grained	Interstitial to plagioclase and CPX.
Sulphides	5	Blebby	Very fine- to medium-grained	Pyrite + chalcopyrite + pyrrhotite. Several large blebs contain an assemblage of sulphides. Minor amounts of pentlandite exsolution occurs in pyrrhotite grains.
Alteration assemblage	10	Anhedral	Very fine-grained	Talc + epidote + chlorite + tremolite. Either overprints or occurs interstitial to all other phases.
Thin Section ID: TS-TG-015	**Sample ID:** A0137379	**Latitude:** 49.63840594	**Longitude:** -89.87375969	**Rock Name:** Olivine orthopyroxenite
Field Description: Medium- to coarse-grained cumulate pyroxene with blebby aggregates of plagioclase, near pyroxenite composition if not for disseminated plagioclase blebs, magnetite also disseminated throughout, minor blebs pyrite, potential block of more mafic material within GABVT, section of trench is breccia.				
Mineralogy	**Abundance (%)**	**Habit**	**Grain size**	**Notes**
Olivine	35	Subhedral, rounded	Very fine- to medium-grained	Preferential alteration occurs along grain boundaries and cracks within individual grains.
Orthopyroxene	15	Subhedral, rounded	Very fine- to fine-grained	
Amphibole	5	Anhedral	Fine-grained	Interstitial to and replaced by alteration assemblage.

Fe-Ti oxides	1	Blebby, minor amounts droplet habit also present	Very fine-grained	Magnetite. Disseminated throughout sample and as infill along cracks in olivine crystals.
Sulphides	1	Blebby	Very fine-grained	Pyrite, disseminated throughout the sample. Larger grains have inclusions of pyrrhotite and chalcopyrite.
Alteration assemblage	45	Anhedral, bladed to granular	Very fine-grained	Epidote + talc + tremolite + calcite + clay group minerals. Occurs throughout the sample as an interstitial phase or overprints and replaces silicates.
Comments: Thin section is highly altered making identification of original morphology difficult.				
Thin Section ID: TS-TG-016	**Sample ID:** A0159036	**Latitude:** 49.68391775	**Longitude:** -89.85880117	**Rock Name:** Mela-pyroxene hornblende gabbro
Field Description: 70:30 ratio pyroxene: plagioclase, plagioclase interstitial to pyroxene with moderate sodic alteration, 5-10% disseminated biotite present, trace pyrite-magnetite in matrix.				
Mineralogy	**Abundance (%)**	**Habit**	**Grain size**	**Notes**
Plagioclase	15	Tabular to equant	Fine-grained	Variable levels of sericite alteration, from weak to moderate.
Clinopyroxene	25	Anhedral	Fine-grained	Alteration internal to crystal is pervasive.
Amphibole	15	Anhedral	Fine-grained	Interstitial to other major phases.

Biotite	5	Tabular	Very fine- to fine-grained.	In close association to amphibole.
Fe-Ti oxides	3	Blebby	Very fine-grained	Magnetite. Disseminated throughout sample.
Sulphides	2	Blebby	Very fine-grained	Pyrite, disseminated throughout sample. Grains rimmed with varying amounts of magnetite.
Alteration assemblage	40	Anhedral	Very fine-grained	Actinolite + talc + epidote + chlorite + clay group minerals. Replaces and occurs interstitial to other phases.
Comments: Sample is intensely altered, with plagioclase and clinopyroxene separated out from the main alteration assemblage so long as there is enough intact grain to make a clear identification.				
Thin Section ID: TS-TG-017	**Sample ID:** A0159033	**Latitude:** 49.68378476	**Longitude:** -89.85868876	**Rock Name:** Pyroxene hornblende gabbro
Field Description: Outcrop is 10x40m trending 70˚, dominantly GAB to GAB-Mt, this sample granular pyroxene-plagioclase of equal proportions, 10% disseminated biotite-hornblende, moderate magnetite, disseminated pyrite in matrix.				
Mineralogy	**Abundance (%)**	**Habit**	**Grain size**	**Notes**
Plagioclase	40	Tabular	Fine- to medium-grained	Weak sericite alteration.
Clinopyroxene	25	Anhedral	Fine- to medium-grained	Alteration internal to crystal is pervasive. Chlorite replacement at rims also common.
Amphibole	15	Anhedral	Very fine-grained	Interstitial to plagioclase and CPX.

Olivine	<5	Rounded	Fine-grained	Associated with magnetite. Iddingsite alteration along cracks within the grain.
Quartz	5	Rounded	Very fine-grained	Associated with magnetite and pyrite.
Fe-Ti oxides	2	Blocky or droplet	Very fine-grained	Magnetite, blocky grains are pitted and disseminated throughout. Droplet texture is extremely fine-grained, and is patterned in swirls.
Sulphides	1	Blebby	Very fine-grained	Pyrite + pyrrhotite, intergrown in some blebs. Magnetite rims occur around some pyrite grains.
Alteration assemblage	10	Anhedral	Very fine-grained	Tremolite + actinolite + calcite. Interstitial to plagioclase and CPX.
Comments: Magnetite droplet habit is extensive, the largest occurrence of this habit in all the thin sections.				
Thin Section ID: TS-TG-018	**Sample ID:** A0159037	**Latitude:** 49.68385954	**Longitude:** -89.85886748	**Rock Name:** Gabbro
Field Description: Coarse-grained cumulate pyroxene groundmass with disseminated blebs of plagioclase up to 10%, along with cross-cutting felsic LGAB veinlets. Groundmass <0.5% disseminated to blebby fine-grained pyrite.				
Mineralogy	**Abundance (%)**	**Habit**	**Grain size**	**Notes**
Plagioclase	5	Massive	Medium-grained	Weak sericite alteration, occurs preferentially along cleavage planes.

Clinopyroxene	45	Anhedral	Fine- to medium-grained	Alteration internal to crystal is pervasive. Replacement by chlorite around rims.
Amphibole	<10	Anhedral	Fine- to medium-grained	Encloses CPX and biotite.
Biotite	<5	Tabular	Fine-grained	Interstitial to CPX.
Fe-Ti oxides	2	Blebby and myrmekitic	Very fine-grained	Magnetite + ilmenite. Disseminated, sometimes forms small aggregates. Mostly blebs, with minor amounts of myrmekitic habit.
Sulphides	1	Blebby	Very fine-grained	Pyrite, disseminated. Grains rimmed with varying amounts of magnetite. Larger grains of pyrite have inclusions of chalcopyrite within them.
Alteration assemblage	40	Anhedral, bladed to granular	Very fine- to fine-grained	Talc + epidote + tremolite + chlorite. Occurs as a groundmass, which surround and infringe onto other mineral phases.
Thin Section ID: TS-TG-019	**Sample ID:** A0137383	**Latitude:** 49.6361587	**Longitude:** -89.87307576	**Rock Name:** Pyroxene hornblende gabbro dike
Field Description: One of two mafic dikes cross-cutting PYXT unit, non magnetic, aphanitic pyroxene-plagioclase.				
Mineralogy	**Abundance (%)**	**Habit**	**Grain size**	**Notes**

Plagioclase	45	Rounded	Very fine-grained	
Clinopyroxene	20	Rounded	Very fine-grained	
Amphibole	30	Rounded	Very fine-grained	
Biotite	~5	Tabular	Very fine-grained	
Fe-Ti oxides	~1	Blebby	Very fine-grained	Magnetite, disseminated throughout.
Sulphides	~1	Blebby	Very fine-grained	Pyrite, almost all grains are rimmed with varying amounts of magnetite.
Alteration assemblage	~1	Rounded	Very fine-grained	Epidote
Comments: One edge hosts coarser grained plagioclase with sericite alteration, which is from the surrounding outcrop the dike was hosted in. The dike morphology is fine-grained with enough preferential orientation of the grains that they appear to flow.				
Thin Section ID: TS-TG-020	**Sample ID:** A0137384	**Latitude:** 49.63626019	**Longitude:** -89.87236586	**Rock Name:** Websterite
Field Description: PYXT outcrop trending north-south for 30m. Medium- to coarse-grained adcumulate pyroxene with interstitial plagioclase. Felsic veins cross-cut throughout. Biotite disseminated within matrix as well up to 10% trace sulfides.				
Mineralogy	**Abundance (%)**	**Habit**	**Grain size**	**Notes**
Plagioclase	5	Anhedral	Medium-grained	Mostly concentrated around the edges of the thin section. Pitted, with some variable amounts of sericite alteration.

Clinopyroxene	~80	Subhedral, subrounded	Very fine- to fine-grained	Cumulate texture, with varying levels of internal alteration minerals, pits, and alteration.
Orthopyroxene	~10	Subhedral, rounded	Fine-grained	
Amphibole	<5	Anhedral	Very fine-grained	Interstitial to pyroxene.
Sulphides	~1	Blebby	Very fine-grained	Pyrite, rimmed with magnetite.
Thin Section ID: TS-TG-021	**Sample ID:** A0137385	**Latitude:** 49.63565748	**Longitude:** -89.87330444	**Rock Name:** Websterite
Field Description: PYXT samples with an increase in plagioclase within matrix typically as pods or aggregates, GAB veins cross-cut along with felsic veins, 10x10m outcrop.				
Mineralogy	**Abundance (%)**	**Habit**	**Grain size**	**Notes**
Plagioclase	5	Massive	Very fine- to medium-grained	Interstitial to pyroxene, with minimal sericite alteration. Small amount of fine-grained sericite groundmass that was possibly once plagioclase.
Clinopyroxene	75	Subhedral	Fine- to medium-grained	Alteration internal to crystal is common. Pits with alteration minerals within them are common.
Orthopyroxene	10	Rounded	Fine- to medium-grained	Not as altered as CPX, though minor amounts of replacement by alteration assemblage around the rims is common.

Amphibole	<5	Anhedral	Very fine-grained	Interstitial to plagioclase and pyroxene.
Sulphides	1	Blebby	Very fine-grained	Pyrite, with minor amounts of magnetite around the rim. Disseminated throughout sample.
Alteration assemblage	~5	Granular	Very fine-grained	Epidote + talc. Partially replaced some of the pyroxene crystals.
Thin Section ID: TS-TG-022	**Sample ID:** A0137386	**Latitude:** 49.63391306	**Longitude:** -89.87140625	**Rock Name:** Clinopyroxenite
Field Description: Medium-grained cumulus pyroxene with anhedral interstitial plagioclase up to 30% and weak potassic-epidote alteration. Trace disseminated pyrite. Some cross-cutting GAB veins producing brecciation.				
Mineralogy	**Abundance (%)**	**Habit**	**Grain size**	**Notes**
Clinopyroxene	~70	Granular	Very fine-grained	Alteration internal to crystal is pervasive and extends to edges, to the point where original grain boundaries are extremely difficult to determine.
Sulphides	~2-3	Blebby	Very fine-grained	Pyrite, disseminated throughout the sample.
Alteration assemblage	~30	Anhedral, bladed to granular	Very fine-grained	Epidote + talc + tremolite + chlorite. Occurs as both an interstitial phase and as a replacement phase, particularly around silicate edges.

Comments: Extremely altered.				
Thin Section ID: TS-TG-023	**Sample ID:** A0137387	**Latitude:** 49.63541522	**Longitude:** -89.87446372	**Rock Name:** Pyroxene hornblende orthopyroxene gabbro
Field Description: Groundmass is PYXT with abundant cross-cutting pegmatite GAB veins. 10x10m outcrop. No obvious trend to veins. PYXT matrix medium-grained adcumulate pyroxene with <10% plagioclase and trace sulfides, pegmatite veins coarse-grained euhedral pyroxene with anhedral plagioclase ~50/50 ratio with disseminated pyrite-chalcopyrite but 0.1%. Sample is mix of PYXT and pegmatite veins.				
Mineralogy	**Abundance (%)**	**Habit**	**Grain size**	**Notes**
Plagioclase	40	Tabular to equant	Very fine- to medium-grained	Variable levels of sericitization, from weak to moderate. Where sericite alteration is weak, it is confined to the centre of the grain.
Clinopyroxene	35	Subhedral to anhedral	Fine- to medium-grained	Alteration internal to crystal is common, as is replacement by tremolite and chlorite, particularly at grain boundaries.
Orthopyroxene	5	Subhedral, rounded	Fine- to medium-grained	Minor amounts of recrystallization.
Amphibole	~7	Anhedral	Medium-grained	Replacement by chlorite occurs at grain boundaries. Interstitial to plagioclase and pyroxene.
Biotite	1	Subhedral	Fine-grained	Interstitial to plagioclase and pyroxene.

Sulphides	<5	Blebby	Very fine-grained	Chalcopyrite + pyrite + pyrrhotite. Disseminated throughout, while forming small aggregates.
Alteration assemblage	~10	Anhedral	Very fine-grained	Tremolite + chlorite. Interstitial to other mineral phases. Chlorite replaces amphibole and pyroxene rims.

Thin Section ID:	**Sample ID:**	**Latitude:**	**Longitude:**	**Rock Name:**
TS-TG-024	A0137388	49.63427671	-89.87548804	Plagioclase bearing hornblende pyroxenite

Field Description:
Fine- to medium-grained granular pyroxene-plagioclase matrix, 60/40 ratio, pyroxene subhedral plagioclase anhedral with weak potassium-epidote alteration. Fine-grained disseminated pyrite within matrix but more associated along plagioclase grain boundaries. LGAB veins show pyrite mineralization as well. Overgrown 10x20m outcrop.

Mineralogy	**Abundance (%)**	**Habit**	**Grain size**	**Notes**
Clinopyroxene	55	Anhedral, granular	Very fine- to fine-grained	Alteration internal to crystal is common. Chlorite replacement occurs around the rims quite often. Talc + epidote alteration common in pits within crystals.
Amphibole	30	Anhedral, massive	Fine- to medium-grained	Overprints and surrounds other mineral phases.
Biotite	1	Tabular	Very fine-grained	Interstitial to amphibole.
Fe-Ti oxides	1	Blebby	Very fine-grained	Magnetite

Sulphides	4	Blebby and skeletal	Very fine-grained	Pyrite, with the occasional pyrrhotite inclusion in larger grains.
Alteration assemblage	10	Anhedral	Very fine-grained	Epidote + talc + calcite + chlorite. Interstitial to amphibole and pyroxene.
Thin Section ID: TS-TG-025	**Sample ID:** A0137389	**Latitude:** 49.63527033	**Longitude:** -89.88350411	**Rock Name:** Leuco-pyroxene hornblende norite
Field Description: 10x20m outcrop in lowlands, medium- to coarse-grained granular pyroxene-plagioclase equal ratio with 5-10% biotite and strongly magnetic, 0.5% fine-grained disseminated pyrite, weak alteration, mafic dikes cross-cutting.				
Mineralogy	**Abundance (%)**	**Habit**	**Grain size**	**Notes**
Plagioclase	50	Tabular to equant	Very fine- to medium-grained	Weak to moderate levels of sericite alteration.
Orthopyroxene	10	Rounded	Medium-grained	Tremolite replacement occurs at the rims.
Amphibole	15	Anhedral, massive	Medium-grained	Occurs interstitial to and intrudes into plagioclase and OPX.
Biotite	5	Tabular	Very fine-grained	Interstitial to plagioclase.
Fe-Ti oxides	4	Blebby	Very fine-grained	Magnetite + ilmenite. Disseminated through sample. Ilmenite occurs within small aggregates of magnetite.

Sulphides	1	Blebby	Very fine-grained	Pyrite, disseminated throughout sample. Magnetite rims around pyrite grains is common.
Alteration assemblage	10	Bladed	Very fine- to fine-grained	Tremolite, interstitial to amphibole and plagioclase.
Thin Section ID: TS-TG-026	**Sample ID:** A0137390	**Latitude:** 49.63434662	**Longitude:** -89.88209906	**Rock Name:** Leuco- orthopyroxene hornblende gabbro
Field Description: medium- to coarse-grained with near pegmatitic sections, granular subhedral purple plagioclase and green pyroxene, trace disseminated pyrite, likely did not move far from original position.				
Mineralogy	**Abundance (%)**	**Habit**	**Grain size**	**Notes**
Plagioclase	45	Subhedral	Fine- to medium-grained	Minor sericite alteration, often more concentrated towards the center of the grain.
Clinopyroxene	10	Anhedral	Fine- to medium-grained	Alteration internal to crystal is common is common, as is infringement and replacement by chlorite and tremolite.
Orthopyroxene	<5	Anhedral, rounded	Fine-grained	Replacement by chlorite at rims.
Amphibole	10	Subhedral to anhedral	Fine- to medium-grained	Surrounds and occurs interstitial to plagioclase and pyroxene.
Fe-Ti oxides	3	Blebby	Very fine-grained	Magnetite, with minor amounts of ilmenite occur as discrete grains in association with magnetite. Disseminated throughout sample.

Sulphides	2	Blebby	Very fine-grained	Pyrite, minor amounts of chalcopyrite occur as separate grains. Disseminated throughout sample.
Alteration assemblage	25	Anhedral, bladed to granular	Very fine-grained	Chlorite + talc + actinolite + tremolite + clay group minerals + epidote. Occurs as a fine-grained groundmass interstitial to plagioclase and pyroxene. Also replaces amphibole grain boundaries.
Thin Section ID: TS-TG-027	**Sample ID:** A0137397	**Latitude:** 49.64486811	**Longitude:** -89.87641291	**Rock Name:** Pyroxene hornblende orthopyroxene gabbro
Field Description: GABVT-Mt 20mx8m ridge trending 40 degrees. Medium- to coarse-grained trace disseminated pyrite 3% biotite.				
Mineralogy	**Abundance (%)**	**Habit**	**Grain size**	**Notes**
Plagioclase	50	Tabular	Medium-grained	Moderate to heavy levels of sericite alteration. Grain boundaries are difficult to determine.
Clinopyroxene	20	Subhedral	Very fine- to medium-grained	Alteration internal to crystal is common. Chlorite replacement occurs at rims.
Orthopyroxene	5	Subhedral, rounded	Fine-grained	Less alteration in the centre of the crystal compared to CPX.
Amphibole	5	Subhedral	Fine-grained	Interstitial to pyroxene crystals. Minor replacement by chlorite occurs at edges.

Fe-Ti oxides	3	Blebby	Very fine-grained	Magnetite + ilmenite. Exsolution of hematite and magnetite are observed in respective mineral phases.
Sulphides	2	Blebby	Very fine-grained	Pyrite, larger grains have inclusions of chalcopyrite within them.
Alteration assemblage	10	Anhedral	Very fine-grained	Epidote + chlorite. Epidote preferentially occurs with magnetite.
Comments: Heavily altered, with alteration affecting many of the crystal boundaries of the primary mineralogy.				
Thin Section ID: TS-TG-028	**Sample ID:** A0137399	**Latitude:** 49.64518098	**Longitude:** -89.8760939	**Rock Name:** Pyroxene hornblende gabbro
Field Description: GABVT medium- to coarse-grained pyroxene: plagioclase ratio is 55:45. trace biotite trace disseminated pyrite. weakly magnetic. Ridge next to lowland area to the west.				
Mineralogy	**Abundance (%)**	**Habit**	**Grain size**	**Notes**
Plagioclase	30	Subhedral	Fine-grained	Heavy sericite alteration, which obscures grain boundaries.
Clinopyroxene	25	Anhedral, bladed	Fine-grained	Alteration internal to crystal is common as is rim replacement by chlorite.
Amphibole	15	Anhedral	Very fine- to fine-grained	Interstitial to CPX and plagioclase. Not as altered as other phases.
Biotite	3	Tabular	Very fine- to medium-grained	Associated with amphibole.

Fe-Ti oxides	2	Blebby	Very fine-grained	Magnetite + ilmenite. Disseminated throughout.
Sulphides	2	Blebby	Very fine-grained	Pyrite + chalcopyrite. Rims of magnetite occur around pyrite grains.
Alteration assemblage	25	Anhedral, bladed	Very fine-grained	Muscovite + chlorite + epidote + clay group minerals + tremolite. Occurs as masses interstitial to other phases.
Thin Section ID: TS-TG-029	**Sample ID:** A0137400	**Latitude:** 49.64530601	**Longitude:** -89.87587989	**Rock Name:** Pyroxene hornblende gabbro
Field Description: GAB high point with adjacent outcrop to the east and west. Low lying area to the west. sample taken at top of slope.				
Mineralogy	**Abundance (%)**	**Habit**	**Grain size**	**Notes**
Plagioclase	50	Tabular	Medium-grained	Sericite alteration is present in each grain, but is weak to moderate in strength.
Clinopyroxene	30	Anhedral	Fine-grained	Alteration internal to crystal and pits are pervasive.
Biotite	1	Tabular	Fine-grained	Occurs with amphibole.
Amphibole	5	Subhedral	Fine-grained	Interstitial to plagioclase and CPX. Chlorite replacement of rims is common.
Sulphides	1	Blebby	Very fine-grained	Pyrite + chalcopyrite, associated together.

Alteration assemblage	10	Anhedral, bladed to granular	Very fine-grained	Epidote + tremolite + actinolite + chlorite. Overprints plagioclase and CPX.
Thin Section ID: TS-TG-030	**Sample ID:** A0137402	**Latitude:** 49.64652232	**Longitude:** -89.87417914	**Rock Name:** Pyroxene hornblende gabbro
Field Description: GAB-Mt on south edge of swamp. Purple green grey. Trace pyrite, moderately to strongly magnetic.				
Mineralogy	**Abundance (%)**	**Habit**	**Grain size**	**Notes**
Plagioclase	50	Equant to tabular	Medium-grained	Weak to intense sericite alteration.
Clinopyroxene	20	Subhedral	Medium-grained	Alteration internal to crystal is variable as are the presence of pits.
Amphibole	10	Anhedral	Very fine-grained	Interstitial to plagioclase and CPX. Freshest mineral phase.
Biotite	10	Tabular	Very fine- to fine-grained	Interstitial to plagioclase and CPX.
Fe-Ti oxides	5	Blocky and myrmekitic	Very fine- to medium-grained	Magnetite + ilmenite. Larger magnetite grains occur in close association to ilmenite.
Sulphides	<5	Blebby	Very fine-grained	Pyrite, disseminated throughout. Slightly larger grains often have inclusions of chalcopyrite.
Alteration assemblage	<5	Anhedral	Very fine-grained	Chlorite + actinolite. Preferentially occurs with biotite and Fe-Ti oxides.

Thin Section ID: TS-TG-031	**Sample ID:** A0137451	**Latitude:** 49.65386499	**Longitude:** -89.85379544	**Rock Name:** Pyroxene hornblende gabbronorite
Field Description: GAB-Mt strongly magnetic. 0.3% disseminated pyrite 5+% disseminated magnetite. trace unidentified red-brown mineral. possibly rutile. Small exposure 4x1m northeast. Black-green-purple-white in colour.				
Mineralogy	**Abundance (%)**	**Habit**	**Grain size**	**Notes**
Plagioclase	55	Equant to tabular	Fine- to medium-grained	Variable amounts of sericite alteration.
Clinopyroxene	15	Subhedral	Fine-grained	Replacement by chlorite and tremolite around rims. S Alteration internal to crystal is pervasive.
Orthopyroxene	15	Subhedral, rounded	Fine-grained	Far less recrystallization present than is observed in CPX.
Amphibole	<5	Anhedral	Fine- to medium-grained	Interstitial to plagioclase.
Biotite	<5	Tabular	Very fine-grained	Associated with magnetite aggregates.
Fe-Ti oxides	3	Blebby	Very fine-grained	Magnetite + ilmenite. Disseminated throughout, with some small aggregates. Ilmenite has exsolution of magnetite.
Sulphides	1	Blebby	Very fine-grained	Pyrite, larger grains have inclusions of chalcopyrite. Disseminated throughout. Pyrite rimmed with varying amounts of magnetite.

Alteration assemblage	~5	Anhedral	Very fine-grained	Chlorite + tremolite. Interstitial to plagioclase and pyroxene.
Thin Section ID: TS-TG-032	**Sample ID:** A0137454	**Latitude:** 49.64472222	**Longitude:** -89.87322222	**Rock Name:** Norite
Field Description: GAB grey-green-black-white-purple in colour. Very fine-grained disseminated pyrite 4x4m exposure.				
Mineralogy	**Abundance (%)**	**Habit**	**Grain size**	**Notes**
Plagioclase	55	Subhedral	Fine-grained	Minor amounts of sericite alteration.
Orthopyroxene	35	Subhedral, rounded	Fine-grained	Minor amounts of internal alteration minerals. Chlorite replacement along rims.
Fe-Ti oxides	~2	Anhedral	Very fine-grained	Magnetite, disseminated throughout sample.
Sulphides	~1	Anhedral	Very fine-grained	Pyrite, minority of grains have magnetite rims. Disseminated throughout sample.
Alteration assemblage	~10	Anhedral	Very fine-grained	Talc + Chlorite + calcite. Interstitial to plagioclase in particular, with chlorite confined mostly to OPX grains.
Thin Section ID: TS-TG-033	**Sample ID:** A0137456	**Latitude:** 49.64559486	**Longitude:** -89.87263784	**Rock Name:** Mela-pyroxene hornblende gabbro

Field Description: MGAB dark green-grey-black-white. Pyroxene: plagioclase 70:30-85:15. Moderate pervasive chlorite-actinolite-epidote alteration. Potassium alteration along exposed surfaces. Poorly exposed outcrop 2x6m trending north. Very fine-grained trace disseminated pyrite.				
Mineralogy	**Abundance (%)**	**Habit**	**Grain size**	**Notes**
Plagioclase	<5	Anhedral	Very fine-grained	Extremely intense sericite alteration to the point that the original grain boundaries are obscured.
Olivine	~50	Subhedral, rounded	Fine-grained	Small sections are quite fresh; however, the majority has iddingsite alteration.
Clinopyroxene	30	Anhedral	Fine-grained	Alteration internal to crystal and pits are pervasive. Replacement by chlorite occurs along rims.
Amphibole	10	Subhedral	Fine-grained	Interstitial to CPX grains. Quite fresh.
Fe-Ti oxides	4	Blebby	Very fine-grained	Magnetite, disseminated throughout.
Sulphides	1	Blebby	Very fine-grained	Pyrite, almost all rimmed by varying amounts of magnetite.
Alteration assemblage	<5	Anhedral	Very fine-grained	Chlorite + talc. Interstitial to pyroxene. Chlorite replacement occurs around CPX rims.

Comments: Olivine and pyroxene preferentially occur, with some sections dominated by olivine and others dominated by pyroxene.				
Thin Section ID: TS-TG-034	**Sample ID:** A0137458	**Latitude:** 49.64575082	**Longitude:** -89.87246899	**Rock Name:** Orthopyroxene gabbro
Field Description: GAB weak to moderate chlorite-actinolite-epidote alteration. Trace very fine-grained disseminated pyrite. Green-grey-black-white. Melano- and mesocratic portions of outcrop. 7x8m northwest exposure.				
Mineralogy	**Abundance (%)**	**Habit**	**Grain size**	**Notes**
Plagioclase	45	Anhedral	Very fine-grained	Heavy amounts of sericite alteration, to the point where it obscures grain boundaries.
Clinopyroxene	20	Anhedral	Very fine- to medium-grained	Alteration internal to crystal are pervasive. Replacement by tremolite occurs along grain boundaries and trends inwards.
Orthopyroxene	<10	Subhedral, rounded	Very fine- to fine-grained	Minor amounts of internal alteration.
Fe-Ti oxides	2	Blebby	Very fine-grained	Magnetite, disseminated throughout section.
Sulphides	2	Blebby	Very fine-grained	Pyrite, occasional grains of chalcopyrite occur as discrete grains and inclusions within pyrite. Magnetite rimmed pyrite grains are also common.

Alteration assemblage	10	Subhedral	Very fine- to fine-grained	Chlorite + epidote + tremolite. Interstitial to plagioclase and pyroxene.
Thin Section ID: TS-TG-035	**Sample ID:** A0137459	**Latitude:** 49.64614598	**Longitude:** -89.87325931	**Rock Name:** hornblende pyroxenite
Field Description: GAB green-grey-black-white-purple. Weak to moderate pervasive chlorite-actinolite-epidote alteration. Pyroxene: plagioclase 65:35-60:40. Very large outcrop visible on satellite photo. Very fine- to medium-grained anhedral to subhedral disseminated to cluster-patchy pyrite. Gossan on weathered surface.				
Mineralogy	**Abundance (%)**	**Habit**	**Grain size**	**Notes**
Olivine	10	Subhedral	Fine- to medium-grained	Strong iddingsite alteration along cracks in the mineral structure and around the edges and rims of each grain.
Clinopyroxene	10	Subhedral to anhedral	Very fine- to fine-grained	Alteration internal to crystal is pervasive. Chlorite and tremolite replacement around CPX rims are common.
Biotite	5	Tabular	Fine-grained	Occurs with amphibole.
Amphibole	10	Subhedral to anhedral	Fine- to medium-grained	Interstitial to olivine and pyroxene.
Fe-Ti oxides	<1	Subhedral to anhedral	Very fine-grained	Magnetite + ilmenite. Disseminated throughout sample.
Sulphides	~2	Blebby	Very fine-grained	Pyrite + chalcopyrite. Disseminated throughout sample.

Alteration assemblage	65	Subhedral to anhedral	Very fine-grained	Muscovite + tremolite + actinolite + clay group minerals + epidote + talc + sericite. Alteration is pervasive and infringes on silicates.
Comments: Sericite is counted under the alteration assemblage because there is no indicator of original plagioclase.				
Thin Section ID: TS-TG-036	**Sample ID:** A0137461	**Latitude:** 49.6425975	**Longitude:** -89.87627187	**Rock Name:** Mela-pyroxene hornblende gabbro
Field Description: GAB green-grey-black-white. Pyroxene: plagioclase 60:40. Moderate to strong pervasive and vein epidote alteration. Weak to moderate pervasive chlorite-actinolite alteration. 0.2% fracture hosted pyrite 4x10m outcrop north.				
Mineralogy	**Abundance (%)**	**Habit**	**Grain size**	**Notes**
Plagioclase	20	Anhedral	Fine- to medium-grained	Moderate to heavy amounts of sericite alteration.
Clinopyroxene	20	Anhedral	Very fine- to fine-grained	Alteration internal to crystal is pervasive. Chlorite replacement around the rim and along cracks in the crystal structure is common. Minor amounts of epidote occur within cleavage planes.
Amphibole	40	Anhedral	Medium-grained	Encloses all silicate phases.

Fe-Ti oxides	~1	Blebby to blocky	Very fine-grained	Magnetite + ilmenite. Disseminated throughout sample. Ilmenite has magnetite exsolution.
Sulphides	~1	Blebby	Very fine-grained	Pyrite, commonly with magnetite rims. Inclusions of chalcopyrite occur in larger pyrite grain.
Alteration assemblage	20	Anhedral	Very fine- to fine-grained	Epidote + talc + chlorite. Epidote and talc often form a fine-grained groundmass which has overtaken other mineral phases.
Thin Section ID: TS-TG-037	**Sample ID:** A0137462	**Latitude:** 49.64251937	**Longitude:** -89.8766546	**Rock Name:** Pyroxene hornblende gabbronorite
Field Description: GAB green-grey-black-white. Along small but extensive rampart outcrop. Weak to moderate pervasive chlorite-actinolite-epidote alteration. Weak to moderate pervasive potassium alteration. With 5% biotite. Pyroxene: plagioclase 60:40-65:35. Sharp grain boundaries. Trace disseminated pyrite 0.2% disseminated magnetite.				
Mineralogy	**Abundance (%)**	**Habit**	**Grain size**	**Notes**
Plagioclase	45	Subhedral to anhedral	Fine- to medium-grained	Weak to heavy amounts of sericite alteration.
Clinopyroxene	15	Anhedral	Fine-grained	Alteration internal to crystal is common. Grain boundaries are degraded by alteration assemblage.
Orthopyroxene	10	Subhedral, rounded	Very fine- to fine-grained	Replacement by chlorite around rims. Typically enclosed by amphibole.

Amphibole	15	Anhedral	Fine-grained	Surrounds and occurs interstitial to pyroxene and plagioclase.
Biotite	<5	Tabular	Very fine-grained	Interstitial to plagioclase.
Fe-Ti oxides	2	Subhedral to anhedral	Very fine-grained	Magnetite + ilmenite. Forms small aggregates throughout sample.
Sulphides	1	Blebby	Very fine-grained	Pyrite + chalcopyrite. Magnetite of varying thickness rims pyrite grains. Disseminated throughout sample.
Alteration assemblage	10	Anhedral	Very fine- to fine-grained	Chlorite + epidote + tremolite. Interstitial to all other mineral phases.
Thin Section ID: TS-TG-038	**Sample ID:** A0137464	**Latitude:** 49.6427574	**Longitude:** -89.87658647	**Rock Name:** Mela-pyroxene hornblende gabbro
Field Description: GAB green-grey-black-white-pink with weak to moderate pervasive chlorite-actinolite-epidote-potassium alteration. Trace very fine-grained disseminated pyrite, 0.3% disseminated magnetite. Moderately foliated. Continuation of GAB outcrop rampart.				
Mineralogy	**Abundance (%)**	**Habit**	**Grain size**	**Notes**
Plagioclase	25	Subhedral to anhedral	Fine-grained	Moderate to heavy amounts of sericite alteration.
Clinopyroxene	15	Anhedral	Fine- to medium-grained	Alteration internal to crystal is common. Chlorite and tremolite replacement around rims.
Amphibole	45	Massive, subhedral	Medium-grained	Encloses plagioclase and pyroxene.

Biotite	2	Tabular	Very fine- to fine-grained	Interstitial to amphibole.
Fe-Ti oxides	1	Anhedral	Very fine- to fine-grained	Magnetite, quite pitted and cracked. Disseminated throughout sample.
Alteration assemblage	~15	Anhedral	Very fine-grained	Epidote + chlorite + calcite + talc + tremolite. Mainly occurs interstitial to other phases, with slight infringement upon grain boundaries.
Thin Section ID: TS-TG-039	**Sample ID:** A0137465	**Latitude:** 49.6415002	**Longitude:** -89.87686446	**Rock Name:** Mela-pyroxene hornblende gabbro
Field Description: GAB green-grey-black-white-pink. Pyroxene: plagioclase 65:35. Weak to moderate pervasive chlorite-actinolite-epidote alteration. Intermittent moderate potassium alteration. Outcrop part of large exposure. 0.3% disseminated pyrite Dominantly medium-grained with few coarse-grained pyroxene-actinolite crystals.				
Mineralogy	**Abundance (%)**	**Habit**	**Grain size**	**Notes**
Plagioclase	25	Anhedral, roughly tabular	Fine- to medium-grained	Moderate to intense levels of sericite alteration. Majority of grains have heavy sericite alteration.
Clinopyroxene	35	Anhedral	Fine-grained	Alteration internal to crystal is common, as is chlorite replacement around the rim.
Amphibole	20	Anhedral	Fine-grained	Alteration internal to crystal is present. Encloses plagioclase and CPX.

Fe-Ti oxides	2	Anhedral, blebby	Very fine-grained	Magnetite + ilmenite. Disseminated throughout. Ilmenite often has magnetite exsolution within.
Sulphides	2	Blebby	Very fine-grained	Pyrite + chalcopyrite + pyrrhotite. Disseminated throughout. Small percentage of pyrite grains have rims of magnetite.
Alteration assemblage	~15	Anhedral, bladed to granular	Very fine-grained	Chlorite + talc + actinolite + tremolite. Infringes on silicate grain boundaries.
Thin Section ID: TS-TG-040	**Sample ID:** A0137467	**Latitude:** 49.64142903	**Longitude:** -89.87666073	**Rock Name:** Plagioclase bearing pyroxenite
Field Description: GABVT green-grey-black-white-pink. Pyroxene: plagioclase 65:35. Moderate pervasive potassium-epidote alteration. Moderate chlorite-actinolite alteration. Dominantly medium-grained with few coarse-grained crystals. Trace disseminated pyrite.				
Mineralogy	**Abundance (%)**	**Habit**	**Grain size**	**Notes**
Clinopyroxene	~45	Anhedral	Very fine- to fine-grained	Large amounts of alteration minerals occur internally in the crystal, though original grain boundaries are usually preserved.
Amphibole	3	Anhedral	Fine-grained	Interstitial to pyroxene.
Fe-Ti oxides	1	Blebby	Very fine-grained	Magnetite, disseminated throughout.

Sulphides	1	Blebby	Very fine-grained	Pyrite, disseminated throughout. Magnetite rims occur around the majority of pyrite grains.
Alteration assemblage	50	Anhedral, bladed to granular	Very fine-grained	Chlorite + sericite + epidote + tremolite + actinolite. Forms a groundmass or infringes onto CPX crystals.
Comments: Sericite is included in the alteration assemblage because there is not any recognizable plagioclase to tie the alteration to.				
Thin Section ID: TS-TG-041	**Sample ID:** A0137468	**Latitude:** 49.64158893	**Longitude:** -89.87697532	**Rock Name:** Mela-pyroxene hornblende orthopyroxene gabbro
Field Description: GABVT green-grey-black-white. Pyroxene: plagioclase 65:35. Intermittent biotite. Moderate chlorite-actinolite-epidote alteration. Trace disseminated pyrite.				
Mineralogy	**Abundance (%)**	**Habit**	**Grain size**	**Notes**
Plagioclase	<5	Anhedral	Very fine-grained	Pervasive sericite alteration to the point where very little of the original grain is preserved.
Orthopyroxene	5	Subhedral, rounded	Very fine- to fine-grained	Pitted and fractured, but without the alteration assemblage that occurs internally in CPX.
Clinopyroxene	25	Anhedral	Fine-grained	Alteration internal to crystal is pervasive. Alteration assemblage also infringes on grain boundaries. Pitted and fractured.

Amphibole	<5	Anhedral	Very fine-grained	Heavily fractured, occurs interstitial to pyroxene.
Fe-Ti oxides	<1	Blebby	Very fine-grained	Magnetite + ilmenite. Exsolution of hematite occurs in magnetite grains and exsolution of magnetite occurs in ilmenite grains. Disseminated throughout.
Sulphides	<1	Blebby	Very fine-grained	Pyrite + chalcopyrite. Magnetite rims some pyrite grains. Disseminated throughout.
Alteration assemblage	65	Anhedral, granular to bladed	Very fine-grained	Chlorite + epidote + talc + tremolite + actinolite + sericite. Forms either a granular groundmass or as radiating bladed crystals.
Comments: Sericite without any recognizable plagioclase is included as part of the alteration assemblage.				
Thin Section ID: TS-TG-042	**Sample ID:** A0137469	**Latitude:** 49.64224897	**Longitude:** -89.87855707	**Rock Name:** Mela-gabbronorite
Field Description: MGAB moderate to strong chlorite-actinolite alteration with strong potassium-alteration in mm-scale veins. 0.3% disseminated pyrite.				
Mineralogy	**Abundance (%)**	**Habit**	**Grain size**	**Notes**
Plagioclase	25	Anhedral	Very fine- to fine-grained	Moderate to intense levels of sericite alteration.

Clinopyroxene	30	Subhedral to anhedral	Fine-grained	Minor to moderate amounts of alteration towards the centre of the grain and zonation.
Orthopyroxene	30	Subhedral, rounded	Very fine- to fine-grained	Highly fractured.
Biotite	1	Tabular	Very fine-grained	Interstitial to plagioclase and pyroxene.
Amphibole	~5	Anhedral	Very fine-grained	Interstitial to pyroxene and plagioclase.
Fe-Ti oxides	1	Blebby	Very fine-grained	Magnetite + ilmenite. Disseminated throughout. Ilmenite displays some magnetite exsolution.
Sulphides	5	Blebby	Very fine-grained	Pyrite + chalcopyrite. Occurs as both disseminated grains and small aggregates.
Alteration assemblage	~5	Anhedral	Very fine-grained	Actinolite + chlorite. Both occur interstitial to pyroxene.
Thin Section ID: TS-TG-043	**Sample ID:** A0137474	**Latitude:** 49.64239244	**Longitude:** -89.87849104	**Rock Name:** Mela-gabbronorite
Field Description: MGAB green-grey-black-white. Pyroxene: plagioclase 70:30-75:25. Moderate to strong pervasive chlorite-actinolite alteration. 0.3% disseminated pyrite with pyrite-bearing oxidized leucocratic plagioclase accumulation. Outcrop part of diabase-capped ridge.				
Mineralogy	**Abundance (%)**	**Habit**	**Grain size**	**Notes**

Plagioclase	15	Anhedral	Fine-grained	Heavy amounts of sericite alteration, to the point where it almost completely obscures grain structure.
Orthopyroxene	20	Subhedral, rounded	Very fine- to fine-grained	Highly fractured.
Clinopyroxene	30	Anhedral	Very fine- to fine-grained	Replacement by chlorite at edges is common. Alteration internal to crystal occurs in many of the grains.
Biotite	15	Tabular	Very fine- to fine-grained	Interstitial to plagioclase and pyroxene.
Olivine	10	Rounded	Medium-grained	Relict only, where the original structure has been replaced by iddingsite.
Amphibole	1	Anhedral	Very fine-grained	Interstitial to pyroxene.
Fe-Ti oxides	2	Blebby and droplet	Very fine-grained	Magnetite, droplet texture is extremely fine-grained, and has almost a myrmekitic texture.
Sulphides	2	Blebby	Very fine-grained	Pyrite + chalcopyrite. Disseminated throughout sample. Pyrite sometimes forms small ringed clusters.
Alteration assemblage	5	Anhedral	Very fine-grained	Actinolite + tremolite. Occurs around pyroxene crystals.

Thin Section ID: TS-TG-044	**Sample ID:** A0137475	**Latitude:** 49.6417582	**Longitude:** -89.87637296	**Rock Name:** Plagioclase bearing hornblende pyroxenite
Field Description: L102N GAB green-grey-black-white. Pyroxene: plagioclase 65:35. Moderate to strong pervasive chlorite-actinolite. 0.2% disseminated pyrite. Weakly to moderately magnetic.				
Mineralogy	**Abundance (%)**	**Habit**	**Grain size**	**Notes**
Plagioclase	5	Anhedral	Fine- to medium-grained	Moderate to intense amounts of sericite alteration.
Orthopyroxene	5	Anhedral, rounded	Fine-grained	Minor amount of rim replacement by chlorite.
Clinopyroxene	40	Anhedral	Fine- to medium-grained	Alteration internal to crystal is pervasive. Rims replaced by chlorite and tremolite.
Biotite	5	Tabular	Very fine-grained	Interstitial to pyroxene.
Amphibole	10	Anhedral	Very fine- to fine-grained	Chlorite replacing edges.
Fe-Ti oxides	2	Anhedral, blebby	Very fine-grained	Magnetite + ilmenite. Disseminated throughout, occasionally forms aggregates.
Sulphides	1	Blebby	Very fine-grained	Pyrite, disseminated throughout sample.
Alteration assemblage	35	Anhedral, granular to bladed	Very fine-grained	Chlorite + talc + clay group minerals + tremolite + actinolite + epidote. Generally forms a groundmass which infringes onto main mineralogy.

Thin Section ID: TS-TG-045	**Sample ID:** A0137476	**Latitude:** 49.64167671	**Longitude:** -89.87651101	**Rock Name:** Plagioclase bearing pyroxenite
Field Description: MGAB at L102N. Green-grey-black-white. Pyroxene: plagioclase 70:30. Moderate to strong pervasive chlorite-actinolite-epidote alteration. Trace disseminated pyrite.				
Mineralogy	**Abundance (%)**	**Habit**	**Grain size**	**Notes**
Plagioclase	5	Anhedral	Fine- to medium-grained	Moderate to heavy amounts of sericite alteration.
Clinopyroxene	45	Anhedral	Very fine- to medium-grained	Alteration internal to crystal is common, to the point where it infringes on and obscures grain boundaries.
Orthopyroxene	20	Anhedral	Fine- to medium-grained	Replacement by chlorite around rims.
Biotite	<5	Tabular	Very fine-grained	Interstitial to pyroxene.
Amphibole	<5	Anhedral	Very fine-grained	Interstitial to pyroxene.
Fe-Ti oxides	1	Anhedral	Very fine-grained	Magnetite, disseminated throughout sample, occasionally forms small aggregates.
Sulphides	1	Blebby	Very fine-grained	Pyrite, disseminated throughout sample.
Alteration assemblage	25	Anhedral, granular to bladed	Very fine-grained	Talc + chlorite + epidote + calcite + tremolite + actinolite. Forma a groundmass that infringes on other phases.

Thin Section ID: TS-TG-046	**Sample ID:** A0137477	**Latitude:** 49.6398947	**Longitude:** -89.88133532	**Rock Name:** Pyroxene hornblende orthopyroxene gabbro
Field Description: Medium-grained granular subhedral pyroxene-plagioclase-hornblende with disseminated magnetite and trace pyrite, weak chlorite-sodium alteration, whaleback outcrop 5x20m.				
Mineralogy	**Abundance (%)**	**Habit**	**Grain size**	**Notes**
Plagioclase	30	Subhedral to anhedral	Very fine- to medium-grained	Weak to moderate levels of sericite alteration.
Clinopyroxene	~25	Anhedral	Very fine- to medium-grained	Alteration internal to crystal is common, as is chlorite replacement around edges. Larger grains enclose plagioclase and OPX.
Orthopyroxene	<5	Anhedral	Very fine- to medium-grained	Chlorite replacement around edges.
Amphibole	25	Anhedral	Medium-grained	Encloses CPX and plagioclase.
Biotite	~5	Tabular	Very fine-grained	Interstitial to plagioclase, pyroxene, and amphibole.
Fe-Ti oxides	2	Blebby	Very fine-grained	Magnetite + ilmenite. Disseminated throughout, with occasional aggregates. Ilmenite occurs with the magnetite aggregates. Ilmenite also has magnetite exsolution.
Sulphides	2	Blebby	Very fine-grained	Pyrite, disseminated throughout. Majority have magnetite rims of varying thickness.

Alteration assemblage	10	Anhedral, granular to bladed	Very fine-grained	Chlorite + epidote + tremolite + actinolite. Forms a groundmass which infringes on other phases.
Thin Section ID: TS-TG-047	**Sample ID:** A0137478	**Latitude:** 49.64345315	**Longitude:** -89.87742564	**Rock Name:** Leuco-pyroxene hornblende gabbro
Field Description: Just off Highway 811 flat 30x20m outcrop, medium- to coarse-grained plagioclase-pyroxene with 5% Biotite, 60/40 plagioclase: pyroxene ratio, and trace disseminated pyrite, moderate alteration.				
Mineralogy	**Abundance (%)**	**Habit**	**Grain size**	**Notes**
Plagioclase	45	Anhedral	Fine-grained	Weak to nearly complete levels of sericite alteration.
Clinopyroxene	10	Anhedral	Very fine- to fine-grained	Alteration internal to crystal and replacement at rims by chlorite and tremolite both occur.
Amphibole	5	Anhedral	Very fine- to fine-grained	Interstitial to plagioclase.
Biotite	10	Tabular	Very fine- to fine-grained	Interstitial to plagioclase and CPX.
Fe-Ti oxides	2	Blebby	Very fine- to fine-grained	Magnetite, disseminated throughout sample, with occasional aggregates.
Sulphides	2	Blebby	Very fine- to fine-grained	Pyrite + chalcopyrite. Chalcopyrite forms much smaller grains. Disseminated throughout sample.

Alteration assemblage	25	Anhedral, granular to bladed	Very fine- to fine-grained	Chlorite + epidote + actinolite + tremolite. Form a groundmass that overprints all other phases to varying degrees.
Thin Section ID: TS-TG-048	**Sample ID:** A0137479	**Latitude:** 49.62117575	**Longitude:** -89.88239007	**Rock Name:** Pyroxene hornblendite
Field Description: Non magnetic GAB, medium-grained granular plagioclase-pyroxene with disseminated biotite, no sulfides, 30x10m outcrop, appears to be more pyroxene-rich to north, with cross-cutting pegmatites and potassium-alteration, this GAB is likely primary unit.				
Mineralogy	**Abundance (%)**	**Habit**	**Grain size**	**Notes**
Plagioclase	5	Anhedral	Very fine-grained	Heavily altered by sericite.
Clinopyroxene	10	Anhedral	Fine-grained	Alteration internal to crystal is pervasive. Replacement by chlorite occurs along edges and propagates along cleavage planes.
Amphibole	35	Subhedral, massive	Fine- to medium-grained	Surrounds and occurs interstitial to plagioclase, pyroxene, and the alteration assemblage.
Sulphides	1	Blebby	Very fine-grained	Pyrite, disseminated throughout sample. Occasional inclusions of chalcopyrite in larger pyrite grains.
Alteration assemblage	50	Anhedral, bladed to granular	Very fine-grained	Chlorite + epidote + talc + tremolite + clay group minerals. Occurs as a groundmass which is interstitial to silicates.

Thin Section ID: TS-TG-049	**Sample ID:** A0137481	**Latitude:** 49.62196483	**Longitude:** -89.88254164	**Rock Name:** Plagioclase bearing hornblende pyroxenite
Field Description: 20x20m outcrop in middle of swamp, homogeneous medium-grained GAB observed for entire outcrop, granular pyroxene-plagioclase trace pyrite.				
Mineralogy	**Abundance (%)**	**Habit**	**Grain size**	**Notes**
Clinopyroxene	30	Subhedral to anhedral	Very fine- to fine-grained	Alteration internal to crystal is common. Alteration assemblage infringes and replaces grain boundaries.
Amphibole	5	Anhedral	Fine-grained	Interstitial to pyroxene.
Sulphides	<5	Blebby	Very fine-grained	Pyrite + minor amounts of chalcopyrite. Disseminated throughout sample. Magnetite rims pyrite grains.
Alteration assemblage	65	Anhedral, granular	Very fine-grained	Sericite + chlorite + epidote + tremolite. Groundmass occurs interstitial to pyroxene or intrudes onto pyroxene crystal boundaries.
Comments: Sericite is included under alteration assemblage because there are no fragments of unaltered plagioclase to identify the original mineralogy.				
Thin Section ID: TS-TG-050	**Sample ID:** A0137480	**Latitude:** 49.62123261	**Longitude:** -89.88222825	**Rock Name:** Plagioclase bearing hornblende pyroxenite
Field Description: Dark green pyroxene cumulate with disseminated coarse-grained potassium-alteration plagioclase, minor disseminated pyrite, trace chalcopyrite but some sporadic rusty				

spots on outcrop, few meter section on northeast part of outcrop with an increase in cross-cutting pegmatite veins.				
Mineralogy	**Abundance (%)**	**Habit**	**Grain size**	**Notes**
Clinopyroxene	45	Anhedral	Fine- to medium-grained	Alteration internal to crystal is pervasive. Cumulate texture.
Amphibole	20	Anhedral, massive	Medium-grained	Surrounds pyroxene crystals. Chlorite replacement occurs at edges.
Sulphides	1	Blebby	Very fine-grained	Pyrite, disseminated throughout. Thick rim of magnetite around nearly all grains.
Alteration assemblage	35	Anhedral	Very fine- to fine-grained	Sericite + epidote + clay group minerals + chlorite + talc + tremolite + actinolite. Forms a granular groundmass, interstitial to pyroxene and amphibole.
Thin Section ID: TS-TG-051	**Sample ID:** A0137490	**Latitude:** 49.61926804	**Longitude:** -89.88885796	**Rock Name:** Mela-pyroxene hornblende gabbro
Field Description: GAB - green-grey-black-white-pink. Weak to moderate pervasive chlorite-actinolite weak potassium-epidote alteration. Trace fine-grained disseminated pyrite. L75 trench.				
Mineralogy	**Abundance (%)**	**Habit**	**Grain size**	**Notes**
Plagioclase	10	Subhedral to anhedral	Very fine- to medium-grained	Weak to intense amounts of plagioclase alteration.
Clinopyroxene	10	Subhedral to anhedral	Very fine- to fine-grained	Alteration internal to crystal is pervasive.

Amphibole	40	Anhedral, massive	Fine- to medium-grained	Interstitial to plagioclase and pyroxene. Alteration assemblage infringes onto grain boundaries.
Fe-Ti oxides	<1	Blebby	Very fine-grained	Magnetite + Ilmenite. Disseminated throughout.
Sulphides	<1	Blebby	Very fine-grained	Pyrite, disseminated throughout. Thin rim of magnetite around most grains.
Alteration assemblage	40	Anhedral, granular	Very fine-grained	Calcite + epidote + actinolite + talc + clay group minerals. Infringes upon the silicates.

Thin Section ID:	**Sample ID:**	**Depth:**	**Rock Name:**
TS-TG-052	RR004-003	81.5 m	Label ¼: clinopyroxenite, middle ½: gabbro, far ¼: mafic dike

Drill Core Description:
Approximately 50-75% mafics. 25-50% plag. Clinopyroxene grains are dark with poor grain boundaries. Plagioclase grains are off-white to weak violet colour. Anhedral to subhedral grains. Moderate pervasive magnetism. The rock gradationally changes from gabbro to pyroxenite. The rock is medium-grained and altered. Colour varies from grey/green to grey/black. From 80.40 to 92.50 is a melanogabbro with gabbroic patches.

Location	**Mineralogy**	**Habit**	**Grain size**	**Notes**
Label ¼	Amphibole	anhedral	Fine-grained	Varying levels of internal alteration and zoning.
Label ¼	clinopyroxene	anhedral	Fine-grained	Varying levels of internal alteration and zoning.

Label ¼	Alteration assemblage	Anhedral	Very fine-grained	Talc + clay group minerals + tremolite. Occurs interstitial to CPX and amphibole.
Middle ½	Plagioclase	Subhedral to anhedral	Very fine- to medium-grained	Weak to moderate sericite alteration.
Middle ½	Amphibole	Anhedral	Very fine-grained	Interstitial to plagioclase.
Middle ½ Gabbro	Clinopyroxene	Anhedral	Fine-grained	Interstitial to plagioclase.
Middle ½	Alteration assemblage	Anhedral	Very fine-grained	Talc + tremolite + actinolite. Interstitial to plagioclase.
Far ¼	Plagioclase	Anhedral, rounded	Very fine-grained	No zoning observed.
Far ¼	Amphibole	Anhedral, rounded	Very fine-grained	No zoning observed.
Far ¼	Clinopyroxene	Anhedral, rounded	Very fine-grained	No zoning observed.
Far ¼	Alteration Assemblage	Anhedral, rounded	Very fine-grained	Tremolite, mainly one small patch of alteration.
Overall opaque mineralogy	Pyrite + ilmenite	Blebby	Very fine-grained	Disseminated throughout.

Comments:
Thin section represents a contact between a mafic dike, gabbro, and melanogabbro. Subsequently it is divided, with ¼ at either end of the thin section being different lithologies to the middle ½. No zoning to the mafic dike.

Thin Section ID:	**Sample ID:**	**Depth:**	**Rock Name:**
TS-TG-053	RR004-003	97.7 m	Troctolite under thin section Leucogabbro by hand sample

Drill Core Description:
The rock gradationally changes from gabbro to pyroxenite. The rock is medium-grained and altered. Colour varies from grey/green to grey/black. Plagioclase content ranges from 25%-50%. Patches of pegmatitic, felsic material.

Mineralogy	Abundance (%)	Habit	Grain size	Notes
Plagioclase	5	Anhedral	Medium- to coarse-grained	Intense levels of sericite alteration.
Olivine	20	Anhedral, rounded	Medium- to coarse-grained	Alteration assemblage infringes onto grain boundaries. Iddingsite alteration propagates along cracks in the crystal structure.
Alteration assemblage	75	Anhedral, granular to bladed	Very fine-grained	Talc + chlorite + clay group minerals + epidote + actinolite + tremolite. Interstitial to and infringes on silicates.
Sulphides	~1	Blebby	Very fine-grained	Pyrite, disseminated throughout.

Comments:
Sample collected of pegmatitic, nearly felsic veinlet. It is possible to see the original grain boundaries when looking at the thin section with the naked eye, but under microscope the majority have simply been replaced by the alteration assemblage.

Thin Section ID:	Sample ID:	Depth:	Rock Name:
TS-TG-054	RR004-003	110.4 m	Mafic: Orthopyroxene gabbro Felsic: Granodiorite

Drill Core Description:
Felsic dike: This unit is mainly quartz and K-feldspar in varying proportions and grain sizes. Areas are medium-grained and equigranular while others are very coarse-grained with no mafics. Feldspar grains are subhedral to euhedral and can be from 2 mm to 2 cm long. Unit somewhat resembles a large pegmatite dike with very little mafic content.

Location	Mineralogy	Habit	Grain size	Notes
Felsic half	Potassium Feldspar	Subhedral to anhedral	Fine- to medium-grained	Majority of the felsic half is potassium feldspar.

Felsic half	Quartz	Subhedral to anhedral, rounded	Very fine-grained	Interstitial to feldspar grains. There is an increase in quartz content towards the mafic half.
Boundary vein	Alteration assemblage	Anhedral	Very fine-grained	Quartz + plagioclase + muscovite + clay group minerals.
Mafic half	Plagioclase	Anhedral	Very fine- to medium-grained	Small percentage of mafic half. Miner amounts of sericite alteration.
Mafic half	Quartz	Subhedral, rounded	Very fine-grained	Small percentage of mafic half. Occurs with plagioclase.
Mafic half	Amphibole	Anhedral	Very fine- to fine-grained	Occurs with plagioclase and quartz. Tremolite infringes on amphibole grain boundaries.
Mafic half	Clinopyroxene	Anhedral	Medium-grained	~1/4 of the mafic half. Replacement by clay group minerals, tremolite, and actinolite occurs at grain boundaries. Alteration internal to crystal occurs.
Mafic half	Orthopyroxene	Anhedral, rounded	Very fine- to fine-grained	Small proportion of mafic half. Clay group minerals infringe upon grain boundaries.
Mafic half	Alteration assemblage	Anhedral, granular to bladed	Very fine- to fine-grained	Tremolite + actinolite + clay group minerals. The majority of the mafic half.

Comments: Sample was picked because it represents a contact point between a felsic dike and mafic intrusion.				
Thin Section ID: TS-TG-055	**Sample ID:** RR004-005	**Depth:** 123.9 m	**Rock Name:** Olivine gabbro	
Drill Core Description: Unit is medium-grained. Relatively homogeneous and moderately to strongly altered. Mineralogy consists of clinopyroxene. chlorite. serpentine. magnetite and plag with minor iddingsite. The rock is a deep green/grey/black colour with white to off-white plag. Plag content fairly consistent throughout at approximately 25%. Alteration is not as strong in upper half of unit where sulfide mineralization is present. Chlorite alteration is present smearing grain boundaries upper half.				
Mineralogy	**Abundance (%)**	**Habit**	**Grain size**	**Notes**
Plagioclase	~5	Anhedral	Fine-grained	Sericite alteration is heavy to complete, with tiny fragments of plagioclase.
Clinopyroxene	15	Subhedral to anhedral	Very fine- to fine-grained	Alteration internal to crystal and pits occur in most grains.
Olivine	20	Anhedral	Fine- to medium-grained	Alteration assemblage replaces grain boundaries. Heavily cracked. Iddingsite propagates along cracks.
Amphibole	15	Massive	Medium-grained	Amphibole encloses plagioclase and pyroxene, including grains that have been completely replaced by the alteration assemblage.
Fe-Ti oxides	<1	Anhedral	Very fine-grained	Occurs in association with sulphides.

Sulphides	~2	Anhedral	Very fine-grained	Chalcopyrite + pyrrhotite + pyrite. Chalcopyrite forms the majority and pyrrhotite and pyrite are more minor phases.
Alteration assemblage	40	Anhedral, granular to bladed	Very fine- to fine-grained	Talc + epidote + chlorite. Generally, occurs as a groundmass which has completely replaced original mineralogy.

Comments:
In drill core, represented a less altered unit of core near where the mafic Titan intrusion began.

Thin Section ID:	**Sample ID:**	**Depth:**	**Rock Name:**
TS-TG-056	RR004-005	144.5	Olivine clinopyroxenite

Drill Core Description:
Unit is medium-grained. Mineralogy consists of clinopyroxene. chlorite. serpentine. magnetite and plag with minor iddingsite. The rock is a deep green/grey/black colour with white to off-white plag. Plag content fairly consistent throughout at approximately 25%. Lower half is strongly altered increasing downhole. Here structurally the rock contains more fractures and shears allowing alteration to take place. A much softer dark green. black and white rock with deep blood red iddingsite and soft serpentine is abundant. Where the alteration intensifies most the plagioclase grains become hard to see. Fractures are covered by very soft slippery serpentine that scratches by a fingernail.

Mineralogy	**Abundance (%)**	**Habit**	**Grain size**	**Notes**
Olivine	30	Anhedral	Medium-grained	Grain boundaries replaced by alteration assemblage. Iddingsite propagates along cracks in crystal structure.

Clinopyroxene	15	Anhedral	Very fine- to medium-grained	Alteration internal to crystal is common.
Biotite	5	Anhedral, roughly tabular	Very fine-grained	Kinks within the crystal structure is common.
Amphibole	10	Subhedral to anhedral	Fine- to medium-grained	Alteration internal to crystal is common, as is replacement by alteration assemblage at grain boundaries.
Sulphides	5	Blebby	Very fine-grained	Pyrite + pyrrhotite + chalcopyrite. Mixture of individual disseminated grains and small aggregates. Aggregates contain all sulphide phases. Extremely thin rims of magnetite occur around pyrite grains.
Alteration assemblage	35	Subhedral to anhedral	Very fine- to medium-grained	Epidote + talc + chlorite + sericite. Epidote overtakes all other phases. Chlorite + talc + sericite form a groundmass.
Comments: Represents a more altered version of TS-TG-055. Sericite is included in the alteration assemblage because there is no recognizable plagioclase to tie back to original mineralogy.				

Appendix II

Whole Rock Geochemistry

sample number	lower detection limits	A0137359	A0137360	A0137361	A0137362	A0137363	A0137364	A0137365	A0137366
northing	UTM83-16	5502808.719	5502817.297	5502822.036	5504885.916	5504805.713	5504815.921	5504851.233	5504658.793
easting		291806.4412	291507.6366	291514.6125	294595.9444	294585.6041	294583.6828	294579.8897	294444.328
SiO_2 (wt%)	0.01	48.9	52.2	51.8	51.6	51.8	50.3	46.8	49.1
TiO_2 (wt%)	0.01	1.35	0.51	0.32	0.59	0.57	1.03	1.06	0.64
Al_2O_3 (wt%)	0.01	13.85	15.1	13.45	13.5	15.8	17.65	14.25	15.25
Fe_2O_3 (wt%)	0.01	14.25	9.01	7.45	9.48	9.1	9.07	14.65	10.25
MnO (wt%)	0.01	0.21	0.15	0.14	0.16	0.13	0.14	0.16	0.15
MgO (wt%)	0.01	6.27	6.49	8.72	7.58	6.08	5.1	5.99	6.5
CaO (wt%)	0.01	9.43	9.04	10.5	9.4	9.42	8.03	9.19	10.75
Na_2O (wt%)	0.01	2.54	2.51	2.09	2.8	3.26	4.18	2.98	2.79
K_2O (wt%)	0.01	0.73	1.49	1.42	1.49	1.51	1.71	1.17	1.42
P_2O_5 (wt%)	0.01	0.14	0.27	0.11	0.29	0.43	0.71	0.39	0.12
LOI	0.01	0.47	1.48	2.01	2.15	1.89	1.45	1.79	2.15
Total		98.21	98.36	98.09	99.17	100.16	99.59	98.56	99.25
Ba (ppm)	0.5	226	354	212	268	418	887	264	291
Ce (ppm)	0.1	22.4	57.7	27.6	58.3	50.9	179	50.5	42.7
Co (ppm)	1	49	39	38	39	38	29	46	47
Cr (ppm)	10	110	30	80	140	60	50	50	40
Cs (ppm)	0.01	1.16	1.5	0.55	0.63	0.55	0.59	0.6	0.69
Cu (ppm)	1	221	94	88	80	89	48	123	134
Dy (ppm)	0.05	5.15	3.07	1.93	3.43	2.6	4.11	3.15	2.62
Er (ppm)	0.03	3.03	1.64	1.05	1.69	1.1	1.69	1.3	1.11
Eu (ppm)	0.02	1.15	1.4	0.87	1.78	1.69	2.64	1.8	1.55
Ga (ppm)	0.1	20.9	16.8	13.6	15.6	16	24.2	18.9	16.4
Gd (ppm)	0.05	4.83	4.04	2.59	5.54	4.79	7.7	5.35	4.38
Hf (ppm)	0.1	3.3	2	1.4	2.8	1.5	6.4	1.8	1.7
Ho (ppm)	0.01	1.01	0.49	0.34	0.57	0.4	0.66	0.44	0.45
In (ppm)	0.005	0.013	0.006	0.0025	0.005	0.0025	0.014	0.007	0.007
La (ppm)	0.1	10	26	11.6	25.4	23	86.5	21.3	17
Li (ppm)	10	20	30	30	20	20	40	30	20
Lu (ppm)	0.01	0.37	0.2	0.14	0.16	0.11	0.2	0.17	0.14
Mo (ppm)	1	2	2	2	1	1	2	2	2
Nb (ppm)	0.1	5.7	4.3	3.4	4.6	3.4	12.3	4.9	5.3
Nd (ppm)	0.1	14.3	31.6	16.5	36.6	29.8	82.4	33.4	28.5
Ni (ppm)	1	108	109	194	83	69	49	51	81
Pb (ppm)	2	8	12	11	2	4	6	<2	6
Pr (ppm)	0.02	3.09	7.21	3.68	7.8	6.83	20.8	6.97	6
Rb (ppm)	0.2	23.5	61.3	57.6	62.6	47.7	48.7	39.9	48.6
Sc (ppm)	1	32	26	34	28	22	15	24	28
Se (ppm)	0.2	0.3	0.3	0.2	<0.2	0.2	0.2	0.2	0.4
Sm (ppm)	0.03	4.12	5.35	3.26	7.04	6	11.45	6.34	6
Sn (ppm)	1	1	1	1	1	1	2	1	1
Sr (ppm)	0.1	197.5	533	435	708	951	958	845	862
Ta (ppm)	0.1	0.4	0.3	0.2	0.2	0.2	0.4	0.3	0.2
Te (ppm)	0.01	0.01	0.02	0.03	0.01	0.01	0.01	0.01	0.01
Tb (ppm)	0.01	0.73	0.5	0.34	0.69	0.48	0.79	0.55	0.53
Th (ppm)	0.05	1.87	4.46	3.29	2.79	2.89	6.35	1.74	2.52
Tl (ppm)	0.02	0.09	0.19	0.03	0.03	0.03	0.16	0.02	0.03
Tm (ppm)	0.01	0.37	0.2	0.12	0.2	0.15	0.22	0.15	0.16
U (ppm)	0.05	0.65	0.89	0.89	0.39	0.59	0.88	0.7	0.92
V (ppm)	5	338	160	128	169	167	151	359	238
W (ppm)	1	3	1	1	1	1	<1	1	3
Y (ppm)	0.1	24.9	14.2	9.3	14.6	10.8	16.6	12.9	11.8
Yb (ppm)	0.03	2.65	1.43	0.88	1.31	0.86	1.59	1.07	1.08
Zn (ppm)	2	146	84	101	95	79	119	104	85
Zr (ppm)	2	106	77	44	100	56	270	69	66
Au (ppb)	0.001	5	3	4	0.5	0.5	0.5	0.5	0.5
Pd (ppb)	0.001	19	2	7	0.5	0.5	0.5	0.5	0.5
Pt (ppb)	0.005	12	2.5	6	2.5	2.5	2.5	2.5	2.5
S (wt%)	0.01	0.04	0.09	0.05	0.08	0.13	0.1	0.15	0.16

sample number	lower detection limits	A0137367	A0137368	A0137369	A0137370	A0137371	A0137373	A0137374	A0137375
northing	UTM83-16	5503411.417	5502925.665	5502543.463	5502487.835	5502516.539	5502464.859	5502444.573	5502427.557
easting		293301.4293	292408.8249	292642.7347	292604.1689	292581.2702	292576.1825	292463.4948	292480.4813
SiO_2 (wt%)	0.01	45.3	47.1	47.7	47.1	46.7	48	46.7	46.4
TiO_2 (wt%)	0.01	0.61	0.5	0.31	0.21	0.27	0.21	0.2	0.35
Al_2O_3 (wt%)	0.01	12.3	13.75	19.35	3.62	17.2	16.4	17.4	13.65
Fe_2O_3 (wt%)	0.01	12.25	10.75	7.33	8.33	8.03	8.16	6.33	9.6
MnO (wt%)	0.01	0.15	0.17	0.13	0.13	0.15	0.13	0.11	0.18
MgO (wt%)	0.01	9.28	9.1	7.04	21	8.58	7.82	9.66	12.5
CaO (wt%)	0.01	13.8	14.35	12.7	14.1	12.6	12.65	15.3	11.4
Na_2O (wt%)	0.01	1.47	1.78	2.33	0.49	1.83	1.77	0.98	1.11
K_2O (wt%)	0.01	0.68	0.55	0.83	0.15	1.22	1.29	0.31	1.56
P_2O_5 (wt%)	0.01	0.31	0.19	0.09	0.05	0.06	0.09	0.04	0.15
LOI	0.01	2.32	1.91	2.29	3.57	2.76	2.66	1.72	3.07
Total		98.61	100.28	100.26	99.14	99.54	99.33	98.87	100.18
Ba (ppm)	0.5	198	180	241	69.6	339	466	98.7	516
Ce (ppm)	0.1	38.6	40.5	26.1	14.6	24.8	32.8	19.4	36.7
Co (ppm)	1	67	56	44	77	51	89	50	59
Cr (ppm)	10	220	60	30	2720	50	80	70	550
Cs (ppm)	0.01	0.72	1.04	2.07	0.23	1.25	1.85	0.69	1.82
Cu (ppm)	1	365	76	87	11	92	960	107	70
Dy (ppm)	0.05	2.4	2.71	1.66	1.3	1.59	1.7	1.31	1.92
Er (ppm)	0.03	0.93	1.11	0.74	0.51	0.75	0.73	0.58	0.7
Eu (ppm)	0.02	1.45	1.63	1.23	0.62	1.07	1.19	0.97	1.21
Ga (ppm)	0.1	14.7	13.8	16.1	4.7	14.1	11.6	13.1	12.4
Gd (ppm)	0.05	4.23	4.56	2.66	1.98	2.94	3.06	2.34	3.26
Hf (ppm)	0.1	1	1.2	0.9	0.7	0.9	1	0.7	0.9
Ho (ppm)	0.01	0.36	0.41	0.24	0.18	0.26	0.26	0.23	0.3
In (ppm)	0.005	0.0025	0.0025	0.0025	0.005	0.0025	0.0025	0.0025	0.0025
La (ppm)	0.1	15	15.8	11.2	6	10.4	13.5	7.6	14.8
Li (ppm)	10	20	10	30	10	40	20	20	30
Lu (ppm)	0.01	0.09	0.11	0.07	0.06	0.09	0.08	0.05	0.09
Mo (ppm)	1	1	1	1	1	1	2	1	1
Nb (ppm)	0.1	1.5	1.8	1.4	0.7	1.1	1.4	0.4	2.3
Nd (ppm)	0.1	28.3	30.5	18.2	10.1	17.6	19.7	13.6	22.2
Ni (ppm)	1	248	62	67	686	84	1035	112	262
Pb (ppm)	2	5	3	3	<2	3	10	9	8
Pr (ppm)	0.02	5.78	5.99	3.86	1.99	3.67	4.4	2.83	5.14
Rb (ppm)	0.2	22.2	14.4	23.9	3.6	40	35.2	12.8	57.3
Sc (ppm)	1	40	41	21	49	27	30	34	25
Se (ppm)	0.2	0.5	0.4	0.3	<0.2	0.3	3.7	0.3	0.3
Sm (ppm)	0.03	6.03	6.79	3.82	2.44	3.87	4.12	2.96	4.97
Sn (ppm)	1	1	0.5	0.5	0.5	0.5	0.5	0.5	1
Sr (ppm)	0.1	840	838	1140	130.5	859	828	906	633
Ta (ppm)	0.1	0.1	0.1	0.1	0.05	0.1	0.1	0.1	0.1
Te (ppm)	0.01	0.04	0.01	0.02	0.01	0.01	0.17	0.01	0.01
Tb (ppm)	0.01	0.45	0.48	0.32	0.23	0.34	0.35	0.29	0.37
Th (ppm)	0.05	0.82	1.27	0.72	0.58	0.82	0.8	0.4	0.73
Tl (ppm)	0.02	0.01	0.02	0.02	1.77	0.04	0.04	0.04	0.06
Tm (ppm)	0.01	0.13	0.13	0.08	0.06	0.09	0.08	0.08	0.1
U (ppm)	0.05	0.18	0.23	0.12	0.12	0.32	0.14	0.09	0.13
V (ppm)	5	285	240	121	124	115	94	107	111
W (ppm)	1	<1	<1	<1	1	1	<1	<1	<1
Y (ppm)	0.1	10.1	10.9	6.5	4.7	6.7	6.8	5.8	7.5
Yb (ppm)	0.03	0.77	0.98	0.56	0.39	0.62	0.59	0.39	0.64
Zn (ppm)	2	76	52	68	66	73	55	40	83
Zr (ppm)	2	32	37	28	22	27	32	21	28
Au (ppb)	0.001	9	0.5	1	0.5	0.5	35	0.5	1
Pd (ppb)	0.001	95	0.5	0.5	1	0.5	109	0.5	2
Pt (ppb)	0.005	29	2.5	2.5	2.5	2.5	44	2.5	6
S (wt%)	0.01	0.49	0.24	0.21	0.07	0.18	1.45	0.11	0.17

sample number	lower detection limits	A0137376	A0137377	A0137378	A0137379	A0137380	A0137381	A0137382	A0137383
northing	UTM83-16	5502440.334	5502403.052	5502384.436	5502394.564	5502481.036	5502554.691	5502146.294	5502142.915
easting		292510.1086	292483.8868	292560.0949	292519.4181	292636.369	292622.7798	292560.9607	292559.2456
SiO_2 (wt%)	0.01	48.5	47.7	60	51.4	47.3	46.2	53.9	48.5
TiO_2 (wt%)	0.01	0.65	0.45	0.88	0.29	0.26	0.3	0.31	1.03
Al_2O_3 (wt%)	0.01	8.76	15.7	15.25	5.19	17.55	16.3	5.51	15.5
Fe_2O_3 (wt%)	0.01	13.8	8.32	6.99	8.39	8.22	10	7.38	10.6
MnO (wt%)	0.01	0.22	0.16	0.11	0.18	0.14	0.17	0.14	0.17
MgO (wt%)	0.01	12.15	8.61	3.89	16.45	8.45	9.43	15.25	7.56
CaO (wt%)	0.01	13.95	12.95	5.32	15.9	11.4	9.85	16.6	9.82
Na_2O (wt%)	0.01	1.09	1.17	3.42	0.66	1.99	2.06	0.81	3.11
K_2O (wt%)	0.01	0.59	1.49	2.76	0.26	0.84	1.35	0.44	1.37
P_2O_5 (wt%)	0.01	0.13	0.17	0.61	0.09	0.11	0.15	0.06	0.74
LOI	0.01	0.89	2.8	1.3	1.89	2.08	2.89	1.24	1.61
Total		101.07	99.71	100.75	101.03	98.51	98.85	101.77	100.23
Ba (ppm)	0.5	159.5	312	1020	74.6	331	343	113	655
Ce (ppm)	0.1	39.1	34.2	135	26.8	31	37.6	32	113
Co (ppm)	1	58	37	21	58	54	70	50	43
Cr (ppm)	10	1970	260	100	2220	50	40	640	200
Cs (ppm)	0.01	0.64	0.5	1.15	0.16	0.88	1.52	0.36	0.78
Cu (ppm)	1	99	70	27	22	81	140	11	71
Dy (ppm)	0.05	3.01	2.22	3.32	2.46	1.53	1.94	2.59	3.8
Er (ppm)	0.03	1.5	0.88	1.42	0.95	0.71	0.74	0.98	1.59
Eu (ppm)	0.02	1.54	1.33	1.99	1.29	1.15	1.38	1.5	2.53
Ga (ppm)	0.1	14.6	15.7	20.3	7.5	14.2	15	8.6	18
Gd (ppm)	0.05	5.32	3.79	6.06	4.43	2.53	3.18	4.54	7.23
Hf (ppm)	0.1	1.3	0.9	5.7	1	1	1.1	1.2	2.9
Ho (ppm)	0.01	0.53	0.35	0.59	0.38	0.23	0.31	0.44	0.56
In (ppm)	0.005	0.0025	0.0025	0.01	0.0025	0.0025	0.0025	0.0025	0.008
La (ppm)	0.1	13.6	13.7	61.6	9.7	13	15.3	11.1	47.1
Li (ppm)	10	20	30	40	20	30	40	20	40
Lu (ppm)	0.01	0.16	0.09	0.16	0.1	0.07	0.09	0.1	0.17
Mo (ppm)	1	1	1	2	1	1	1	3	1
Nb (ppm)	0.1	1.2	1.6	13.4	0.5	1.5	2.3	0.9	10.3
Nd (ppm)	0.1	30.1	21.3	58.6	22.7	18.6	22.7	27.1	62.4
Ni (ppm)	1	288	135	48	421	102	94	319	123
Pb (ppm)	2	4	5	10	<2	2	4	<2	3
Pr (ppm)	0.02	6.17	4.81	15.6	4.39	4.15	5.03	5.27	15
Rb (ppm)	0.2	19.1	65.2	88.9	10.4	24.4	48.4	18.4	36.1
Sc (ppm)	1	44	28	11	45	20	20	53	26
Se (ppm)	0.2	0.4	0.3	<0.2	<0.2	0.3	0.4	<0.2	<0.2
Sm (ppm)	0.03	6.71	4.79	9.64	5.23	3.85	5.01	5.97	11.35
Sn (ppm)	1	1	0.5	1	0.5	0.5	1	1	1
Sr (ppm)	0.1	403	967	715	239	1035	894	212	919
Ta (ppm)	0.1	0.1	0.1	0.8	0.05	0.1	0.1	0.1	0.4
Te (ppm)	0.01	0.01	0.01	0.01	0.005	0.01	0.02	0.01	0.01
Tb (ppm)	0.01	0.57	0.4	0.6	0.47	0.32	0.34	0.5	0.69
Th (ppm)	0.05	0.57	0.56	8.73	0.42	1.1	0.9	0.77	1.53
Tl (ppm)	0.02	0.02	0.02	0.24	0.01	0.03	0.03	0.03	0.07
Tm (ppm)	0.01	0.15	0.11	0.18	0.13	0.07	0.08	0.14	0.19
U (ppm)	0.05	0.09	0.14	1.92	0.13	0.24	0.19	0.18	0.39
V (ppm)	5	343	183	115	146	108	119	138	178
W (ppm)	1	<1	1	7	<1	<1	1	<1	2
Y (ppm)	0.1	13.1	8.6	14.4	10	6.4	7.6	10.5	15.5
Yb (ppm)	0.03	1.08	0.63	1.23	0.74	0.46	0.64	0.7	1.25
Zn (ppm)	2	100	66	100	77	70	95	54	121
Zr (ppm)	2	42	26	227	27	32	38	39	106
Au (ppb)	0.001	1	1	0.5	0.5	2	1	2	0.5
Pd (ppb)	0.001	14	3	0.5	4	1	0.5	218	1
Pt (ppb)	0.005	15	2.5	2.5	2.5	2.5	2.5	219	2.5
S (wt%)	0.01	0.15	0.11	0.07	0.04	0.16	0.31	0.02	0.09

sample number	lower detection limits	A0137384	A0137385	A0137386	A0137387	A0137388	A0137389	A0137390	A0137396
northing	UTM83-16	5502152.173	5502087.736	5501888.646	5502064.041	5501940.376	5502072.929	5501966.441	5503083.113
easting		292610.9305	292540.6512	292670.2676	292455.8757	292377.1114	291802.6316	291900.1305	292352.2501
SiO_2 (wt%)	0.01	52.4	52.2	51.4	52.5	47.2	45.4	49.5	47.1
TiO_2 (wt%)	0.01	0.33	0.31	0.34	0.28	0.43	1.2	0.23	0.31
Al_2O_3 (wt%)	0.01	5.43	5.24	4.99	7.48	9.74	17.8	18.8	18.25
Fe_2O_3 (wt%)	0.01	6.7	6.91	7.59	6.67	9.8	12.7	7.23	6.92
MnO (wt%)	0.01	0.14	0.15	0.16	0.14	0.18	0.16	0.11	0.13
MgO (wt%)	0.01	14	13.65	16.15	13.4	12.8	6.02	7.61	7.73
CaO (wt%)	0.01	17.9	17.15	16.75	15.4	13.45	9.61	11.15	13.05
Na_2O (wt%)	0.01	0.89	0.9	0.42	1.25	1.24	3.2	2.46	1.76
K_2O (wt%)	0.01	0.41	0.39	0.13	0.49	0.7	1.14	0.55	1.1
P_2O_5 (wt%)	0.01	0.04	0.04	0.13	0.19	0.28	1.38	0.05	0.1
LOI	0.01	1.18	1.22	2.09	1.19	3.04	2.55	1.69	2.93
Total		99.68	98.3	100.31	99.15	99.11	101.47	99.58	99.52
Ba (ppm)	0.5	126	130.5	93.7	180.5	256	1015	227	287
Ce (ppm)	0.1	28.5	32.3	37.4	41.4	65.9	108.5	22	40.8
Co (ppm)	1	38	43	51	43	50	44	38	45
Cr (ppm)	10	1800	920	930	590	1160	40	60	40
Cs (ppm)	0.01	0.35	0.26	0.09	0.42	0.41	0.8	1.28	1.74
Cu (ppm)	1	9	21	38	252	104	96	53	130
Dy (ppm)	0.05	2.54	2.75	2.75	2.54	2.92	3.93	1.58	2
Er (ppm)	0.03	0.94	1.13	1.17	1	1.1	1.41	0.62	1.07
Eu (ppm)	0.02	1.77	1.69	1.87	1.59	1.79	2.81	0.97	1.64
Ga (ppm)	0.1	8.1	8.7	7.4	8.8	10.6	20.6	15.1	15
Gd (ppm)	0.05	5.48	5.14	5.7	4.95	5.12	8	2.38	3.86
Hf (ppm)	0.1	1.1	1.5	1.3	1.3	1.8	0.6	0.7	1.2
Ho (ppm)	0.01	0.39	0.5	0.45	0.39	0.46	0.59	0.25	0.36
In (ppm)	0.005	0.0025	0.0025	0.0025	0.0025	0.0025	0.008	0.0025	0.005
La (ppm)	0.1	9.3	11.1	13.1	15.1	26	44.9	9.9	14.6
Li (ppm)	10	20	20	10	20	30	20	20	20
Lu (ppm)	0.01	0.11	0.1	0.11	0.12	0.13	0.14	0.05	0.09
Mo (ppm)	1	1	1	2	1	1	1	1	<1
Nb (ppm)	0.1	0.7	0.8	1.5	0.8	2.6	8	1.3	4.2
Nd (ppm)	0.1	27.9	27.4	32	29	40	64.9	13.7	27.6
Ni (ppm)	1	222	223	333	345	231	47	79	111
Pb (ppm)	2	3	7	4	5	4	2	5	3
Pr (ppm)	0.02	5.04	5.17	6	6.15	9.02	14.8	2.97	6.21
Rb (ppm)	0.2	17.5	15.3	4.5	16.8	14.5	26.5	12.5	35.8
Sc (ppm)	1	51	53	48	42	38	16	14	20
Se (ppm)	0.2	<0.2	<0.2	<0.2	0.2	0.5	0.3	0.2	0.215
Sm (ppm)	0.03	7.06	6.25	7.28	6.33	7.8	11.75	2.94	5.96
Sn (ppm)	1	1	1	1	0.5	0.5	1	0.5	1
Sr (ppm)	0.1	195	211	249	470	460	1615	1430	1095
Ta (ppm)	0.1	0.1	0.1	0.1	0.1	0.1	0.3	0.1	0.2
Te (ppm)	0.01	0.01	0.005	0.01	0.03	0.02	0.01	0.01	0.02
Tb (ppm)	0.01	0.56	0.56	0.55	0.52	0.58	0.77	0.29	0.44
Th (ppm)	0.05	0.66	0.72	1.34	0.62	2.89	0.65	0.39	1.11
Tl (ppm)	0.02	0.01	0.01	0.01	0.02	0.02	0.07	0.01	0.04
Tm (ppm)	0.01	0.1	0.13	0.13	0.11	0.12	0.19	0.06	0.12
U (ppm)	0.05	0.15	0.17	0.36	0.15	0.53	0.17	0.11	0.24
V (ppm)	5	158	184	160	113	206	258	93	111
W (ppm)	1	<1	<1	<1	<1	1	<1	<1	1
Y (ppm)	0.1	11.1	11.8	10.9	10.1	11.5	15.8	5.5	9.9
Yb (ppm)	0.03	0.73	0.86	0.75	0.66	0.94	1.01	0.5	0.67
Zn (ppm)	2	50	52	107	50	78	91	58	58
Zr (ppm)	2	37	44	41	35	67	18	22	41
Au (ppb)	0.001	1	1	2	13	5	2	1	1
Pd (ppb)	0.001	79	11	48	13	9	1	0.5	0.5
Pt (ppb)	0.005	41	8	30	8	9	2.5	2.5	2.5
S (wt%)	0.01	0.02	0.03	0.07	0.05	0.36	0.2	0.11	0.12

sample number	lower detection limits	A0137397	A0137399	A0137400	A0137401	A0137402	A0137451	A0137453	A0137454
northing	UTM83-16	5503120.176	5503154.089	5503167.386	5503294.48	5503297.86	5504057.985	5502970.416	5503095.131
easting		292355.4001	292379.7583	292395.7387	292489.7991	292523.6812	294025.9421	292460.9881	292585.1045
SiO_2 (wt%)	0.01	44.7	46.7	47.4	45.6	43.1	46.4	47.8	46.4
TiO_2 (wt%)	0.01	1	0.29	0.25	0.77	0.72	0.96	0.17	0.31
Al_2O_3 (wt%)	0.01	16.15	17.9	18.15	13.8	18	15.45	20.2	13.9
Fe_2O_3 (wt%)	0.01	17.65	6.71	6.42	14.85	13.2	16.1	5.21	7.45
MnO (wt%)	0.01	0.14	0.12	0.12	0.18	0.12	0.17	0.09	0.13
MgO (wt%)	0.01	5.59	7.76	7.51	8.27	4.8	5.92	6.41	10.35
CaO (wt%)	0.01	10.5	13.15	12.65	13.15	11.2	9.29	13.2	15.75
Na_2O (wt%)	0.01	2.41	1.81	2.05	2.06	2.55	2.76	1.78	1.01
K_2O (wt%)	0.01	1.23	1.34	0.86	0.38	0.75	0.91	1.04	0.7
P_2O_5 (wt%)	0.01	0.1	0.08	0.08	0.65	0.08	0.04	0.05	0.04
LOI	0.01	1.82	3.3	2.84	0.78	1.6	1.17	2.71	2.29
Total		101.44	99.32	98.5	100.64	96.3	99.28	98.84	98.47
Ba (ppm)	0.5	264	380	276	209	223	282	273	269
Ce (ppm)	0.1	32.6	35.6	37.3	52.4	24.2	29.1	22.7	20.8
Co (ppm)	1	69	41	38	51	64	76	39	49
Cr (ppm)	10	10	30	160	50	30	20	80	280
Cs (ppm)	0.01	1.42	2.06	2.22	0.42	0.62	0.68	1.87	2.32
Cu (ppm)	1	88	108	49	75	102	66	79	46
Dy (ppm)	0.05	1.89	1.48	1.46	3.29	1.45	2.36	1.53	1.79
Er (ppm)	0.03	0.89	0.77	0.74	1.28	0.68	1.24	0.61	0.59
Eu (ppm)	0.02	1.33	1.36	1.23	2.18	1.28	1.22	0.99	1.25
Ga (ppm)	0.1	21.3	14.2	14	18.6	19.7	21.1	15.4	11.6
Gd (ppm)	0.05	3.34	3.17	3.01	5.88	2.46	3.27	1.8	3.45
Hf (ppm)	0.1	1	1	1.1	1	0.9	1.4	0.6	0.7
Ho (ppm)	0.01	0.3	0.22	0.25	0.5	0.26	0.37	0.16	0.27
In (ppm)	0.005	0.006	0.0025	0.0025	0.009	0.006	0.008	0.0025	0.0025
La (ppm)	0.1	13.5	13.9	16.5	19.5	10.3	12.9	10.1	7.6
Li (ppm)	10	20	20	20	10	20	20	20	20
Lu (ppm)	0.01	0.09	0.08	0.06	0.12	0.08	0.17	0.06	0.1
Mo (ppm)	1	<1	<1	<1	<1	<1	<1	<1	<1
Nb (ppm)	0.1	2.3	2.5	3.8	1.9	2.5	4	1.1	1.8
Nd (ppm)	0.1	20.3	20.8	22	36.2	14.6	18.3	14.4	17.9
Ni (ppm)	1	17	67	81	30	52	16	111	171
Pb (ppm)	2	7	6	8	4	7	6	5	4
Pr (ppm)	0.02	4.54	5.04	4.79	7.85	3.2	3.95	3.17	3.32
Rb (ppm)	0.2	41.2	43.6	28.7	6.5	20	27	46.4	27.3
Sc (ppm)	1	26	29	26	33	20	28	16	42
Se (ppm)	0.2	0.239	<0.2	<0.2	<0.2	0.229	<0.2	<0.2	<0.2
Sm (ppm)	0.03	4.17	4.81	4.41	7.69	3.37	3.94	3.17	4.17
Sn (ppm)	1	1	1	1	1	1	1	0.5	0.5
Sr (ppm)	0.1	1055	977	1045	1085	1240	609	1315	658
Ta (ppm)	0.1	0.1	0.1	0.2	0.1	0.1	0.3	0.1	0.1
Te (ppm)	0.01	0.01	0.01	0.01	0.02	0.02	0.01	0.03	0.02
Tb (ppm)	0.01	0.37	0.32	0.34	0.63	0.3	0.41	0.22	0.37
Th (ppm)	0.05	1.21	1.52	1.72	0.76	0.8	1.91	0.91	0.43
Tl (ppm)	0.02	0.03	0.05	0.04	0.1	0.06	0.06	0.03	0.03
Tm (ppm)	0.01	0.11	0.09	0.09	0.15	0.08	0.19	0.06	0.08
U (ppm)	0.05	0.33	0.45	0.44	0.17	0.24	0.45	0.14	0.19
V (ppm)	5	478	136	108	368	448	514	77	155
W (ppm)	1	<1	<1	1	<1	<1	<1	<1	<1
Y (ppm)	0.1	7.2	7.5	6.6	12.5	6.3	10.6	5	7.6
Yb (ppm)	0.03	0.58	0.5	0.7	0.78	0.56	1.16	0.37	0.61
Zn (ppm)	2	77	52	57	81	75	111	43	51
Zr (ppm)	2	36	38	42	34	30	51	24	24
Au (ppb)	0.001	0.5	1	0.5	0.5	0.5	0.5	1	1
Pd (ppb)	0.001	0.5	0.5	0.5	1	2	0.5	1	140
Pt (ppb)	0.005	2.5	2.5	2.5	2.5	2.5	2.5	2.5	51
S (wt%)	0.01	0.4	0.09	0.05	0.11	0.31	0.37	0.13	0.09

sample number	lower detection limits	A0137455	A0137456	A0137458	A0137459	A0137460	A0137461	A0137462	A0137464
northing	UTM83-16	5503101.26	5503190.561	5503207.438	5503253.519	5503270.295	5502867.467	5502859.739	5502886.003
easting		292590.8354	292630.9679	292643.8314	292588.4853	292577.8564	292355.9195	292327.9414	292333.9279
SiO_2 (wt%)	0.01	43	48.4	48.6	46.9	47.8	48.5	47.6	47.7
TiO_2 (wt%)	0.01	0.86	0.38	0.34	0.22	0.37	0.65	0.72	0.68
Al_2O_3 (wt%)	0.01	14.25	8.69	10.5	17.55	18.15	14.1	14.7	14.25
Fe_2O_3 (wt%)	0.01	15.55	8.66	8.2	6.3	9.55	9.64	9.52	9.47
MnO (wt%)	0.01	0.16	0.17	0.16	0.12	0.11	0.16	0.15	0.15
MgO (wt%)	0.01	8.24	12.5	12	8.53	6.64	9.35	8.69	8.69
CaO (wt%)	0.01	12.75	17.1	15.5	13.35	12.65	13.8	13.05	13.8
Na_2O (wt%)	0.01	1.43	0.71	1.06	1.33	2.21	1.66	2.12	1.68
K_2O (wt%)	0.01	0.69	0.63	0.55	1.78	1	0.79	1.23	0.99
P_2O_5 (wt%)	0.01	0.08	0.03	0.05	0.1	0.12	0.13	0.23	0.21
LOI	0.01	1.69	1.77	2.31	3.72	2.47	2.82	1.81	2.07
Total		98.82	99.22	99.38	100.03	101.21	101.73	99.97	99.89
Ba (ppm)	0.5	186	133.5	143.5	399	209	207	405	834
Ce (ppm)	0.1	27.9	21.5	27.8	26	26.9	44.2	53	53.5
Co (ppm)	1	78	51	55	43	60	57	55	51
Cr (ppm)	10	180	950	280	110	30	70	80	100
Cs (ppm)	0.01	1.26	0.91	1	2.1	0.96	1.31	1.72	0.72
Cu (ppm)	1	251	52	65	41	81	75	77	41
Dy (ppm)	0.05	2.6	2.51	2.88	1.54	1.32	3.24	3.73	3.21
Er (ppm)	0.03	1.12	1.17	1.28	0.56	0.45	1.3	1.2	1.45
Eu (ppm)	0.02	1.61	1.49	1.61	1.09	1.04	2.14	2.3	2.3
Ga (ppm)	0.1	20.4	9.7	10	12.7	16.6	14.4	14.7	14.5
Gd (ppm)	0.05	4.2	4.44	4.95	2.44	2.13	6.35	6.14	6.61
Hf (ppm)	0.1	1.1	0.9	1.1	0.6	0.7	1.4	1.6	1.7
Ho (ppm)	0.01	0.42	0.41	0.43	0.22	0.26	0.51	0.61	0.5
In (ppm)	0.005	0.005	0.0025	0.0025	0.0025	0.0025	0.007	0.007	0.007
La (ppm)	0.1	11.3	6.6	9.8	11.3	12	16.2	20.2	19.9
Li (ppm)	10	20	30	20	30	20	20	20	10
Lu (ppm)	0.01	0.1	0.1	0.08	0.07	0.07	0.13	0.12	0.18
Mo (ppm)	1	<1	<1	<1	<1	<1	<1	<1	<1
Nb (ppm)	0.1	2	1.4	1.1	3.6	4.1	6.2	6.4	6.3
Nd (ppm)	0.1	22	20.7	25	17.8	16.5	36.3	39.2	40.9
Ni (ppm)	1	149	166	185	118	58	77	71	58
Pb (ppm)	2	4	8	4	4	4	4	7	5
Pr (ppm)	0.02	4.46	3.72	4.71	3.77	3.62	7.09	7.76	8.54
Rb (ppm)	0.2	21.7	37	22.5	84.3	34.2	27.5	41.3	26.5
Sc (ppm)	1	33	58	51	25	21	45	45	45
Se (ppm)	0.2	0.53	<0.2	<0.2	<0.2	0.326	<0.2	<0.2	<0.2
Sm (ppm)	0.03	4.81	5.11	5.86	3.54	3.3	7.66	8.16	8.54
Sn (ppm)	1	1	1	1	0.5	0.5	1	0.5	1
Sr (ppm)	0.1	741	314	535	620	1050	878	761	815
Ta (ppm)	0.1	0.1	0.1	0.1	0.1	0.2	0.3	0.3	0.4
Te (ppm)	0.01	0.02	0.01	0.01	0.01	0.01	0.01	0.01	0.01
Tb (ppm)	0.01	0.43	0.46	0.5	0.28	0.25	0.67	0.74	0.64
Th (ppm)	0.05	0.88	0.5	0.76	0.84	1.35	0.63	0.97	1.18
Tl (ppm)	0.02	0.03	0.02	0.02	0.05	0.05	0.02	0.03	0.03
Tm (ppm)	0.01	0.12	0.15	0.15	0.05	0.06	0.17	0.14	0.18
U (ppm)	0.05	0.16	0.13	0.19	0.22	0.32	0.18	0.21	0.31
V (ppm)	5	603	212	155	95	269	224	222	228
W (ppm)	1	<1	<1	<1	<1	<1	1	<1	1
Y (ppm)	0.1	10.3	10.8	11.2	6.1	5.6	13.1	14.4	14.5
Yb (ppm)	0.03	0.86	0.85	0.8	0.49	0.5	1.23	1.29	1.12
Zn (ppm)	2	86	65	60	56	58	75	67	74
Zr (ppm)	2	39	31	39	31	35	47	53	56
Au (ppb)	0.001	2	2	2	1	0.5	0.5	0.5	0.5
Pd (ppb)	0.001	3	9	93	15	1	0.5	0.5	1
Pt (ppb)	0.005	2.5	5	26	11	2.5	2.5	2.5	2.5
S (wt%)	0.01	0.31	0.05	0.07	0.07	0.23	0.12	0.2	0.06

sample number	lower detection limits	A0137465	A0137466	A0137467	A0137468	A0137469	A0137472	A0137474	A0137475
northing	UTM83-16	5502747.052	5502733.564	5502738.603	5502757.25	5502834.994	5502862.338	5502850.701	5502774.376
easting		292308.5142	292311.9032	292322.862	292300.8785	292189.4937	292213.6045	292194.87	292345.0515
SiO_2 (wt%)	0.01	48.9	47.2	48.2	46.6	51	49.4	51.1	47.4
TiO_2 (wt%)	0.01	0.38	0.31	0.29	0.34	0.42	0.28	0.42	0.29
Al_2O_3 (wt%)	0.01	12.7	9.56	7.9	9.06	8.01	15.85	8.13	11.8
Fe_2O_3 (wt%)	0.01	9	8.32	8.12	9	9.06	7.92	9.3	9.25
MnO (wt%)	0.01	0.15	0.16	0.17	0.17	0.18	0.14	0.19	0.16
MgO (wt%)	0.01	11.6	12.75	14.25	13.35	12.55	8.69	12.1	13.1
CaO (wt%)	0.01	13.25	16.4	15.65	16.35	15.05	13.3	14.55	14.35
Na_2O (wt%)	0.01	1.33	0.74	0.83	0.71	1.48	2.06	1.62	0.97
K_2O (wt%)	0.01	0.96	0.49	0.37	0.49	0.64	0.86	0.78	0.69
P_2O_5 (wt%)	0.01	0.15	0.05	0.03	0.05	0.28	0.05	0.38	0.08
LOI	0.01	2.82	3.14	2.74	2.96	1.96	2.31	1.6	3.14
Total		101.42	99.24	98.72	99.2	100.74	101	100.28	101.38
Ba (ppm)	0.5	300	111	85.5	112.5	215	301	273	208
Ce (ppm)	0.1	28.7	18.2	19.8	20.1	40.9	23.1	58.8	21.4
Co (ppm)	1	60	56	53	52	50	46	50	63
Cr (ppm)	10	730	480	860	520	390	80	320	630
Cs (ppm)	0.01	1.17	0.59	0.34	0.69	0.35	3.52	0.69	1.75
Cu (ppm)	1	62	116	20	70	225	115	193	64
Dy (ppm)	0.05	2.22	2.29	2.07	2.44	3.44	1.98	4.01	1.8
Er (ppm)	0.03	0.85	1.13	0.74	1.15	1.25	0.83	1.69	0.93
Eu (ppm)	0.02	1.02	1.08	1.13	1.08	2.05	1.44	2.37	1.18
Ga (ppm)	0.1	12.3	9.9	9	9	11.1	13.6	11.6	11
Gd (ppm)	0.05	3.21	4.09	3.18	3.89	5.98	3.05	6.88	2.74
Hf (ppm)	0.1	0.9	0.8	0.7	0.9	1.3	0.8	1.7	0.9
Ho (ppm)	0.01	0.37	0.36	0.4	0.45	0.57	0.23	0.57	0.33
In (ppm)	0.005	0.0025	0.0025	0.0025	0.0025	0.006	0.006	0.005	0.0025
La (ppm)	0.1	11.9	6.5	7.8	7.2	13.6	9.2	22.7	8.6
Li (ppm)	10	20	10	10	10	20	40	20	10
Lu (ppm)	0.01	0.13	0.13	0.12	0.11	0.21	0.09	0.21	0.12
Mo (ppm)	1	<1	<1	<1	<1	<1	1	<1	<1
Nb (ppm)	0.1	1.9	1	1.5	1.2	1.2	1.2	3.3	1.6
Nd (ppm)	0.1	19.1	16.7	14.3	17.5	37.6	18	46.3	14.9
Ni (ppm)	1	195	199	210	177	261	159	258	225
Pb (ppm)	2	6	5	6	4	73	3	7	5
Pr (ppm)	0.02	3.92	3.09	3.02	3.04	6.93	3.6	8.88	2.97
Rb (ppm)	0.2	38.5	19.4	11.2	18.1	22.1	27.8	29.4	30
Sc (ppm)	1	42	54	60	54	46	25	43	43
Se (ppm)	0.2	<0.2	<0.2	<0.2	<0.2	0.31	0.222	0.288	<0.2
Sm (ppm)	0.03	3.69	4.35	3.59	4.45	8.74	3.98	9.91	3.56
Sn (ppm)	1	1	1	1	1	1	0.5	1	0.5
Sr (ppm)	0.1	418	375	295	348	313	823	415	497
Ta (ppm)	0.1	0.1	0.1	0.1	0.1	0.1	0.2	0.2	0.1
Te (ppm)	0.01	0.01	0.01	0.01	0.005	0.03	0.01	0.02	0.01
Tb (ppm)	0.01	0.39	0.43	0.36	0.5	0.74	0.33	0.75	0.42
Th (ppm)	0.05	1.1	0.52	0.78	0.69	0.69	0.57	1.71	0.84
Tl (ppm)	0.02	0.03	0.02	0.01	0.02	0.02	0.03	0.04	0.03
Tm (ppm)	0.01	0.09	0.15	0.15	0.12	0.14	0.07	0.22	0.11
U (ppm)	0.05	0.21	0.16	0.25	0.16	0.15	0.15	0.4	0.18
V (ppm)	5	204	187	179	208	179	137	193	171
W (ppm)	1	<1	<1	<1	<1	<1	<1	<1	<1
Y (ppm)	0.1	8.9	9.6	8.9	10.7	14.3	7.6	16.2	8.3
Yb (ppm)	0.03	0.72	0.77	0.74	0.97	0.94	0.64	1.4	0.61
Zn (ppm)	2	66	57	60	54	149	52	77	57
Zr (ppm)	2	33	29	24	32	40	26	51	32
Au (ppb)	0.001	1	0.5	0.5	0.5	6	1	4	0.5
Pd (ppb)	0.001	14	2	6	2	1	1	1	10
Pt (ppb)	0.005	2.5	2.5	2.5	2.5	2.5	2.5	2.5	6
S (wt%)	0.01	0.11	0.06	0.02	0.05	0.16	0.15	0.16	0.08

sample number	lower detection limits	A0137476	A0137477	A0137478	A0137479	A0137480	A0137481	A0137482	A0137489
northing	UTM83-16	5502765.748	5502581.016	5502965.697	5500503.228	5500509.117	5500591.351	5500612.536	5500299.872
easting		292334.7525	291978.936	292276.2647	291822.9659	291834.9059	291815.355	291678.1111	291343.5026
SiO_2 (wt%)	0.01	48.3	48.6	49.5	47.3	49.6	48.5	46.5	48.1
TiO_2 (wt%)	0.01	0.37	0.39	0.35	0.27	0.4	0.2	0.22	0.21
Al_2O_3 (wt%)	0.01	8.24	16.3	17.35	15.2	5.61	15.35	6.94	16.4
Fe_2O_3 (wt%)	0.01	8.09	8.8	8.75	7.28	9.61	6.34	10.2	6.08
MnO (wt%)	0.01	0.16	0.14	0.14	0.11	0.17	0.14	0.15	0.1
MgO (wt%)	0.01	12.85	8.36	7.98	12.15	16.7	12.6	19.35	11.6
CaO (wt%)	0.01	18.75	12.25	11.65	11.95	13.95	11.25	12.45	10.9
Na_2O (wt%)	0.01	0.68	2.19	2.3	1.44	0.55	1.48	0.58	1.76
K_2O (wt%)	0.01	0.47	1.1	1.37	1	0.2	1.29	0.2	1.17
P_2O_5 (wt%)	0.01	0.05	0.13	0.14	0.07	0.04	0.05	0.02	0.06
LOI	0.01	1.82	2.02	2.22	2.6	2.45	3.92	2.08	3.81
Total		99.9	100.43	101.91	99.55	99.54	101.32	98.88	100.38
Ba (ppm)	0.5	148.5	350	443	318	39.5	345	70.9	356
Ce (ppm)	0.1	22.4	43.4	42.4	34.3	30.5	27.3	17.1	27.8
Co (ppm)	1	44	54	58	57	83	54	94	52
Cr (ppm)	10	430	40	10	560	1760	740	1130	550
Cs (ppm)	0.01	0.73	0.94	2	1.61	0.08	1.19	0.44	1.25
Cu (ppm)	1	58	92	175	70	176	67	81	116
Dy (ppm)	0.05	2.81	2.29	2.09	1.41	2.31	1.15	1.37	1.21
Er (ppm)	0.03	0.89	1.1	0.73	0.73	0.9	0.71	0.59	0.46
Eu (ppm)	0.02	1.32	1.71	1.35	0.99	1.08	0.65	0.79	0.64
Ga (ppm)	0.1	9.3	15	14.4	13.1	9	12.9	7.5	13.4
Gd (ppm)	0.05	3.58	4.56	2.93	2.27	3.62	1.93	1.91	2.19
Hf (ppm)	0.1	1.2	1.2	1.2	1.6	1.5	1.1	1.1	1.2
Ho (ppm)	0.01	0.47	0.4	0.31	0.24	0.32	0.2	0.21	0.23
In (ppm)	0.005	0.0025	0.0025	0.0025	0.0025	0.0025	0.0025	0.0025	0.0025
La (ppm)	0.1	7.4	18.7	18.7	16.2	12.1	13.2	6.4	14
Li (ppm)	10	10	20	20	20	10	30	5	20
Lu (ppm)	0.01	0.14	0.1	0.1	0.07	0.11	0.06	0.05	0.06
Mo (ppm)	1	<1	<1	<1	<1	<1	<1	<1	<1
Nb (ppm)	0.1	1.1	3.2	3.5	2.7	2.6	2	0.8	2.2
Nd (ppm)	0.1	21.2	29.8	25.8	18	21.8	15.5	13.1	14.2
Ni (ppm)	1	148	74	49	286	519	316	532	285
Pb (ppm)	2	5	5	11	6	3	7	4	3
Pr (ppm)	0.02	3.93	6.21	5.79	4.32	4.3	3.49	2.56	3.43
Rb (ppm)	0.2	19.2	32	56.5	31.4	2.3	53.9	5.1	47
Sc (ppm)	1	69	31	27	26	50	24	39	21
Se (ppm)	0.2	<0.2	0.199	0.453	<0.2	0.412	<0.2	<0.2	0.209
Sm (ppm)	0.03	4.8	5.69	4.35	3.42	4.68	2.33	2.55	2.86
Sn (ppm)	1	1	0.5	0.5	0.5	1	0.5	0.5	1
Sr (ppm)	0.1	313	810	835	561	154.5	505	217	595
Ta (ppm)	0.1	0.1	0.1	0.2	0.2	0.2	0.2	0.1	0.1
Te (ppm)	0.01	0.01	0.01	0.02	0.01	0.06	0.02	0.02	0.03
Tb (ppm)	0.01	0.46	0.43	0.39	0.26	0.4	0.18	0.23	0.23
Th (ppm)	0.05	0.56	2	2.09	2.54	1.82	2.16	0.79	2.1
Tl (ppm)	0.02	0.02	0.03	0.06	0.03	0.01	0.02	0.07	0.03
Tm (ppm)	0.01	0.13	0.11	0.08	0.07	0.11	0.05	0.06	0.07
U (ppm)	0.05	0.12	0.26	0.43	0.38	0.26	0.33	0.11	0.42
V (ppm)	5	242	152	139	95	137	78	102	74
W (ppm)	1	<1	<1	<1	1	<1	<1	<1	1
Y (ppm)	0.1	11.6	10.3	7.4	6.2	9	5.1	5.8	5.2
Yb (ppm)	0.03	0.75	0.7	0.76	0.6	0.82	0.39	0.43	0.38
Zn (ppm)	2	42	56	75	59	79	66	67	52
Zr (ppm)	2	34	59	44	58	57	48	28	53
Au (ppb)	0.001	1	0.5	0.5	0.5	4	0.5	1	0.5
Pd (ppb)	0.001	22	1	0.5	2	9	1	1	2
Pt (ppb)	0.005	17	2.5	2.5	2.5	14	2.5	2.5	2.5
S (wt%)	0.01	0.05	0.17	0.13	0.1	0.2	0.08	0.1	0.2

sample number	lower detection limits	A0137490	A0137492	A0137493	A0137499	A0137500	A0159001	A0159002	A0159003
northing	UTM83-16	5500309.087	5500300.613	5500294.681	5502498.402	5502467.689	5502460.95	5502465.409	5502463.899
easting		291347.7342	291355.359	291349.4284	292551.8738	292554.6774	292541.7644	292559.0724	292557.5634
SiO_2 (wt%)	0.01	48.5	47.6	46.8	43.7	46.8	47.2	46.1	44.7
TiO_2 (wt%)	0.01	0.34	0.3	0.26	1.01	0.42	0.26	0.42	0.75
Al_2O_3 (wt%)	0.01	12.75	13.5	13.7	18.05	18.05	18.7	15.6	12.3
Fe_2O_3 (wt%)	0.01	7	6.94	6.73	12.35	9.4	8.9	10.35	11.7
MnO (wt%)	0.01	0.11	0.11	0.11	0.13	0.14	0.13	0.15	0.18
MgO (wt%)	0.01	13.15	13	12.65	6.67	6.42	8.54	9.51	12.75
CaO (wt%)	0.01	11.2	12.6	12.35	10.8	10.7	11.75	12.4	11.4
Na_2O (wt%)	0.01	1.6	1.27	1.45	3.08	3.13	1.95	1.99	1.76
K_2O (wt%)	0.01	0.77	0.59	0.61	0.47	0.36	0.39	0.84	0.55
P_2O_5 (wt%)	0.01	0.13	0.08	0.07	1.39	1.11	0.11	0.52	0.53
LOI	0.01	3.15	2.98	3.13	1.05	1.68	0.91	2.67	1.14
Total		98.88	99.15	98.03	98.93	98.42	98.99	100.74	98.01
Ba (ppm)	0.5	245	209	215	313	259	240	270	293
Ce (ppm)	0.1	43	34.6	31.1	108	63.5	24.9	60.2	80
Co (ppm)	1	58	59	57	56	38	62	58	60
Cr (ppm)	10	780	710	710	160	110	30	330	1100
Cs (ppm)	0.01	0.83	0.91	0.82	0.24	0.44	0.45	0.93	0.3
Cu (ppm)	1	64	81	72	139	43	44	76	60
Dy (ppm)	0.05	1.65	1.68	1.52	4.52	2.39	1.24	2.77	4.43
Er (ppm)	0.03	0.71	0.69	0.71	1.73	1.04	0.74	1.05	1.77
Eu (ppm)	0.02	0.86	1.01	0.91	3.45	2.29	1.15	1.98	2.75
Ga (ppm)	0.1	13.1	13	12.7	21.4	19.1	15.8	14.5	15.6
Gd (ppm)	0.05	2.78	2.48	2.41	9.45	4.59	2.68	5.36	7.96
Hf (ppm)	0.1	2.2	1.4	1.3	1.3	0.5	0.7	1.1	2.7
Ho (ppm)	0.01	0.26	0.26	0.26	0.75	0.28	0.25	0.36	0.63
In (ppm)	0.005	0.0025	0.0025	0.0025	0.01	0.0025	0.0025	0.005	0.012
La (ppm)	0.1	22.5	15.6	14.7	45.4	29.1	11.6	26.2	31.6
Li (ppm)	10	20	10	10	10	10	10	20	10
Lu (ppm)	0.01	0.09	0.08	0.06	0.12	0.07	0.05	0.07	0.14
Mo (ppm)	1	8	<1	<1	<1	<1	<1	<1	<1
Nb (ppm)	0.1	3.8	2.9	2.5	5.6	0.7	1.1	2	5.8
Nd (ppm)	0.1	21.3	20.3	17.3	70.6	38.9	16.5	38	55.6
Ni (ppm)	1	362	327	311	95	71	92	126	328
Pb (ppm)	2	2	4	5	5	4	3	4	5
Pr (ppm)	0.02	5.35	4.65	4.23	16.4	9.28	3.78	8.93	12.35
Rb (ppm)	0.2	24	17.4	19	4.1	7	8.8	20.7	6.3
Sc (ppm)	1	29	30	28	20	13	20	26	30
Se (ppm)	0.2	<0.2	<0.2	<0.2	0.223	<0.2	<0.2	<0.2	<0.2
Sm (ppm)	0.03	3.81	3.96	3.3	12.65	7.19	3.43	6.89	11.85
Sn (ppm)	1	1	1	1	1	1	0.5	0.5	1
Sr (ppm)	0.1	435	548	521	1575	1480	1115	945	761
Ta (ppm)	0.1	0.2	0.2	0.2	0.3	0.1	0.1	0.1	0.3
Te (ppm)	0.01	0.02	0.02	0.02	0.01	0.005	0.01	0.01	0.01
Tb (ppm)	0.01	0.29	0.29	0.23	0.87	0.47	0.3	0.5	0.78
Th (ppm)	0.05	4.47	2.26	2.38	1.08	0.71	0.77	1.38	0.81
Tl (ppm)	0.02	0.02	0.02	0.03	0.01	0.01	0.02	0.02	0.01
Tm (ppm)	0.01	0.08	0.07	0.07	0.2	0.11	0.05	0.12	0.15
U (ppm)	0.05	0.67	0.48	0.37	0.23	0.12	0.09	0.26	0.09
V (ppm)	5	110	103	100	291	179	130	176	238
W (ppm)	1	<1	1	<1	<1	<1	<1	<1	<1
Y (ppm)	0.1	7.7	7.7	6.8	19	9.9	5.9	11.2	17.3
Yb (ppm)	0.03	0.49	0.63	0.61	1.21	0.51	0.51	0.65	1.45
Zn (ppm)	2	61	54	51	86	82	59	71	91
Zr (ppm)	2	89	57	54	40	15	26	39	85
Au (ppb)	0.001	0.5	0.5	0.5	1	0.5	1	0.5	0.5
Pd (ppb)	0.001	2	2	2	2	1	1	6	5
Pt (ppb)	0.005	2.5	2.5	2.5	2.5	2.5	2.5	5	2.5
S (wt%)	0.01	0.07	0.12	0.14	0.18	0.08	0.09	0.14	0.1

sample number	lower detection limits	A0159004	A0159005	A0159006	A0159007	A0159008	A0159009	A0159010	A0159011
northing	UTM83-16	5502475.067	5502471.668	5502471.708	5502462.34	5502456.441	5502458.93	5502457.311	5502448.842
easting		292556.6894	292546.5882	292545.7224	292543.1909	292543.1827	292544.8731	292552.4675	292543.9743
SiO_2 (wt%)	0.01	47.9	48.3	48.2	49.8	46.9	49.5	47.7	46.6
TiO_2 (wt%)	0.01	0.27	0.26	0.25	0.4	0.49	0.31	0.48	0.36
Al_2O_3 (wt%)	0.01	17.3	17.8	17.8	11.05	10.75	5.76	10.75	18.05
Fe_2O_3 (wt%)	0.01	7.98	7.87	7.79	9.24	10.35	7.99	10.5	9.02
MnO (wt%)	0.01	0.13	0.13	0.12	0.14	0.17	0.12	0.18	0.14
MgO (wt%)	0.01	8.42	8.09	8.48	13.15	12.8	20.4	13.75	9.63
CaO (wt%)	0.01	13	12.7	12.5	12.4	14.35	12.8	13.4	11.15
Na_2O (wt%)	0.01	1.97	2.17	1.84	1.45	1.27	0.69	1.28	2.13
K_2O (wt%)	0.01	0.47	0.66	0.32	0.46	0.4	0.3	0.43	0.55
P_2O_5 (wt%)	0.01	0.09	0.07	0.06	0.21	0.32	0.13	0.28	0.45
LOI	0.01	2.06	3	1.06	1.24	1.58	1.7	1.37	2.71
Total		99.74	101.22	98.56	99.82	99.58	100.14	100.36	100.96
Ba (ppm)	0.5	254	250	169.5	189.5	162.5	145	180.5	221
Ce (ppm)	0.1	28.5	25	20.5	31.1	55.3	30.9	45	34.7
Co (ppm)	1	56	49	58	61	65	74	63	66
Cr (ppm)	10	50	40	40	1360	940	3080	1270	130
Cs (ppm)	0.01	0.89	1.41	0.49	0.71	0.35	0.47	0.38	1.13
Cu (ppm)	1	117	104	117	80	63	5	53	328
Dy (ppm)	0.05	1.54	1.4	1.19	1.89	3.53	1.73	3.04	2.13
Er (ppm)	0.03	0.85	0.77	0.73	0.72	1.46	0.66	1.33	0.7
Eu (ppm)	0.02	1.29	1.16	1.13	1.34	2.24	0.83	2.12	1.42
Ga (ppm)	0.1	15.1	14.8	15.4	12.6	12.4	8.1	13	15
Gd (ppm)	0.05	3.13	3.21	2.23	3.56	6.52	2.91	5.76	3.67
Hf (ppm)	0.1	1.1	0.9	0.8	1.1	1.7	1.3	2	0.9
Ho (ppm)	0.01	0.31	0.26	0.23	0.3	0.58	0.22	0.51	0.36
In (ppm)	0.005	0.0025	0.0025	0.0025	0.0025	0.007	0.0025	0.007	0.005
La (ppm)	0.1	12.3	11.6	9.5	12.9	21	14.5	17.3	15.2
Li (ppm)	10	10	20	10	10	10	10	10	20
Lu (ppm)	0.01	0.08	0.07	0.05	0.05	0.12	0.09	0.11	0.08
Mo (ppm)	1	<1	<1	<1	<1	<1	<1	<1	<1
Nb (ppm)	0.1	1.4	1.3	0.9	1.4	2.9	2.4	2.4	1.6
Nd (ppm)	0.1	19.5	16.7	14.2	22.7	41.6	16.9	36.2	23.1
Ni (ppm)	1	101	86	98	337	223	779	282	272
Pb (ppm)	2	5	3	4	3	5	4	5	6
Pr (ppm)	0.02	4.43	3.6	3.04	5.06	8.86	3.97	7.46	5.26
Rb (ppm)	0.2	11.9	21.7	9.3	12.1	7.2	7.9	8	13.2
Sc (ppm)	1	29	27	26	31	47	28	42	18
Se (ppm)	0.2	0.268	0.199	0.239	0.307	<0.2	<0.2	<0.2	0.548
Sm (ppm)	0.03	4.17	3.4	2.81	4.37	9.65	3.55	7.87	4.93
Sn (ppm)	1	0.5	0.5	0.5	0.5	1	0.5	1	0.5
Sr (ppm)	0.1	1100	1145	1035	528	548	217	543	1020
Ta (ppm)	0.1	0.1	0.1	0.1	0.1	0.1	0.1	0.1	0.1
Te (ppm)	0.01	0.02	0.01	0.01	0.01	0.02	0.005	0.01	0.04
Tb (ppm)	0.01	0.34	0.29	0.22	0.37	0.67	0.31	0.61	0.43
Th (ppm)	0.05	0.67	0.95	0.43	0.43	1.07	2.35	1.17	0.67
Tl (ppm)	0.02	0.01	0.02	0.03	0.05	0.01	0.03	0.02	0.02
Tm (ppm)	0.01	0.07	0.09	0.06	0.09	0.15	0.08	0.15	0.1
U (ppm)	0.05	0.09	0.17	0.07	0.11	0.23	0.42	0.17	0.13
V (ppm)	5	137	118	120	156	231	86	207	103
W (ppm)	1	<1	<1	<1	<1	<1	<1	<1	<1
Y (ppm)	0.1	7.7	6.7	5.9	9.1	14.9	6.8	13.5	8.1
Yb (ppm)	0.03	0.63	0.58	0.52	0.61	1.23	0.58	0.86	0.52
Zn (ppm)	2	53	52	52	74	72	65	85	73
Zr (ppm)	2	32	29	26	35	60	57	58	27
Au (ppb)	0.001	0.5	0.5	0.5	1	1	0.5	0.5	8
Pd (ppb)	0.001	0.5	1	1	6	16	3	13	34
Pt (ppb)	0.005	2.5	2.5	2.5	7	11	2.5	9	18
S (wt%)	0.01	0.28	0.21	0.05	0.06	0.21	0.03	0.11	0.29

sample number	lower detection limits	A0159012	A0159013	A0159014	A0159015	A0159018	A0159019	A0159020	A0159021
northing	UTM83-16	5502434.365	5502450.432	5502442.814	5502445.413	5500623.524	5500628.073	5500625.324	5502145.014
easting		292543.999	292537.2457	292535.5058	292543.1992	291678.9605	291670.8218	291672.6689	292559.6166
SiO_2 (wt%)	0.01	40.5	44.3	49.7	47.9	47.8	46.8	43.8	51.4
TiO_2 (wt%)	0.01	0.12	0.15	0.54	0.25	0.38	0.3	0.16	0.32
Al_2O_3 (wt%)	0.01	13.3	18.85	13.55	15.05	6.66	7.7	8.38	4.55
Fe_2O_3 (wt%)	0.01	13.05	10.8	11	7.92	8.53	8.21	11.35	7.78
MnO (wt%)	0.01	0.2	0.13	0.14	0.11	0.16	0.14	0.15	0.16
MgO (wt%)	0.01	17.4	11.3	9.83	8.72	16.55	16.15	20.7	15.8
CaO (wt%)	0.01	6.95	9.49	11.6	16.3	14.2	14.1	9.25	16.95
Na_2O (wt%)	0.01	0.61	1.3	2.15	1.41	0.94	0.72	0.57	0.75
K_2O (wt%)	0.01	0.41	0.43	0.57	0.45	0.34	0.3	0.23	0.33
P_2O_5 (wt%)	0.01	0.08	0.05	0.21	0.06	0.09	0.04	0.04	0.06
LOI	0.01	5.59	3.59	0.91	2.16	3.44	3.55	4.1	1.72
Total		98.25	100.52	100.41	100.46	99.28	98.19	98.82	99.94
Ba (ppm)	0.5	151	179.5	266	153	124.5	113	99.3	110
Ce (ppm)	0.1	14	14.9	37.7	23.9	36.7	25	19.6	30.1
Co (ppm)	1	130	91	61	78	66	69	113	50
Cr (ppm)	10	20	50	710	220	1330	1140	520	670
Cs (ppm)	0.01	1.04	1.31	0.59	1.41	0.49	0.49	0.44	0.36
Cu (ppm)	1	701	1220	148	3560	63	107	122	13
Dy (ppm)	0.05	0.81	0.56	2.27	1.95	2.34	1.87	1.04	2.81
Er (ppm)	0.03	0.26	0.29	0.97	0.81	0.93	0.8	0.39	1.23
Eu (ppm)	0.02	0.52	0.62	1.51	1.24	1.21	0.97	0.52	1.75
Ga (ppm)	0.1	9.2	12.9	16.9	11.8	9.3	8.4	8.3	7.9
Gd (ppm)	0.05	1.24	1.01	3.72	3.42	3.58	2.77	1.48	5.23
Hf (ppm)	0.1	0.5	0.4	1.2	0.9	1.9	1.1	0.9	1.4
Ho (ppm)	0.01	0.15	0.1	0.33	0.29	0.36	0.33	0.16	0.46
In (ppm)	0.005	0.0025	0.005	0.0025	0.009	0.0025	0.0025	0.0025	0.0025
La (ppm)	0.1	6.7	8	17.1	9.6	15.3	9.9	8.9	10.5
Li (ppm)	10	40	20	20	10	10	10	10	20
Lu (ppm)	0.01	0.03	0.01	0.1	0.09	0.11	0.09	0.04	0.11
Mo (ppm)	1	<1	<1	<1	<1	<1	<1	<1	<1
Nb (ppm)	0.1	0.8	0.6	1.7	0.7	2.5	1.6	1.2	1
Nd (ppm)	0.1	8.7	7.7	24.6	18.8	21.8	16.7	10.8	27.2
Ni (ppm)	1	757	489	201	1420	391	392	586	281
Pb (ppm)	2	3	2	2	4	4	<2	21	3
Pr (ppm)	0.02	2.06	1.98	5.68	3.95	5.26	3.75	2.63	5.38
Rb (ppm)	0.2	12.8	13.7	16.2	18	7.5	7.5	5.2	13.9
Sc (ppm)	1	7	8	29	46	49	45	24	53
Se (ppm)	0.2	1.62	2.81	0.261	3.95	0.2	0.2	0.4	<0.2
Sm (ppm)	0.03	2.08	1.6	5.1	4.38	5.27	3.85	2.2	6.69
Sn (ppm)	1	0.5	0.5	1	1	1	1	0.5	1
Sr (ppm)	0.1	231	928	770	697	181	218	132.5	158.5
Ta (ppm)	0.1	0.1	0.05	0.1	0.1	0.2	0.1	0.1	0.1
Te (ppm)	0.01	0.26	0.47	0.01	0.4	0.02	0.02	0.08	0.01
Tb (ppm)	0.01	0.11	0.15	0.44	0.38	0.44	0.33	0.19	0.58
Th (ppm)	0.05	0.37	0.42	0.71	0.49	2.26	1.56	1.54	0.81
Tl (ppm)	0.02	0.02	0.18	0.05	0.26	0.05	0.01	0.19	0.02
Tm (ppm)	0.01	0.03	0.03	0.13	0.11	0.13	0.11	0.04	0.15
U (ppm)	0.05	0.09	0.11	0.15	0.07	0.4	0.26	0.27	0.15
V (ppm)	5	40	60	256	129	179	124	70	146
W (ppm)	1	<1	<1	<1	<1	<1	1	<1	<1
Y (ppm)	0.1	3.2	2.5	9.6	8.3	9.6	8.2	4.6	11.9
Yb (ppm)	0.03	0.31	0.22	0.82	0.62	0.85	0.57	0.29	0.88
Zn (ppm)	2	131	74	83	51	71	64	94	58
Zr (ppm)	2	14	15	38	29	68	45	35	39
Au (ppb)	0.001	85	123	0.5	152	1	4	3	0.5
Pd (ppb)	0.001	99	513	4	717	1	4	17	171
Pt (ppb)	0.005	59	181	2.5	175	2.5	2.5	8	171
S (wt%)	0.01	0.35	0.53	0.14	1.18	0.06	0.17	0.29	0.01

sample number	lower detection limits	A0159022	A0159023	A0159024	A0159025	A0159033	A0159034	A0159036	A0159037
northing	UTM83-16	5502147.704	5502160.321	5502172.969	5502167.54	5507397.195	5507398.465	5507412.282	5507406.023
easting		292553.2838	292555.1391	292614.468	292599.1555	293799.3628	293798.1095	293791.8509	293786.8456
SiO_2 (wt%)	0.01	52.3	51.6	51.5	51.4	48.8	48.5	47.8	46.4
TiO_2 (wt%)	0.01	0.29	0.27	0.31	0.37	0.38	0.35	0.37	0.76
Al_2O_3 (wt%)	0.01	6.12	10.2	5.81	4.81	12.65	11.45	10.5	9.1
Fe_2O_3 (wt%)	0.01	8.89	7.44	6.6	6.92	9.61	9.92	9.63	14.5
MnO (wt%)	0.01	0.18	0.15	0.13	0.15	0.16	0.16	0.16	0.2
MgO (wt%)	0.01	15.7	12.45	13.7	14.4	12.3	13.8	13.45	14.6
CaO (wt%)	0.01	13.55	12.9	17.3	17.65	12.75	12.55	11.55	9.92
Na_2O (wt%)	0.01	0.98	1.72	1.1	0.99	1.71	1.59	1.48	1.14
K_2O (wt%)	0.01	0.45	0.69	0.48	0.47	0.64	0.59	0.95	1.02
P_2O_5 (wt%)	0.01	0.11	0.11	0.23	0.06	0.2	0.2	0.22	0.35
LOI	0.01	2.19	2.14	1.17	1.43	0.97	1.36	1.7	2.27
Total		100.88	99.81	98.57	98.86	100.38	100.71	98.06	100.56
Ba (ppm)	0.5	184.5	225	150.5	153.5	287	268	301	284
Ce (ppm)	0.1	33.7	32.1	42.7	35.3	43.7	41.2	47.8	59.3
Co (ppm)	1	57	48	41	43	55	60	59	69
Cr (ppm)	10	590	460	1570	1370	840	1120	1340	1870
Cs (ppm)	0.01	0.69	0.55	0.51	0.86	0.7	0.75	1.7	3.51
Cu (ppm)	1	38	83	14	4	84	69	49	71
Dy (ppm)	0.05	2.37	2.19	2.96	2.97	2.24	2.26	2.26	3.15
Er (ppm)	0.03	1.03	1.1	1.07	1.2	1.13	0.97	1.16	1.35
Eu (ppm)	0.02	1.32	1.29	1.89	1.86	1.46	1.2	1.31	1.67
Ga (ppm)	0.1	9.8	12.2	8.6	8.2	11.6	11	11.6	13
Gd (ppm)	0.05	4.47	3.75	5.48	5.75	3.74	3.49	3.88	5.03
Hf (ppm)	0.1	1.4	1.2	1.2	1.5	1.2	1.2	1.4	1.9
Ho (ppm)	0.01	0.39	0.32	0.42	0.42	0.41	0.41	0.4	0.51
In (ppm)	0.005	0.0025	0.0025	0.0025	0.0025	0.005	0.005	0.006	0.007
La (ppm)	0.1	13	13.2	15.5	12.2	18.5	17.4	20.5	24.9
Li (ppm)	10	20	20	20	20	10	10	20	30
Lu (ppm)	0.01	0.15	0.11	0.15	0.11	0.16	0.13	0.14	0.15
Mo (ppm)	1	1	1	<1	<1	<1	<1	1	<1
Nb (ppm)	0.1	1.6	1	1.3	1.3	2.5	2.4	3.3	3.9
Nd (ppm)	0.1	26.5	22.7	32.8	30.1	26.4	24.9	29.3	35.3
Ni (ppm)	1	226	214	211	209	238	298	318	357
Pb (ppm)	2	3	4	3	2	2	2	4	4
Pr (ppm)	0.02	5.44	4.75	6.97	6.2	6.22	5.84	6.13	8.08
Rb (ppm)	0.2	19	27.1	18.5	24.8	18.6	17.7	37.1	36.4
Sc (ppm)	1	46	37	50	53	39	39	35	37
Se (ppm)	0.2	<0.2	0.2	<0.2	<0.2	0.3	0.2	0.2	0.2
Sm (ppm)	0.03	5.54	4.77	7.88	7.76	5.27	5.06	5.12	6.87
Sn (ppm)	1	1	0.5	1	1	0.5	1	1	1
Sr (ppm)	0.1	229	482	263	192	487	446	393	224
Ta (ppm)	0.1	0.2	0.1	0.1	0.1	0.2	0.1	0.2	0.2
Te (ppm)	0.01	0.01	0.01	0.005	0.005	0.03	0.03	0.03	0.04
Tb (ppm)	0.01	0.49	0.44	0.55	0.6	0.41	0.41	0.43	0.54
Th (ppm)	0.05	2.31	1.39	1.35	0.88	1.97	1.88	2.63	2.23
Tl (ppm)	0.02	0.03	0.03	0.04	0.02	0.13	0.09	0.09	0.16
Tm (ppm)	0.01	0.17	0.12	0.1	0.15	0.12	0.13	0.18	0.18
U (ppm)	0.05	0.38	0.35	0.3	0.27	0.39	0.43	0.62	0.65
V (ppm)	5	143	122	137	156	132	117	138	266
W (ppm)	1	<1	<1	<1	1	<1	<1	<1	1
Y (ppm)	0.1	11	9.5	11.6	12	11.4	10.8	11.3	13.6
Yb (ppm)	0.03	1.06	0.76	0.8	0.76	1.08	1	1.01	1.3
Zn (ppm)	2	77	60	50	58	67	69	68	99
Zr (ppm)	2	40	37	40	45	49	50	59	71
Au (ppb)	0.001	0.5	3	0.5	0.5	6	1	3	2
Pd (ppb)	0.001	14	12	24	1	30	27	26	79
Pt (ppb)	0.005	11	5	27	2.5	11	10	11	26
S (wt%)	0.01	0.06	0.06	0.02	0.01	0.08	0.09	0.07	0.07

sample number	lower detection limits	A0159038	A0159039	A0159040	A0159042	A0159043	A0159044	A0159045	A0159046
northing	UTM83-16	5503081.794	5503065.717	5503045.371	5503053.239	5503010.088	5503008.089	5502054.313	5502056.342
easting		292578.7387	292588.8976	292611.3181	292624.0579	292617.0572	292614.2289	292451.1673	292456.3044
SiO_2 (wt%)	0.01	42.8	41.7	41.9	42.6	47.6	47	50.4	52.8
TiO_2 (wt%)	0.01	0.81	0.86	1.08	1.48	0.88	0.82	0.35	0.29
Al_2O_3 (wt%)	0.01	14.05	14.6	18.3	17.45	16.05	13.7	5.64	5.48
Fe_2O_3 (wt%)	0.01	14.4	15.2	11.65	13.45	10.7	9.84	7.25	7.9
MnO (wt%)	0.01	0.16	0.14	0.12	0.12	0.15	0.15	0.13	0.16
MgO (wt%)	0.01	8.65	8.12	7.76	8.14	7.13	8.72	14.65	14.7
CaO (wt%)	0.01	13.2	14.8	13.05	11.8	10.4	11.9	16.5	16.65
Na_2O (wt%)	0.01	1.4	1.23	1.76	1.83	3.2	2.35	0.89	0.99
K_2O (wt%)	0.01	0.49	0.54	1.03	1.29	0.87	0.86	0.4	0.32
P_2O_5 (wt%)	0.01	0.09	0.09	0.18	0.05	0.88	0.68	0.19	0.18
LOI	0.01	2.09	1.9	2.88	2.67	1.49	2.33	1.52	1.18
Total		98.27	99.29	99.85	101.01	99.56	98.49	98.09	100.8
Ba (ppm)	0.5	132.5	149	286	226	505	404	181	104.5
Ce (ppm)	0.1	27.1	25.6	31	23.6	118.5	82.1	40.8	48.3
Co (ppm)	1	65	63	51	54	47	47	60	55
Cr (ppm)	10	260	100	70	60	140	150	900	780
Cs (ppm)	0.01	0.81	0.81	1.53	1.02	0.85	2.38	0.28	0.33
Cu (ppm)	1	169	202	91	60	175	55	433	35
Dy (ppm)	0.05	2.65	2.48	3.15	3.13	3.81	3.1	2.64	3.25
Er (ppm)	0.03	1.06	1.04	1.23	1.4	1.33	1.28	0.95	1.19
Eu (ppm)	0.02	1.52	1.58	1.81	1.82	2.9	2.46	1.61	1.82
Ga (ppm)	0.1	17.8	18.3	18.9	18.2	18.6	15.6	7.5	7.7
Gd (ppm)	0.05	3.85	3.99	4.68	4.83	6.99	6.59	4.84	5.37
Hf (ppm)	0.1	1	1	1	1.2	1.4	0.9	1	1.3
Ho (ppm)	0.01	0.45	0.4	0.4	0.5	0.6	0.53	0.38	0.51
In (ppm)	0.005	0.006	0.007	0.01	0.012	0.008	0.009	0.0025	0.0025
La (ppm)	0.1	10	9.5	11.9	7.8	49.6	33.1	15.3	17.1
Li (ppm)	10	10	10	10	10	20	20	20	20
Lu (ppm)	0.01	0.11	0.1	0.12	0.11	0.14	0.14	0.09	0.16
Mo (ppm)	1	<1	<1	1	<1	1	<1	<1	<1
Nb (ppm)	0.1	1.8	3.6	8.1	3.3	5	6.3	2.4	1.2
Nd (ppm)	0.1	23.3	21.7	25.4	22.5	70.5	53	31.3	37.5
Ni (ppm)	1	105	171	97	76	103	129	466	339
Pb (ppm)	2	<2	2	<2	<2	5	3	6	4
Pr (ppm)	0.02	4.2	4.14	4.93	3.99	15.85	11.5	6.45	7.53
Rb (ppm)	0.2	13.8	17.2	35.6	43.8	24.5	38.5	14.7	9.9
Sc (ppm)	1	30	34	32	38	22	35	52	51
Se (ppm)	0.2	0.3	0.5	<0.2	0.2	0.2	<0.2	0.2	<0.2
Sm (ppm)	0.03	5.35	5.42	6.28	6.24	12	9.65	6.71	8.14
Sn (ppm)	1	1	1	1	1	1	1	1	1
Sr (ppm)	0.1	768	711	785	640	1140	653	278	258
Ta (ppm)	0.1	0.1	0.2	0.2	0.1	0.2	0.3	0.2	0.1
Te (ppm)	0.01	0.01	0.02	0.01	0.01	0.01	0.01	0.07	0.01
Tb (ppm)	0.01	0.46	0.44	0.61	0.6	0.79	0.64	0.5	0.52
Th (ppm)	0.05	0.68	0.88	1.03	0.49	1.29	0.89	0.97	1.18
Tl (ppm)	0.02	0.02	0.03	0.03	0.04	0.07	0.1	0.04	0.02
Tm (ppm)	0.01	0.14	0.12	0.16	0.13	0.18	0.15	0.11	0.15
U (ppm)	0.05	0.2	0.15	0.27	0.45	0.43	0.92	0.22	0.23
V (ppm)	5	466	559	450	457	197	189	122	128
W (ppm)	1	<1	<1	<1	<1	1	1	1	0.5
Y (ppm)	0.1	9.8	9.9	12.1	12.1	14.5	12.8	9.3	12.3
Yb (ppm)	0.03	0.84	0.87	0.88	1.07	0.91	0.99	0.56	0.99
Zn (ppm)	2	87	75	65	77	99	94	59	71
Zr (ppm)	2	33	33	37	32	47	32	42	39
Au (ppb)	0.001	6	2	1	0.5	1	0.5	45	4
Pd (ppb)	0.001	1	4	0.5	1	2	20	80	21
Pt (ppb)	0.005	2.5	2.5	2.5	2.5	2.5	7	67	13
S (wt%)	0.01	0.25	0.33	0.11	0.05	0.17	0.13	0.03	0.01

sample number	lower detection limits	A0159047	A0159050	A0159451	A0159452	RR04-TG-001
northing	UTM83-16	5501894.095	5501937.647	5502059.812	5502064.071	depth
easting		292393.9906	292375.8497	292441.4702	292434.6921	88.05 m
SiO_2 (wt%)	0.01	49.9	51.2	52	51.5	43.8
TiO_2 (wt%)	0.01	0.4	0.41	0.33	0.37	1.05
Al_2O_3 (wt%)	0.01	6.06	5.62	5.22	5.31	17.15
Fe_2O_3 (wt%)	0.01	8.98	8.52	7.88	8.15	11.16
MnO (wt%)	0.01	0.18	0.17	0.15	0.16	0.17
MgO (wt%)	0.01	14.05	13.7	15.7	15.65	6.71
CaO (wt%)	0.01	17.95	17.7	16.45	16.25	10.1
Na_2O (wt%)	0.01	0.66	0.83	0.77	0.76	3.5
K_2O (wt%)	0.01	0.39	0.39	0.27	0.29	0.87
P_2O_5 (wt%)	0.01	0.04	0.32	0.14	0.16	1.01
LOI	0.01	1.52	2.02	1.34	1.73	1.42
Total		100.25	101.02	100.51	100.59	97.58
Ba (ppm)	0.5	123.5	97.8	98	96.4	442
Ce (ppm)	0.1	22.8	34.9	34.7	35.7	175.5
Co (ppm)	1	60	52	61	62	46
Cr (ppm)	10	680	750	1820	1770	80
Cs (ppm)	0.01	0.3	0.2	0.4	0.36	2.71
Cu (ppm)	1	60	71	34	37	97
Dy (ppm)	0.05	2.86	3.86	2.75	3.25	4.4
Er (ppm)	0.03	1.3	1.58	1.06	1.42	1.36
Eu (ppm)	0.02	1.54	2.04	1.71	1.79	3.99
Ga (ppm)	0.1	7.7	8.5	7.6	7.7	19.2
Gd (ppm)	0.05	5.13	6.01	4.85	5.25	9.54
Hf (ppm)	0.1	1.2	1.3	1.1	1.1	3
Ho (ppm)	0.01	0.47	0.54	0.4	0.46	0.66
In (ppm)	0.005	0.0025	0.005	0.0025	0.0025	0.014
La (ppm)	0.1	6.9	12.1	11.1	11.7	59.4
Li (ppm)	10	20	10	10	20	20
Lu (ppm)	0.01	0.15	0.14	0.11	0.11	0.15
Mo (ppm)	1	<1	1	<1	<1	<1
Nb (ppm)	0.1	0.8	0.7	1	1.1	6.3
Nd (ppm)	0.1	23.7	34.8	30.9	31.3	98.6
Ni (ppm)	1	254	297	402	386	81
Pb (ppm)	2	3	2	4	<2	6
Pr (ppm)	0.02	4.01	6.13	5.8	5.99	20.8
Rb (ppm)	0.2	14.3	14.2	11.1	10.6	16.4
Sc (ppm)	1	58	54	51	51	18
Se (ppm)	0.2	<0.2	<0.2	<0.2	<0.2	0.3
Sm (ppm)	0.03	6.47	8.44	6.94	7.3	15.7
Sn (ppm)	1	1	0.5	1	0.5	1
Sr (ppm)	0.1	155	259	202	213	1050
Ta (ppm)	0.1	0.1	0.1	0.1	0.1	0.2
Te (ppm)	0.01	0.005	0.05	0.01	0.01	0.01
Tb (ppm)	0.01	0.54	0.7	0.51	0.55	0.96
Th (ppm)	0.05	0.58	0.89	0.68	0.74	1.04
Tl (ppm)	0.02	0.01	0.01	0.02	0.01	0.09
Tm (ppm)	0.01	0.14	0.19	0.12	0.14	0.19
U (ppm)	0.05	0.13	0.26	0.19	0.2	0.59
V (ppm)	5	182	158	140	144	191
W (ppm)	1	<1	<1	2	<1	<1
Y (ppm)	0.1	12.1	13.9	10.2	11.4	16.4
Yb (ppm)	0.03	0.88	1.05	0.77	0.83	0.95
Zn (ppm)	2	61	73	66	70	95
Zr (ppm)	2	35	41	39	39	125
Au (ppb)	0.001	1	12	1	3	NA
Pd (ppb)	0.001	42	254	7	5	NA
Pt (ppb)	0.005	33	143	6	8	NA
S (wt%)	0.01	0.05	0.04	0.01	0.01	0.35

Appendix III

SIMS Sulphur Isotopes

Pyrite

Thin Section	Region of interest #	Spot #	Grain #	$^{33}S/^{32}S$	$\delta^{33}S$ (VCDT)	2σ (‰)	$^{34}S/^{32}S$	$\delta^{34}S$ (VCDT)	2σ (‰)	$\Delta^{33}S$	2σ (‰)
TS_TG_049	1	1	1	0.0078801	0.36	0.15	0.0442063	0.99	0.12	-0.15	0.15
TS_TG_049	1	2	1	0.0078816	0.56	0.15	0.0442267	1.45	0.12	-0.19	0.15
TS_TG_049	1	3	1	0.0078813	0.51	0.15	0.0442210	1.32	0.13	-0.17	0.15
TS_TG_049	1	4	1	0.0078820	0.60	0.17	0.0442182	1.26	0.12	-0.05	0.15
TS_TG_049	1	5	1	0.0078819	0.59	0.15	0.0442177	1.25	0.12	-0.06	0.15
TS_TG_049	1	6	1	0.0078821	0.61	0.19	0.0442277	1.47	0.13	-0.15	0.15
TS_TG_049	1	7	2	0.0078842	0.88	0.15	0.0442366	1.68	0.13	0.02	0.15
TS_TG_049	1	8	2	0.0078774	0.02	0.16	0.0441761	0.31	0.12	-0.14	0.15
TS_TG_047	2	1	1	0.0078371	-5.10	0.16	0.0437226	-9.96	0.14	0.04	0.15
TS_TG_047	2	2	2	0.0078403	-4.69	0.15	0.0437647	-9.01	0.12	-0.04	0.15
TS_TG_047	2	3	2	0.0078340	-5.48	0.17	0.0437002	-10.47	0.13	-0.08	0.15
TS_TG_047	2	4	2	0.0078328	-5.64	0.15	0.0436845	-10.82	0.12	-0.05	0.15
TS_TG_047	2	5	2	0.0078370	-5.11	0.16	0.0437311	-9.77	0.14	-0.07	0.15
TS_TG_047	3	1	3	0.0078666	-1.35	0.15	0.0440514	-2.52	0.13	-0.05	0.15
TS_TG_047	3	2	3	0.0078662	-1.41	0.15	0.0440468	-2.62	0.13	-0.06	0.15
TS_TG_047	3	3	2	0.0078616	-1.99	0.16	0.0439953	-3.79	0.12	-0.04	0.15
TS_TG_047	3	4	3	0.0078639	-1.70	0.17	0.0440265	-3.08	0.12	-0.11	0.15
TS_TG_047	3	5	3	0.0078653	-1.52	0.16	0.0440392	-2.79	0.14	-0.08	0.15
TS_TG_047	3	6	3	0.0078611	-2.05	0.15	0.0439868	-3.98	0.13	0.00	0.15
TS_TG_047	3	7	3	0.0078597	-2.23	0.16	0.0439800	-4.13	0.13	-0.10	0.15
TS_TG_047	3	8	1	0.0078542	-2.93	0.15	0.0439091	-5.74	0.12	0.03	0.15
TS_TG_047	4	1	1	0.0078611	-2.05	0.15	0.0439971	-3.75	0.12	-0.12	0.15
TS_TG_047	4	2	1	0.0078611	-2.04	0.17	0.0439904	-3.90	0.12	-0.04	0.15
TS_TG_047	4	3	1	0.0078608	-2.09	0.15	0.0439796	-4.14	0.13	0.04	0.15
TS_TG_047	4	4	1	0.0078618	-1.95	0.17	0.0440004	-3.67	0.12	-0.06	0.15
TS_TG_047	4	5	1	0.0078634	-1.76	0.20	0.0440203	-3.22	0.12	-0.10	0.15
TS_TG_043	5	1	1	0.0078759	-0.17	0.19	0.0441568	-0.13	0.13	-0.10	0.15
TS_TG_043	5	2	2	0.0078760	-0.16	0.15	0.0441499	-0.29	0.12	-0.01	0.15
TS_TG_043	5	3	3	0.0078771	-0.01	0.15	0.0441531	-0.21	0.13	0.10	0.15
TS_TG_043	5	4	4	0.0078750	-0.28	0.15	0.0441413	-0.48	0.11	-0.04	0.15
TS_TG_043	5	5	5	0.0078756	-0.21	0.15	0.0441503	-0.28	0.13	-0.07	0.15
TS_TG_043	6	1	1	0.0078764	-0.10	0.16	0.0441665	0.09	0.11	-0.15	0.15
TS_TG_043	6	2	1	0.0078757	-0.20	0.16	0.0441546	-0.18	0.12	-0.10	0.15
TS_TG_043	6	3	1	0.0078770	-0.03	0.15	0.0441641	0.03	0.13	-0.05	0.15
TS_TG_043	6	4	2	0.0078772	0.00	0.15	0.0441646	0.05	0.13	-0.03	0.15
TS_TG_043	6	5	3	0.0078770	-0.03	0.17	0.0441668	0.10	0.13	-0.08	0.15
TS_TG_043	6	6	4	0.0078784	0.15	0.17	0.0441815	0.43	0.11	-0.07	0.15
TS_TG_043	6	7	5	0.0078770	-0.03	0.18	0.0441651	0.06	0.11	-0.06	0.15
TS_TG_043	6	8	6	0.0078770	-0.03	0.17	0.0441650	0.06	0.14	-0.06	0.15
TS_TG_043	6	9	7	0.0078782	0.12	0.15	0.0441737	0.25	0.12	-0.01	0.15
TS_TG_043	6	10	8	0.0078764	-0.11	0.15	0.0441624	0.00	0.12	-0.11	0.15
TS_TG_043	7	1	1	0.0078762	-0.13	0.18	0.0441465	-0.36	0.15	0.06	0.15
TS_TG_043	7	2	2	0.0078754	-0.23	0.17	0.0441513	-0.25	0.13	-0.10	0.15
TS_TG_043	7	3	3	0.0078741	-0.39	0.15	0.0441301	-0.73	0.17	-0.02	0.15
TS_TG_043	7	4	3	0.0078740	-0.41	0.16	0.0441387	-0.54	0.13	-0.14	0.15
TS_TG_043	7	5	4	0.0078735	-0.48	0.17	0.0441299	-0.74	0.13	-0.10	0.15
TS_TG_043	7	6	5	0.0078740	-0.42	0.15	0.0441350	-0.62	0.13	-0.10	0.15
TS_TG_043	7	7	6	0.0078756	-0.21	0.15	0.0441563	-0.14	0.13	-0.14	0.15
TS_TG_043	7	8	6	0.0078766	-0.08	0.16	0.0441507	-0.27	0.11	0.06	0.15
TS_TG_042	8	1	1	0.0078781	0.11	0.15	0.0441722	0.22	0.12	0.00	0.15
TS_TG_042	8	2	1	0.0078774	0.02	0.15	0.0441661	0.08	0.12	-0.02	0.15
TS_TG_042	8	3	1	0.0078771	-0.02	0.15	0.0441749	0.28	0.11	-0.16	0.15
TS_TG_042	9	1	1	0.0078743	-0.37	0.15	0.0441262	-0.82	0.12	0.05	0.15
TS_TG_042	9	2	1	0.0078768	-0.06	0.17	0.0441678	0.12	0.14	-0.12	0.15
TS_TG_042	9	3	2	0.0078782	0.12	0.15	0.0441770	0.33	0.13	-0.05	0.15
TS_TG_042	9	4	3	0.0078749	-0.30	0.15	0.0441436	-0.43	0.14	-0.08	0.15
TS_TG_042	9	5	4	0.0078745	-0.35	0.17	0.0441424	-0.46	0.14	-0.12	0.15
TS_TG_042	9	6	5	0.0078783	0.13	0.18	0.0441854	0.52	0.16	-0.14	0.15
TS_TG_042	9	7	5	0.0078741	-0.39	0.16	0.0441459	-0.38	0.11	-0.20	0.15
TS_TG_042	9	8	6	0.0078771	-0.02	0.19	0.0441622	-0.01	0.12	-0.01	0.15
TS_TG_042	9	9	5	0.0078777	0.06	0.16	0.0441739	0.26	0.11	-0.08	0.15
TS_TG_042	9	10	5	0.0078746	-0.34	0.19	0.0441459	-0.38	0.13	-0.14	0.15
TS_TG_042	10	1	1	0.0078774	0.02	0.15	0.0441700	0.17	0.13	-0.06	0.15
TS_TG_042	10	2	1	0.0078769	-0.04	0.17	0.0441682	0.13	0.12	-0.11	0.15

Thin Section	Region of interest #	Spot #	Grain #	$^{33}S/^{32}S$	$\delta^{33}S$ (VCDT)	2σ (‰)	$^{34}S/^{32}S$	$\delta^{34}S$ (VCDT)	2σ (‰)	$\Delta^{33}S$	2σ (‰)
TS_TG_042	10	3	1	0.0078771	-0.02	0.17	0.0441705	0.18	0.12	-0.11	0.15
TS_TG_042	10	4	2	0.0078747	-0.32	0.15	0.0441587	-0.09	0.13	-0.28	0.15
TS_TG_042	10	5	2	0.0078746	-0.34	0.18	0.0441538	-0.20	0.12	-0.23	0.15
TS_TG_042	10	6	2	0.0078747	-0.32	0.16	0.0441584	-0.09	0.13	-0.27	0.15
TS_TG_040	11	1	1	0.0079011	3.03	0.15	0.0444375	6.22	0.11	-0.17	0.15
TS_TG_040	11	2	1	0.0078811	0.49	0.15	0.0442139	1.16	0.12	-0.11	0.15
TS_TG_040	11	3	2	0.0078978	2.61	0.16	0.0444050	5.49	0.14	-0.21	0.15
TS_TG_040	11	4	2	0.0078987	2.72	0.17	0.0444127	5.66	0.12	-0.19	0.15
TS_TG_040	11	5	2	0.0078956	2.34	0.18	0.0443841	5.02	0.12	-0.24	0.15
TS_TG_040	11	6	2	0.0078981	2.65	0.15	0.0444027	5.44	0.11	-0.15	0.15
TS_TG_040	11	7	2	0.0078977	2.59	0.16	0.0444029	5.44	0.13	-0.21	0.15
TS_TG_040	11	8	3	0.0078957	2.35	0.18	0.0443825	4.98	0.12	-0.21	0.15
TS_TG_040	11	9	4	0.0078969	2.49	0.16	0.0443902	5.15	0.14	-0.16	0.15
TS_TG_040	11	10	5	0.0078775	0.03	0.15	0.0441748	0.28	0.12	-0.12	0.15
TS_TG_040	12	1	1	0.0078932	2.03	0.19	0.0443469	4.17	0.12	-0.12	0.15
TS_TG_040	12	2	1	0.0078913	1.78	0.16	0.0443171	3.50	0.12	-0.02	0.15
TS_TG_040	12	3	1	0.0078904	1.67	0.15	0.0443159	3.47	0.12	-0.12	0.15
TS_TG_040	12	4	2	0.0078813	0.51	0.15	0.0442162	1.22	0.11	-0.11	0.15
TS_TG_040	12	5	3	0.0078878	1.34	0.17	0.0442803	2.67	0.12	-0.03	0.15
TS_TG_040	12	6	4	0.0078970	2.51	0.16	0.0443870	5.08	0.11	-0.11	0.15
TS_TG_040	12	7	4	0.0078878	1.34	0.15	0.0442810	2.68	0.11	-0.04	0.15
TS_TG_040	12	8	5	0.0078795	0.29	0.15	0.0441909	0.64	0.12	-0.04	0.15
TS_TG_040	12	9	5	0.0078956	2.33	0.17	0.0443622	4.52	0.12	0.00	0.15
TS_TG_037	13	1	1	0.0078686	-1.09	0.15	0.0440823	-1.82	0.13	-0.16	0.15
TS_TG_037	13	2	1	0.0078648	-1.58	0.15	0.0440360	-2.87	0.13	-0.10	0.15
TS_TG_037	13	3	1	0.0078588	-2.34	0.16	0.0439728	-4.30	0.12	-0.13	0.15
TS_TG_037	13	4	2	0.0078622	-1.91	0.17	0.0439976	-3.73	0.12	0.02	0.15
TS_TG_037	13	5	2	0.0078635	-1.74	0.16	0.0440136	-3.37	0.13	0.00	0.15
TS_TG_037	13	6	3	0.0078614	-2.01	0.17	0.0439948	-3.80	0.13	-0.05	0.15
TS_TG_037	13	7	3	0.0078648	-1.59	0.16	0.0440352	-2.88	0.11	-0.10	0.15
TS_TG_037	13	8	4	0.0078710	-0.79	0.19	0.0440927	-1.58	0.12	0.02	0.15
TS_TG_037	13	9	5	0.0078684	-1.12	0.15	0.0440659	-2.19	0.12	0.01	0.15
TS_TG_037	13	10	5	0.0078667	-1.34	0.15	0.0440467	-2.62	0.13	0.01	0.15
TS_TG_037	13	11	6	0.0078714	-0.74	0.19	0.0440975	-1.47	0.12	0.02	0.15
TS_TG_034	14	1	1	0.0078780	0.09	0.15	0.0441754	0.29	0.13	-0.06	0.15
TS_TG_034	14	2	1	0.0078781	0.11	0.17	0.0441786	0.36	0.11	-0.08	0.15
TS_TG_034	14	3	1	0.0078779	0.08	0.15	0.0441654	0.06	0.12	0.05	0.15
TS_TG_034	14	4	1	0.0078787	0.18	0.18	0.0441787	0.37	0.13	0.00	0.15
TS_TG_034	14	5	1	0.0078785	0.16	0.15	0.0441773	0.33	0.13	-0.01	0.15
TS_TG_033	15	1	1	0.0078756	-0.21	0.16	0.0441484	-0.32	0.13	-0.05	0.15
TS_TG_033	15	2	1	0.0078731	-0.53	0.15	0.0441219	-0.92	0.13	-0.06	0.15
TS_TG_033	15	3	1	0.0078817	0.56	0.15	0.0442062	0.99	0.13	0.05	0.15
TS_TG_033	15	4	1	0.0078814	0.52	0.17	0.0442061	0.99	0.14	0.02	0.15
TS_TG_033	15	5	2	0.0078701	-0.91	0.21	0.0440844	-1.77	0.21	0.00	0.15
TS_TG_033	15	6	3	0.0078707	-0.84	0.18	0.0440905	-1.63	0.15	0.00	0.15
TS_TG_033	15	7	4	0.0078714	-0.74	0.15	0.0440953	-1.52	0.16	0.05	0.15
TS_TG_033	15	8	4	0.0078757	-0.20	0.15	0.0441469	-0.35	0.12	-0.02	0.15
TS_TG_033	15	9	5	0.0078759	-0.17	0.15	0.0441490	-0.31	0.12	-0.01	0.15
TS_TG_033	15	10	5	0.0078764	-0.11	0.15	0.0441574	-0.12	0.13	-0.05	0.15
TS_TG_031	16	1	1	0.0078787	0.18	0.15	0.0441816	0.43	0.14	-0.04	0.15
TS_TG_031	16	2	1	0.0078773	0.01	0.15	0.0441632	0.01	0.12	0.00	0.15
TS_TG_031	16	3	2	0.0078783	0.14	0.15	0.0441724	0.22	0.12	0.02	0.15
TS_TG_031	16	4	2	0.0078787	0.19	0.17	0.0441814	0.43	0.14	-0.03	0.15
TS_TG_031	16	5	2	0.0078781	0.11	0.15	0.0441800	0.40	0.15	-0.09	0.15
TS_TG_031	16	6	3	0.0078741	-0.40	0.15	0.0441367	-0.58	0.14	-0.10	0.15
TS_TG_031	16	7	4	0.0078693	-1.01	0.16	0.0440838	-1.78	0.13	-0.09	0.15
TS_TG_031	16	8	4	0.0078702	-0.90	0.15	0.0440911	-1.62	0.11	-0.06	0.15
TS_TG_031	16	9	5	0.0078730	-0.54	0.17	0.0441216	-0.93	0.14	-0.07	0.15
TS_TG_031	16	10	5	0.0078706	-0.84	0.15	0.0441000	-1.42	0.12	-0.11	0.15
TS_TG_030	17	1	1	0.0078784	0.14	0.15	0.0441678	0.12	0.14	0.08	0.15
TS_TG_030	17	2	1	0.0078776	0.05	0.15	0.0441673	0.11	0.13	-0.01	0.15
TS_TG_030	17	3	2	0.0078817	0.56	0.15	0.0442125	1.13	0.13	-0.02	0.15
TS_TG_030	17	4	2	0.0078717	-0.70	0.18	0.0441098	-1.19	0.12	-0.09	0.15
TS_TG_030	17	5	3	0.0078784	0.15	0.16	0.0441862	0.53	0.13	-0.13	0.15
TS_TG_030	17	6	3	0.0078747	-0.32	0.15	0.0441374	-0.57	0.13	-0.03	0.15
TS_TG_030	17	7	4	0.0078758	-0.18	0.15	0.0441561	-0.15	0.13	-0.11	0.15
TS_TG_030	17	8	4	0.0078777	0.06	0.15	0.0441820	0.44	0.12	-0.17	0.15
TS_TG_030	18	1	1	0.0078765	-0.09	0.16	0.0441615	-0.02	0.12	-0.08	0.15
TS_TG_030	18	2	1	0.0078740	-0.41	0.17	0.0441364	-0.59	0.14	-0.11	0.15
TS_TG_030	18	3	2	0.0078732	-0.52	0.15	0.0441305	-0.73	0.11	-0.15	0.15
TS_TG_030	18	4	3	0.0078769	-0.05	0.15	0.0441747	0.27	0.13	-0.19	0.15
TS_TG_030	18	5	2	0.0078778	0.07	0.18	0.0441875	0.57	0.16	-0.23	0.15
TS_TG_030	18	6	2	0.0078748	-0.31	0.16	0.0441506	-0.27	0.13	-0.18	0.15
TS_TG_030	18	7	4	0.0078755	-0.22	0.15	0.0441525	-0.23	0.14	-0.10	0.15

Thin Section	Region of interest #	Spot #	Grain #	$^{33}S/^{32}S$	$\delta^{33}S$ (VCDT)	2σ (‰)	$^{34}S/^{32}S$	$\delta^{34}S$ (VCDT)	2σ (‰)	$\Delta^{33}S$	2σ (‰)
TS_TG_030	18	8	5	0.0078759	-0.17	0.19	0.0441667	0.09	0.13	-0.22	0.15
TS_TG_030	19	1	1	0.0078725	-0.60	0.18	0.0441219	-0.92	0.12	-0.13	0.15
TS_TG_030	19	2	1	0.0078768	-0.06	0.15	0.0441790	0.37	0.13	-0.25	0.15
TS_TG_030	19	3	1	0.0078799	0.34	0.15	0.0441954	0.74	0.13	-0.04	0.15
TS_TG_030	19	4	2	0.0078781	0.10	0.15	0.0441859	0.53	0.12	-0.17	0.15
TS_TG_030	19	5	2	0.0078690	-1.05	0.18	0.0440851	-1.75	0.19	-0.15	0.15
TS_TG_030	19	6	3	0.0078765	-0.09	0.19	0.0441743	0.27	0.12	-0.23	0.15
TS_TG_030	19	7	3	0.0078763	-0.13	0.18	0.0441563	-0.14	0.13	-0.05	0.15

Chalcopyrite

Thin Section	Region of interest #	Spot #	Grain #	$^{33}S/^{32}S$	$\delta^{33}S$ (VCDT)	2σ (‰)	$^{34}S/^{32}S$	$\delta^{34}S$ (VCDT)	2σ (‰)	$\Delta^{33}S$	2σ (‰)
TS_TG_049	1	1	1	0.0078807	0.44	0.16	0.0442134	1.15	0.23	-0.15	0.15
TS_TG_049	1	2	1	0.0078814	0.53	0.14	0.0442201	1.30	0.19	-0.14	0.15
TS_TG_049	1	3	1	0.0078826	0.68	0.17	0.0442215	1.34	0.20	-0.01	0.15
TS_TG_047	2	1	1	0.0078351	-5.35	0.15	0.0437219	-9.98	0.19	-0.20	0.15
TS_TG_047	2	2	2	0.0078321	-5.73	0.15	0.0436933	-10.62	0.18	-0.25	0.15
TS_TG_047	2	3	3	0.0078418	-4.49	0.15	0.0437842	-8.57	0.25	-0.07	0.15
TS_TG_047	2	4	3	0.0078347	-5.39	0.24	0.0437208	-10.00	0.35	-0.23	0.15
TS_TG_047	2	5	3	0.0078282	-6.23	0.18	0.0436492	-11.62	0.35	-0.23	0.15
TS_TG_047	3	1	1	0.0078562	-2.67	0.18	0.0439480	-4.86	0.21	-0.17	0.15
TS_TG_047	4	1	1	0.0078488	-3.61	0.19	0.0438532	-7.00	0.19	0.01	0.15
TS_TG_047	4	2	2	0.0078560	-2.70	0.15	0.0439417	-5.00	0.20	-0.12	0.15
TS_TG_047	4	3	3	0.0078488	-3.61	0.16	0.0438629	-6.78	0.20	-0.11	0.15
TS_TG_047	4	4	4	0.0078496	-3.51	0.15	0.0438747	-6.52	0.18	-0.14	0.15
TS_TG_047	4	5	5	0.0078616	-1.99	0.18	0.0440036	-3.60	0.22	-0.13	0.15
TS_TG_047	4	6	6	0.0078539	-2.97	0.21	0.0439163	-5.58	0.31	-0.09	0.15
TS_TG_043	5	1	1	0.0078740	-0.42	0.17	0.0441324	-0.68	0.19	-0.07	0.15
TS_TG_043	5	2	2	0.0078734	-0.49	0.16	0.0441386	-0.54	0.21	-0.21	0.15
TS_TG_043	5	3	2	0.0078743	-0.37	0.15	0.0441415	-0.48	0.18	-0.13	0.15
TS_TG_043	5	4	2	0.0078752	-0.26	0.20	0.0441509	-0.26	0.26	-0.12	0.15
TS_TG_043	5	5	2	0.0078775	0.03	0.13	0.0441682	0.13	0.22	-0.04	0.15
TS_TG_043	5	6	2	0.0078602	-2.16	0.24	0.0439893	-3.92	0.36	-0.14	0.15
TS_TG_043	6	1	1	0.0078757	-0.20	0.13	0.0441531	-0.21	0.20	-0.09	0.15
TS_TG_043	7	2	1	0.0078760	-0.15	0.18	0.0441645	0.04	0.20	-0.17	0.15
TS_TG_042	8	1	1	0.0078747	-0.33	0.13	0.0441405	-0.50	0.18	-0.07	0.15
TS_TG_042	8	2	1	0.0078785	0.15	0.11	0.0441854	0.52	0.18	-0.11	0.15
TS_TG_042	8	3	2	0.0078753	-0.25	0.13	0.0441520	-0.24	0.22	-0.13	0.15
TS_TG_042	8	4	3	0.0078778	0.07	0.12	0.0441806	0.41	0.19	-0.14	0.15
TS_TG_042	8	5	4	0.0078761	-0.14	0.13	0.0441589	-0.08	0.17	-0.10	0.15
TS_TG_042	8	6	3	0.0078778	0.07	0.22	0.0441753	0.29	0.18	-0.08	0.15
TS_TG_042	8	7	3	0.0078785	0.16	0.12	0.0441832	0.47	0.18	-0.08	0.15
TS_TG_042	8	8	5	0.0078779	0.08	0.21	0.0441848	0.50	0.18	-0.18	0.15
TS_TG_042	10	1	1	0.0078760	-0.16	0.14	0.0441585	-0.09	0.22	-0.11	0.15
TS_TG_034	14	1	1	0.0078750	-0.29	0.13	0.0441464	-0.37	0.20	-0.10	0.15
TS_TG_034	14	2	1	0.0078699	-0.94	0.27	0.0441026	-1.36	0.38	-0.24	0.15
TS_TG_034	14	3	1	0.0078754	-0.23	0.19	0.0441412	-0.48	0.20	0.02	0.15
TS_TG_034	14	4	2	0.0078700	-0.93	0.16	0.0440898	-1.65	0.18	-0.08	0.15
TS_TG_030	18	1	1	0.0078636	-1.73	0.21	0.0440176	-3.28	0.25	-0.04	0.15
TS_TG_030	19	1	1	0.0078711	-0.78	0.19	0.0441006	-1.40	0.17	-0.05	0.15
TS_TG_030	19	2	1	0.0078695	-0.98	0.14	0.0440864	-1.73	0.15	-0.09	0.15
TS_TG_030	19	3	1	0.0078675	-1.23	0.14	0.0440598	-2.33	0.23	-0.03	0.15
TS_TG_030	19	4	2	0.0078715	-0.72	0.15	0.0441096	-1.20	0.21	-0.11	0.15

Reference Materials

Reference Material	Session	Spot #	$^{33}S/^{32}S$	$\delta^{33}S$ (VCDT)	2σ (‰)	$^{34}S/^{32}S$	$\delta^{34}S$ (VCDT)	2σ (‰)	$\Delta^{33}S$	2σ (‰)
S0302A test	IP22018A	5	0.0078780	0.10	0.11	0.0441644	0.04	0.06	0.08	0.11
S0302A test	IP22018A	6	0.0078765	-0.09	0.11	0.0441639	0.03	0.09	-0.11	0.12
S0302A test	IP22018A	7	0.0078779	0.08	0.11	0.0441623	-0.01	0.05	0.09	0.11
S0302A test	IP22018A	8	0.0078779	0.09	0.11	0.0441634	0.02	0.07	0.08	0.11
S0302A test	IP22018A	9	0.0078766	-0.08	0.14	0.0441620	-0.01	0.08	-0.08	0.14
S0302A test	IP22018A	10	0.0078773	0.00	0.12	0.0441587	-0.09	0.09	0.05	0.13
S0302A	IP22018A	10	0.0078769	-0.04	0.11	0.0441621	-0.01	0.07	-0.03	0.11
S0302A	IP22018A	12	0.0078770	-0.03	0.12	0.0441637	0.03	0.08	-0.05	0.13
S0302A	IP22018A	13	0.0078772	-0.01	0.11	0.0441614	-0.03	0.08	0.00	0.11
S0302A	IP22018A	14	0.0078770	-0.03	0.11	0.0441602	-0.05	0.06	-0.01	0.11

S0302A	IP22018A	15	0.0078767	-0.06	0.12	0.0441627	0.00	0.07	-0.06	0.12
S0302A	IP22018A	16	0.0078778	0.06	0.12	0.0441637	0.03	0.08	0.05	0.13
S0302A	IP22018A	17	0.0078774	0.02	0.11	0.0441630	0.01	0.05	0.02	0.11
S0302A	IP22018A	18	0.0078769	-0.05	0.12	0.0441645	0.04	0.08	-0.07	0.12
S0302A	IP22018A	19	0.0078773	0.01	0.15	0.0441642	0.04	0.07	-0.01	0.15
S0302A	IP22018A	20	0.0078770	-0.03	0.11	0.0441655	0.07	0.07	-0.07	0.11
S0302A	IP22018A	21	0.0078772	-0.01	0.14	0.0441590	-0.08	0.07	0.03	0.14
S0302A	IP22018A	22	0.0078776	0.04	0.11	0.0441592	-0.08	0.08	0.08	0.11
S0302A	IP22018A	23	0.0078769	-0.04	0.11	0.0441606	-0.04	0.06	-0.02	0.11
S0302A	IP22018A	24	0.0078768	-0.06	0.11	0.0441630	0.01	0.05	-0.06	0.11
S0302A	IP22018A	25	0.0078781	0.11	0.11	0.0441647	0.05	0.07	0.08	0.11
S0302A	IP22018B	26	0.0078774	0.01	0.15	0.0441615	-0.02	0.08	0.03	0.15
S0302A	IP22018B	27	0.0078766	-0.09	0.15	0.0441647	0.05	0.08	-0.11	0.15
S0302A	IP22018B	28	0.0078772	0.00	0.15	0.0441655	0.07	0.08	-0.04	0.15
S0302A	IP22018B	29	0.0078779	0.09	0.11	0.0441634	0.02	0.09	0.08	0.12
S0302A	IP22018B	30	0.0078774	0.02	0.11	0.0441605	-0.05	0.08	0.04	0.12
S0302A	IP22018B	31	0.0078773	0.01	0.14	0.0441599	-0.06	0.10	0.04	0.15
S0302A	IP22018B	32	0.0078762	-0.13	0.13	0.0441604	-0.05	0.07	-0.11	0.13
S0302A	IP22018B	33	0.0078774	0.01	0.13	0.0441637	0.03	0.06	0.00	0.13
S0302A	IP22018B	34	0.0078776	0.05	0.15	0.0441635	0.02	0.07	0.03	0.15
S0302A	IP22018B	35	0.0078768	-0.06	0.12	0.0441640	0.03	0.10	-0.08	0.13
S0302A	IP22018B	36	0.0078775	0.03	0.15	0.0441647	0.05	0.07	0.01	0.15
S0302A	IP22018B	37	0.0078773	0.01	0.11	0.0441591	-0.08	0.09	0.05	0.12
S0302A	IP22018B	38	0.0078775	0.03	0.11	0.0441604	-0.05	0.07	0.06	0.11
S0302A	IP22018B	39	0.0078777	0.05	0.11	0.0441607	-0.04	0.09	0.08	0.12
S0302A	IP22018B	40	0.0078766	-0.08	0.11	0.0441638	0.03	0.09	-0.09	0.12
S0302A	IP22018B	41	0.0078772	-0.01	0.11	0.0441639	0.03	0.07	-0.03	0.11
S0321	IP22018	11	0.0078782	0.12	0.21	0.0441738	0.26	0.22	-0.01	0.24
S0321	IP22018	12	0.0078786	0.17	0.15	0.0441705	0.18	0.20	0.08	0.19
S0321	IP22018	13	0.0078784	0.15	0.14	0.0441688	0.14	0.21	0.08	0.18
S0321	IP22018	14	0.0078775	0.04	0.14	0.0441738	0.25	0.22	-0.09	0.18
S0321	IP22018	15	0.0078778	0.07	0.18	0.0441724	0.22	0.21	-0.04	0.21
S0321	IP22018	16	0.0078778	0.07	0.18	0.0441699	0.17	0.21	-0.01	0.21
S0321	IP22018	17	0.0078777	0.06	0.15	0.0441695	0.16	0.18	-0.03	0.18
S0321	IP22018	18	0.0078779	0.08	0.15	0.0441722	0.22	0.20	-0.03	0.18
S0321	IP22018	19	0.0078784	0.15	0.15	0.0441703	0.17	0.21	0.06	0.19
S0321	IP22018	20	0.0078786	0.17	0.18	0.0441721	0.22	0.19	0.06	0.21
S0321	IP22018	21	0.0078783	0.14	0.16	0.0441730	0.24	0.17	0.02	0.18
S0321	IP22018	23	0.0078777	0.06	0.14	0.0441724	0.22	0.21	-0.06	0.17
S0321	IP22018	25	0.0078780	0.10	0.11	0.0441697	0.16	0.19	0.01	0.15
S0321	IP22018	26	0.0078781	0.11	0.21	0.0441727	0.23	0.18	0.00	0.23
S0321	IP22018	27	0.0078781	0.11	0.18	0.0441709	0.19	0.18	0.02	0.21

Appendix IV

Sm-Nd Isotopes

Sample Name	Nd (ppm)	Sm (ppm)	143Nd/144Nd (current)	Error (2σ)	147Sm/144Nd*	143Nd/144Nd initial*	Nd143/Nd144 initial+	ε_{Nd}
A0159050	32.21	8.065	0.511892	0.000029	0.1514	0.511693	0.50994	1.14
A0159043	68.46	11.77	0.511067	0.000021	0.1040	0.510931	0.50922	1.48
A0159042	23.66	6.135	0.511998	0.000030	0.1568	0.511793	0.50922	1.35
A0159040	24.7	5.962	0.511816	0.000028	0.1459	0.511625	0.50923	1.55
A0159037	34.81	6.658	0.511259	0.000023	0.1156	0.511108	0.50921	1.18
A0159034	23.66	4.643	0.511323	0.000023	0.1187	0.511168	0.50922	1.39
A0159021	26.2	6.457	0.511861	0.000028	0.1490	0.511666	0.50922	1.36
A0159020	9.898	1.971	0.511349	0.000024	0.1204	0.511191	0.50921	1.29
A0137379	22.63	5.44	0.511819	0.000028	0.1454	0.511629	0.50924	1.82
A0137378	60.72	9.218	0.510812	0.000019	0.0918	0.510692	0.50918	0.72
A0137371	18.81	4.068	0.511528	0.000025	0.1307	0.511356	0.50921	1.19
A0137370	9.911	2.273	0.511691	0.000027	0.1386	0.511509	0.50923	1.63
A0137368	31.69	6.938	0.511566	0.000025	0.1324	0.511393	0.50922	1.37
A0137362	35.39	7.245	0.511379	0.000024	0.1237	0.511217	0.50918	0.70

Appendix V

Sulphide Mineral Chemistry

Note: where there are two pyrite zones denotes that Co and Ni had differing trends throughout the crystal or where there are two differing trends in Pt. Additionally, b.l.d is below limits of detection, which are individual for each isotope and sample.

Samples (ppm)	Reference material	Pyrite 1	Pyrite 2 zone 1	Pyrite 2 zone 2	Pyrite 3	Pyrite 4	Pyrite 5 zone 1	Pyrite 5 zone 2	Chalcopyrite 6
Mean S^{33}	MASS-1	236223.13	238829.88	246878.83	241324.17	241968.46	254053.55	222558.72	265263.50
Mean S^{34}	MASS-1	307198.23	311564.18	310114.07	330192.57	311668.39	331675.76	302681.99	259621.03
Mean V^{51}	MASS-1	0.28	0.35	0.23	0.30	0.27	0.24	0.30	0.36
Mean Co^{59}	MASS-1	17213.44	1360.70	28293.31	25947.44	25.71	3057.99	512.32	b.l.d
Mean Ni^{61}	MASS-1	272.33	679.60	161.99	160.42	654.72	531.10	595.41	b.l.d
Mean Cu^{63}	MASS-1	b.l.d	b.l.d	b.l.d	1.2377	2.6500	1.0305	0.7709	294474.90
Mean Cu^{65}	MASS-1	0.31	0.43	0.29	8.60	6.86	1.32	8.58	284566.47
Mean Zn^{66}	MASS-1	b.l.d	b.l.d	b.l.d	b.l.d	b.l.d	b.l.d	b.l.d	10.54
Mean Zn^{68}	MASS-1	b.l.d	b.l.d	b.l.d	b.l.d	b.l.d	b.l.d	b.l.d	11.53
Mean As^{75}	MASS-1	7.5031	b.l.d	b.l.d	b.l.d	b.l.d	b.l.d	b.l.d	b.l.d
Mean Se^{77}	MASS-1	14.93	16.07	17.45	32.31	33.06	31.63	32.72	57.75
Mean Se^{78}	MASS-1	8.56	11.19	13.73	30.47	23.98	28.25	20.57	b.l.d
Mean Se^{82}	MASS-1	13.75	18.52	15.89	32.24	28.29	31.12	28.03	52.63
Mean Ru^{101}	Po725	b.l.d	b.l.d	b.l.d	b.l.d	b.l.d	b.l.d	b.l.d	b.l.d
Mean Rh^{103}	Po725	b.l.d	b.l.d	b.l.d	b.l.d	b.l.d	b.l.d	b.l.d	0.62
Mean Pd^{105}	Po725	b.l.d	b.l.d	b.l.d	b.l.d	b.l.d	b.l.d	b.l.d	b.l.d
Mean Pd^{106}	Po725	b.l.d	b.l.d	b.l.d	b.l.d	b.l.d	b.l.d	b.l.d	b.l.d
Mean Pd^{108}	Po725	b.l.d	b.l.d	b.l.d	b.l.d	b.l.d	b.l.d	b.l.d	b.l.d
Mean Ag^{109}	MASS-1	b.l.d	0.0093	b.l.d	b.l.d	b.l.d	b.l.d	b.l.d	1.1977
Mean Cd^{111}	MASS-1	b.l.d	b.l.d	b.l.d	b.l.d	b.l.d	b.l.d	b.l.d	b.l.d
Mean Sn^{118}	MASS-1	b.l.d	b.l.d	b.l.d	b.l.d	b.l.d	b.l.d	b.l.d	b.l.d
Mean Sn^{120}	MASS-1	b.l.d	b.l.d	b.l.d	b.l.d	b.l.d	b.l.d	b.l.d	b.l.d
Mean Sb^{121}	MASS-1	b.l.d	b.l.d	b.l.d	b.l.d	b.l.d	b.l.d	b.l.d	b.l.d
Mean Sb^{123}	MASS-1	b.l.d	b.l.d	b.l.d	b.l.d	b.l.d	b.l.d	b.l.d	0.52
Mean Te^{125}	MASS-1	b.l.d	b.l.d	b.l.d	b.l.d	b.l.d	0.28	0.34	0.89
Mean Os^{189}	Po725	b.l.d	b.l.d	b.l.d	0.05	b.l.d	b.l.d	b.l.d	b.l.d
Mean Ir^{193}	Po725	b.l.d	b.l.d	b.l.d	b.l.d	b.l.d	b.l.d	b.l.d	b.l.d
Mean Pt^{194}	Po725	0.04	b.l.d	b.l.d	b.l.d	b.l.d	b.l.d	b.l.d	b.l.d
Mean Pt^{195}	Po725	0.03	b.l.d	b.l.d	b.l.d	b.l.d	0.03	b.l.d	b.l.d
Mean Au^{197}	MASS-1	b.l.d	b.l.d	b.l.d	0.01	b.l.d	b.l.d	b.l.d	b.l.d
Mean Pb^{208}	MASS-1	b.l.d	b.l.d	b.l.d	b.l.d	b.l.d	b.l.d	b.l.d	b.l.d
Mean Bi^{209}	MASS-1	b.l.d	b.l.d	b.l.d	b.l.d	b.l.d	b.l.d	b.l.d	0.09

Samples (ppm)	Reference material	Pyrite 7	Pyrite 8	Pyrite 9 zone 1	Pyrite 9 zone 2	Pyrite 10	Pyrite 11	Pyrite 12	Pyrite 13
Mean S^{33}	MASS-1	256009.16	232762.20	251259.13	264524.74	276452.51	279488.77	291052.69	304450.57
Mean S^{34}	MASS-1	325525.28	295181.24	355112.48	354873.66	360394.16	356645.04	358133.62	362488.75
Mean V^{51}	MASS-1	0.28	0.25	0.29	0.26	0.30	0.34	0.20	0.29
Mean Co^{59}	MASS-1	20647.62	4343.89	7423.07	6173.53	16566.16	3960.19	43810.81	25420.80
Mean Ni^{61}	MASS-1	132.93	472.46	320.30	313.44	301.08	383.01	2648.94	1776.56
Mean Cu^{63}	MASS-1	1.40	1.71	4.60	2.36	1.17	0.74	b.l.d	b.l.d
Mean Cu^{65}	MASS-1	1.25	20.15	4.27	8.29	1.73	1.13	0.48	0.42
Mean Zn^{66}	MASS-1	b.l.d	b.l.d	b.l.d	0.40	0.71	0.43	0.75	0.54
Mean Zn^{68}	MASS-1	b.l.d	b.l.d	b.l.d	b.l.d	b.l.d	b.l.d	b.l.d	b.l.d
Mean As^{75}	MASS-1	b.l.d	2.22	3.19	45.93	b.l.d	b.l.d	b.l.d	b.l.d
Mean Se^{77}	MASS-1	20.96	15.78	24.62	32.47	45.22	33.59	78.52	89.69
Mean Se^{78}	MASS-1	25.58	12.10	24.02	40.26	46.67	38.70	79.49	86.52
Mean Se^{82}	MASS-1	24.76	12.34	24.92	39.24	47.27	37.69	79.51	87.09
Mean Ru^{101}	Po725	b.l.d	b.l.d	b.l.d	0.2384	b.l.d	b.l.d	0.05	b.l.d
Mean Rh^{103}	Po725	b.l.d	0.0201	b.l.d	b.l.d	b.l.d	b.l.d	0.17	b.l.d
Mean Pd^{105}	Po725	b.l.d	b.l.d	b.l.d	b.l.d	b.l.d	b.l.d	b.l.d	b.l.d
Mean Pd^{106}	Po725	b.l.d	b.l.d	b.l.d	b.l.d	b.l.d	b.l.d	b.l.d	b.l.d
Mean Pd^{108}	Po725	b.l.d	b.l.d	b.l.d	b.l.d	b.l.d	b.l.d	b.l.d	b.l.d
Mean Ag^{109}	MASS-1	b.l.d	b.l.d	b.l.d	b.l.d	b.l.d	b.l.d	0.01	b.l.d
Mean Cd^{111}	MASS-1	b.l.d	b.l.d	b.l.d	b.l.d	b.l.d	b.l.d	b.l.d	b.l.d
Mean Sn^{118}	MASS-1	b.l.d	b.l.d	b.l.d	b.l.d	b.l.d	b.l.d	b.l.d	b.l.d
Mean Sn^{120}	MASS-1	b.l.d	b.l.d	b.l.d	b.l.d	b.l.d	b.l.d	b.l.d	b.l.d
Mean Sb^{121}	MASS-1	b.l.d	b.l.d	b.l.d	b.l.d	b.l.d	b.l.d	b.l.d	b.l.d
Mean Sb^{123}	MASS-1	b.l.d	b.l.d	b.l.d	b.l.d	b.l.d	b.l.d	b.l.d	b.l.d
Mean Te^{125}	MASS-1	b.l.d	b.l.d	b.l.d	b.l.d	0.26	b.l.d	b.l.d	0.24
Mean Os^{189}	Po725	b.l.d	b.l.d	0.21	b.l.d	0.05	b.l.d	b.l.d	b.l.d
Mean Ir^{193}	Po725	b.l.d	b.l.d	0.13	0.24	0.02	b.l.d	b.l.d	0.05
Mean Pt^{194}	Po725	b.l.d	b.l.d	0.72	14.79	b.l.d	1.45	b.l.d	b.l.d
Mean Pt^{195}	Po725	b.l.d	b.l.d	1.02	15.99	b.l.d	1.57	0.14	0.03
Mean Au^{197}	MASS-1	b.l.d	b.l.d	b.l.d	b.l.d	b.l.d	b.l.d	b.l.d	b.l.d
Mean Pb^{208}	MASS-1	b.l.d	b.l.d	b.l.d	b.l.d	b.l.d	b.l.d	b.l.d	b.l.d
Mean Bi^{209}	MASS-1	b.l.d	b.l.d	b.l.d	b.l.d	b.l.d	b.l.d	b.l.d	b.l.d

Samples (ppm)	Reference material	Chalcopyrite 14	Pyrite 15	Chalcopyrite 16	Pyrite 17	Pyrite 18	Pyrite 19	Pyrite 20	Pyrite 21
Mean S^{33}	MASS-1	309373.04	285317.64	275721.72	263157.09	279944.42	270427.80	247466.13	247444.10
Mean S^{34}	MASS-1	284794.33	381788.46	262438.73	321279.80	351883.98	336480.49	310002.87	312848.79
Mean V^{51}	MASS-1	b.l.d	0.29	0.44	0.35	0.24	0.16	0.21	0.15
Mean Co^{59}	MASS-1	b.l.d	13988.20	b.l.d	20189.71	10251.62	21118.64	11066.81	6651.53
Mean Ni^{61}	MASS-1	b.l.d	4599.38	b.l.d	3893.32	2538.21	39.90	54.97	77.28
Mean Cu^{63}	MASS-1	336524.82	b.l.d	293684.28	b.l.d	0.23	3.14	1.14	0.33
Mean Cu^{65}	MASS-1	308231.55	0.49	286812.89	0.49	0.38	5.75	2.92	1.07
Mean Zn^{66}	MASS-1	3.98	1.03	14.93	1.20	1.38	1.17	1.04	1.10
Mean Zn^{68}	MASS-1	b.l.d	b.l.d	18.03	b.l.d	b.l.d	b.l.d	b.l.d	b.l.d
Mean As^{75}	MASS-1	b.l.d	2.02	b.l.d	138.35	3.21	b.l.d	b.l.d	b.l.d
Mean Se^{77}	MASS-1	72.32	44.94	77.43	60.81	33.38	4.85	4.97	2.56
Mean Se^{78}	MASS-1	116.65	45.52	b.l.d	66.20	28.03	b.l.d	b.l.d	b.l.d
Mean Se^{82}	MASS-1	52.77	40.43	71.76	55.77	36.22	3.42	3.86	b.l.d
Mean Ru^{101}	Po725	0.52	b.l.d	b.l.d	b.l.d	b.l.d	b.l.d	b.l.d	0.06
Mean Rh^{103}	Po725	0.29	b.l.d	0.19	b.l.d	b.l.d	b.l.d	b.l.d	b.l.d
Mean Pd^{105}	Po725	b.l.d	b.l.d	b.l.d	b.l.d	b.l.d	b.l.d	b.l.d	b.l.d
Mean Pd^{106}	Po725	b.l.d	b.l.d	b.l.d	0.04	b.l.d	b.l.d	b.l.d	b.l.d
Mean Pd^{108}	Po725	b.l.d	b.l.d	b.l.d	b.l.d	b.l.d	b.l.d	b.l.d	b.l.d
Mean Ag^{109}	MASS-1	23.67	b.l.d	44.85	b.l.d	b.l.d	b.l.d	b.l.d	b.l.d
Mean Cd^{111}	MASS-1	b.l.d	b.l.d	b.l.d	b.l.d	b.l.d	b.l.d	b.l.d	b.l.d
Mean Sn^{118}	MASS-1	b.l.d	b.l.d	b.l.d	b.l.d	b.l.d	b.l.d	b.l.d	b.l.d
Mean Sn^{120}	MASS-1	b.l.d	b.l.d	b.l.d	b.l.d	b.l.d	b.l.d	b.l.d	b.l.d
Mean Sb^{121}	MASS-1	b.l.d	b.l.d	b.l.d	b.l.d	b.l.d	b.l.d	b.l.d	b.l.d
Mean Sb^{123}	MASS-1	b.l.d	b.l.d	b.l.d	b.l.d	b.l.d	b.l.d	b.l.d	b.l.d
Mean Te^{125}	MASS-1	1.60	0.15	b.l.d	0.2441	b.l.d	b.l.d	b.l.d	b.l.d
Mean Os^{189}	Po725	b.l.d	b.l.d	b.l.d	b.l.d	b.l.d	b.l.d	b.l.d	b.l.d
Mean Ir^{193}	Po725	b.l.d	b.l.d	b.l.d	b.l.d	b.l.d	b.l.d	b.l.d	b.l.d
Mean Pt^{194}	Po725	b.l.d	b.l.d	b.l.d	0.33	b.l.d	b.l.d	b.l.d	b.l.d
Mean Pt^{195}	Po725	b.l.d	0.05	b.l.d	0.26	0.02	b.l.d	b.l.d	b.l.d
Mean Au^{197}	MASS-1	b.l.d	b.l.d	b.l.d	b.l.d	0.01	b.l.d	b.l.d	b.l.d
Mean Pb^{208}	MASS-1	1.83	0.48	3.98	1.00	1.27	b.l.d	b.l.d	b.l.d
Mean Bi^{209}	MASS-1	0.26	b.l.d	0.18	b.l.d	b.l.d	b.l.d	0.08	b.l.d

Samples (ppm)	Reference material	Pyrite 22	Pyrite 23	Pyrite 24	Pyrite 25 zone 1	Pyrite 25 zone 2	Pyrite 26	Pyrite 27 zone 1	Pyrite 27 zone 2
Mean S^{33}	MASS-1	231098.87	219625.47	228146.13	198875.26	205402.27	204366.58	195441.72	164923.84
Mean S^{34}	MASS-1	296921.91	284869.78	301035.26	259546.60	276421.98	260465.76	266013.08	245463.26
Mean V^{51}	MASS-1	0.13	0.14	0.12	0.20	0.04	0.12	0.17	0.14
Mean Co^{59}	MASS-1	21020.74	2100.96	21715.43	4483.86	456.49	22890.32	17232.85	652.47
Mean Ni^{61}	MASS-1	44.67	368.51	599.35	62.21	400.52	219.56	260.58	774.73
Mean Cu^{63}	MASS-1	1.31	0.76	1.71	0.47	0.76	0.74	1.92	1.71
Mean Cu^{65}	MASS-1	1.83	0.95	1.59	1.02	0.53	1.57	1.93	1.45
Mean Zn^{66}	MASS-1	0.78	0.44	0.81	0.39	0.86	0.90	0.51	1.03
Mean Zn^{68}	MASS-1	b.l.d	b.l.d	b.l.d	b.l.d	b.l.d	b.l.d	b.l.d	b.l.d
Mean As^{75}	MASS-1	b.l.d	4.74	52.50	b.l.d	b.l.d	b.l.d	2.00	b.l.d
Mean Se^{77}	MASS-1	4.9150	5.12	6.13	3.91	8.64	7.11	4.30	6.3608
Mean Se^{78}	MASS-1	b.l.d	b.l.d	b.l.d	b.l.d	b.l.d	6.38	b.l.d	b.l.d
Mean Se^{82}	MASS-1	3.92	4.74	6.32	b.l.d	9.84	6.32	4.27	7.14
Mean Ru^{101}	Po725	b.l.d	b.l.d	b.l.d	b.l.d	b.l.d	b.l.d	b.l.d	b.l.d
Mean Rh^{103}	Po725	b.l.d	b.l.d	b.l.d	b.l.d	b.l.d	b.l.d	b.l.d	b.l.d
Mean Pd^{105}	Po725	b.l.d	b.l.d	b.l.d	b.l.d	b.l.d	b.l.d	b.l.d	b.l.d
Mean Pd^{106}	Po725	b.l.d	b.l.d	b.l.d	b.l.d	b.l.d	b.l.d	b.l.d	b.l.d
Mean Pd^{108}	Po725	b.l.d	b.l.d	b.l.d	b.l.d	b.l.d	b.l.d	b.l.d	b.l.d
Mean Ag^{109}	MASS-1	0.01	b.l.d	b.l.d	b.l.d	b.l.d	b.l.d	b.l.d	b.l.d
Mean Cd^{111}	MASS-1	b.l.d	b.l.d	b.l.d	b.l.d	b.l.d	b.l.d	b.l.d	b.l.d
Mean Sn^{118}	MASS-1	b.l.d	b.l.d	b.l.d	b.l.d	b.l.d	b.l.d	b.l.d	b.l.d
Mean Sn^{120}	MASS-1	b.l.d	b.l.d	b.l.d	b.l.d	b.l.d	b.l.d	b.l.d	b.l.d
Mean Sb^{121}	MASS-1	b.l.d	b.l.d	b.l.d	b.l.d	b.l.d	b.l.d	b.l.d	b.l.d
Mean Sb^{123}	MASS-1	b.l.d	b.l.d	b.l.d	b.l.d	b.l.d	b.l.d	b.l.d	b.l.d
Mean Te^{125}	MASS-1	b.l.d	b.l.d	b.l.d	b.l.d	b.l.d	b.l.d	b.l.d	b.l.d
Mean Os^{189}	Po725	b.l.d	b.l.d	b.l.d	b.l.d	b.l.d	b.l.d	b.l.d	b.l.d
Mean Ir^{193}	Po725	b.l.d	b.l.d	b.l.d	b.l.d	b.l.d	b.l.d	b.l.d	b.l.d
Mean Pt^{194}	Po725	b.l.d	b.l.d	b.l.d	b.l.d	b.l.d	b.l.d	b.l.d	b.l.d
Mean Pt^{195}	Po725	b.l.d	b.l.d	1.44	b.l.d	b.l.d	b.l.d	b.l.d	b.l.d
Mean Au^{197}	MASS-1	b.l.d	b.l.d	1.39	b.l.d	0.15	b.l.d	0.0827	0.0631
Mean Pb^{208}	MASS-1	b.l.d	b.l.d	b.l.d	b.l.d	b.l.d	b.l.d	b.l.d	0.0112
Mean Bi^{209}	MASS-1	0.03	0.03	0.03	0.08	b.l.d	0.04	0.0861	0.1197

Samples (ppm)	Reference material	Pyrite 28	Pyrite 29 zone 1	Pyrite 29 zone 2	Pyrite 30	Pyrite 31	Pyrite 32 zone 1	Pyrite 32 zone 2	Pyrite 33
Mean S^{33}	MASS-1	167394.17	166231.15	154274.05	180682.77	169890.97	178319.30	185848.42	180977.17
Mean S^{34}	MASS-1	235114.05	211843.69	214926.66	253808.34	224442.30	220761.14	222120.58	216796.57
Mean V^{51}	MASS-1	0.14	0.17	0.14	0.15	0.15	0.08	0.07	0.15
Mean Co^{59}	MASS-1	302.21	448.89	2415.51	5764.32	1517.30	1879.13	343.34	19954.57
Mean Ni^{61}	MASS-1	334.12	2701.41	941.74	1056.56	380.37	7089.78	2076.62	380.32
Mean Cu^{63}	MASS-1	0.31	0.51	0.98	0.42	0.57	0.42	2.03	1.37
Mean Cu^{65}	MASS-1	2.39	0.63	4.16	1.48	4.98	0.38	2.86	1.31
Mean Zn^{66}	MASS-1	0.70	0.48	0.41	0.80	0.37	0.33	0.76	0.43
Mean Zn^{68}	MASS-1	b.l.d	b.l.d	b.l.d	b.l.d	b.l.d	b.l.d	b.l.d	b.l.d
Mean As^{75}	MASS-1	b.l.d	b.l.d	b.l.d	b.l.d	b.l.d	1.90	b.l.d	8.10
Mean Se^{77}	MASS-1	b.l.d	26.94	21.48	21.30	17.93	28.37	20.17	26.67
Mean Se^{78}	MASS-1	b.l.d	24.93	19.06	13.45	11.64	24.38	21.61	23.96
Mean Se^{82}	MASS-1	b.l.d	29.95	20.71	21.65	16.73	25.27	16.55	23.77
Mean Ru^{101}	Po725	b.l.d	b.l.d	b.l.d	b.l.d	b.l.d	0.15	b.l.d	b.l.d
Mean Rh^{103}	Po725	b.l.d	b.l.d	b.l.d	b.l.d	b.l.d	b.l.d	b.l.d	b.l.d
Mean Pd^{105}	Po725	b.l.d	b.l.d	b.l.d	b.l.d	b.l.d	b.l.d	b.l.d	b.l.d
Mean Pd^{106}	Po725	b.l.d	b.l.d	b.l.d	b.l.d	b.l.d	0.31	0.04	b.l.d
Mean Pd^{108}	Po725	b.l.d	b.l.d	b.l.d	b.l.d	b.l.d	0.24	0.13	b.l.d
Mean Ag^{109}	MASS-1	b.l.d	0.16	0.11	b.l.d	b.l.d	0.14	2.44	b.l.d
Mean Cd^{111}	MASS-1	b.l.d	b.l.d	b.l.d	b.l.d	b.l.d	b.l.d	b.l.d	b.l.d
Mean Sn^{118}	MASS-1	b.l.d	b.l.d	b.l.d	b.l.d	b.l.d	b.l.d	b.l.d	b.l.d
Mean Sn^{120}	MASS-1	b.l.d	b.l.d	b.l.d	b.l.d	b.l.d	0.21	b.l.d	b.l.d
Mean Sb^{121}	MASS-1	b.l.d	b.l.d	b.l.d	b.l.d	b.l.d	b.l.d	0.08	b.l.d
Mean Sb^{123}	MASS-1	b.l.d	0.08	b.l.d	b.l.d	0.04	b.l.d	0.08	b.l.d
Mean Te^{125}	MASS-1	b.l.d	0.60	1.56	1.30	b.l.d	0.29	0.33	b.l.d
Mean Os^{189}	Po725	b.l.d	b.l.d	b.l.d	b.l.d	b.l.d	b.l.d	b.l.d	b.l.d
Mean Ir^{193}	Po725	b.l.d	b.l.d	b.l.d	b.l.d	b.l.d	b.l.d	b.l.d	b.l.d
Mean Pt^{194}	Po725	b.l.d	b.l.d	b.l.d	b.l.d	b.l.d	b.l.d	b.l.d	b.l.d
Mean Pt^{195}	Po725	b.l.d	b.l.d	b.l.d	b.l.d	b.l.d	b.l.d	b.l.d	b.l.d
Mean Au^{197}	MASS-1	b.l.d	b.l.d	b.l.d	b.l.d	b.l.d	b.l.d	b.l.d	b.l.d
Mean Pb^{208}	MASS-1	b.l.d	b.l.d	b.l.d	b.l.d	b.l.d	b.l.d	0.10	b.l.d
Mean Bi^{209}	MASS-1	0.03	2.87	3.81	0.02	0.04	0.34	6.44	0.03

Samples (ppm)	Reference material	Pyrite 34	Pyrite 35	Pyrite 36	Pyrite 37	Pyrite 38	Pyrite 39	Pyrite 40	Pyrite 41
Mean S^{33}	MASS-1	171857.57	173149.79	180092.78	169317.78	160542.88	36565.62	41324.40	50161.40
Mean S^{34}	MASS-1	217050.98	213622.59	225821.01	229034.75	201086.72	63832.68	51614.74	54417.41
Mean V^{51}	MASS-1	0.14	0.10	0.10	0.13	0.05	0.12	0.14	0.16
Mean Co^{59}	MASS-1	15227.99	8557.86	6842.34	374.39	7197.54	10041.96	2321.85	4792.66
Mean Ni^{61}	MASS-1	843.60	971.32	726.21	298.10	119.31	136.36	60.86	127.34
Mean Cu^{63}	MASS-1	0.59	0.89	0.58	0.50	0.43	1.81	2.33	4.74
Mean Cu^{65}	MASS-1	2.65	1.04	0.74	1.62	2.25	1.67	2.14	3.13
Mean Zn^{66}	MASS-1	0.40	0.57	0.65	0.61	0.29	0.35	0.63	1.63
Mean Zn^{68}	MASS-1	b.l.d	b.l.d	b.l.d	b.l.d	b.l.d	1.61	2.46	1.61
Mean As^{75}	MASS-1	97.41	20.53	10.79	b.l.d	1.22	4.40	1.36	1.94
Mean Se^{77}	MASS-1	30.74	35.36	24.35	14.26	28.10	10.37	4.97	18.61
Mean Se^{78}	MASS-1	27.68	34.03	30.65	14.48	28.18	8.87	9.99	21.50
Mean Se^{82}	MASS-1	27.02	33.05	25.99	12.73	26.52	9.14	3.39	23.25
Mean Ru^{101}	Po725	b.l.d	b.l.d	b.l.d	b.l.d	b.l.d	0.0020	0.0023	0.0023
Mean Rh^{103}	Po725	0.013	b.l.d	b.l.d	b.l.d	b.l.d	0.0005	0.0458	0.0006
Mean Pd^{105}	Po725	b.l.d	b.l.d	b.l.d	b.l.d	b.l.d	0.0010	0.0012	0.0013
Mean Pd^{106}	Po725	0.021	b.l.d	b.l.d	b.l.d	b.l.d	0.0007	0.0009	0.0010
Mean Pd^{108}	Po725	b.l.d	b.l.d	b.l.d	b.l.d	b.l.d	0.0010	0.0012	0.0014
Mean Ag^{109}	MASS-1	b.l.d	b.l.d	b.l.d	0.021	b.l.d	0.060	0.05	0.0007
Mean Cd^{111}	MASS-1	0.16	b.l.d	b.l.d	b.l.d	b.l.d	0.0032	0.37	0.0037
Mean Sn^{118}	MASS-1	b.l.d	b.l.d	b.l.d	b.l.d	b.l.d	0.22	0.42	0.44
Mean Sn^{120}	MASS-1	b.l.d	b.l.d	b.l.d	b.l.d	b.l.d	0.21	0.38	0.23
Mean Sb^{121}	MASS-1	b.l.d	b.l.d	b.l.d	b.l.d	b.l.d	0.06	0.08	0.08
Mean Sb^{123}	MASS-1	b.l.d	b.l.d	b.l.d	b.l.d	b.l.d	0.0709	0.0596	0.0047
Mean Te^{125}	MASS-1	b.l.d	b.l.d	b.l.d	b.l.d	b.l.d	0.0025	0.2402	0.0027
Mean Os^{189}	Po725	b.l.d	b.l.d	b.l.d	b.l.d	b.l.d	b.l.d	b.l.d	b.l.d
Mean Ir^{193}	Po725	b.l.d	b.l.d	b.l.d	b.l.d	b.l.d	0.0011	0.0013	0.0014
Mean Pt^{194}	Po725	b.l.d	b.l.d	b.l.d	b.l.d	b.l.d	0.0003	0.0004	0.0004
Mean Pt^{195}	Po725	b.l.d	b.l.d	b.l.d	b.l.d	b.l.d	0.0008	0.0009	0.0009
Mean Au^{197}	MASS-1	b.l.d	b.l.d	b.l.d	b.l.d	b.l.d	0.0005	0.2046	0.0007
Mean Pb^{208}	MASS-1	b.l.d	b.l.d	b.l.d	0.0095	b.l.d	0.0003	0.4455	0.5578
Mean Bi^{209}	MASS-1	0.054	0.055	0.058	0.053	0.018	0.1513	0.2139	0.1379

Samples (ppm)	Reference material	Pyrite 42	Pyrite 43 zone 1	Pyrite 43 zone 2	Pyrite 44	Chalcopyrite 45
Mean S^{33}	MASS-1	29978.09	52177.45	73028.24	76256.34	293451.60
Mean S^{34}	MASS-1	51408.87	45747.55	71669.99	76545.03	298456.70
Mean V^{51}	MASS-1	0.14	0.38	0.26	0.38	b.l.d
Mean Co^{59}	MASS-1	2861.77	3.54	5509.23	444.44	b.l.d
Mean Ni^{61}	MASS-1	57.14	583.67	24.14	130.58	b.l.d
Mean Cu^{63}	MASS-1	10.43	1.53	23.76	3.51	305002.92
Mean Cu^{65}	MASS-1	14.64	1.07	2.48	8.59	293129.73
Mean Zn^{66}	MASS-1	0.70	0.68	1.26	1.30	2.3704
Mean Zn^{68}	MASS-1	1.15	0.72	13.69	5.23	b.l.d
Mean As^{75}	MASS-1	1.84	1.03	6.99	59.82	b.l.d
Mean Se^{77}	MASS-1	7.52	8.63	2.42	8.22	83.4803
Mean Se^{78}	MASS-1	11.60	14.97	12.44	13.61	b.l.d
Mean Se^{82}	MASS-1	8.56	7.36	4.08	7.22	82.1706
Mean Ru^{101}	Po725	0.0016	0.0024	0.0036	0.0034	0.6341
Mean Rh^{103}	Po725	0.048	0.0007	0.0010	0.11	0.4586
Mean Pd^{105}	Po725	0.0009	0.0014	0.0021	0.0020	b.l.d
Mean Pd^{106}	Po725	0.0008	0.0012	0.0019	0.0019	b.l.d
Mean Pd^{108}	Po725	0.0010	0.0016	0.0025	0.0024	b.l.d
Mean Ag^{109}	MASS-1	0.074	0.34	0.0011	0.12	61.9029
Mean Cd^{111}	MASS-1	0.0026	0.0039	0.48	0.66	b.l.d
Mean Sn^{118}	MASS-1	0.15	0.50	0.16	0.46	b.l.d
Mean Sn^{120}	MASS-1	0.18	0.32	0.23	0.50	b.l.d
Mean Sb^{121}	MASS-1	0.057	0.08	0.06	0.08	b.l.d
Mean Sb^{123}	MASS-1	0.068	0.09	0.14	0.20	b.l.d
Mean Te^{125}	MASS-1	0.002	0.44	0.004	0.004	b.l.d
Mean Os^{189}	Po725	b.l.d	b.l.d	b.l.d	b.l.d	b.l.d
Mean Ir^{193}	Po725	0.0010	0.0015	0.0023	0.0023	b.l.d
Mean Pt^{194}	Po725	0.0003	0.0004	0.0006	0.0005	b.l.d
Mean Pt^{195}	Po725	0.0006	0.0009	0.0013	0.0012	b.l.d
Mean Au^{197}	MASS-1	0.20	0.0008	0.0010	0.27	b.l.d
Mean Pb^{208}	MASS-1	1.51	1.11	1.07	0.61	b.l.d
Mean Bi^{209}	MASS-1	0.25	0.97	0.27	0.12	0.26